



## Durham E-Theses

---

### *Pyroelectricity in langmuir-blodgett films*

Jones, Carole A.

#### How to cite:

---

Jones, Carole A. (1987) *Pyroelectricity in langmuir-blodgett films*, Durham theses, Durham University. Available at Durham E-Theses Online: <http://etheses.dur.ac.uk/6784/>

#### Use policy

---

The full-text may be used and/or reproduced, and given to third parties in any format or medium, without prior permission or charge, for personal research or study, educational, or not-for-profit purposes provided that:

- a full bibliographic reference is made to the original source
- a [link](#) is made to the metadata record in Durham E-Theses
- the full-text is not changed in any way

The full-text must not be sold in any format or medium without the formal permission of the copyright holders.

Please consult the [full Durham E-Theses policy](#) for further details.

PYROELECTRICITY IN  
LANGMUIR-BLODGETT FILMS

BY

CAROLE A. JONES, B. Sc.

The copyright of this thesis rests with the author.  
No quotation from it should be published without  
his prior written consent and information derived  
from it should be acknowledged.

A Thesis submitted for the Degree of  
Doctor of Philosophy in the  
University of Durham

July 1987



-5 NOV 1987

It is asserted, too, that these stones, when heated by the sun or rubbed between the fingers, will attract chaff and filaments of paper.

Pliny the Elder (c. 5 B.C.)

## DECLARATION

I hereby declare that the work reported in this thesis has not previously been submitted for any degree, and is not being currently submitted in candidature for any other degree.

The work reported in this thesis was carried out by the candidate.

## STATEMENT OF COPYRIGHT

The copyright of this Thesis rests with the author. No quotation from it should be published without her prior written consent, and information derived from it should be acknowledged.

## ACKNOWLEDGEMENTS

I would like to express my thanks to the many friends and colleagues at Durham University who have helped me during the course of this work. Primarily, I wish to thank my supervisors, Dr. Mike Petty and Professor Gareth Roberts, for their invaluable guidance and encouragement throughout my studies. I would also like to thank Dr. Graham Russell, who performed the RHEED experiments, and whose sense of humour never failed to cheer me up. I am also grateful to Dr. Gerald Davies for obtaining the infrared spectra, and to Dr. Steve Roser (Bristol University) for performing the X-ray measurements.

The materials used in this work were supplied by several people, but I would particularly like to acknowledge Dr. Norman Ratcliffe (Bristol University) and Dr. Malcolm Stewart (RARDE, Waltham Abbey) for synthesizing the 4-octadecylaniline and the PBD respectively. Much of the equipment was constructed in the departmental workshops, and I am most grateful to the technical staff, headed by Mr. Frank Spence, for contributing their skills. My thanks also go to Mr. Norman Thompson and Miss Kay Cummins for their patient and accurate reproduction of the diagrams. I gratefully acknowledge financial support from the Procurement Executive, Ministry of Defence.

Finally, I would like to thank my parents and sister for their continual support and encouragement throughout my university career, and most of all my husband, Patrick, for his patience and understanding.

## ABSTRACT

The fabrication of pyroelectric devices using the Langmuir-Blodgett (LB) technique is described. Studies of a wide range of materials are reported; however, the thesis concentrates on electrical and structural investigations of two specific alternate layer films: 22-tricosenoic acid/1-docosylamine and 22-tricosenoic acid/4-octadecylaniline. The latter system possesses a pyroelectric coefficient of  $0.65 \text{ nCcm}^{-2}\text{K}^{-1}$ , representing the largest reported value, to date, for an LB film. The pyroelectric figure of merit ( $p/\epsilon_r'$ ) of such films is approximately  $0.22 \text{ nCcm}^{-2}\text{K}^{-1}$ , which is comparable with the values for commercially available materials. The difference in pyroelectric coefficient of the two types of alternate layer film is attributed to differences in inter-layer bonding, as revealed by infrared spectroscopy. The dependence of the pyroelectric coefficients on parameters such as film thickness, substrate thickness and temperature is investigated. Structural studies, performed using electron and X-ray diffraction techniques, are also described. These provide information on the orientation of the molecules relative to the substrate and on the d-spacing of the LB films.

It is shown that the substrate has a deleterious effect on the responsiveness of LB film devices, and studies of films deposited onto different substrate materials indicate that there is a significant piezoelectrically induced secondary effect contributing to the overall pyroelectric coefficient. This secondary effect is small at low temperatures, but becomes dominant at around 250 K. The results of thermally stimulated discharge experiments indicate that both free charges and dipolar groups are incorporated in the films during deposition, and become tightly bound within the polar structure.

# CONTENTS

	Page
<b>1 INTRODUCTION</b>	<b>1</b>
<b>2 PYROELECTRIC MATERIALS: THEIR PROPERTIES AND APPLICATIONS</b>	<b>4</b>
<b>2.0 Introduction</b>	<b>4</b>
<b>2.1 An historic outline</b>	<b>4</b>
<b>2.2 Definitions</b>	<b>6</b>
2.2.1 Crystal symmetry and pyroelectricity	6
2.2.2 Ferroelectricity	7
2.2.3 Primary pyroelectricity	9
2.2.4 Secondary pyroelectricity	10
2.2.5 Tertiary effects	10
<b>2.3 Thermodynamic model</b>	<b>11</b>
<b>2.4 Conventional pyroelectric materials</b>	<b>14</b>
2.4.1 Inorganic single crystals	15
2.4.2 Inorganic ceramics	16
2.4.3 Organic crystals	16
(a) Triglycine sulphate	17
(b) Meta-dinitrobenzene	17
<b>2.5 Applications of pyroelectric materials</b>	<b>18</b>
2.5.1 Thermal imaging cameras	18
2.5.2 Other applications	20
<b>2.6 Summary</b>	<b>21</b>



	<b>Page</b>
<b>3 THIN FILM PYROELECTRIC STRUCTURES</b>	<b>23</b>
<b>3.0 Introduction</b>	<b>23</b>
<b>3.1 Conventional thin film pyroelectrics</b>	<b>23</b>
3.1.1 Inorganic thin films	23
3.1.2 Pyroelectric polymers	24
3.1.3 Liquid crystals	25
<b>3.2 Langmuir-Blodgett films</b>	<b>26</b>
3.2.1 LB films of a single material	27
3.2.2 Alternate layer structures	28
<b>3.3 Effect of a thick substrate</b>	<b>29</b>
3.3.1 Mechanical clamping	29
3.3.2 Thermal clamping	31
<b>3.4 Thin substrates</b>	<b>35</b>
<b>3.5 Summary</b>	<b>37</b>
<b>4 EXPERIMENTAL TECHNIQUES</b>	<b>38</b>
<b>4.0 Introduction</b>	<b>38</b>
<b>4.1 The Langmuir trough</b>	<b>38</b>
4.1.1 The conventional trough	38
4.1.2 The alternate layer trough	40
4.1.3 Pressure-area isotherms	40
4.1.4 Film deposition	41

	<b>Page</b>
<b>4.2 Device fabrication</b>	42
4.2.1 Substrate preparation	42
(a) Glass	42
(b) Aluminised glass	42
(c) Silicon	42
4.2.2 Fabrication of MIM devices	43
4.2.3 Surface blacking	43
<b>4.3 Structural characterisation</b>	43
4.3.1 Reflection high energy electron diffraction	43
4.3.2 Fourier transform infrared spectroscopy	45
4.3.3 X-ray low angle diffraction	46
<b>4.4 Pyroelectric and dielectric characterisation</b>	46
4.4.1 Static pyroelectric detection	46
4.4.2 Dynamic pyroelectric detection	48
4.4.3 Surface potential characterisation	49
4.4.4 Measurement of relative permittivity	51
4.4.5 Thermally stimulated discharge	53
<b>4.5 Summary</b>	53
<b>5 DEPOSITION AND STRUCTURAL CHARACTERISATION OF ACID/AMINE FILMS: RESULTS AND DISCUSSION</b>	<b>55</b>
<b>5.0 Introduction</b>	<b>55</b>
<b>5.1 Film characterisation and deposition</b>	<b>55</b>
5.1.1 Pressure-area isotherms	55
5.1.2 Film deposition and device fabrication	56

	Page
<b>5.2 Fourier transform infrared spectroscopy</b>	57
5.2.1 22-TA/docosylamine	57
5.2.2 22-TA/aminobenzoate	58
5.2.3 22-TA/aniline	59
<b>5.3 Reflection high energy electron diffraction</b>	60
5.3.1 22-tricosenoic acid	60
5.3.2 Acid/amine alternate layers	62
<b>5.4 X-ray low angle diffraction</b>	63
<b>5.5 Summary</b>	64
<b>6 DIELECTRIC AND PYROELECTRIC CHARACTERISATION OF ACID/AMINE FILMS: RESULTS AND DISCUSSION, PART I</b>	66
<b>6.0 Introduction</b>	66
<b>6.1 Dielectric characterisation</b>	66
6.1.1 Determination of $\epsilon'_r$	66
6.1.2 Temperature dependence of $\epsilon'_r$	67
6.1.3 Frequency dependence of $\epsilon'_r$	67
<b>6.2 Pyroelectric characterisation</b>	68
6.2.1 Static and dynamic measurements	68
6.2.2 Dependence of $p$ on film thickness	71
6.2.3 Dependence of $p$ on substrate thickness	72
6.2.4 Dependence of $p$ on $\alpha_{1s}$	73
<b>6.3 Summary</b>	75

	Page
<b>7 DIELECTRIC AND PYROELECTRIC CHARACTERISATION OF ACID/AMINE FILMS: RESULTS AND DISCUSSION, PART II</b>	76
<b>7.0 Introduction</b>	76
<b>7.1 Temperature dependence of <math>p</math></b>	76
<b>7.2 Thermally stimulated discharge</b>	79
7.2.1 Results of TSD experiments	80
7.2.2 Feature A	81
7.2.3 Feature D	82
7.2.4 Features B and C	83
7.2.5 Origins of excess charges and dipoles	85
<b>7.3 Summary</b>	86
<b>8 OTHER MATERIALS: RESULTS AND DISCUSSION</b>	88
<b>8.0 Introduction</b>	88
<b>8.1 Other alternate layer systems</b>	88
8.1.1 Highly polarisable systems	88
8.1.2 Systems with large dipole moments	90
8.1.3 Other alternate layer systems	91
<b>8.2 Ionically terminated polymers</b>	92
8.2.1 Ammonium terminated PBD	93
8.2.2 Boron terminated PBD	93
8.2.3 Ammonium terminated polystyrene	94
8.2.4 Acid terminated PBD	94
8.2.5 m-DNB terminated PBD	94

	Page
8.3 Esters of stearic acid	96
8.3.1 Ethyl stearate	96
8.3.2 Vinyl stearate	96
8.4 Summary	98
9 CONCLUSIONS AND SUGGESTIONS FOR FURTHER WORK	100
9.1 Summary	100
9.2 Suggestions for further work	103
9.3 Conclusions	104
REFERENCES	106
APPENDIX 1	125

## CHAPTER 1

### INTRODUCTION

It is widely anticipated that the steadily decreasing size of microelectronic components will lead ultimately to the exploitation of devices of molecular dimensions [1]. The ability to precisely tailor the structure of organic molecules means that these materials offer a much broader range of properties than is likely to be achieved with their inorganic counterparts. There is therefore a growing interest in the use of molecular materials for electronic [2], optical [3] and sensor [4] applications. The research presented in this thesis concentrates on one such application, namely the use of organic materials as thermal detectors.

The present generation of high performance thermal imaging devices relies mainly on the narrow band gap semiconductor cadmium mercury telluride (CMT) [5]. Although this system has a high sensitivity, it suffers from the inherent disadvantage of requiring cooling, and hence is bulky and expensive. Moreover, the spectral sensitivity of CMT detectors is not flat over the infrared region of the electromagnetic spectrum. An alternative type of thermal detector is based on the pyroelectric materials [6]; these are crystals which possess a temperature dependent spontaneous polarisation. Pyroelectric detectors can be operated at room temperature, and have a flat spectral response over a very broad wavelength range.

The largest pyroelectric effects occur in single crystal and ceramic materials such as barium titanate, triglycine sulphate and strontium barium niobate [7]. However, for device applications, it is advantageous to prepare the material in thin film form [8], and pyroelectric polymers such as polyvinylidene fluoride (PVDF) have been widely exploited for this purpose [9]. In order to render PVDF pyroelectric, it is necessary to subject it to a so-called "poling" process, in which an electric field is applied to the stretched film at an elevated temperature. The minimum thickness to which pyroelectric polymers can be reduced is thus limited by electrical breakdown. There is a need, therefore, to find new pyroelectric materials which can be deposited in the form of very thin films and



which do not require poling. This thesis describes one such class of materials.

The Langmuir-Blodgett (LB) technique is an elegant method for producing uniform, high quality organic thin films, and can be used to create novel structures with a precisely defined symmetry [10]. In the LB technique, a solid substrate is passed through a water surface on which a close-packed monolayer of an amphiphilic material is floating. In general, a monomolecular layer of the amphiphile is deposited onto the substrate with each traversal through the air-water interface. Because the film is built up layer by layer, the structure can be tailored to possess the specific symmetry requirements necessary for the observation of the pyroelectric effect, without the need for poling the film.

This thesis reports on the use of LB films as pyroelectric detectors, and concentrates mainly on systems consisting of alternate layers of a fatty acid and a fatty amine, although a range of other materials has also been investigated. The principal aims of the present work can be summarised as follows:

(1) To identify those LB film materials which form the most efficient pyroelectric detectors.

(2) To study the fundamental physical mechanisms responsible for the pyroelectric effect.

(3) To investigate the potential of LB film pyroelectric materials for practical device applications.

Chapters 2 and 3 cover the theoretical background of the pyroelectric effect, and include literature reviews of previous work in the field. Chapter 2 concentrates on bulk pyroelectric materials, whilst chapter 3 is concerned with the specific properties of thin films. The deleterious effect of using a thick substrate is emphasised in chapter 3, and expressions are derived to describe the thermal and mechanical clamping effects of the substrate. In chapter 4 the various experimental techniques used in the course of this work are described. The theoretical background of each technique is discussed, and detailed descriptions are given of the equipment used and the procedures adopted.

Chapters 5, 6 and 7 contain the results of experiments on acid/amine alternate layer films. The first of these chapters deals with the structural characterisation of the films using the techniques of infrared spectroscopy, electron

diffraction and X-ray diffraction. Chapters 6 and 7 are both concerned with dielectric and pyroelectric characterisation of acid/amine films. In chapter 6, fundamental electrical measurements are reported, whilst chapter 7 describes two more sophisticated investigations, namely the temperature dependence of the pyroelectric coefficient and thermally stimulated discharge of the films. Chapter 8 reviews the results of experiments on other LB film materials, including vinyl stearate and ionically terminated polybutadiene. Finally, chapter 9 summarises all the results, and suggests the directions in which future research should be aimed.



## CHAPTER 2

### PYROELECTRIC MATERIALS: THEIR PROPERTIES AND APPLICATIONS

#### 2.0 INTRODUCTION

If the crystal structure of a material is such that the centres of positive and negative charge do not coincide, then a spontaneous polarisation will exist across the crystal. In general, this polarisation will vary with temperature, giving rise to the pyroelectric effect. This chapter is concerned with the general properties of bulk pyroelectric materials and with their applications. The specific case of thin films is considered separately in chapter 3.

After a brief historical review, the basic properties of pyroelectric materials are defined and described in section 2.2. This is followed in section 2.3 by the development of a simple thermodynamic model, which relates pyroelectricity to macroscopic crystal properties. Section 2.4 describes the structure, preparation and properties of some specific pyroelectric materials. Finally, some important applications of pyroelectric devices are reviewed in section 2.5.

#### 2.1 AN HISTORICAL OUTLINE

The study of pyroelectricity can be traced back over 2300 years [1] to the Greek philosopher Theophrastus [2] who, in 315 B.C., described the ability of a stone known as *lyngourion* (probably tourmaline), when heated, to attract small objects. *Lyngourion* (or *lyncurium* in Latin) was greatly prized for its reputed medicinal properties, and was frequently referred to in the literature of the Greek and Roman periods [3] and the Dark and Middle Ages [4].

The first description of pyroelectricity in a scientific journal was published by Louis Lemery [5] in the *Histoire de l'Académie Royale des Sciences* in 1717, and was followed in 1756 by a systematic study of the properties of tourmaline by the Prussian physicist Dr. Franz Ulrich Theodor Aepinus [6], who formulated five "laws of the electricity of tourmaline". In 1759, John Canton [7] observed that the cooling of tourmaline caused its electrical polarity to be the reverse of

that found on heating, and further discovered that the quantities of positive and negative charge produced were equal. It is interesting to note that Canton was a correspondent of Benjamin Franklin, whose experiments on the spreading of oil films on Clapham Common [8] formed the basis for future work on Langmuir-Blodgett films.

The term “pyroelectricity” was first used by David Brewster, famous for his work on optics; in a paper published in 1824 [9], he listed a series of substances which exhibited the pyroelectric effect, including Rochelle salt, the material which led to the discovery of ferroelectricity almost a century later. During the nineteenth century, the first theoretical analyses of pyroelectricity were published [10–12], and the relationship between crystal symmetry and pyroelectricity was postulated, leading in 1880 to the discovery of piezoelectricity by Jacques and Pierre Curie [13].

During the early twentieth century, the study of pyroelectricity became rather esoteric, and several eminent theoreticians, including Schrödinger [14] and Born [15], applied the newly-developed concepts of quantum mechanics to dielectric and pyroelectric materials. In 1938, Yeou Ta [16] published a paper entitled “Action of Radiation on Pyroelectric Crystals”, proposing the use of tourmaline as an infrared detector, and the first dynamic pyroelectric detector was patented by Leon Sivian in 1942 [17]. These developments, along with Chynoweth’s work on barium titanate [18], provided the foundation for the great upsurge of interest in pyroelectric materials since 1960.

Current research into pyro- and ferroelectricity covers a wide range of materials, including ceramics, single crystals, polymers and molecular assemblies such as liquid crystals and Langmuir-Blodgett films. Figure 2.1 shows the logarithmic increase in the number of publications on ferroelectrics and related subjects over the last 50 years. The growth of interest in this subject is also manifested by the holding every three or four years of an international meeting [19], a regional European meeting [20], an IEEE applications conference [21] and national meetings in the USSR. There is an international journal, “Ferroelectrics” [22], devoted to the subject, and Lang’s Annual Literature Guide to Pyroelectricity [23] provides a major source of bibliographic information on this

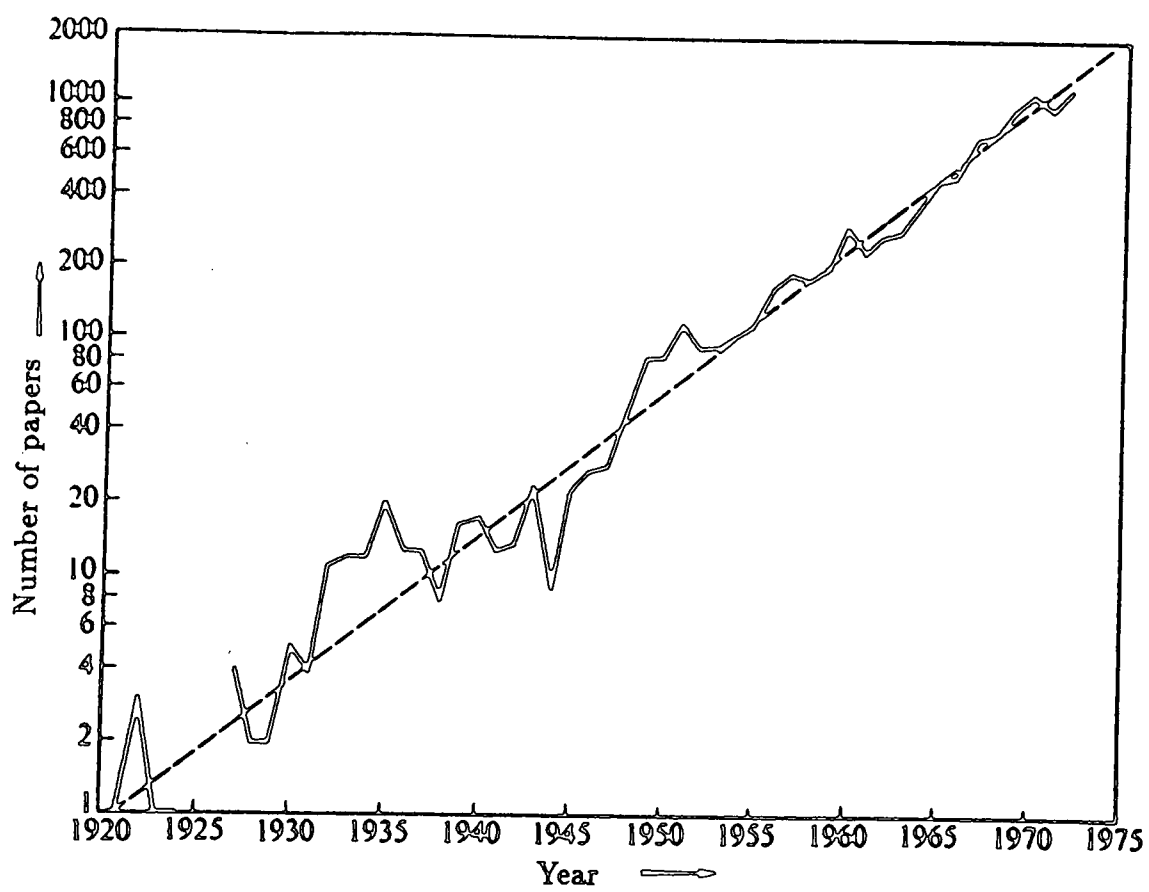


Figure 2.1 Publications on ferroelectricity and related topics as a function of year.

very important class of materials.

## 2.2 DEFINITIONS

### 2.2.1 Crystal symmetry and pyroelectricity

Crystals are classified into seven systems depending on the geometry of their unit cell; these are termed triclinic, monoclinic, orthorhombic, tetragonal, trigonal, hexagonal and cubic. The seven systems are, in turn, divided into point groups (crystal classes) according to their symmetry with respect to a point; there are 32 such crystal classes. Of the 32 classes, 20 are non-centrosymmetric and exhibit the piezoelectric effect: that is, when mechanical stress is applied along certain crystallographic directions, the crystals develop an electric polarisation whose magnitude is proportional to the applied stress. Conversely, when an electric field is applied along certain directions in a piezoelectric crystal, it is strained by an amount proportional to the applied field.

10 of the 20 non-centrosymmetric crystal classes possess a unique polar axis and hence a spontaneous electrical polarisation (*ie.* they have a finite dipole moment per unit volume in the absence of any applied electric field) and are called polar. The polar axis is defined [24] as that direction which is parallel to the spontaneous polarisation vector. When a polar crystal is heated or cooled, electrical conduction generally cannot provide enough current to compensate for the change in polarisation with temperature, and the crystal develops an electric charge on its surface; this is termed the pyroelectric effect. If the material forms the dielectric in a capacitor, and an external resistance is connected between the electrodes, a pyroelectric current,  $i$ , will flow in the external circuit;  $i$  is given by the expression

$$i = pA \frac{dT}{dt} \quad (2.1)$$

where  $dT/dt$  is the rate of change of temperature,  $A$  the device area, and  $p$  is termed the pyroelectric coefficient.

The pyroelectric coefficient is a useful parameter with which to compare different pyroelectric materials. However,  $p$  provides a measure of the current generated by a given rate of change of temperature, and not of the induced

COMPOUND	FORM	$P$ ( $nCcm^{-2}K^{-1}$ )	$\epsilon_r'$	$P/\epsilon_r'$ ( $nCcm^{-2}K^{-1}$ )
$LiTaO_3$	Single crystal	19	46	0.41
TGS	Single crystal	30	50	0.6
PVDF	Polymer film	3	10	0.3
$Sr_{0.6}Ba_{0.4}Nb_2O_6$	Ceramic	85	607	0.14

Table 2.1 Pyroelectric coefficients and figures of merit for some common pyroelectric materials.

voltage, which is the parameter measured in a pyroelectric detection system. The following proof demonstrates that it is possible to compare the pyroelectric voltages generated by different materials if the dielectric constant,  $\epsilon'_r$ , (*ie.* the real part of the relative permittivity) is also taken into account.

Consider a parallel plate capacitor of area  $A$  and thickness  $d$ , in which the dielectric is a pyroelectric material. A small change  $dT$  in the temperature will generate an amount of charge  $dQ$ , where

$$dQ = pAdT. \quad (2.2)$$

The charge  $dQ$  is associated with a small voltage  $dV$  given by

$$dQ = CdV, \quad (2.3)$$

where  $C$  is the capacitance of the pyroelectric element. Equating (2.2) and (2.3), we obtain

$$CdV = pAdT. \quad (2.4)$$

But,

$$C = \frac{\epsilon_0 \epsilon'_r A}{d}, \quad (2.5)$$

where  $\epsilon_0$  is the permittivity of free space. Therefore,

$$\frac{dV}{dT} = \frac{p}{\epsilon'_r \epsilon_0} d. \quad (2.6)$$

Thus, we can see that the quantity  $p/\epsilon'_r$  provides a useful figure of merit for a pyroelectric material [25], and represents a measure of the induced voltage per unit change of temperature. Therefore, a good pyroelectric material should have a large pyroelectric coefficient and a small dielectric constant [26]. Table 2.1 lists the values of  $p$ ,  $\epsilon'_r$  and  $p/\epsilon'_r$  for some conventional pyroelectric materials. This demonstrates that a material with a relatively low pyroelectric coefficient can form a good pyroelectric detector if its dielectric constant is correspondingly low.

### 2.2.2 Ferroelectricity

Ferroelectrics are a sub-group of the polar materials, and hence are both piezo- and pyroelectric. They are characterised by the reversibility or reorientability of their spontaneous polarisation on application of a sufficiently large

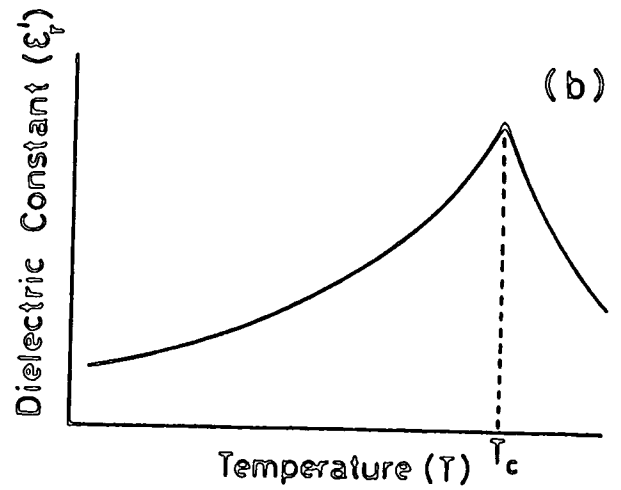
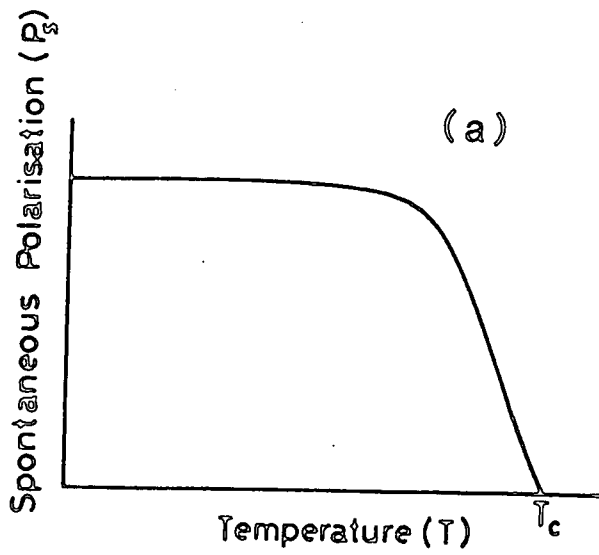
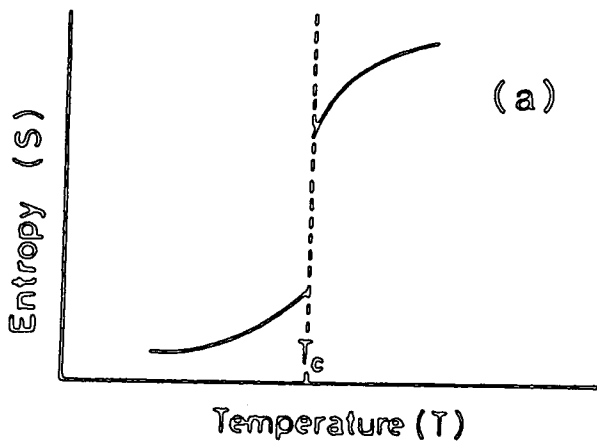
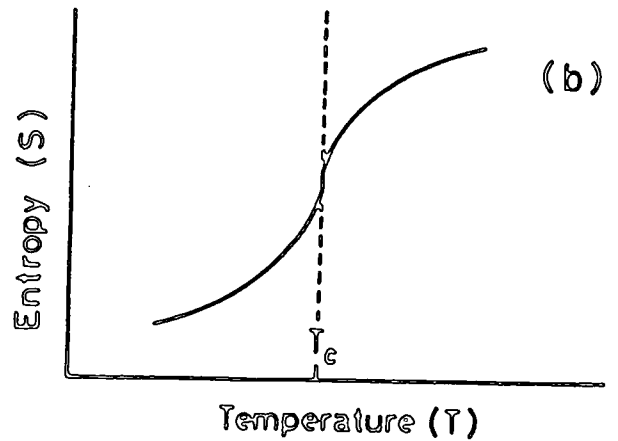


Figure 2.2 (a) Spontaneous polarisation and (b) dielectric constant of a ferroelectric material as a function of temperature.



FIRST ORDER



SECOND ORDER

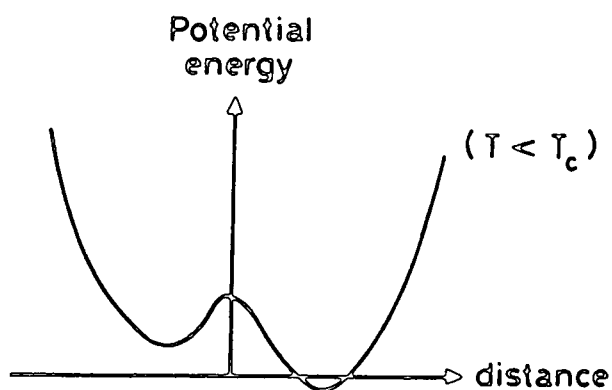
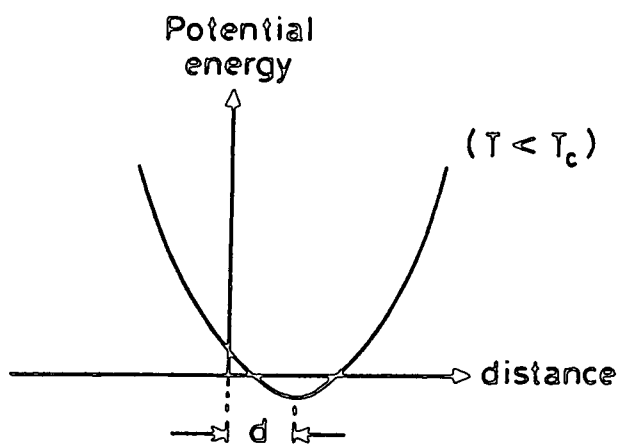
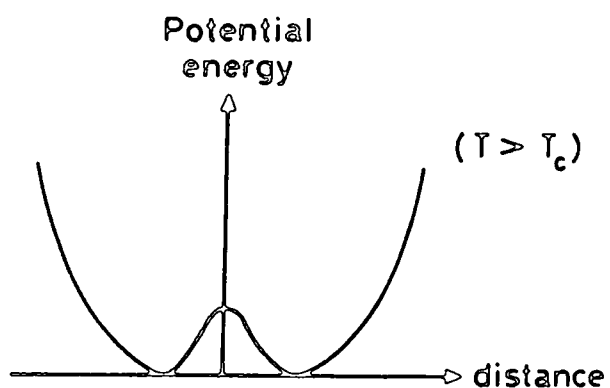
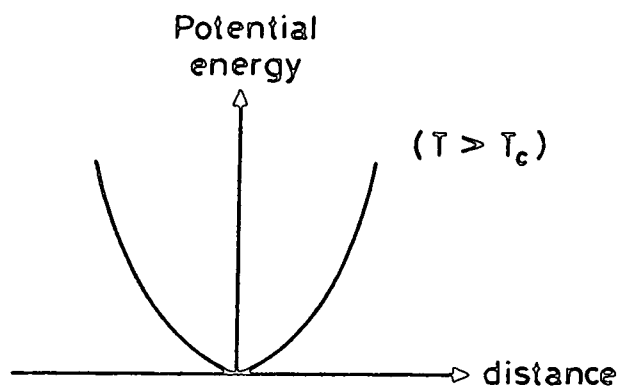
Figure 2.3 Entropy versus temperature for (a) a first order, and (b) a second order ferroelectric phase transition.

electric field. Ferroelectric behaviour is largely analogous with ferromagnetism, and ferroelectric materials exhibit effects such as hysteresis, Curie-Weiss behaviour and bistable switching. As with ferromagnetism, a Curie temperature,  $T_c$ , can be defined, at which a structural phase transition occurs. At temperatures below  $T_c$ , the material is polar and ferroelectric; as  $T_c$  is approached, the spontaneous polarisation decreases rapidly, and vanishes at the Curie point (figure 2.2a). The non-polar phase above  $T_c$  is known as a paraelectric phase. The dielectric constant,  $\epsilon_r'$ , also shows anomalous behaviour at the Curie point (figure 2.2b).

Ferroelectric materials are classified according to the nature of their transition from the paraelectric state to the ferroelectric state [27]. The most commonly used classification is based on the thermodynamics of the system, and distinguishes those materials whose phase transition is first order and those whose transition is second order. A first order transition is characterised by a finite discontinuity in the entropy,  $S$ , at  $T_c$ , whereas a second order phase transition involves a continuous change in entropy, although  $\partial S/\partial T$  is discontinuous. Figure 2.3 shows the entropy plotted as a function of temperature for first and second order transitions.

Another widely used system for classifying ferroelectrics is to describe the phase transition as either displacive or order-disorder. This classification is best explained by considering the potential energy of a single dipole. In the paraelectric phase, materials exhibiting a displacive phase transition can be thought of as consisting of dipoles occupying a minimum energy position in a single potential well. The transition to the ferroelectric phase is characterised by a small spontaneous displacement by some of the dipoles, to occupy new minimum energy positions, displaced a distance  $d$  from the original equilibrium position (figure 2.4a). For an order-disorder transition, the paraelectric phase is associated with two equally probable minimum energy positions for a dipolar group. In the ferroelectric phase, the symmetric double potential well becomes distorted, such that one of the positions is preferred (figure 2.4b). In table 2.2, the types of phase transition and Curie temperatures of some common ferroelectric materials are summarised.





(a) DISPLACIVE

(b) ORDER - DISORDER

Figure 2.4 Potential energy diagrams above and below the Curie temperature for (a) a displacive and (b) an order-disorder phase transition.

COMPOUND	ORDER-DISORDER OR DISPLACIVE TRANSITION	FIRST OR SECOND ORDER TRANSITION	T <sub>c</sub> (°C)
BaTiO <sub>3</sub>	Displacive	First order	120
LiNbO <sub>3</sub>	Displacive	Second order	1210
NaNbO <sub>3</sub>	Order-disorder	First order	163
KDP	Order-disorder	First order	-150
TGS	Order-disorder	Second order	49
Pb Zr <sub>x</sub> Ti <sub>(1-x)</sub> O <sub>3</sub> (PZT)	Displacive	Second order	217

Table 2.2 Classification of phase transitions for some ferroelectric materials.

In general, the pyroelectric coefficient of a ferroelectric material increases as the Curie temperature is approached; it is therefore advantageous to use such materials at temperatures close to the Curie point. However, figure 2.2b shows that the dielectric constant also tends to increase at this point; consequently, the figure of merit,  $p/\epsilon_r'$ , often shows an anomalous temperature dependence. There is therefore considerable advantage to be gained from using pyroelectric materials which are not ferroelectric, and hence do not show discontinuities in  $p/\epsilon_r'$  as a function of temperature.

### 2.2.3 Primary pyroelectricity

In order for a material to be pyroelectric, each unit cell of the substance must have an electric dipole; this dipole is produced because the centres of positive and negative charge do not coincide. If the dipoles throughout the sample are aligned in such a way that they do not cancel one another, then the material will exhibit a spontaneous electric polarisation. An increase or decrease in temperature will change the strength of the dipoles by causing shifts in the atomic positions or by modifying the interatomic bonding; this is generally known as the primary (or "true") pyroelectric effect.

The preceding discussion has referred only to single crystals. However, it is important to note that polycrystalline aggregates can also be pyroelectric. The spontaneous polarisation,  $P_S$ , is defined as the dipole moment,  $\mu$ , per unit volume, averaged over the volume,  $v$ , of the substance. This can be expressed mathematically as

$$P_S = \frac{1}{v} \iiint \mu \, dv. \quad (2.7)$$

In order for  $P_S$  to be non-zero, not only must  $\mu$  be non-zero in at least a part of the material, but it is also necessary that the integration process should not cause cancellation of all the terms. Hence, a polycrystalline sample can be pyroelectric, so long as the crystallites are oriented such that the average dipole moment is not equal to zero. This is frequently achieved by a process known as poling, in which a d.c. electric field is applied along a particular direction, causing the dipoles to orient in this direction.

It should be noted that a pyroelectric effect might also be generated by

a change in the angle between the dipoles and the polar axis as a result of a change in temperature. This is a familiar concept in the field of ferroelectric liquid crystals [28], and we shall also consider this possibility in pyroelectric Langmuir-Blodgett films in a later section.

#### 2.2.4 Secondary pyroelectricity

Because pyroelectrics are a sub-group of piezoelectrics, any material which is pyroelectric must also be piezoelectric. Therefore, when a pyroelectric material is heated (or cooled) and undergoes thermal expansion (or contraction), resulting in the generation of a mechanical strain, there will be a change in polarisation due to the piezoelectric effect. This so-called secondary effect is additional to the primary pyroelectric effect which will also result from heating the crystal, and, in practice, it is extremely difficult to distinguish between primary and secondary pyroelectricity. One important difference between the two phenomena is that the primary effect is due purely to a coupling between the thermal and electrical properties of the crystal, whilst the secondary effect also involves the mechanical properties. This is of extreme significance when considering thin films which are mechanically constrained by the substrate on which they are deposited, and will be discussed further in chapter 3.

It should be noted that a crystal which is piezoelectric but not pyroelectric will not develop a surface charge when uniformly heated or subjected to a hydrostatic stress. In such a crystal, dipolar arrangements are present, but are arranged in several compensating directions such that there is no net crystal dipole. In quartz, for example, there are three polar axes at  $120^\circ$  in a plane, and a uniform stress will effect each axis equally, such that the net change in polarisation will be zero.

#### 2.2.5 Tertiary effects

In addition to primary and secondary pyroelectricity, there are several phenomena which can give rise to spurious, and generally undesirable, tertiary effects. Such phenomena can create an effective polar axis within a centrosymmetric crystal and lead to a pyroelectric effect in a material which would not

be expected, on the basis of its crystal symmetry, to be pyroelectric. Tertiary pyroelectricity has recently been proposed [29] as the basis of a detection system for high intensity radiation pulses.

The first such effect is due to non-uniform heating, which leads to non-uniform stresses and can produce a polarisation along an effective polar axis in the direction of the temperature gradient. Secondly, if a crystal is not homogeneous (*ie.* if its properties are not independent of position), then an asymmetric distribution of space-charge may exist at defects such as grain boundaries and dislocations; in general this space-charge distribution will be temperature dependent. Even in a perfectly homogeneous crystal, such effects are likely to occur at the surfaces [30] where surface states can trap free carriers, and this effect becomes particularly dominant in thin films where the surface layers constitute a large proportion of the total thickness.

### 2.3 THERMODYNAMIC MODEL

The previous section described the microscopic origins of pyroelectricity, and predicted in which materials the effect should be observed. In this section, we consider the macroscopic crystal properties (*ie.* those which are experimentally determinable), and relate these to the piezo- and pyroelectric coefficients.

The total internal energy,  $U$ , of a crystal can be completely defined by its thermal, electrical and mechanical properties [31]. Quantitatively, each of these three properties is described by a pair of variables:

**Thermal:** Temperature ( $T$ ) and Entropy ( $S$ )

**Electrical:** Electric field ( $E_m$ ) and Displacement ( $D_n$ ) ( $m, n = 1 - 3$ )

**Mechanical:** Stress ( $\sigma_j$ ) and Strain ( $\epsilon_i$ ) ( $i, j = 1 - 6$ )

Of course, either quantity in each pair may be chosen as the independent variable; however, in a discussion of pyroelectricity, it is clear that temperature must be an independent variable and displacement a dependent variable. Here, we choose stress as the third independent variable.

Consider a small reversible change in temperature,  $dT$ , giving rise to a small change in entropy,  $dS$ , defined by the expression

$$dS = \left( \frac{c}{T} \right) dT \quad (2.8)$$

where  $c$  is the specific heat capacity. Similarly, a change in electric field,  $dE_m$ , produces a change in displacement,  $dD_n$ , given by

$$dD_n = k_{nm}dE_m \quad (2.9)$$

where  $k_{nm}$  is the permittivity. A change in stress,  $d\sigma_j$ , produces a change in strain,  $d\epsilon_i$ , given by

$$d\epsilon_i = s_{ij}d\sigma_j \quad (2.10)$$

where  $s_{ij}$  is the elastic compliance.

If we expand the dependent variables as perfect differentials, then we obtain the following set of equations:

$$dS = \left( \frac{\partial S}{\partial T} \right)_{E,\sigma} dT + \left( \frac{\partial S}{\partial E_m} \right)_{\sigma,T} dE_m + \left( \frac{\partial S}{\partial \sigma_j} \right)_{E,T} d\sigma_j \quad (2.11a)$$

$$dD_n = \left( \frac{\partial D_n}{\partial T} \right)_{E,\sigma} dT + \left( \frac{\partial D_n}{\partial E_m} \right)_{\sigma,T} dE_m + \left( \frac{\partial D_n}{\partial \sigma_j} \right)_{E,T} d\sigma_j \quad (2.11b)$$

$$d\epsilon_i = \left( \frac{\partial \epsilon_i}{\partial T} \right)_{E,\sigma} dT + \left( \frac{\partial \epsilon_i}{\partial E_m} \right)_{\sigma,T} dE_m + \left( \frac{\partial \epsilon_i}{\partial \sigma_j} \right)_{E,T} d\sigma_j \quad (2.11c)$$

where the subscripts to the bracketed derivatives denote the independent variables which are held constant during partial differentiation. This may be expressed in matrix form thus:

$$[dS \quad dD_n \quad d\epsilon_i] = \begin{bmatrix} \left( \frac{\partial S}{\partial T} \right)_{E,\sigma} & \left( \frac{\partial S}{\partial E_m} \right)_{\sigma,T} & \left( \frac{\partial S}{\partial \sigma_j} \right)_{E,T} \\ \left( \frac{\partial D_n}{\partial T} \right)_{E,\sigma} & \left( \frac{\partial D_n}{\partial E_m} \right)_{\sigma,T} & \left( \frac{\partial D_n}{\partial \sigma_j} \right)_{E,T} \\ \left( \frac{\partial \epsilon_i}{\partial T} \right)_{E,\sigma} & \left( \frac{\partial \epsilon_i}{\partial E_m} \right)_{\sigma,T} & \left( \frac{\partial \epsilon_i}{\partial \sigma_j} \right)_{E,T} \end{bmatrix} \begin{bmatrix} dT \\ dE_m \\ d\sigma_j \end{bmatrix} \quad (2.12)$$

We can immediately see that the leading diagonal of the matrix of partial derivatives gives the ‘‘direct’’ effects described by equations (2.8), (2.9) and (2.10), whilst the off-diagonal elements give the coupled effects, namely, piezoelectricity, pyroelectricity and thermal expansion. It has been shown [31] that there is a symmetry in the off-diagonal components such that:

$$\left( \frac{\partial \epsilon_i}{\partial E_m} \right)_{\sigma,T} = \left( \frac{\partial D_n}{\partial \sigma_j} \right)_{E,T} = d_{nj}^T \quad (2.13a)$$

$$\left(\frac{\partial \epsilon_i}{\partial T}\right)_{E,\sigma} = \left(\frac{\partial S}{\partial \sigma_j}\right)_{E,T} = \alpha_i^E \quad (2.13b)$$

$$\left(\frac{\partial D_n}{\partial T}\right)_{E,\sigma} = \left(\frac{\partial S}{\partial E_m}\right)_{\sigma,T} = p_n^\sigma \quad (2.13c)$$

where  $d_{nj}^T$ ,  $\alpha_i^E$  and  $p_n^\sigma$  are the piezoelectric, thermal expansion and pyroelectric coefficients, respectively, and where the superscripts denote constant quantities.

Figure 2.5 illustrates interactions between the thermal, electrical and mechanical properties of a crystal; the heavy lines indicate the direct effects, whilst the faint lines denote the various coupled effects which can occur. Combining equations (2.11) and (2.13), we obtain:

$$dS = \alpha_i^E d\sigma_j + p_n^\sigma dE_m + \left(\frac{c}{T}\right)^{E,\sigma} dT \quad (2.14a)$$

$$dD_n = d_{nj}^T d\sigma_j + k_{nm}^{\sigma,T} dE_m + p_n^\sigma dT \quad (2.14b)$$

$$d\epsilon_i = s_{ij}^{E,T} d\sigma_j + d_{nj}^T dE_m + \alpha_i^E dT. \quad (2.14c)$$

The electric displacement,  $dD_n$ , is related to the polarisation,  $dP_n$ , by the expression

$$dD_n = dP_n + \epsilon_0 dE_m \quad (2.15)$$

where  $\epsilon_0$  is the permittivity of free space. As the electric field is constant ( $dE_m = 0$ ), then

$$dD_n = dP_n. \quad (2.16)$$

If the crystal is free to expand and contract, then it is in a situation of constant stress ( $d\sigma_j = 0$ ), and equation (2.14b) becomes

$$dP_n = p_n^\sigma dT. \quad (2.17)$$

Thus, the pyroelectric coefficient at constant stress is defined as

$$p_n^\sigma = \left(\frac{dP_n}{dT}\right)_\sigma \quad (2.18)$$

This includes both primary and secondary pyroelectric terms. We can separate these out by re-writing equations (2.14b) and (2.14c) under conditions of constant electric field. Neglecting entropy changes, we obtain,

$$dP_n = d_{nj}^T d\sigma_j + p_n^\sigma dT \quad (2.19a)$$

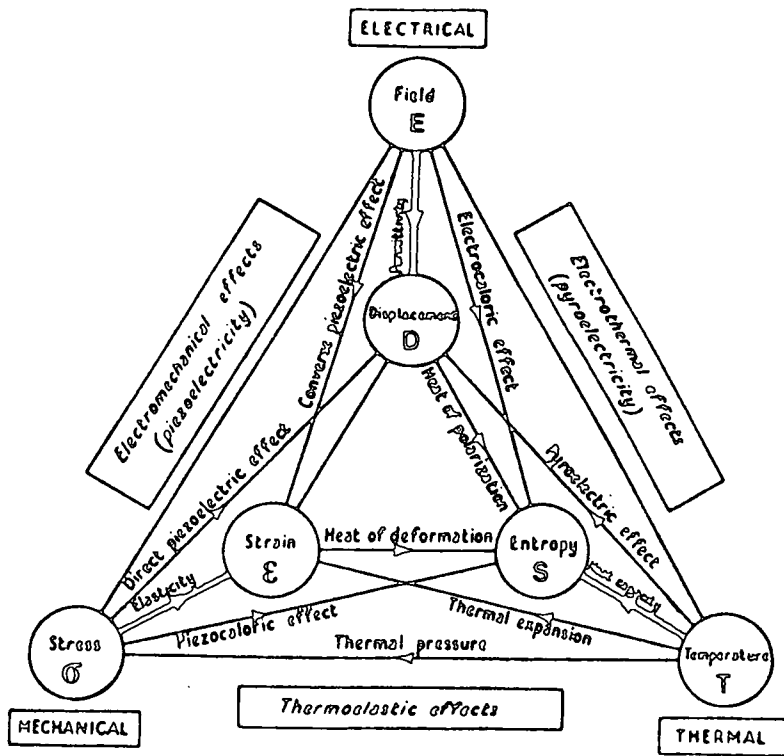


Figure 2.5 The relationships between the thermal, electrical and mechanical properties of a crystal.

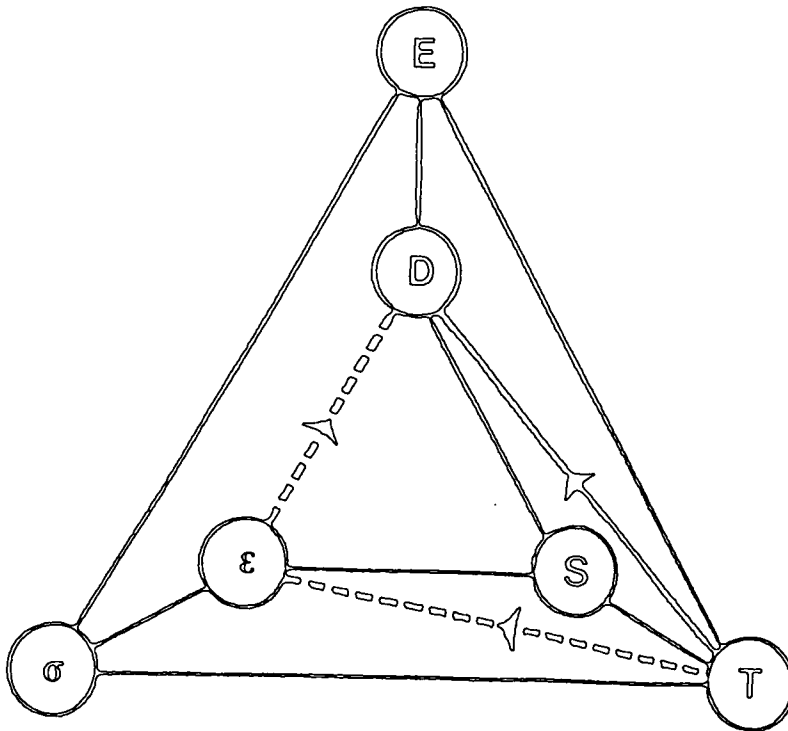


Figure 2.6 The relationship of primary pyroelectricity (full arrow) and secondary pyroelectricity (broken arrow) to the thermodynamic variables.



$$d\epsilon_i = s_{ij}^{E,T} d\sigma_j + \alpha_i^E dT. \quad (2.19b)$$

Putting  $d\sigma_j = 0$  (constant stress), and equating, we obtain

$$\frac{d\epsilon_i}{s_{ij}} - \frac{\alpha_i^E dT}{s_{ij}} = \frac{dP_n}{d_{nj}} - \frac{p_n^\sigma dT}{d_{nj}} \quad (2.20)$$

which leads to

$$p_n^\sigma = \left( \frac{dP_n}{dT} \right)_\epsilon + \frac{\alpha_i d_{nj}}{s_{ij}} \quad (2.21)$$

But,

$$\left( \frac{dP_n}{dT} \right)_\epsilon = p^\epsilon$$

where  $p^\epsilon$  is the pyroelectric coefficient at constant strain. Also,  $s_{ij}^{-1} = c_{ij}$ , where  $c_{ij}$  is the elastic stiffness. Therefore,

$$p_n^\sigma = p_n^\epsilon + d_{nj} c_{ij} \alpha_i. \quad (2.22)$$

The interpretation of equation (2.22) is that the total pyroelectric coefficient in a free crystal (constant stress) is the sum of the pyroelectric coefficient under constant strain and a term dependent on the piezoelectric coefficient. These two terms are, of course, the primary and secondary effects, and we can see that a crystal which is mechanically clamped (constant strain) will exhibit only a primary pyroelectric effect. This concept will be developed further in chapter 3 when we consider thin films which are mechanically clamped in the plane of the film, but are free to expand and contract in the direction perpendicular to this plane.

Figure 2.6 shows how primary and secondary pyroelectric effects are related to the basic thermodynamic variables. The full arrow denotes the primary pyroelectric effect, whilst the broken arrow indicates the secondary effect.

## 2.4 CONVENTIONAL PYROELECTRIC MATERIALS

Polar materials may be fabricated in single crystal, ceramic or thin film forms, and the form chosen will depend on such factors as cost, reproducibility, specimen quality and dimensions. This section reviews some conventional bulk single crystal and ceramic pyroelectrics; thin films are discussed in chapter 3.

### 2.4.1 Inorganic single crystals

Single crystals are widely used for basic pyro- and ferroelectric studies, where the polar material needs to be as near perfect as possible, and where cost is not a limiting factor. The most common methods of preparation of single crystals are growth from solution and Czochralski growth [32], both of which rely on nucleation of material onto a seed crystal. Figure 2.7 contains a comprehensive listing of pyroelectric single crystals that have been grown by various techniques.

One of the most widely studied classes of pyroelectric crystals is the perovskites, which have the general formula  $ABO_3$  where A is a mono- or divalent metal and B is a tetra- or pentavalent one. The perfect perovskite structure is illustrated in figure 2.8. It is immediately apparent that this structure is cubic and centrosymmetric and hence is not pyroelectric. However, most perovskites adopt a structure which is based on the cubic prototype, but which is slightly distorted; the most common distortion being a tilting of the oxygen octahedra in the unit cell, resulting in a polar structure. Perhaps the best-known example is barium titanate ( $BaTiO_3$ ) [30], which has a pyroelectric coefficient of approximately  $30 \text{ nCcm}^{-2}\text{K}^{-1}$ .  $BaTiO_3$  adopts a tetragonal structure at temperatures below  $120^\circ\text{C}$ , in which the  $Ti^{4+}$  and  $Ba^{2+}$  ions are shifted slightly relative to the  $O^{2-}$  framework, which also becomes distorted. Figure 2.9 shows a projection of the tetragonal  $BaTiO_3$  unit cell onto the (100) plane. Other perovskites which have been widely studied include  $KNbO_3$  [34],  $PbTiO_3$  [35],  $NaNbO_3$  [36] and  $KTaO_3$  [37].

There are several other structures commonly adopted by inorganic ferroelectric crystals [38–42]; the most common of these are tabulated in table 2.3. In view of the importance of hydrogen bonds in Langmuir-Blodgett films, it is interesting to note that hydrogen bonding plays an important part in ferroelectric switching in the  $KH_2PO_4$  (KDP) type materials. KDP itself possesses a structure which essentially consists of two interpenetrating body-centred lattices of  $PO_4$  tetrahedra and two interpenetrating body-centred K lattices, with every  $PO_4$  linked to four other  $PO_4$  groups by hydrogen bonds (figure 2.10). Several authors have proposed models to account for the structural changes

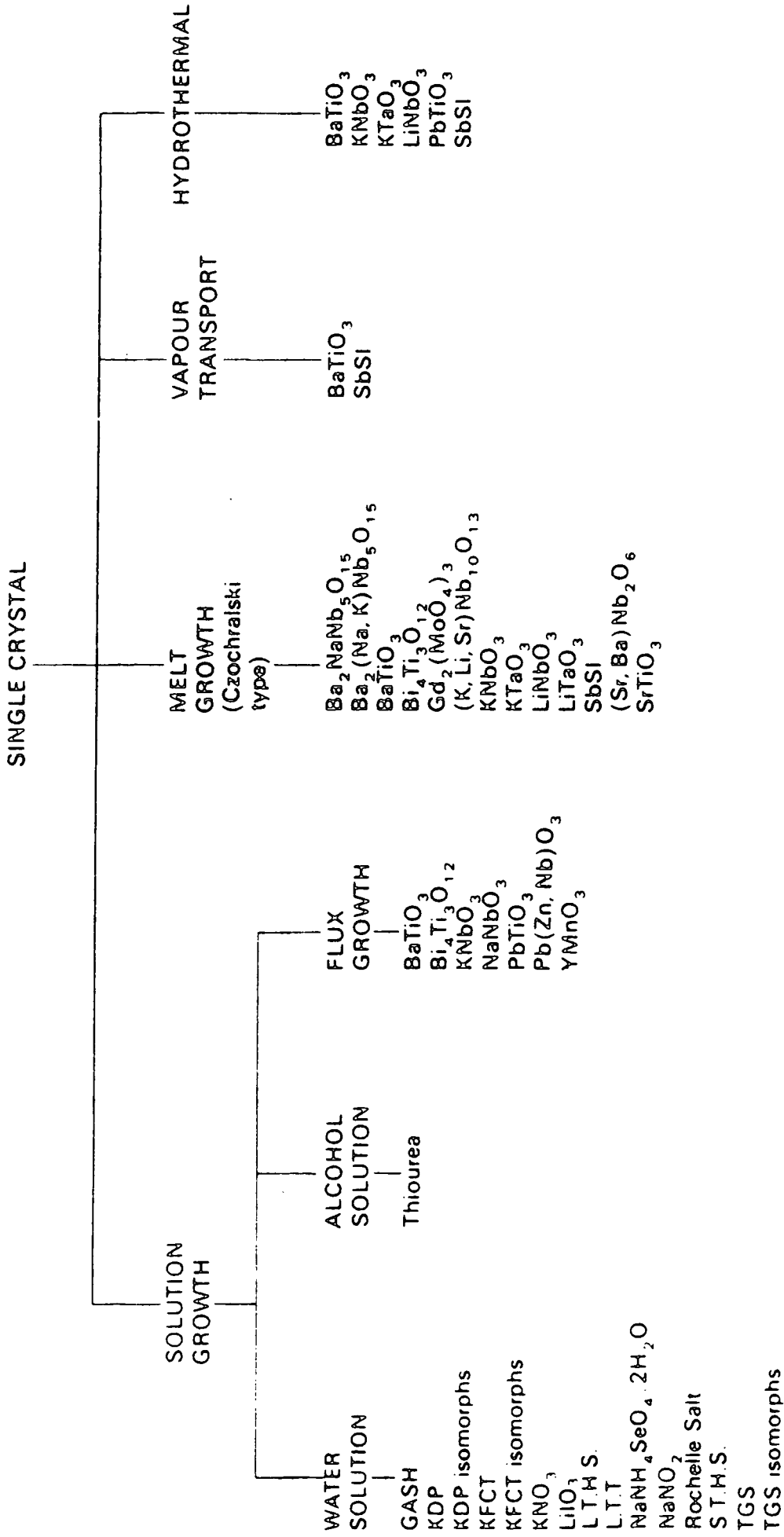


Figure 2.7 Single crystal polar materials that have been grown by various techniques.

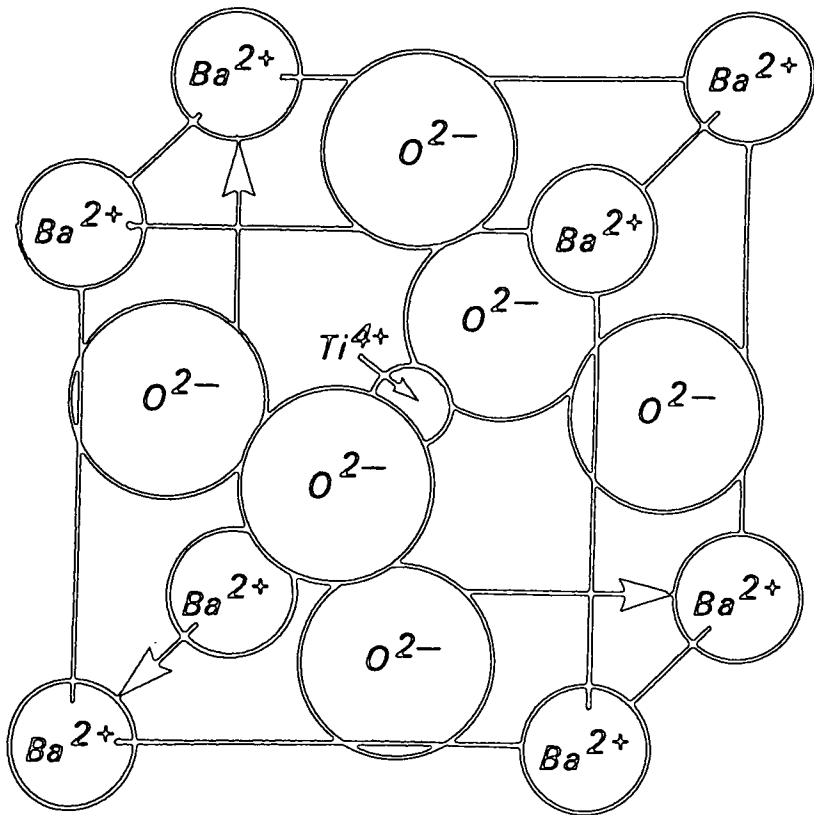


Figure 2.8 Cubic unit cell of barium titanate.

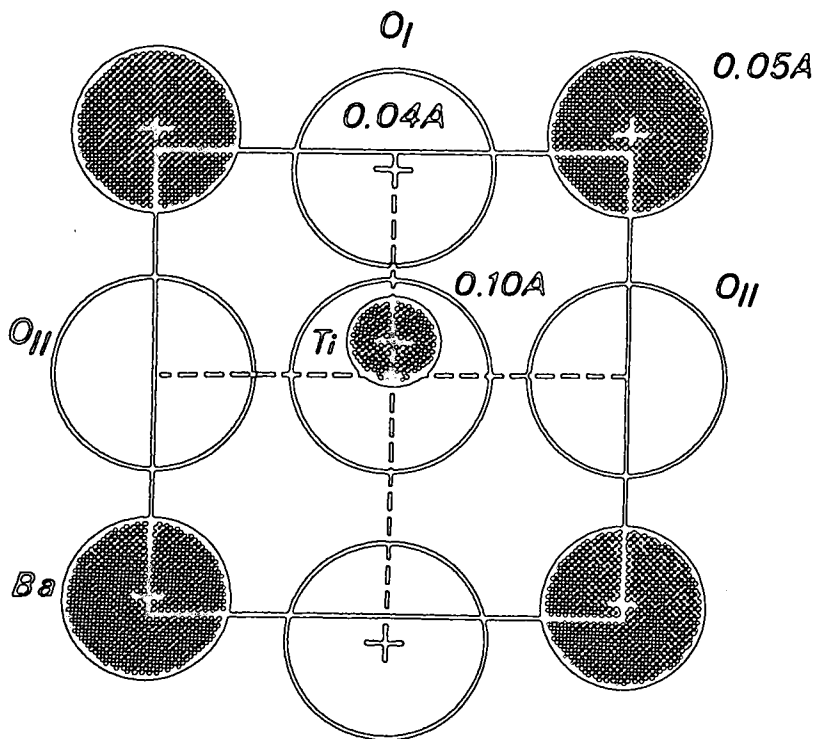


Figure 2.9 Projection onto the (100) plane of the tetragonal unit cell of barium titanate.

TYPE OF STRUCTURE	EXAMPLES	FEATURES	REFERENCES
Perovskite	$\text{BaTiO}_3$ , $\text{KNbO}_3$	Derived from cubic prototype, based on oxygen octahedra.	[33-37]
Lithium niobate type	$\text{LiNbO}_3$ , $\text{LiTaO}_3$	Based on oxygen octahedra, but with two formula units per unit cell.	[38]
Tungsten-bronze type	$\text{Ba}_2\text{Sr}_{1-x}\text{Nb}_{10}\text{O}_{30}$ (SBN)	$\text{ABO}_3$ type structure based on ten linked $\text{BO}_6$ octahedra. Partially disordered structure due to the large number of available A and B sites.	[39]
KDP-type	$\text{KH}_2\text{PO}_4$ (KDP)	Based on two interpenetrating body centred cubic (bcc) lattices of $\text{PO}_4$ tetrahedra and two interpenetrating bcc K lattices. Extensive hydrogen bonding plays important role in ferroelectric switching.	[40]
Sodium nitrite	$\text{NaNO}_2$	Body centred orthorhombic structure.	[41]
V-VI-VII compounds	SbSI	Semiconducting. Structure consists of chains of atoms.	[42]

Table 2.3 Summary of inorganic pyroelectric materials.

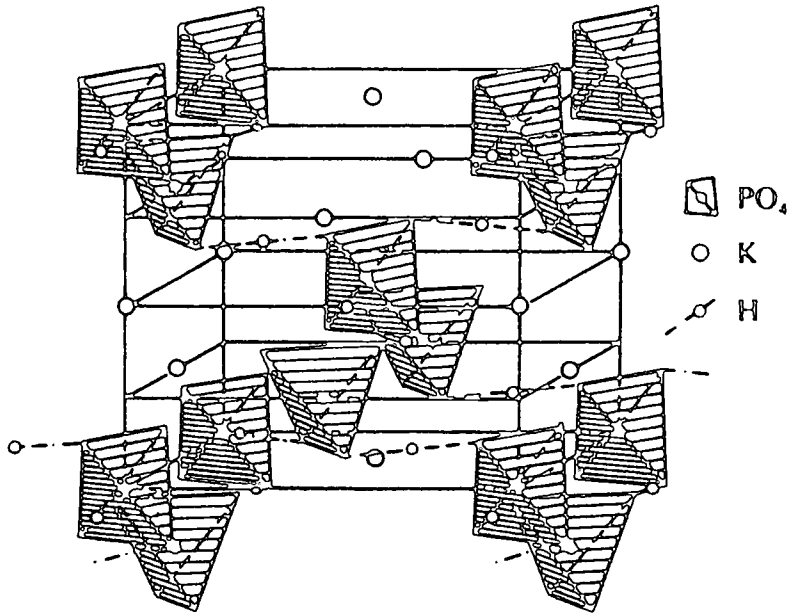


Figure 2.10 The structure of potassium dihydrogen phosphate (KDP).

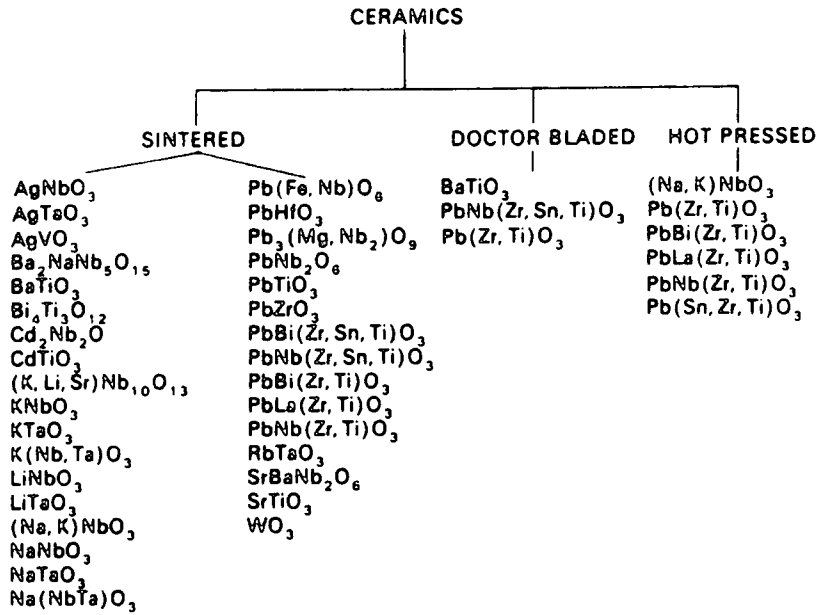


Figure 2.11 Ceramic polar materials that have been fabricated by various techniques.

which occur during ferroelectric switching; these have been reviewed by Lines and Glass [43]. Early treatments relied on a model in which polarisation reversal was achieved simply by a movement of protons along the asymmetric hydrogen bonds. More recently, it has been recognised that motion of the K, P and O atoms also occurs; nevertheless, the large increase in Curie temperature (around 80% ) which results from replacing the protons with deuterons indicates that protonic movement plays a crucial role in the ferroelectric transition.

### 2.4.2 Inorganic ceramics

For studies of the fundamental properties of a material, large homogeneous single crystals are usually desirable. However, ceramics have the advantage of being cheaper and easier to prepare than their single crystal counterparts [44]. Figure 2.11 contains a list of pyroelectric ceramics which have been prepared, and indicates that the most common technique for forming pyroelectric ceramics is sintering. In this process, the constituents of the polar material are mixed in the correct proportions with an organic binder and pressed into a structure of the desired shape and dimensions. This structure is then fired at an appropriate temperature, which causes the binder to be burnt out and the pressed materials to react chemically and form the desired polar material.

Each grain within the ceramic has properties similar to a polar single crystal, but the overall structure is isotropic and shows no directional behaviour such as pyroelectricity; an electric field must therefore be applied to a ceramic in order to render it pyroelectric. Pyroelectric coefficients of  $85 \text{ nCcm}^{-2}\text{K}^{-1}$  have been achieved for strontium barium niobate ceramics; however, the dielectric constant is also very high due to interfacial polarisation mechanisms at the numerous grain boundaries. Consequently,  $p/\epsilon_r'$  is usually quite small.

### 2.4.3 Organic crystals

In order to deduce which organic materials can be used to create pyroelectric Langmuir-Blodgett films, it is helpful to first examine the origins of pyroelectricity in conventional bulk organic materials; in this section we discuss two such materials, triglycine sulphate (TGS) and meta-dinitrobenzene (m-DNB). A

more comprehensive review of organic pyroelectric materials has been compiled by Gagulin and Chayanov [45].

#### (a) Triglycine sulphate

Triglycine sulphate,  $(\text{NH}_2\text{CH}_2\text{COOH})_3\cdot\text{H}_2\text{SO}_4$  (abbreviated as TGS), is a water soluble ferroelectric material, which is widely used in pyroelectric detectors. The crystal structure of TGS was elucidated by Hoshino, Okaya and Pepinsky [46] using a combination of X-ray diffraction and neutron scattering data, and was refined by later workers [47,48]. These studies showed that the sulphuric acid group donates both of its protons to two of the glycine units, usually designated glycine I and glycine III, creating glycinium ions; glycine II, on the other hand, exists in a zwitter-ion configuration. Thus, the correct chemical formula for TGS is  $(\text{NH}_3^+\text{CH}_2\text{COOH})_2(\text{NH}_3^+\text{CH}_2\text{COO}^-)\cdot\text{SO}_4^{2-}$ .

The structure of TGS is shown schematically in figure 2.12; most of the hydrogen atoms have been omitted for clarity. The proton designated X forms a hydrogen bond between glycines II and III, and, in the ferroelectric phase, is in a position closer to glycine III than to glycine II. The other region of marked asymmetry is at the glycine I nitrogen location, designated Y. The dipole reversal mechanism in TGS is very interesting: the proton, X, "flips" to a position which is closer to glycine II; this provides a driving force for the movement of the nitrogen atom, Y, as indicated by the arrows, bringing about a reversal of the polar axis. It should be noted, however, that deuteration of TGS does not produce the vast changes in dielectric properties which result from deuteration of KDP. This suggests that the role of hydrogen bonds may be much less dominant in TGS.

#### (b) Meta-dinitrobenzene

m-DNB is one of the simplest of a series of pyroelectric benzene derivatives, and has a pyroelectric coefficient of around  $1.3 \text{ nCcm}^{-2}\text{K}^{-1}$ . Some of the more complex derivatives are described by Asaji and Weiss [49]. The molecular and crystalline structures of m-DNB are shown in figure 2.13; the large dipole moment,  $\mu$ , arises from the distortion of the delocalised  $\pi$ -electron system of the



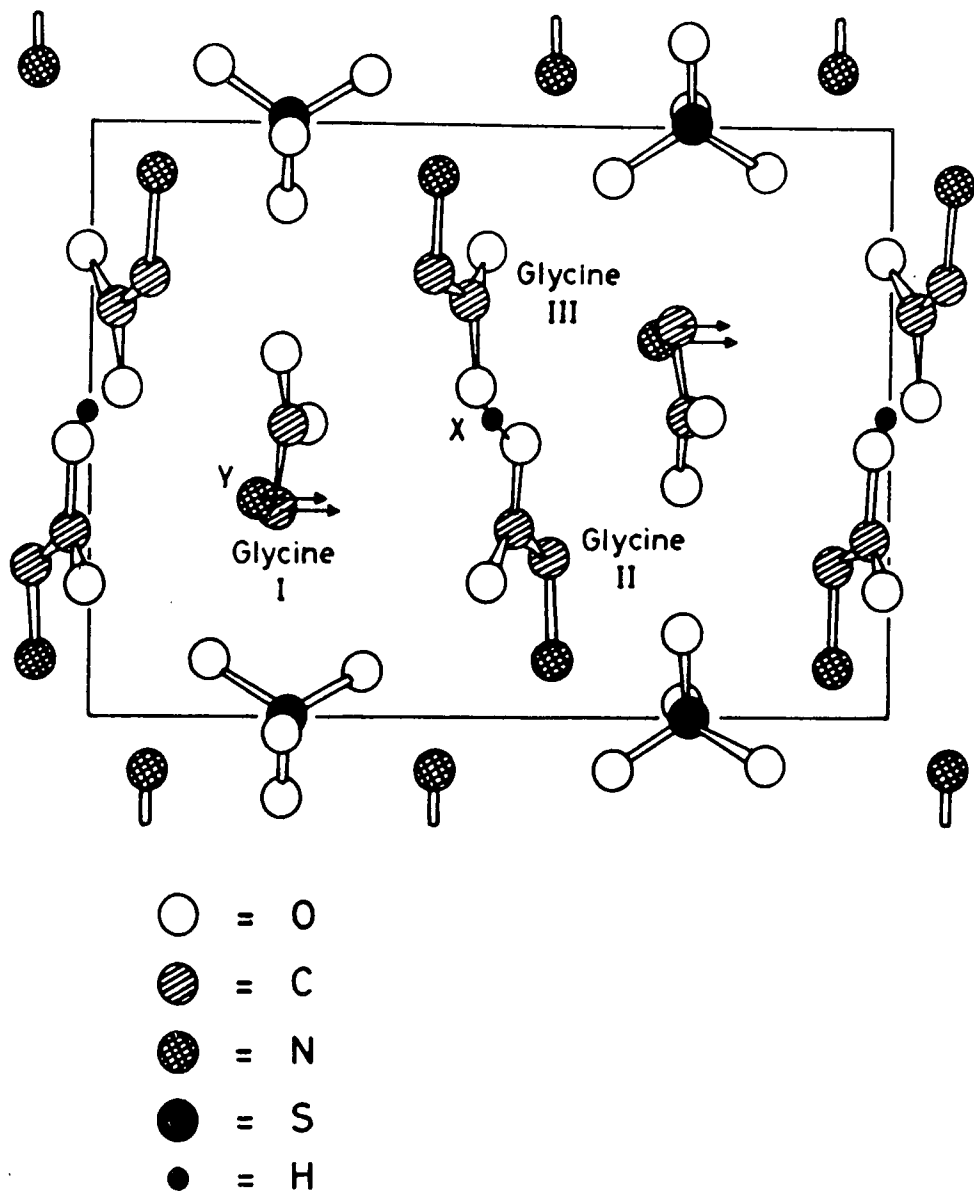


Figure 2.12 The crystal structure of triglycine sulphate (TGS).

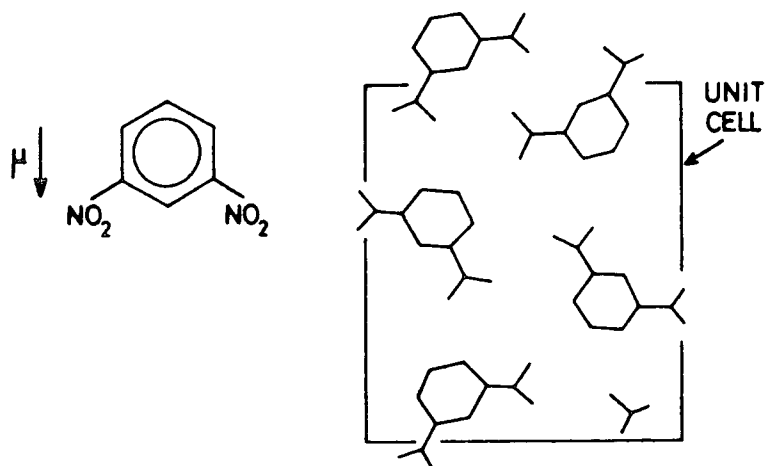


Figure 2.13 Molecular and crystal structures of meta-dinitrobenzene (m-DNB).

benzene ring by the strongly polar NO<sub>2</sub> groups.

As the temperature increases, there are two competing effects within the m-DNB crystal: firstly, anharmonic lattice vibrations give rise to changes of the average orientation of the molecules, and tend to increase the polarisation. On the other hand, there exists an anharmonic internal vibration due to twisting of the NO<sub>2</sub> groups [50], which changes the charge distribution within the molecules and decreases their dipole moment. These opposing effects are thought to be responsible for the complex temperature dependence of the primary pyroelectric coefficient in m-DNB [51]. In the present work, it was attempted to exploit the pyroelectric activity of m-DNB by incorporating this group into Langmuir-Blodgett film-forming molecules.

## 2.5 APPLICATIONS OF PYROELECTRIC MATERIALS

There are numerous applications for piezo-, pyro- and ferroelectric materials [52]: these include ultrasonic transducers [53], bistable switches [54], PTC thermistors [55] and non-linear optical materials [56]. However, in this section we shall be concerned only with those applications which directly exploit the pyroelectric effect. The most important such use is in infrared imaging; however, other possible applications are also reviewed in the following sections.

### 2.5.1 Thermal imaging cameras

Infrared imaging systems are widely used for both military and civilian applications. The present generation of high performance devices relies mainly on semiconductor quantum detectors, in which the incident radiation excites electrons from states near the top of the valence band into states near the bottom of the conduction band, producing electron-hole pairs, and changing the electrical properties of the material. The semiconductor must be chosen to have a band-gap which corresponds to the energy of the longest wavelength of the radiation which is to be detected.

Unfortunately, the atmosphere is largely opaque to infrared radiation, and the only "windows" of high infrared transmission occur in the 3–5  $\mu\text{m}$  and 8–14  $\mu\text{m}$  wavelength ranges. There is no shortage of materials with bandgaps

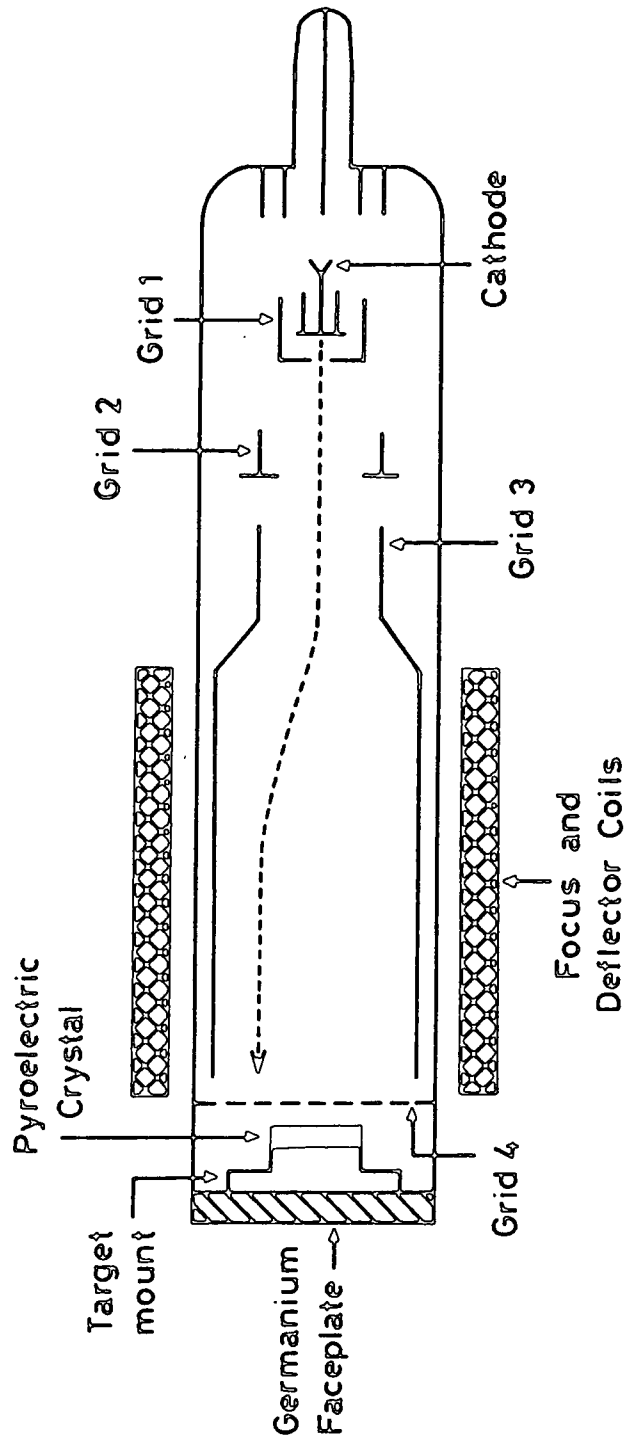


Figure 2.14 Schematic diagram of the pyroelectric vidicon.

sponding to the 3–5  $\mu\text{m}$  range (0.41–0.25 eV); however, no elemental or compound semiconductor is known with a band-gap of only 0.09 eV, corresponding to a wavelength of 14  $\mu\text{m}$ . The semiconductor alloy  $\text{Hg}_{1-x}\text{Cd}_x\text{Te}$  (cadmium mercury telluride or CMT) was therefore developed as a narrow band-gap semiconductor, capable of detecting 8–14  $\mu\text{m}$  radiation [57].

However, detectors based on CMT suffer from the inherent disadvantage of requiring cooling, in order to reduce the Johnson noise associated with the thermal generation of large numbers of carriers in a narrow bandgap semiconductor. CMT detectors are therefore both cumbersome and expensive; moreover, the sensitivity of these detectors is not constant over the required wavelength range. Thermal detectors based on the pyroelectric effect, on the other hand, do not require cooling and have a sensitivity versus frequency response which is flat over a broad wavelength range. Considerable progress has been made in producing CMT which can be used at temperatures close to ambient. However, such material is insensitive to long wavelength radiation. There has therefore been considerable interest in recent years in producing pyroelectric thermal imaging devices [58–62].

A simple pyroelectric detector consists of a slice of pyroelectric material with metal electrodes on opposite faces, the material being oriented such that its polar axis is perpendicular to the electroded faces. The performance of the detector is affected by a number of factors including the pyroelectric material used, the dimensions of the detector chip, the method of mounting and encapsulating the chip and the type of amplifier used. These factors have been considered by several authors [58–61]. The performance of a detector is usually characterised either by its responsivity,  $R_v$ , (the voltage output per unit incident radiation power), or by its specific detectivity,  $D^*$ , which takes into account the various noise sources in the detector.

The most well-established type of thermal-imaging camera is the pyroelectric vidicon [61,63], which is illustrated schematically in figure 2.14. This consists, essentially, of a vidicon tube with a pyroelectric target and germanium faceplate. The target is a disc of pyroelectric material (usually TGS) with a transparent front electrode. An infrared lens produces a thermal image on this

target, and the resulting charge distribution is read off the back surface by a raster-scanning electron beam.

Since, with a steady flux of incident radiation, the target will rapidly reach thermal equilibrium, it is necessary to modulate the flux; for this reason, a mechanical chopper is incorporated into the device. The major factor limiting spatial resolution is thermal diffusion within the target. Pyroelectric targets are therefore reticulated [63]: that is, grooves are etched using ion beam milling or laser ablation, creating a matrix of thermally isolated islands.

The pyroelectric vidicon is gradually being superseded by flat-panel infrared image sensors, using self-scanned arrays of detectors. Such a device has been described by Schlosser and Glower [64], who fabricated an array of elements by depositing rows and columns of electrodes onto a substrate of pyroelectric ceramic; intersections of the row and column electrodes define the location of individual pyroelectric elements. The scanning electron beam is replaced by a set of FET analogue switches, one for each row and column, which are actuated in sequence by digital signals generated in the vertical and horizontal scan circuits. A complete frame of video information is obtained by sampling the voltage on each of the array elements in turn. The device is illustrated schematically in figures 2.15a and b.

### 2.5.2 Other applications

In addition to their use in thermal-imaging cameras, pyroelectrics have several other applications as detectors of electromagnetic radiation. The pyroelectric detector is particularly well suited to such applications in view of its flat spectral sensitivity. Pyroelectric materials have been used to calibrate the power generated by ultraviolet, visible and infrared radiation sources [65]. The detector is biased by an a.c. electrical signal out of phase with the input radiation. The applied voltage is adjusted to give a nil pyroelectric output, and the optical power is then equal to the electrical power supplied. A similar application is the pyrometer [66], which is used to measure the temperature of remote bodies; once the radiation power has been calculated, the temperature can be deduced from Stefan's law. The pyroelectric detector can also be used as a very

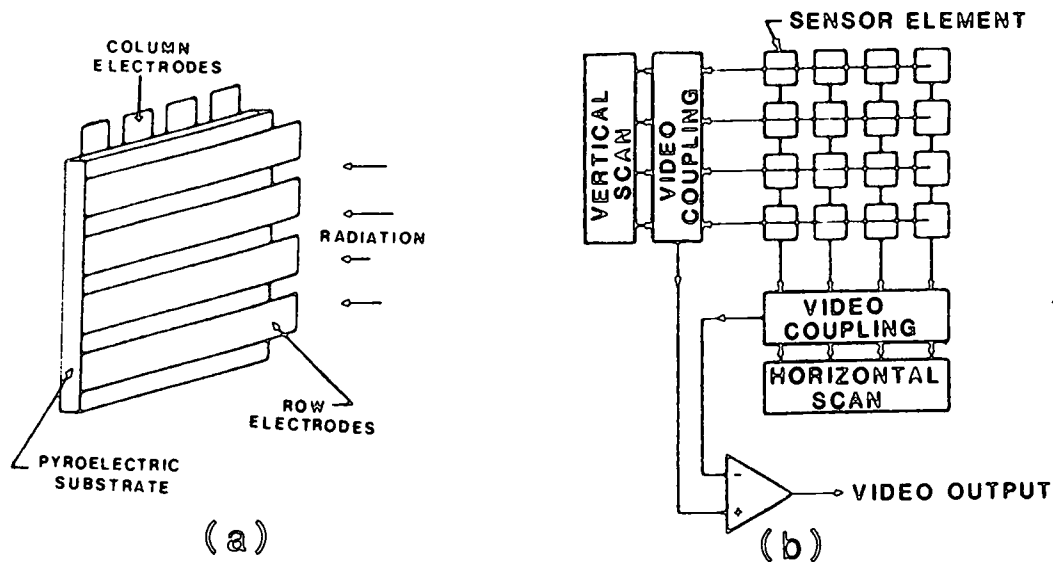


Figure 2.15 Schematic diagram of a self-scanned pyroelectric thermal imaging device.

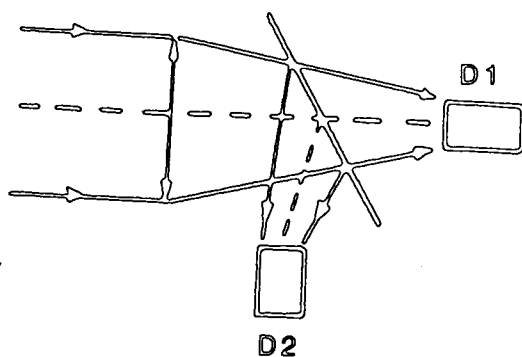


Figure 2.16 Schematic diagram of a pyroelectric solar energy converter.

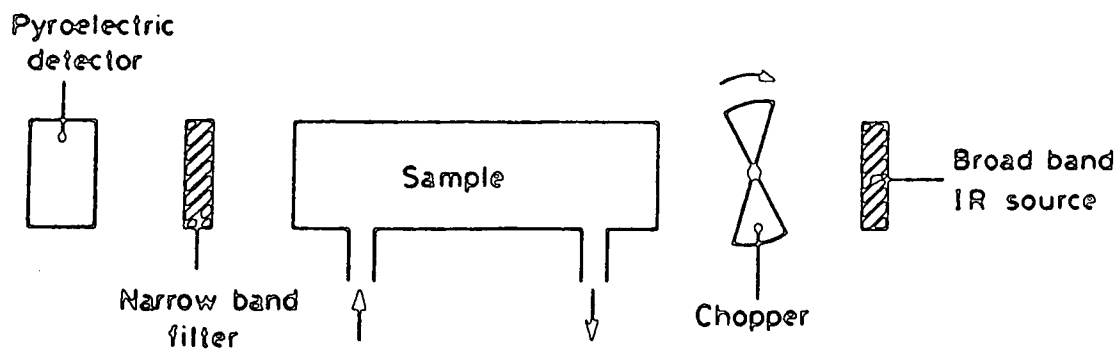


Figure 2.17 Schematic diagram of a gas pollutant monitor, using a pyroelectric detector.

sensitive thermometer [67], which is able to detect temperature changes as small as  $6 \times 10^{-6}^\circ \text{C}$ .

By detecting the infrared radiation emitted by the human body, pyroelectric detectors can be used in intruder detection systems [68]. Pyroelectric materials respond readily to a varying infrared signal but not to a steady radiation level, and movement of the intruder provides the required modulation of the infrared signal.

The pyroelectric detector can be considered as a high impedance thermo-electric converter, and as such can be used for solar energy conversion [69]. A typical converter is illustrated in figure 2.16. The incident radiation is mechanically chopped, and when light is stopped from reaching detector 1, it is reflected to detector 2, so that the full power of the light is used. To date, the best results have been obtained with TGS, for which the efficiency is approximately 1% .

Broadband infrared sources and pyroelectric detectors can be used to monitor pollutants in gaseous samples [68]; a typical monitor is shown in figure 2.17. The wavelengths of the incident radiation absorbed by the sample will depend upon the molecular species present. The insertion of various narrow band optical filters into the beam enables the spectral regions corresponding to standard gas absorptions to be monitored. By inserting different filters, many pollutants can be monitored in rapid succession. The inclusion of a mechanical chopper allows a.c. amplifiers and phase sensitive detection techniques to be employed.

## 2.6 SUMMARY

We have shown that for a material to be pyroelectric it must possess a non-centrosymmetric crystal structure with a unique polar axis. The primary pyroelectric effect is that which would be observed under conditions of constant strain (ie. if the sample were mechanically clamped). If the sample is allowed to deform, then this primary effect is augmented by a piezoelectrically induced secondary effect. It has also been shown that there are mechanisms which can give rise to spurious tertiary effects.

Some actual organic and inorganic single crystal and ceramic pyroelectric materials have been described, and some of the applications of pyroelectric de-

vices have been discussed. In the next chapter, we discuss the limitations of bulk materials and show that, for many applications, it is advantageous to use thin film pyroelectrics.



## CHAPTER 3

### THIN FILM PYROELECTRIC STRUCTURES

#### 3.0 INTRODUCTION

Chapter 2 introduced the concepts of pyroelectricity and described the basic properties and applications of pyroelectric materials; in this chapter we discuss the advantages of using thin films of such materials. Section 3.1 describes some of the more conventional types of thin film, including inorganic layers, organic polymers and liquid crystals. This is followed in section 3.2 by a brief introduction to Langmuir-Blodgett (LB) films, with emphasis on how polar structures can be produced using the LB technique.

Section 3.3 discusses the constraints placed on an LB film by deposition onto a thick substrate, and derives mathematical expressions to describe two such effects, namely mechanical and thermal clamping. Finally, it is shown in section 3.4 that thermal clamping can be reduced by using a thin substrate.

#### 3.1 CONVENTIONAL THIN FILM PYROELECTRICS

There has recently been much interest in producing thin films of polar materials [1]. For device applications, thin films have several important advantages over bulk materials; these include the ability to produce large area devices, and the possibility of forming the film directly on the semiconductor amplifying circuits. In the case of unsupported films, however, the prime reason for using the material in thin film form is to achieve higher sensitivity, as the voltage responsivity is approximately inversely proportional to the thickness of the active element [2]. It will be shown later, though, that the situation is more complicated for films which are supported on substrates [3], and that the thickness of this substrate can often dominate the response of the pyroelectric film.

##### 3.1.1 Inorganic thin films

Figure 3.1 lists some polar inorganic materials which have been produced in thin film form by various techniques. With the exception of r.f. sputtering,

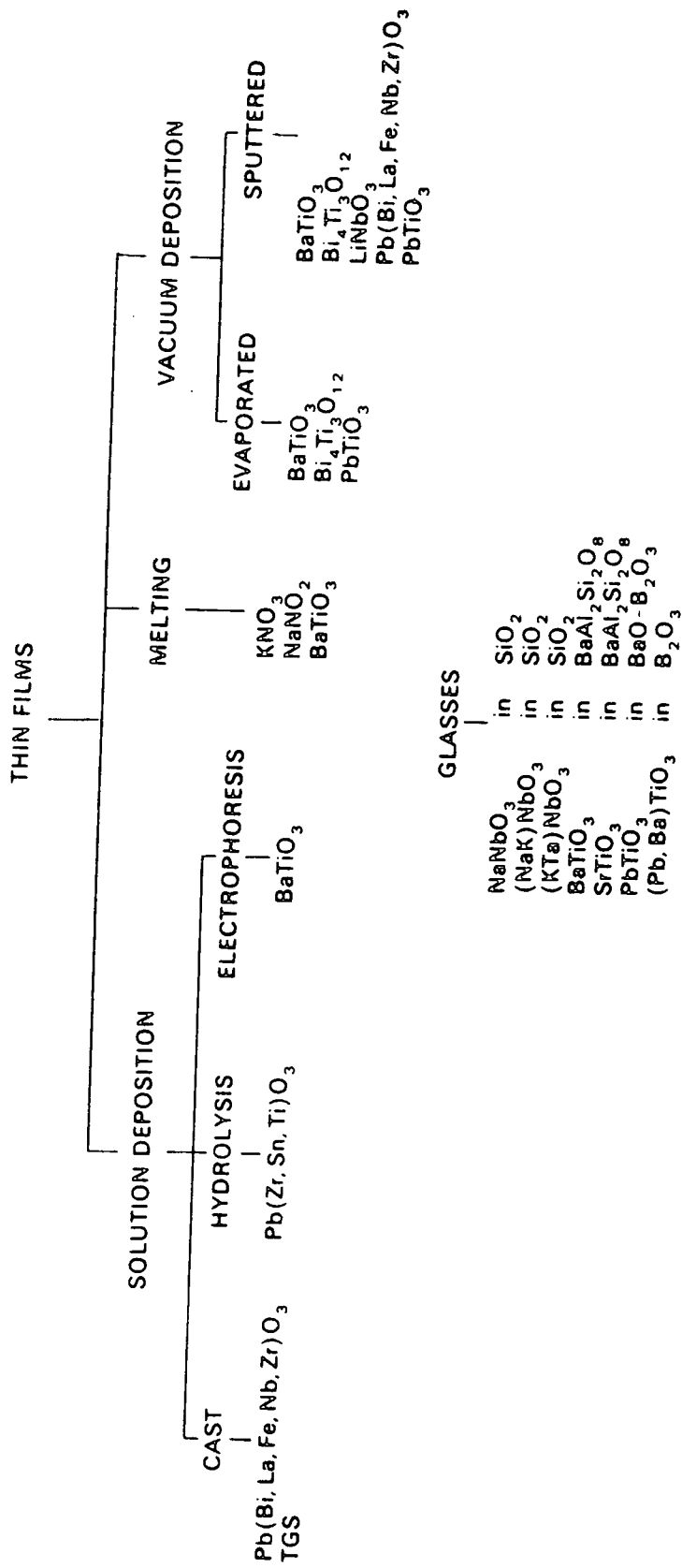


Figure 3.1 Thin film polar materials that have been formed by various techniques.

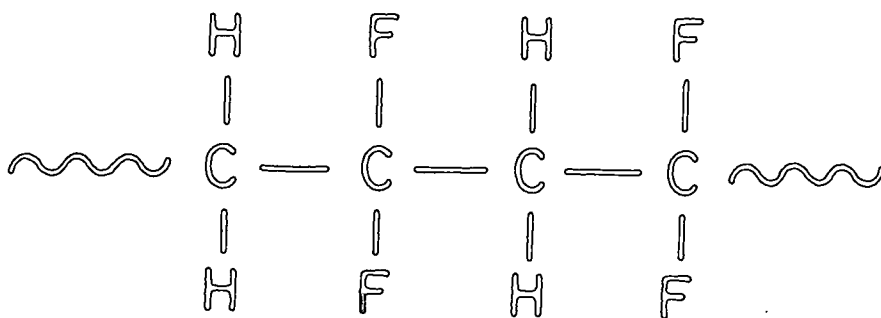
these techniques all produce polycrystalline films which have properties similar to ceramics and, like ceramics, must be poled in order to build in a unique polar axis. R.f. sputtering is probably the most satisfactory method for producing thin films of polar inorganic materials, as it offers good control over stoichiometry and thickness, and, in some cases, produces crystalline epitaxial layers [4]. In general, a ceramic target of the correct composition is used in a suitable atmosphere (usually oxygen and argon). The substrate, which is heated to around 600°C, is generally a single crystal whose crystal lattice and orientation are chosen such that the sputtered film is aligned along a desired preferred direction, thus obviating the need to pole the film.

Despite the development of such techniques for producing inorganic thin films, researchers are now investigating the use of organic materials as pyroelectric detectors. Organic materials generally lend themselves to thin film deposition; and the wealth of compounds available, coupled with the skill of organic chemists, means that the molecular structure can be precisely tailored to give the desired physical properties.

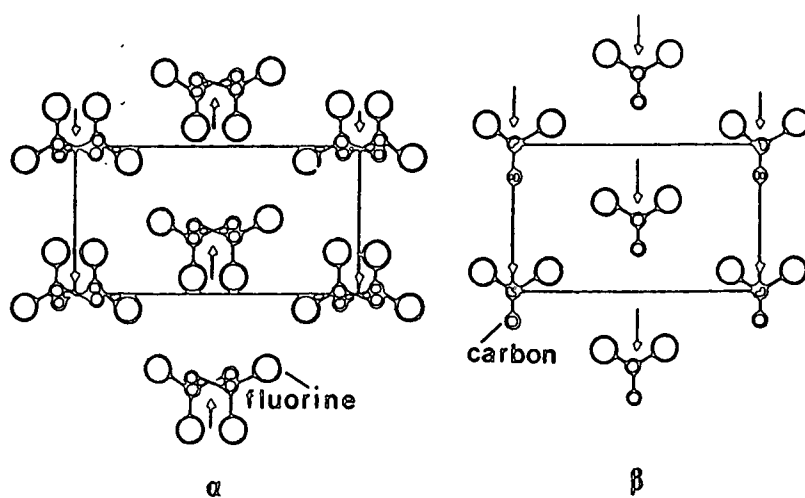
### 3.1.2 Pyroelectric polymers

Piezo- and pyroelectricity in synthetic polymers were first reported by Kawai in 1969 [5]. Pyroelectric polymers possess the specific advantages of flexibility, ease of fabrication and low density. Of the pyroelectric polymers, polyvinylidene fluoride (PVDF) (figure 3.2a) has attracted particular attention because of the large piezo- and pyroelectric coefficients which can be induced in this material, and the literature abounds with references to potential transducer applications of PVDF [6].

The production of PVDF has been described by Pantelis [7]. The film is initially crystallised from the melt, and adopts the so-called  $\alpha$  form, which is not polar. Conversion to the polar  $\beta$  form is effected by stretching the film between rollers to align the polymer backbones, followed by poling to align the fluorine atoms (figure 3.2b). Poling may be carried out either by applying an electric field at an elevated temperature (thermal poling) or by employing a corona discharge at ambient temperature (corona poling) [8]. Unfortunately,



(a)



(b)

Figure 3.2 Polyvinylidene fluoride (PVDF): (a) molecular structure, (b) unit cells of the  $\alpha$  and  $\beta$  forms, looking down the carbon backbone (hydrogen atoms omitted).

the minimum thickness to which pyroelectric PVDF can be prepared is limited by the breakdown strength of the polymer and by the fact that the pyroelectric coefficient diminishes for very thin films.

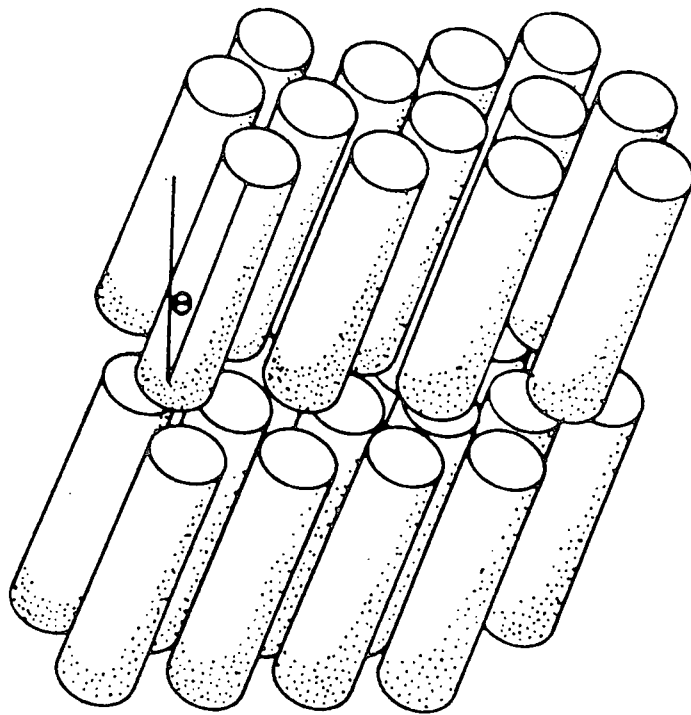
PVDF has found wide application as a piezoelectric material, and has been used in piezoelectric keyboards, microphones, underwater hydrophones and as an ultrasonic transducer for medical imaging applications. PVDF has also been used as a pyroelectric vidicon target material, in which its low thermal conductivity reduces thermal spreading; however, the responsivity is only 70% that of a TGS target. There have recently been several reports of pyroelectric activity in various copolymers of VDF and other materials [9–12], and there is a continual search for new polymers with enhanced pyroelectric properties.

### 3.1.3 Liquid crystals

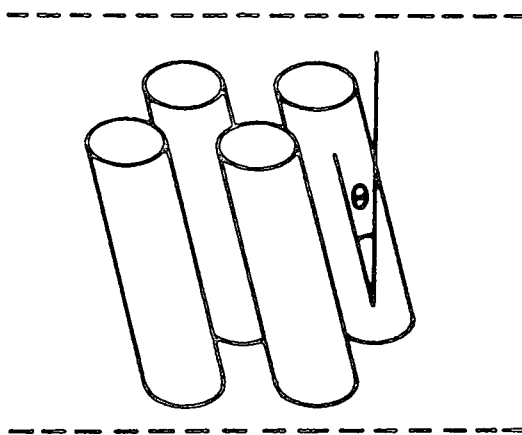
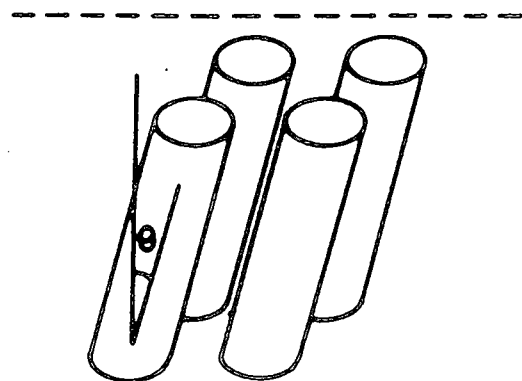
In 1975, it was proposed by Meyer *et al* [13] that certain liquid crystalline phases are pyroelectric and, indeed, ferroelectric. There has recently been a great deal of interest in the ferroelectric chiral smectic C\* (SmC\*) phase [14,15]; the principal advantage of these materials being their low dielectric constant [16,17].

Liquid crystal phases are adopted by elongated rod-like molecules which pack into well-defined but fluid structures. In the achiral smectic C (SmC) phase (figure 3.3a), the molecules are randomly packed in layers, and in a particular domain the molecules are tilted in a single direction with respect to the layer planes; the tilt angle,  $\theta$ , varies with temperature. If the constituent molecules are chiral, then the structure is denoted SmC\*: in this case, the tilt direction precesses around the layer normal on passing from one layer to the next, creating a macromolecular helical structure (figure 3.3b). An individual layer is therefore polar, while the bulk phase is not, since the net polarisation is averaged to zero. In order to observe polar behaviour, the helix must be “unwound” by application of an electric field [18], or by making the device thinner than the wavelength of the helix [15].

Despite their advantages, ferroelectric liquid crystals are unlikely to form the basis for efficient pyroelectric detectors, because of the necessity for encapsu-



(a)



(b)

Figure 3.3 Smectic liquid crystal phases: (a) smectic C (SmC), (b) chiral smectic C (SmC\*).

lation in a glass cell, which acts as a heat sink and greatly increases the thermal mass of the device.

### 3.2 LANGMUIR-BLODGETT FILMS

Langmuir-Blodgett (LB) films are ultra-thin, highly ordered organic layers and are formed from molecules which possess both hydrophilic and hydrophobic groups. They are produced by dissolving a small amount of a suitable amphiphilic material in an organic solvent, spreading the solution on a clean water surface, allowing the solvent to evaporate, and compressing the resultant monolayer to produce a close-packed structure which is a two-dimensional analogue of a solid phase. If a suitable substrate is passed through the water surface, then, in general, a single monolayer of the amphiphilic material is transferred to the substrate with each traversal through the interface. The LB film can therefore be built up to the desired thickness by repeatedly depositing monolayers.

There are many advantages which make LB films particularly attractive candidates for pyroelectric devices. The most important of these is that the sequential deposition of single monolayers enables the symmetry of the film to be precisely defined; in particular, layers of different materials can be built up to produce a highly polar structure. Secondly, the polarisation of an LB film is "frozen in" during deposition, and it is therefore not necessary to subject the film to the poling process which must be used for pyroelectric polymers. This also implies that ferroelectric behaviour would not be expected in LB films, as the polarisation cannot be reversed without breaking down the entire structure. The third advantage of the LB technique is that it enables very much thinner films to be prepared than any of the methods thus far described. Finally, LB films are produced at ambient temperatures, and can be deposited onto a wide variety of substrates. A pyroelectric LB film could therefore be deposited directly onto a silicon chip which incorporates the circuitry for amplifying the pyroelectric signal.

### 3.2.1 LB films of a single material

One of the pioneers of the LB technique, Katharine Blodgett, postulated three possible modes of LB film deposition and named them X, Y and Z type [19], as illustrated in figure 3.4. The majority of materials deposit in the Y type mode (figure 3.4a), where material is transferred on both up- and down-strokes of the substrate, resulting in a structure in which the molecules are packed in a head-to-head and tail-to-tail sequence. It should be noted that, if a hydrophilic substrate is used, Y type pick-up does not commence until the first up-stroke. Y type structures comprising an even number of monolayers are, of course, centrosymmetric and hence cannot be pyroelectric.

X type deposition (figure 3.4b) is the situation where material is transferred to the substrate only on the downstroke, and is common for fatty acid esters such as ethyl stearate [20] and vinyl stearate [21]. X type deposition also occurs when fatty acid salts are dipped at very high pH levels; however, X-ray diffraction has revealed that the molecules undergo rearrangement during, or subsequent to, deposition, reverting to the energetically more favourable Y type structure [22]. Finally, Z type deposition (figure 3.4c) refers to transfer only on the upstroke, and had not been observed when described by Blodgett. Since then, Z type dipping has been reported in the phthalocyanines [23]. It is obvious from figure 3.4 that both X and Z type deposition produce non-centrosymmetric polar structures, which should exhibit pyroelectricity.

Christie *et al* [24] have described the fabrication of polar LB films of polybutadiene. Multilayers of this material deposit in an X type conformation, providing the film is irradiated with ultra-violet light after deposition of each monolayer, to initiate cross-linking of the polymer chains. Although surface potential measurements confirmed that the films possessed a large polarisation, no pyroelectric signal was detected. The authors attribute this to the rigidity of the cross-linked structure causing mechanical clamping [25].

Blinov has reported pyroelectric activity in mono- and multilayer LB films of a series of amphiphilic azoxy compounds [26–29]. Blinov reports that these materials can be deposited in X, Y or Z type modes depending on the conditions used, and that both X and Z type deposition lead to the formation of pyroelectric



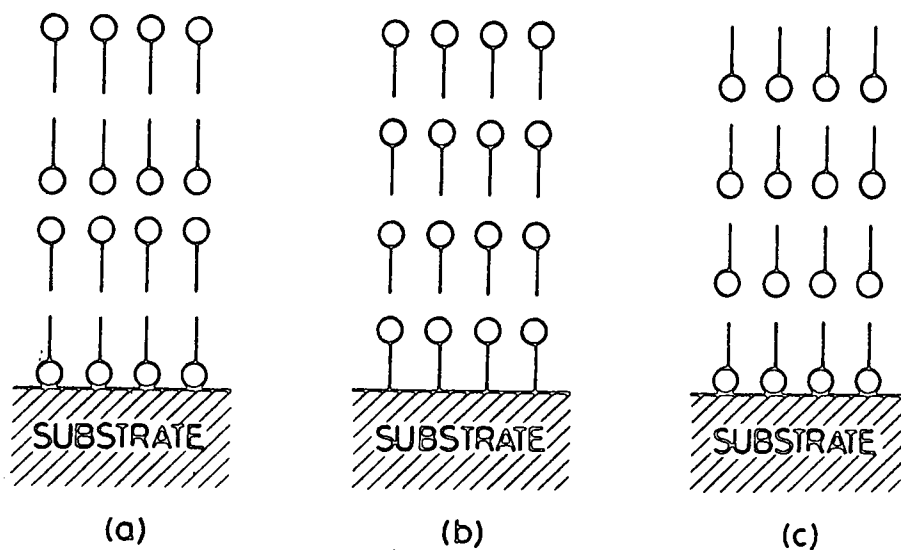


Figure 3.4 Modes of LB film deposition: (a) Y type, (b) X type, (c) Z type.

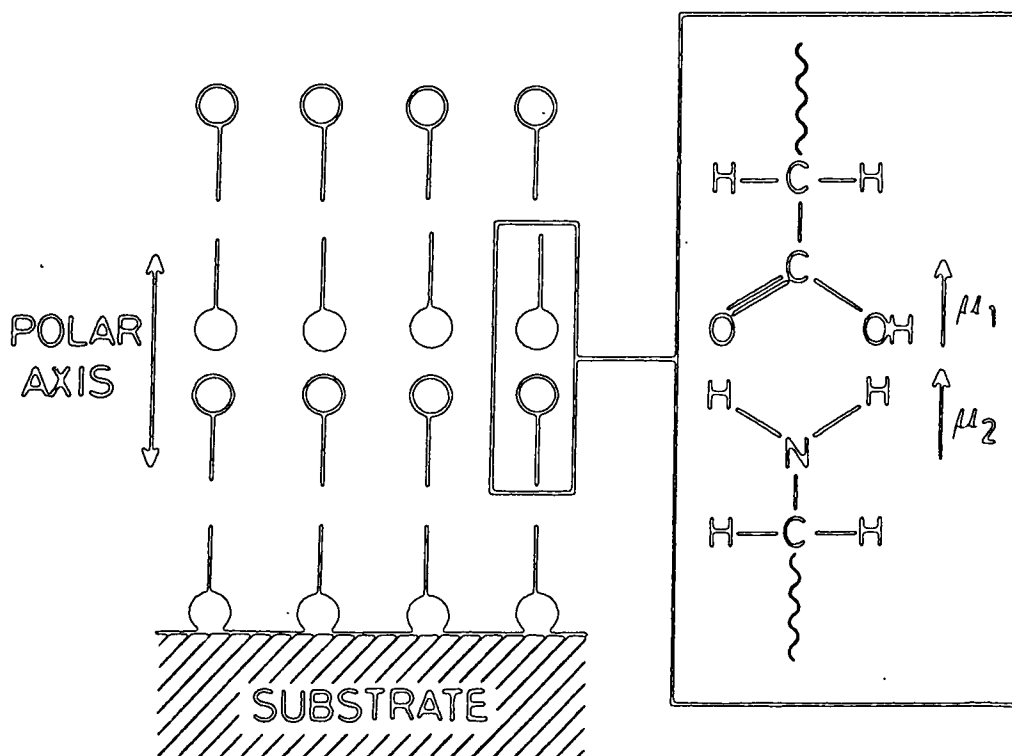


Figure 3.5 Alternate layer deposition of a fatty acid and a fatty amine, to produce a polar structure.

structures, whilst Y type layers are not pyroelectric. It should be noted, however, that this behaviour is most unusual: LB materials usually deposit in a single mode (X, Y or Z) and, although they can sometimes be constrained to deposit in a different mode, rearrangement usually occurs, and the structure reverts to its preferred form [21, 22].

Blinov has reported pyroelectric coefficients as high as  $0.3 \text{ nCcm}^{-2}\text{K}^{-1}$ , and attributes the effect to a predominantly primary mechanism on the basis of the observed temperature dependence of the electrical polarisation. Piezoelectricity and the linear Stark effect were also reported in these films.

### 3.2.2 Alternate layer structures

In recent years, several LB troughs have been constructed which can be used to deposit alternate layers of two different materials [30–32]. If the two materials possess polar head groups whose dipole moments are in opposite senses with respect to the hydrocarbon chain, then, although the molecules deposit in a head-to-head and tail-to-tail fashion, the dipoles will not cancel, but will reinforce one another and the structure will be highly polar. An example is shown in figure 3.5; in this case the two materials are a fatty acid and a fatty amine. The acid/amine system might also have an additional contribution to the polarisation due to the transfer of protons from the acid to the amine and the resultant formation of amino and carboxylate ions [33]. Rather than using two highly polar materials in alternate layers, it is possible to use one material with a large polarisation and a second material which acts as a spacer layer to prevent cancellation of the dipoles in the active layer.

Pyroelectricity in alternate layer LB films has been described by two previous authors [34, 35], both of whom used fatty acid/fatty amine alternate layers. Smith *et al* [34] achieved pyroelectric coefficients of around  $0.05 \text{ nCcm}^{-2}\text{K}^{-1}$  using stearylamine with a series of straight chain fatty acids; slightly higher coefficients were obtained by replacing the fatty acid with a polar amphiphilic dye. These authors concluded that the pyroelectric effect was predominantly secondary, because of the small pyroelectric coefficient which resulted from a relatively large polarisation.

Smith *et al* observed these effects in very thick LB films (several hundred monolayers); however, Christie *et al* [35] have reported a pyroelectric coefficient of  $0.3 \text{ nCcm}^{-2}\text{K}^{-1}$  for 11 layer samples of 1-docosylamine and 22-tricosenoic acid, increasing to  $1 \text{ nCcm}^{-2}\text{K}^{-1}$  for 99 layer films of the same two materials. One of the aims of the present work was to further investigate the 1-docosylamine/22- tricosenoic acid system, and to gain an insight into the nature of the polarisation, with a view to selecting new materials for LB film deposition, with enhanced pyroelectric activity.

### 3.3 EFFECT OF A THICK SUBSTRATE

One method for producing pyroelectric devices is to deposit an LB film onto an electrically conducting substrate; to thermally evaporate top electrodes; and finally to coat the resulting devices with a layer of infrared absorbing material, such as bismuth black [36]. The substrate is usually an aluminised glass microscope slide of thickness  $\sim 1 \text{ mm}$ , whilst the blacking layer has a thickness of  $\sim 1 \mu\text{m}$ , and the electrodes are  $\sim 40 \text{ nm}$  thick. The LB film, whose thickness is of the order of  $100 \text{ nm}$ , is therefore extremely thin compared with the substrate on which it is deposited and the blacking layer with which it is coated.

The thick substrate imposes two restraints on the pyroelectric response of the LB film: firstly, secondary pyroelectricity is limited by the thermal expansion of the substrate (mechanical clamping); and, secondly, the substrate acts as a heat sink, reducing the excess temperature of the LB film over ambient (thermal clamping). The following sections propose models to account for these two effects.

#### 3.3.1 Mechanical clamping

In section 2.3, we developed a general thermodynamic model which demonstrated that the total pyroelectric coefficient in a free crystal is given by the sum of the pyroelectric coefficient for the fully clamped crystal and a secondary term which depends on the piezoelectric coefficient of the crystal. This model will now be applied to the case of an LB film, which is mechanically clamped in the plane of the substrate, but is free to expand and contract in the direction

perpendicular to the substrate (partial clamping) [37].

In section 2.3, we derived the following pair of equations:

$$dP_n = d_{n_j}^T d\sigma_j + p_n^\sigma dT \quad (3.1a)$$

$$d\epsilon_i = s_{i_j}^{E,T} d\sigma_j + \alpha_i^E dT, \quad (3.1b)$$

where all symbols have the same meaning as in chapter 2. The model used for the case of an LB film on a substrate is shown in figure 3.6; a coordinate system is defined, in which the substrate is in the plane of the 1 and 2 axes, and the polar axis is assumed to be perpendicular to the substrate. It will be shown later, however, that this model is not always accurate, since some films adopt a structure in which the polar axis is inclined at a small angle to the substrate normal. Assuming the polar axis is perpendicular to the substrate plane, then

$$dP_1 = dP_2 = 0.$$

We shall also make the assumption that the polar axis has 3-fold or greater symmetry, so that there is isotropy in the plane of the substrate. Therefore,

$$\alpha_1 = \alpha_2 \text{ and } \alpha_4 = \alpha_5 = \alpha_6 = 0$$

$$s_{11} = s_{22} \text{ and } s_{12} = s_{21}$$

$$d_{31} = d_{32}.$$

Furthermore, it will be assumed that the temperature of the substrate changes, such that there are non-zero stresses and strains in the substrate plane:

$$d\sigma_1 = d\sigma_2, \quad d\sigma_3 = 0 \text{ and } d\epsilon_1 = d\epsilon_2.$$

Since the film is much thinner than the substrate, the strains  $d\epsilon_1$  and  $d\epsilon_2$  are determined by the thermal expansion coefficient of the substrate,  $\alpha_{1s}$ :

$$\alpha_{1s} = \frac{d\epsilon_1}{dT} = \frac{d\epsilon_2}{dT}.$$

If we expand equations (3.1a) and (3.1b), and use the substitutions stated above, we obtain the following pair of equations:

$$d\epsilon_1 = (s_{11} + s_{12})d\sigma_1 + \alpha_1 dT \quad (3.2a)$$

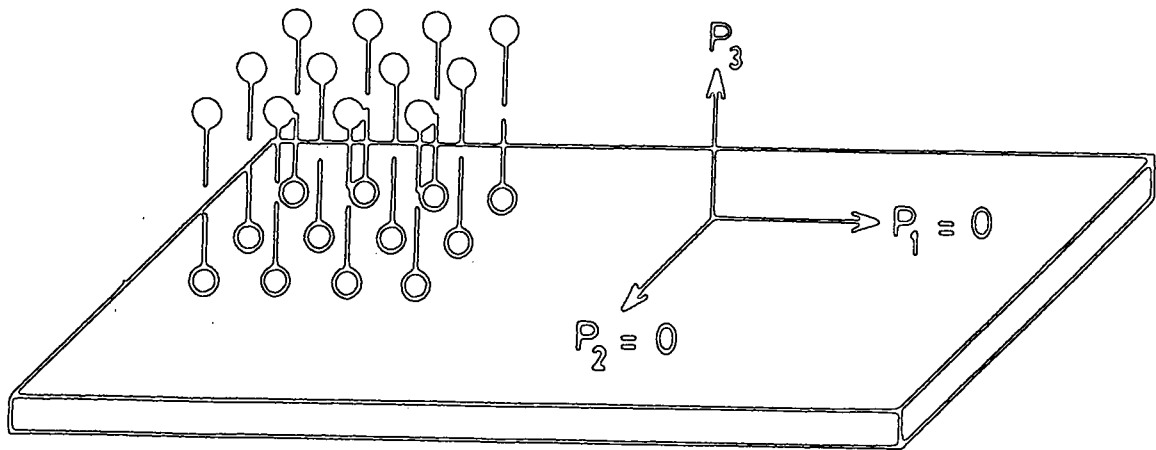


Figure 3.6 Model for partial clamping when an LB film is deposited onto a thick substrate.

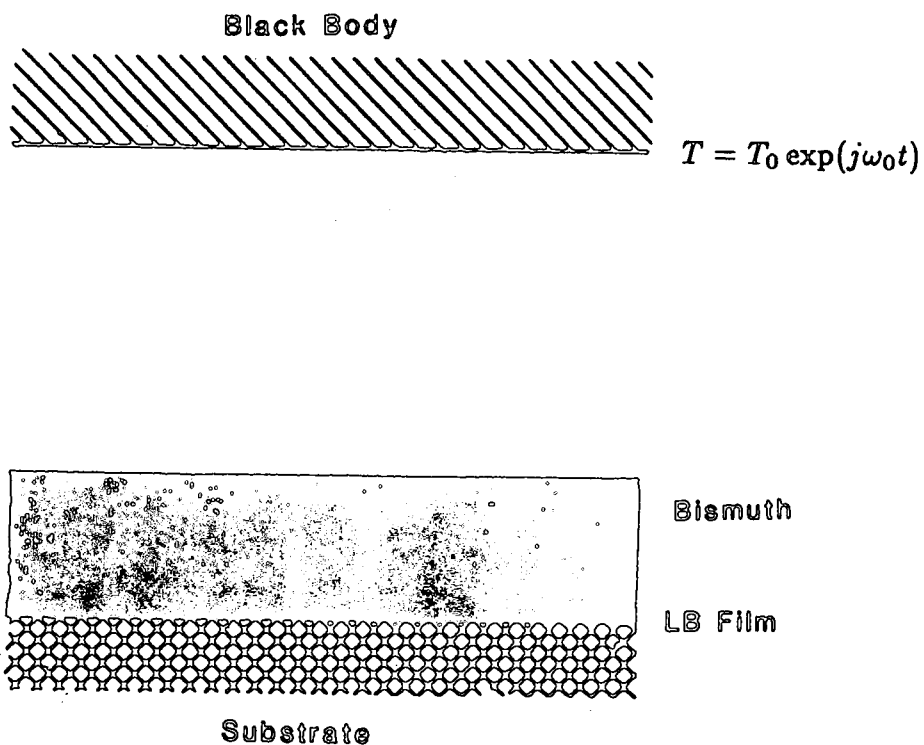


Figure 3.7 Thermal model for an LB film pyroelectric detector.

$$dP_3 = 2d_{31}d\sigma_1 + p_3^\sigma dT, \quad (3.2b)$$

where we have dropped all superscripts except for  $p^\sigma$ .

However,  $d\epsilon_1 = \alpha_{1s}dT$ , therefore (3.2a) gives,

$$\frac{d\sigma_1}{dT} = -\left(\frac{\alpha_1 - \alpha_{1s}}{s_{11} + s_{12}}\right). \quad (3.3)$$

The partially clamped pyroelectric coefficient,  $p_3^{pc}$  is defined as

$$p_3^{pc} = \frac{dP_3}{dT}.$$

Differentiating (3.2b) with respect to temperature,

$$p_3^{pc} = 2d_{31}\frac{d\sigma_1}{dT} + p_3^\sigma. \quad (3.4)$$

Substituting from (3.3) to (3.4), we obtain:

$$p_3^{pc} = p_3^\sigma - \frac{2d_{31}(\alpha_1 - \alpha_{1s})}{s_{11} + s_{12}}. \quad (3.5)$$

Thus, we can see that the effect of the substrate is to reduce the pyroelectric coefficient of the free crystal by an amount given by the second term on the right hand side of equation (3.5). Furthermore, this reduction can be minimised by matching the thermal expansion coefficients of the film and substrate, rendering the film effectively free in all three directions. Equation (3.5) also demonstrates that partial clamping by the substrate does not affect the primary component of the total pyroelectric coefficient. Mechanical clamping would therefore not be a problem in films whose pyroelectric effect was predominantly primary in origin.

### 3.3.2 Thermal clamping

Several theories [38–40] have been proposed to account for the heat sinking effect when a thin pyroelectric element is deposited on a thick substrate. However, these all assume that the pyroelectric film is sufficiently thick for an appreciable temperature gradient to exist across its thickness; these theories are therefore not relevant to the case of LB films. In this section, a novel model will be developed, in which we assume that the thermal mass of the LB film is negligible when compared to those of the substrate and of the blacking layer,

and we apply the heat flow equation to such a device irradiated by sinusoidally modulated radiation.

The dynamic method of Chynoweth [41] is a commonly used technique for observing pyroelectric activity; the device is heated by a black-body source which is modulated by a mechanical chopper, and the resulting pyroelectric voltage is detected, amplified and displayed by a phase-sensitive detection system synchronised to the modulation frequency. The thermal analysis developed here enables pyroelectric coefficients to be calculated from the measured pyroelectric voltages.

The model used in this analysis is shown in figure 3.7 [42]. The device is assumed to consist of an infinitesimally thin pyroelectric film sandwiched between a thick substrate, which acts as a heat sink, and a black radiation-absorbing layer. The metal electrodes are also assumed to have negligible thermal mass, as they are thin compared with the substrate and the blacking layer. The device is heated by a black body of temperature  $T_0$ , separated from the device by a medium of radiation transfer conductance  $H$ , and sinusoidally modulated at an angular frequency,  $\omega_0$ .

The problem is essentially that of a two layer structure on a heat sink, a case which has been solved by Holeman [38], assuming a temperature variation of the form

$$\theta = \theta_0 + T(x) \exp(j\omega_0 t). \quad (3.6)$$

For a thin upper layer and low modulation frequency, the temperature  $T(x)$  in the upper layer was calculated to be

$$T(x) = \frac{HT_0}{H + K\omega}, \quad (3.7)$$

where

$$\omega = \left( \frac{j\rho c\omega_0}{K} \right)^{\frac{1}{2}}. \quad (3.8)$$

$K$ ,  $\rho$  and  $c$  are, respectively, the thermal conductivity, density and specific heat capacity of the substrate.

We extend this model to the case of LB films by assuming that the film does not contribute to the thermal properties of the device, and hence the temperature of the LB film is given by the temperature  $T_i$  at the interface between

the substrate and the blacking layer, and

$$T_i \approx T(x).$$

Therefore, assuming  $K\omega/H \gg 1$ ,

$$T_i = \frac{HT_0}{K\omega}. \quad (3.9)$$

Using Stefan's law for black body radiation, the incident radiation power per unit area,  $W$ , is given by

$$W = \sigma\eta_L T_0^4, \quad (3.10)$$

where  $\sigma$  is Stefan's constant and  $\eta_L$  the emissivity of the radiator.

$H$  is defined [38] as

$$H = 4\sigma T_K^3 \eta_L \eta_B, \quad (3.11)$$

where  $T_K$  is the average temperature of the radiator and the blacking layer, and  $\eta_B$  is the emissivity of the blacking layer. Assuming there is no re-radiation from the blacking layer, then

$$H = \frac{1}{2}\sigma T_0^3 \eta_L \eta_B. \quad (3.12)$$

Hence,

$$HT_0 = \frac{1}{2}W\eta_B.$$

Using this substitution, and also substituting for  $\omega$ ,

$$T_i = \frac{W\eta_B(j^{-\frac{1}{2}})}{2(K\rho c\omega_0)^{\frac{1}{2}}}. \quad (3.13)$$

We model the pyroelectric element as a current source in parallel with a resistor  $R$  and a capacitor  $C$ , where  $R$  and  $C$  are the total resistance and capacitance due to the LB film in parallel with the input impedance of the amplifier.

The pyroelectric current,  $i$ , is defined by the equation

$$i = pA \frac{d\theta}{dt}, \quad (3.14)$$

where  $p$  is the pyroelectric coefficient and  $A$  the area of the device. Substituting from (3.6) we obtain

$$i = pAT_i\omega_0 \exp\left[j\left(\omega_0 t + \frac{\pi}{2}\right)\right]. \quad (3.15)$$



The pyroelectric voltage,  $v$ , is given by

$$v = iZ, \quad (3.16)$$

where  $Z$  is the impedance. As the device area is typically  $\sim 2 \text{ cm}^2$ , then  $C > 1 \text{ nF}$ . Also,  $R \sim 10^{11} \Omega$  and  $\omega_0 \sim (1-20) \times 2\pi \text{ rad s}^{-1}$ . Therefore,  $\omega_0^2 R^2 C^2 \gg 1$ , and the impedance approximates to

$$Z = -\frac{j}{\omega_0 C}. \quad (3.17)$$

Hence,

$$|v| = \frac{pAT_i}{C}. \quad (3.18)$$

If we write

$$C = \frac{\epsilon_0 \epsilon_r' A}{Nd}, \quad (3.19)$$

where  $\epsilon_r'$  is the relative permittivity of the LB film,  $N$  is the number of monolayers and  $d$  is the thickness of a monolayer, then

$$p = \frac{2|v|\epsilon_0 \epsilon_r' (\omega_0 K \rho c)^{\frac{1}{2}} (j^{\frac{1}{2}})}{W \eta_B Nd}. \quad (3.20)$$

Noting that

$$j^{\frac{1}{2}} = \frac{1+j}{\sqrt{2}},$$

then

$$|p| = \frac{2\sqrt{2}v_m \epsilon_0 \epsilon_r' (\omega_0 K \rho c)^{\frac{1}{2}}}{W \eta_B Nd}, \quad (3.21)$$

where  $v_m$  is the measured root mean square pyroelectric voltage, which is similar in form to the equation used by Blinov *et al* [28]; and the measured pyroelectric voltage,  $v_m$ , is given by

$$v_m = \frac{|p|W \eta_B Nd (\omega_0)^{-\frac{1}{2}}}{2\sqrt{2}\epsilon_0 \epsilon_r' (K \rho c)^{\frac{1}{2}}}. \quad (3.22)$$

All of the parameters on the right hand side of equation (3.21) are known or can be experimentally determined, and it is therefore possible to calculate dynamic pyroelectric coefficients of LB films. The heat sinking effect of the substrate can be examined by comparing equation (3.21) with the equation for the dynamic pyroelectric coefficient of a bulk material [43]:

$$p = \frac{2\sqrt{2}v_m G}{W \eta_B \omega_0 AR}, \quad (3.23)$$

where  $G$  is the thermal conductance of the material and  $R$  its electrical resistance. It is interesting to note that for a bulk detector the pyroelectric voltage,  $v_m$ , is proportional to  $\omega_0$ , whilst for an LB film detector  $v_m$  is proportional to  $(\omega_0)^{-\frac{1}{2}}$ ; LB film detectors are therefore expected to be best suited to low frequency applications. Furthermore, the performance can be optimised by selecting a substrate with suitable values of thermal conductivity, density and specific heat capacity.

### 3.4 THIN SUBSTRATES

It has already been demonstrated that the pyroelectric response of an LB film detector is limited by the heat sinking effect of the substrate; we will now show that an efficient device must incorporate a thin substrate in order to minimise this effect. Consider a small change  $dT$  in the temperature of a pyroelectric element, generating an amount of charge  $dQ$ , given by

$$dQ = pAdT, \quad (3.24)$$

where  $p$  is the pyroelectric coefficient and  $A$  the device area. If the voltage generated is  $dV$  and the capacitance of the device is  $C$ , then

$$dV = \frac{pA}{C}dT. \quad (3.25)$$

According to Putley [43],  $dT$  is given by the ratio of the radiative power absorbed to the total thermal admittance,  $Y_t$ , which can be expressed thus:

$$dT = \frac{W\eta}{Y_t}, \quad (3.26)$$

where  $W$  is the radiative power emitted by the object and  $\eta$  the emissivity of the detector. Therefore,

$$dV = \frac{pAW\eta}{CY_t}. \quad (3.27)$$

Hence, it is desirable that the thermal admittance,  $Y_t$ , should be as small as possible.

$Y_t$  has components due to thermal conductance,  $G_t$ , and thermal capacitance,  $C_t$ , such that

$$Y_t^2 = G_t^2 - (j\omega_0 C_t)^2. \quad (3.28)$$

But,

$$C_t = cdA, \quad (3.29)$$

where  $c$  is the volume specific heat capacity of the film and  $d$  the total thickness of the device (film plus substrate). Therefore,

$$Y_t^2 = G_t^2 + \omega_0^2 c^2 d^2 A^2. \quad (3.30)$$

The thermal conductance term is dominated by the metal electrodes and connecting leads, and is difficult to control; therefore, the performance of the detector can only be improved by minimising the thermal capacitance term,  $\omega_0 cdA$ . In order to achieve this, however, the thermal capacitance term must dominate in the expression for thermal admittance; that is,

$$\omega_0 cdA > G_t. \quad (3.31)$$

Consider a typical LB film device, where the total thickness of the metal electrodes is  $t$ , and the top and bottom electrodes are both connected to wires of length  $b$  and diameter  $w$ .  $G_t$  is given by:

$$G_t = \frac{2Ktw}{b}, \quad (3.32)$$

where  $K$  is the thermal conductivity of the metal electrodes. If

$$K = 200 \text{ Wm}^{-1}\text{K}^{-1}$$

$$t = 5 \times 10^{-8} \text{ m}$$

$$w = 10^{-3} \text{ m}$$

$$b = 10^{-2} \text{ m},$$

then,

$$G_t = 2 \times 10^{-6} \text{ WK}^{-1}.$$

Therefore, the requirement for the capacitance term to dominate is:

$$d > \frac{10^{-7}}{\omega_0 c A}. \quad (3.33)$$

If  $\omega_0 = 16\pi \text{ rad s}^{-1}$ ,  $c = 10^3 \text{ Jkg}^{-1}\text{K}^{-1}$  and  $A = 10^{-4} \text{ m}^2$ , then  $d > 400 \text{ nm}$ . Hence, we can see that, whilst equations (3.27) and (3.30) indicate that the voltage responsivity can be improved by making the total device thickness,  $d$ , as small as possible,  $d$  must not be smaller than about 400 nm, otherwise the thermal conductance of the metal electrodes will dominate. In practice,  $d$  can be reduced by using a thin substrate.

### 3.5 SUMMARY

It has been shown that there are considerable advantages in using LB films as pyroelectric infrared detectors. These advantages include precise control over thickness and symmetry, high sensitivity, ease of deposition onto integrated circuits, low dielectric constant, and built-in polarisation, removing the need to pole the films. However, the response of a thin film detector can be dramatically reduced if a thick substrate is employed, due to the effects of thermal and mechanical clamping. Thermal clamping can be reduced by using a thin substrate; mechanical clamping is a more fundamental problem, but could be avoided by using a material in which the total pyroelectric effect includes a large primary component, or by selecting a substrate material with an appropriate thermal expansion coefficient.

## CHAPTER 4

### EXPERIMENTAL TECHNIQUES

#### 4.0 INTRODUCTION

This chapter provides a general description of the techniques used in the fabrication and characterisation of pyroelectric LB film structures. The Langmuir trough and the procedures adopted for the characterisation of new materials and the deposition of LB films are described in section 4.1. Section 4.2 describes the fabrication of LB film devices, and sections 4.3 and 4.4 discuss, respectively, their structural and electrical assessment. For each technique the theoretical background is presented, and this is followed by a detailed description of the equipment used and the procedure adopted.

#### 4.1 THE LANGMUIR TROUGH

The trough used by Langmuir and Blodgett in their pioneering work [1] consisted of a metal container, coated with paraffin wax to render it hydrophobic, and filled to the brim with water. The floating monolayer was compressed using a film of piston oil, which was separated from the LB film by a waxed thread floating on the water and fastened to the sides of the trough. The substrate was raised and lowered by means of a crude hand winder, the piston oil maintaining a constant surface pressure as material was removed from the surface.

Modern Langmuir troughs bear little resemblance to this early version; sophisticated electronic circuitry controls the surface pressure, high grade materials are used in their manufacture, and systems are often housed in microelectronics clean rooms to avoid the problems associated with dust. The troughs used for the present work are described in the following sections.

##### 4.1.1 The conventional trough

The trough used for the deposition of single materials was of the constant perimeter barrier type [2], and is illustrated schematically in figure 4.1; the inset illustrates the maximum and minimum areas contained within the barrier. The barrier was made of PTFE-coated glass fibre, and was held taut by three pairs

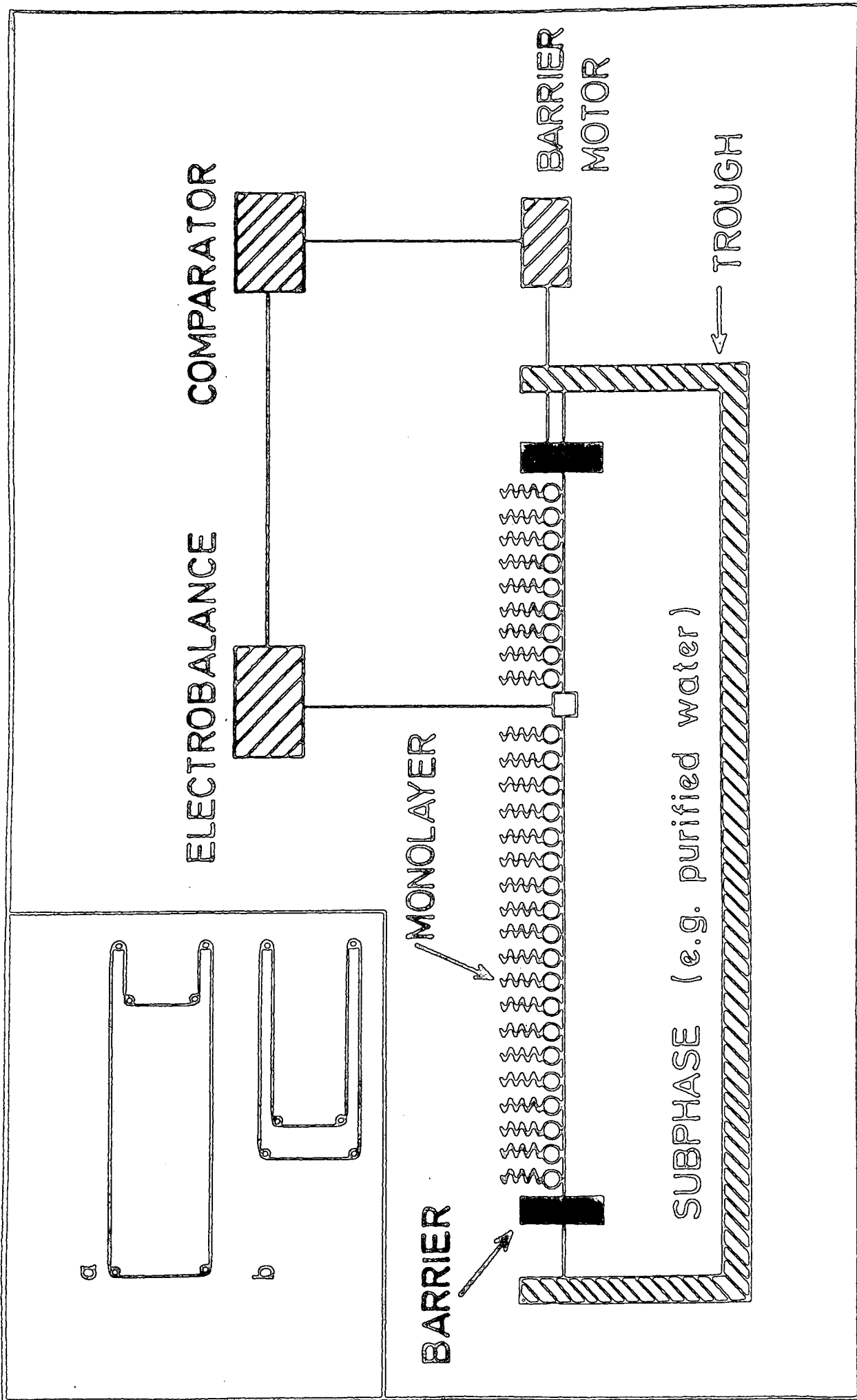


Figure 4.1 Schematic diagram of the constant perimeter barrier Langmuir trough.

of rollers mounted on cross-members; the cross-members were pulled by means of toothed rubber belts driven by an electric motor. The trough itself was made of glass and was mounted on a platform which could be raised and lowered. The surface pressure was monitored using a Wilhelmy plate, consisting of a 1 cm wide strip of filter paper; this was suspended in the water by a thread from a CI microbalance head. The microbalance was an integral component of the control system, and formed part of a feedback loop, such that any change in surface pressure during film deposition could be compensated for by movement of the constant perimeter barrier. Movement of the barrier could also be achieved by manual forward and reverse controls. The dipping head consisted of a metal screw clamp, in which substrates could be held, affixed to a motor driven micrometer screw. The complete assembly was housed in a glass-doored cabinet, incorporating an extractor fan to aid solvent evaporation, and was mounted on a pneumatic anti-vibration table. The trough was located in a class 10,000 microelectronics clean room.

The water used as the subphase in the trough was purified using an Elgastat Spectrum SC31 reverse osmosis unit, and a Milli Q double deionisation and 0.2  $\mu\text{m}$  filtration system. In-line monitors confirmed that the resistivity was close to its theoretical maximum of 18  $\text{M}\Omega\text{ cm}$ , and that the total organic carbon content was less than 20 ppb. The water was delivered to the trough via high quality polypropylene tubing. The trough water was changed at frequent intervals, as rapid bacterial growth is known to occur when water is left in the trough for periods of several days [3]. In addition, a regular cleaning procedure was employed, in which the barrier and rollers were removed and refluxed in propan-2-ol, and the trough was rinsed with chloroform, propan-2-ol and purified water. On re-assembly, the Wilhelmy plate was renewed and the instrumentation recalibrated. Immediately prior to monolayer spreading, the water surface was cleaned with a fine nozzled glass pipe, connected to an aspirator suction pump.

A Bryans 29000 X-Y chart recorder was used to plot surface pressure versus surface area isotherms, and a Bryans 312 2Y-T chart recorder plotted both area and pressure as functions of time. The pH of the subphase was continuously monitored using a Pye Unicam PW 9409 pH meter.

#### 4.1.2 The alternate layer trough

The trough used to deposit alternate layers [4] was identical in many respects to that described above; however, the area defined by the constant perimeter barrier was divided into two by a fixed PTFE beam (figure 4.2). Two microbalances and barrier motors were used, enabling the surface pressures of the two separate monolayers to be controlled independently. The substrate was mounted on a PTFE cylinder, which was accommodated within the central fixed beam. This cylinder rotated about a central axis, entering the water through one monolayer, and leaving through the other. The water purification and cleaning processes described above were also employed for the alternate layer trough.

#### 4.1.3 Pressure-area isotherms

The first step in the assessment of a new LB film material is the determination of its surface pressure-area ( $\pi$ - $A$ ) isotherm. This involves spreading a monolayer onto the water surface, slowly compressing it by means of the moving barrier, and monitoring the surface pressure ( $\pi$ ) as a function of the area enclosed by the barrier ( $A$ ). If the number of molecules spread on the surface is known, then the average area occupied by a molecule can be deduced. An ideal  $\pi$ - $A$  isotherm of a fatty acid is shown in figure 4.3a; three distinct regions are present, corresponding to two dimensional analogues of gas, liquid and solid phases. It should be noted, however, that isotherms of many materials do not show this distinct structure; for example, the isotherm of ammonium terminated polybutadiene [5] is expanded (figure 4.3b), with no abrupt phase changes. In figures 4.3a and b, the high pressure region of the curve has been extrapolated down to the X-axis; the point of intersection gives the molecular area at zero surface pressure, an important parameter in the characterisation of a material.

The procedure adopted for the screening of new materials was as follows: the material was first dissolved in an organic solvent (invariably "Aristar" grade chloroform) to an accurately known concentration (usually close to 1 mg ml<sup>-1</sup>). A known volume (typically 100  $\mu$ l) was then deposited onto the clean water surface, using a Kloehn microlitre syringe, and the extractor fan was switched on for several minutes to aid solvent evaporation. A  $\pi$ - $A$  isotherm was then



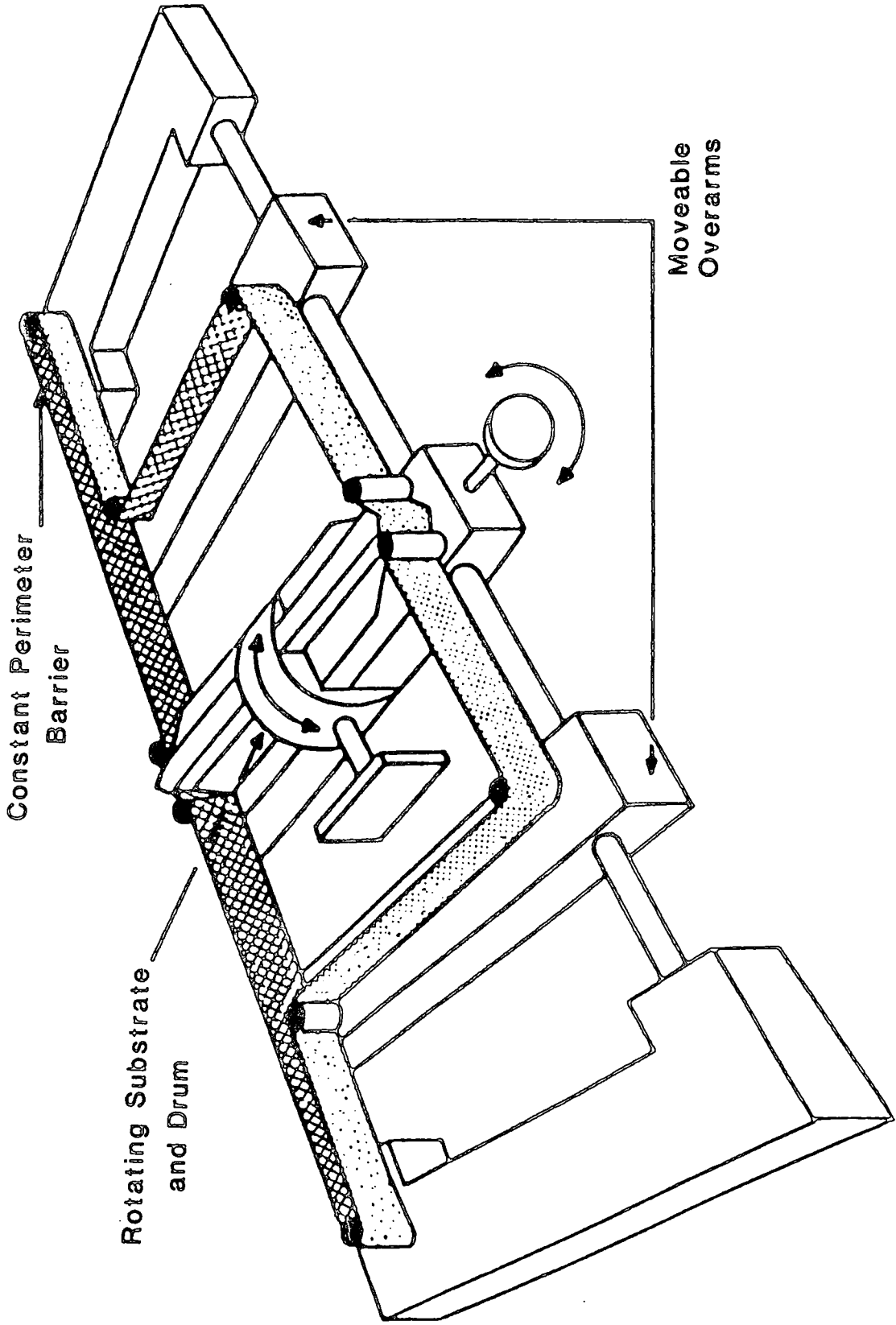


Figure 4.2 Schematic diagram of the alternate layer trough.

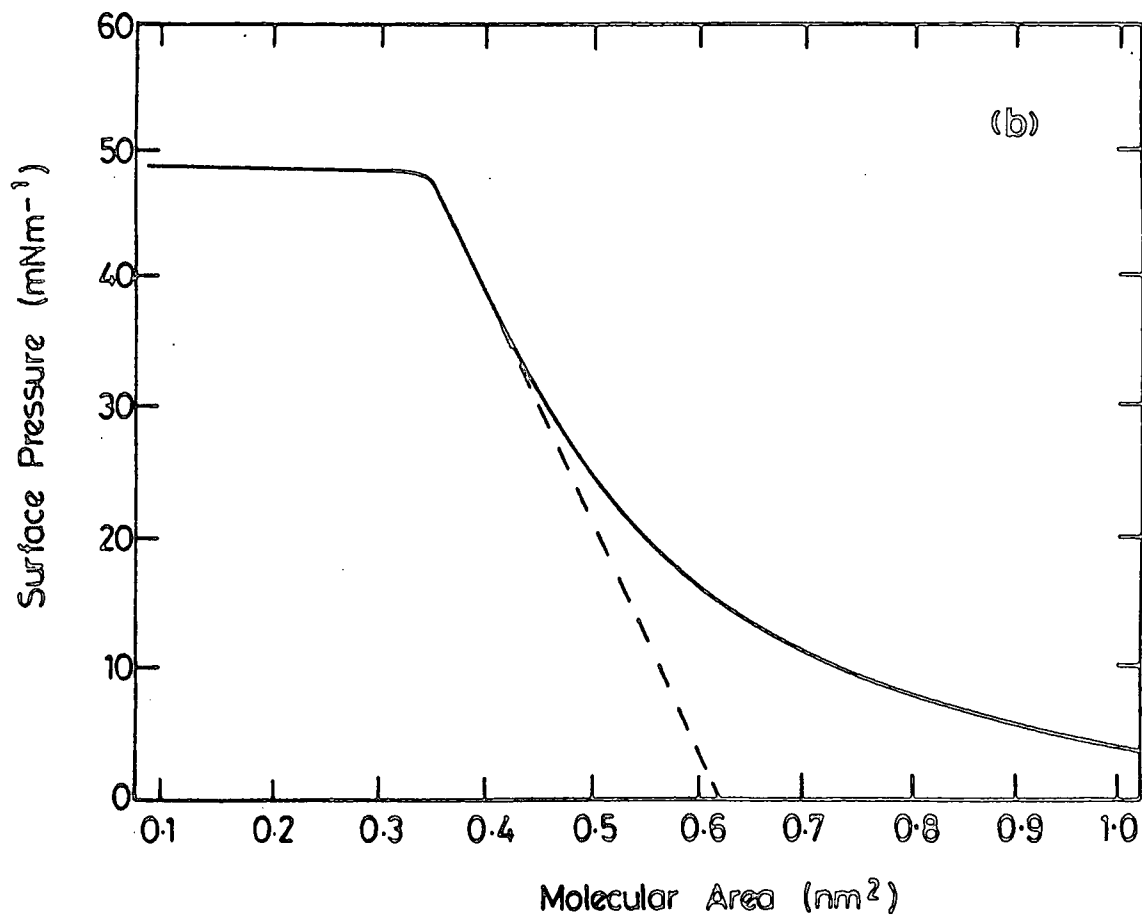
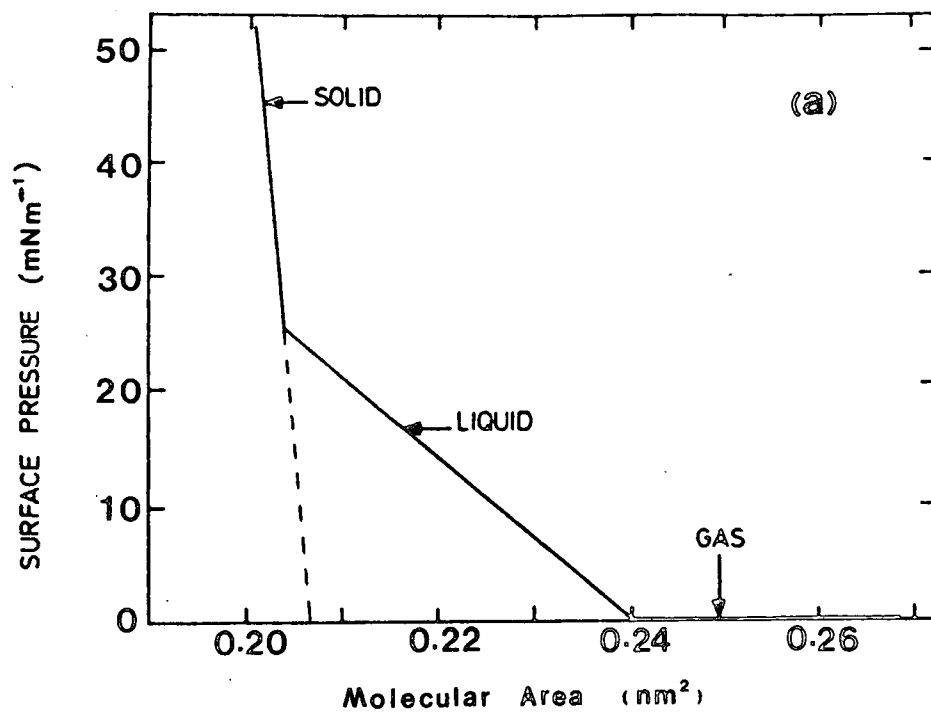


Figure 4.3 Surface pressure-area isotherms for (a) a "classical" fatty acid, and (b) an ammonium terminated polybutadiene.

plotted on the X-Y chart recorder by compressing the film at a fixed rate.

The molecular area at zero pressure was calculated from the isotherm, and this value was compared with that obtained from measurements on space filling molecular models. Poor agreement between these values indicates instabilities in the film due to dissolution into the subphase, evaporation or buckling of the film [6]. The film stability was further investigated by selecting a value of surface pressure within the condensed region of the isotherm, controlling the film pressure at this value, and monitoring the surface area as a function of time. It was found that the rate of dissolution could sometimes be controlled by altering the pH of the subphase with the addition of hydrochloric acid or ammonium hydroxide solutions.

If the molecular area was in reasonable agreement with the theoretical value, and the surface area at constant pressure was relatively stable, then a material was judged to be suitable for LB film deposition.

#### **4.1.4 Film deposition**

Most of the films deposited during the course of this work adopted the Y type structure, and were fabricated on hydrophilic substrates; material was therefore not transferred until the first withdrawal of the substrate through the monolayer. For this reason, the substrate was immersed through a clean water surface prior to the spreading of the film. After the film had been spread and the solvent allowed to evaporate, the system was switched to "control" mode, such that the surface pressure was maintained at a pre-selected value. It was found that high quality films could usually be produced if the first withdrawal of the substrate was performed extremely slowly, and was followed by a "draining" period of around 30 minutes before subsequent layers were deposited at a faster rate.

The deposition was characterised by monitoring the surface area as a function of time. Figure 4.4 shows schematically the traces that would be expected for X, Y and Z type deposition onto a hydrophilic substrate. In each case, deposition does not commence until the first withdrawal of the substrate (if the substrate is hydrophilic); thereafter, X, Y and Z type deposition occur, as de-

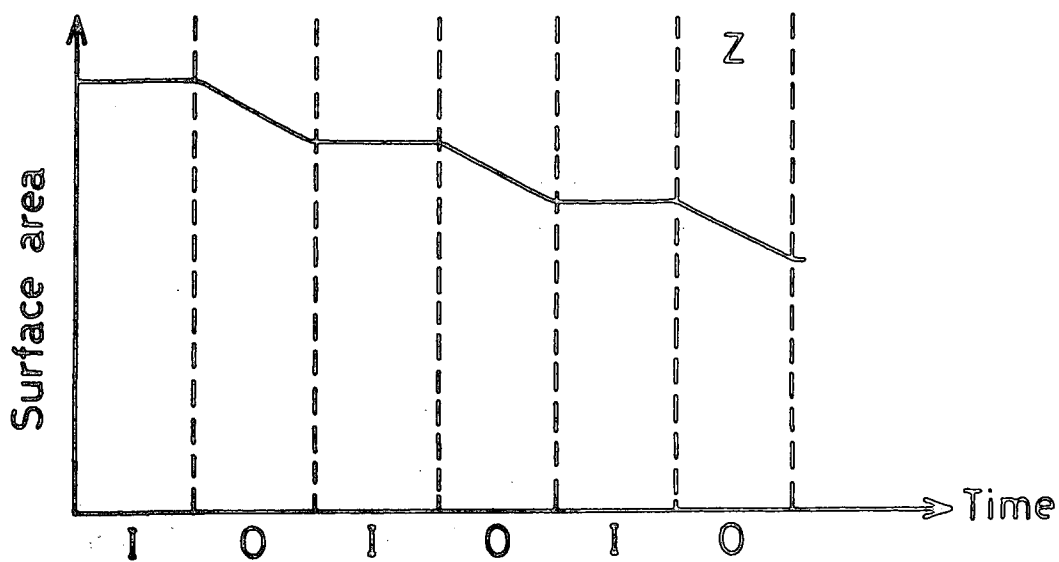
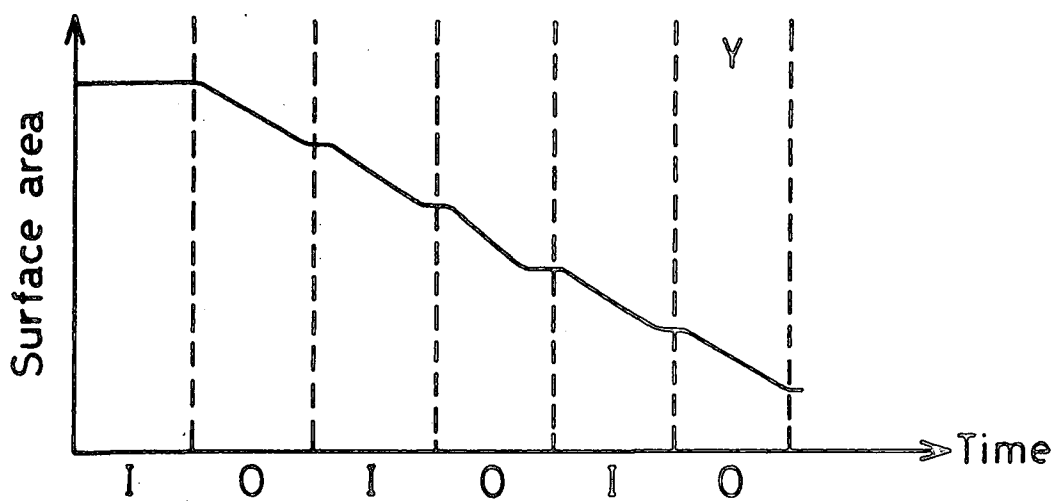
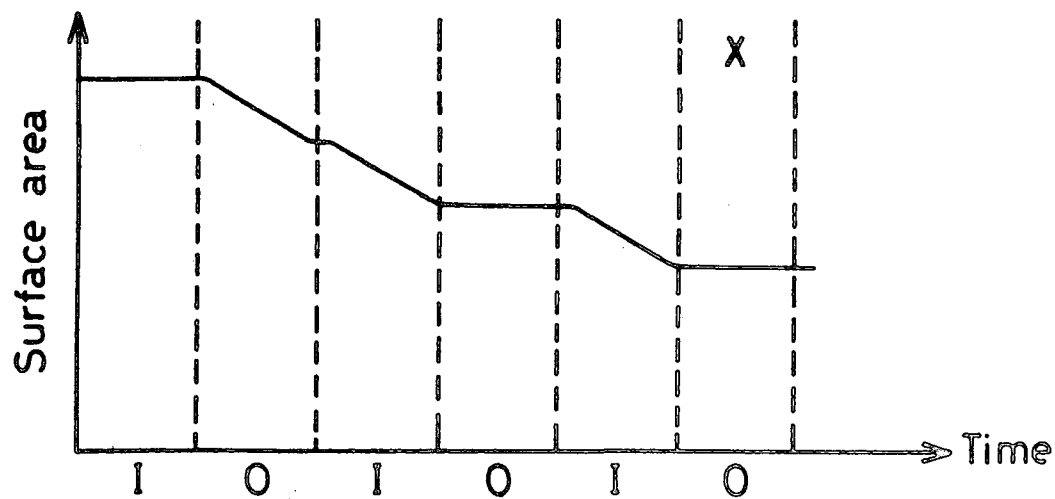


Figure 4.4 Surface area versus time graphs for X, Y and Z type LB film deposition. I denotes substrate moving into the water; O denotes substrate moving out of the water.

scribed in section 3.2.1. A deposition ratio was also calculated; this is defined as the ratio of the decrease in surface area to the area of the substrate immersed; thus, no pick-up corresponds to a ratio of zero, whilst complete coverage corresponds to a ratio of unity.

## 4.2 DEVICE FABRICATION

### 4.2.1 Substrate preparation

#### (a) Glass

Several glasses with different thermal expansion coefficients were used; however, routine measurements were performed on ordinary Chance-Propper laboratory microscope slides. The glasses were all cleaned rigourously before being used as substrates. Initially, the slides were wiped with lint-free lens cleaning tissue, soaked in propan-2-ol, to remove large particles of dust. They were then ultrasonically agitated in a 5% solution of "Decon 90" de-greasing agent, and rinsed twice in ultrasonically agitated deionised water. Finally, the slides were refluxed in boiling propan-2-ol for several hours.

#### (b) Aluminised glass

Highly conducting substrates were produced by evaporating a layer of aluminium onto glass which had been cleaned by the process described above. The evaporation was performed in an Edwards E306A vacuum coating system, at pressures of less than  $10^{-5}$  torr, using a resistively heated tungsten filament as the evaporation source. Substrates prepared in this way were refluxed in propan-2-ol immediately before use, in order to produce a uniformly hydrophilic surface.

#### (c) Silicon

Silicon wafers were used as substrates for infrared spectroscopy and electron microscopy experiments. For this purpose, n-type silicon of either {100} or {111} orientation was used; the wafers were cleaned by refluxing in 1,1,1-trichloroethane. The native oxide on the silicon provided a hydrophilic surface, onto which Y type deposition did not occur until the first withdrawal of the substrate through the floating monolayer; hence, it was only possible to deposit odd numbers of monomolecular layers onto such surfaces. When an even num-

ber of layers was required, the surface was rendered hydrophobic by adding a small amount of dimethyldichlorosilane to the 1,1,1-trichloroethane reflux. The hydrochloric acid produced by the reaction with the surface oxide was removed by rinsing with deionised water.

#### **4.2.2 Fabrication of MIM devices**

Electrical measurements were made on devices in which the LB film formed the dielectric layer of a metal-insulator-metal (MIM) capacitor. Films were deposited onto aluminised glass slides, and were then stored in a desiccator under a low pressure of dry nitrogen for two days. Capacitor structures were produced by evaporating aluminium discs of approximate area  $1.8 \text{ cm}^2$  onto the LB film; these discs were connected to an unmetallised portion of the glass substrate by narrow aluminium strips, enabling silver paste contacts to be made to both lower and upper electrodes without damage to the organic layer. The resulting device is illustrated in figure 4.5.

#### **4.2.3 Surface blacking**

As the top electrodes were highly reflective, and hence inefficient at absorbing infrared radiation, it was necessary to coat the MIM devices with a layer of metal black [7]. Metal blacks are produced when a metallic or semimetallic element is evaporated under a low pressure of an inert gas, and the metal particles condense into colloidal aggregates. In this case, the metal used was bismuth, and the inert gas nitrogen. A special evaporation chamber was constructed, into which nitrogen could be admitted and maintained at a pressure of 1 mbar by means of a rotary pump. The bismuth, which was in the form of granules, was evaporated from a resistively heated molybdenum boat.

### **4.3 STRUCTURAL CHARACTERISATION**

#### **4.3.1 Reflection high energy electron diffraction**

Reflection high energy electron diffraction (RHEED) is a powerful and convenient technique for studying the orientation of LB film molecules relative to the substrate surface, and has been widely used for this purpose [8-15]. Un-

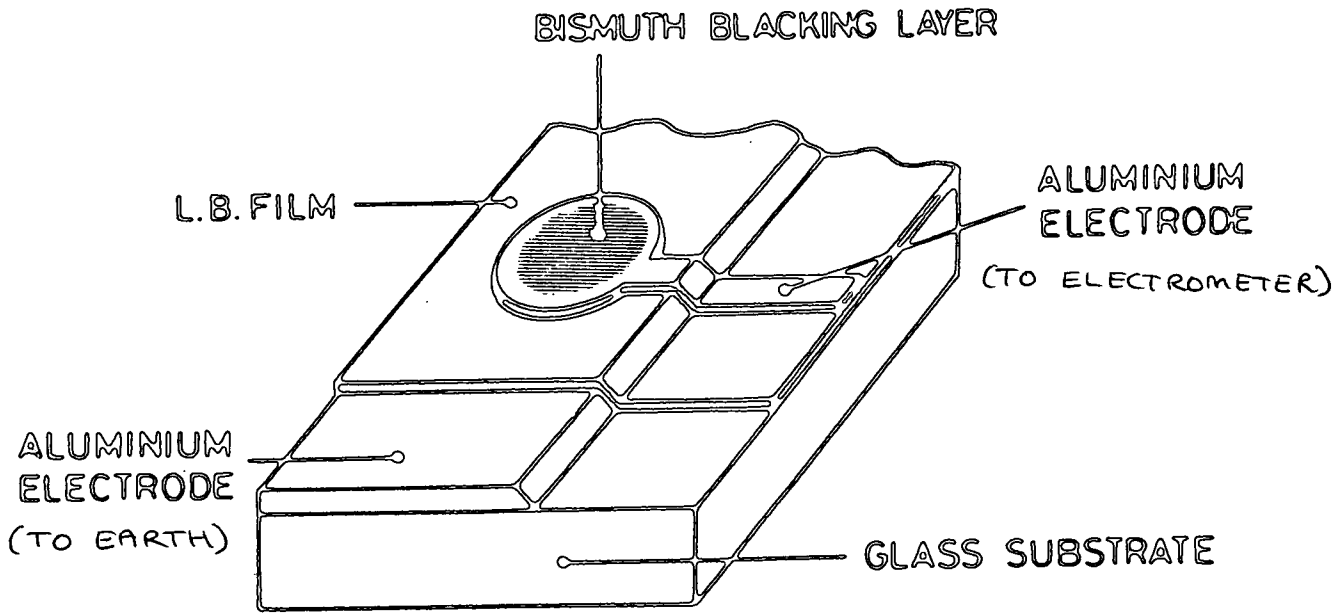


Figure 4.5 Langmuir-Blodgett film MIM capacitor device.

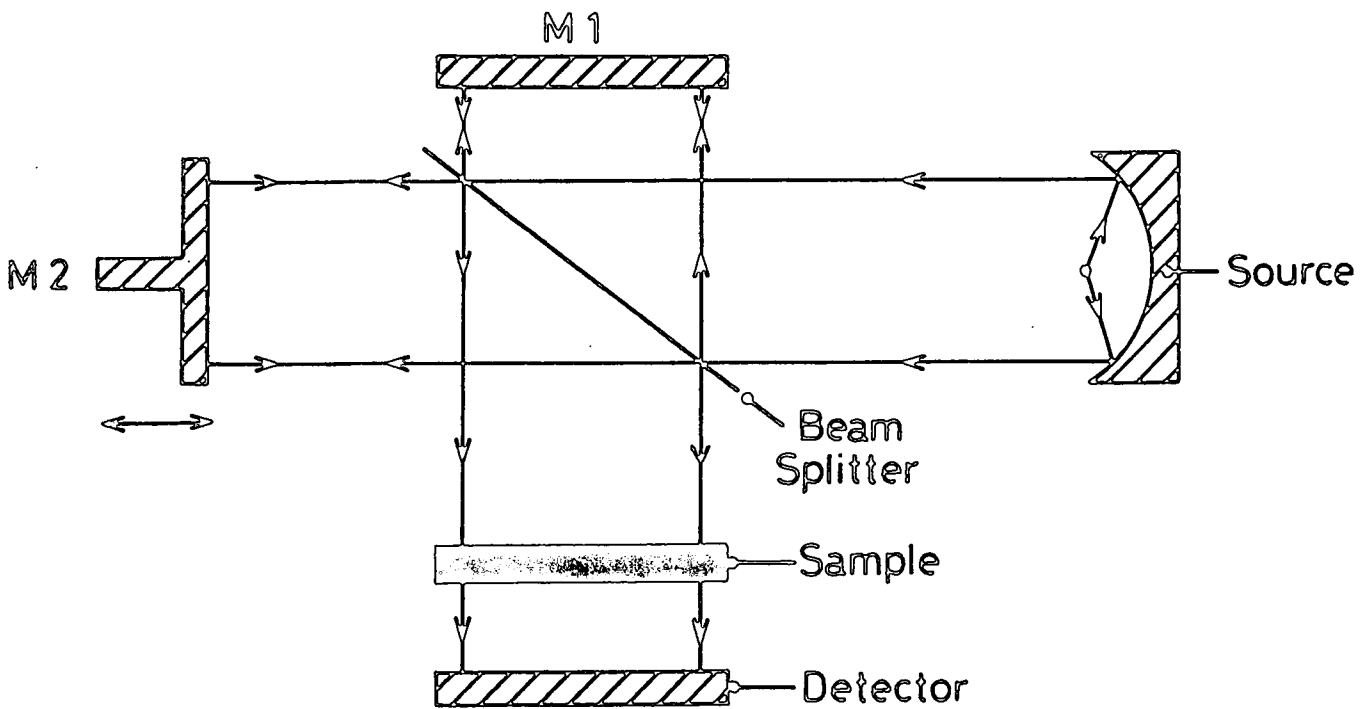


Figure 4.6 The Michelson interferometer.

like transmission electron diffraction (TED), RHEED does not require that the sample be prepared in the form of a very thin film; hence, an LB film deposited onto a thick silicon or aluminised glass substrate can readily be examined by this technique. RHEED is particularly useful for examining surface films, since the geometry is such that the electron beam samples a very thin surface layer over a large area.

In the RHEED technique, the specimen is mounted in a transmission electron microscope, such that the incident electron beam strikes it at grazing incidence. Diffraction will occur according to the usual Bragg relationship; however, since the wavelength of the electron beam is typically 0.01 nm, and the interplanar spacing for most crystals is of the order of 0.2 nm, the Bragg angle,  $\theta$ , will vary from about 1.5 to 0.5°. Consequently, in RHEED, only those crystal planes which are inclined at less than a few degrees to the surface of the specimen will diffract an electron beam that strikes it at grazing incidence.

Typical d-spacings of LB films are considerably greater than 0.2 nm ( $\sim 6$  nm); however, the hydrocarbon chains of LB film molecules are comprised of regular  $C_2H_4$  repeat units, and the RHEED pattern which is obtained from an LB film specimen corresponds to diffraction from planes of these  $C_2H_4$  subcells. It has been established [12] that the structure of fatty acid LB films is granular, with the molecules within all of the grains inclined at approximately the same angle to the substrate surface, but with the azimuth of this inclination varying by a small amount from grain to grain. Thus the structure of an LB film is somewhat disordered within the substrate plane, but exhibits a preferred common orientation of the molecules perpendicular to this plane. The RHEED patterns characteristic of such a structure consist of arcs of intensity [16]. In these patterns, the angle between the shadow edge of the sample and the diffraction arc corresponding to the preferential plane of packing provides a measurement of the inclination of the molecules relative to the substrate normal.

The present studies were performed in a JEM 120 transmission electron microscope operated at 100 kV, with the sample stage located at the top of the projection chamber. In order to investigate the presence of any anisotropy in the films, RHEED studies were performed with the incident electron beam inclined



at a range of azimuths, varying from parallel to perpendicular to the direction of dipping [15].

#### 4.3.2 Fourier transform infrared spectroscopy

The characteristic vibrational frequencies of most chemical bonds lie in the range  $4000$  to  $200\text{ cm}^{-1}$ , corresponding to the infrared (IR) region of the electromagnetic spectrum. If a vibration causes a periodic change in the electric dipole moment associated with a bond, then IR radiation of the same frequency will interact, producing a resonant energy transfer, where radiation is absorbed. Each type of bond corresponds to a particular characteristic frequency; this frequency depends not only on the atomic masses of the bonding species, but also on the nature of the local environment. As the environment of a bond is unique to a particular molecule, an infrared spectrum provides a "finger print" of the molecule, from which it can be characterised. In this case, IR spectroscopy was used to study head group interactions in acid/amine alternate layer LB films, since this technique can detect hydrogen bonding and proton transfer from the acid to the amine.

Conventional dispersive IR spectroscopy involves passing broad band IR radiation through the sample, frequency analysing the transmitted beam, and comparing this with a reference beam. The Fourier transform infrared (FTIR) technique, on the other hand, is based on the Michelson interferometer, which is shown in figure 4.6. A parallel beam of broad band light is incident on a beam splitter, from which half is reflected to M1 (fixed mirror), and the remainder passes through to M2 (moveable mirror). The radiation is then reflected back to the beam splitter, where it recombines, passes through the sample and is detected. The detected radiation corresponds to an interferogram produced by constructive and destructive interference between the beams which have been reflected by M1 and M2, with characteristic frequencies absorbed by the sample. A normal absorption spectrum is calculated by taking the Fourier transform of the detected signal. The main advantage of FTIR over dispersive spectroscopy is the speed with which the spectrum can be obtained, since the entire spectrum is contained in the interferogram. In addition, the intensity of radiation incident

on the sample is greater (Jacquinot's advantage), and the signal to noise ratio is improved (Fellgett's advantage) [17].

In this study, a Mattson Sirius 100 Fourier transform spectrometer was used. Transmission spectra were obtained using films deposited onto silicon wafers; also, reflection absorption infrared spectroscopy (RAIRS) experiments were performed, using aluminised glass substrates, with an average angle of reflection of  $81^\circ$ .

#### 4.3.3 X-ray low angle diffraction

The wavelength of copper  $K\alpha$  radiation is approximately 0.15 nm; such radiation will therefore be diffracted by the planes formed by the layers of LB film molecules, rather than by the  $C_2H_4$  subcells. Hence, X-ray diffraction provides a means of determining the d-spacing of LB films. Since the d-spacing of an LB film is typically of the order of 6 nm, the first order (001) reflection will occur at a Bragg angle of less than  $1^\circ$ . The criterion for observing X-ray diffraction from LB films is, therefore, that the beam should strike the sample at grazing incidence; for this reason, the technique of X-ray low angle diffraction (XRLAD) was employed [18-21].

All measurements were performed at Bristol University, using a specially constructed glancing angle diffractometer, which utilised copper  $K\alpha$  radiation. The detector was interfaced to a microcomputer which plotted the diffracted intensity as a function of detector position. The system was calibrated such that a value of  $\theta$  could be readily calculated for each position of the detector. The resultant spectra consisted of a series of equally spaced peaks due to reflections from the (00*l*) planes (*ie.* those planes which are parallel to the substrate surface). Values of  $\theta$ , and ultimately of the d-spacing were calculated from each reflection, and an average value was taken.

### 4.4 PYROELECTRIC AND DIELECTRIC CHARACTERISATION

#### 4.4.1 Static pyroelectric detection

It was stated in chapter 2 that the pyroelectric current,  $i$ , generated by a

device of area  $A$  is given by

$$i = pA \frac{dT}{dt} \quad (4.1)$$

where  $dT/dt$  is the rate of change of temperature and  $p$  the pyroelectric coefficient.\* If a pyroelectric sample of known area is heated or cooled at a constant rate, a constant current will therefore flow; by measuring this current, the pyroelectric coefficient can be calculated. The value of  $p$  obtained using this simple technique is very accurate, since equation (4.1) makes no assumptions about the thermal and electrical properties of the sample.

In this case, the heating and cooling of the sample were performed using a Cambion model 801-3958-01 thermoelectric element. This was mounted on a heat sink consisting of a copper block through which cold water continuously circulated; thus, the bottom face of the thermoelectric element was maintained at a constant temperature, and the top face was heated or cooled relative to this. LB film devices in the form of MIM capacitors deposited on glass substrates were mounted on top of the thermoelectric module, and good thermal contact was established using zinc oxide heat sink compound. Also mounted on the thermoelectric element was a piece of glass identical to the substrate material, supporting a platinum resistance thermometer; this enabled the temperature of the LB film to be measured without damaging the specimen. Contacts were made to the sample using platinum wires and silver paste.

The assembly was mounted inside a brass chamber which could be evacuated; containers of silica gel desiccant were housed in the base. A schematic diagram of the chamber is shown in figure 4.7. The pyroelectric current was measured using a Keithley 600B electrometer, and the output was displayed on one channel of a Rikadenki R-52 2Y-T chart recorder. The other channel displayed the temperature measured by the platinum resistance thermometer.

The following procedure was adopted for the measurement of the pyroelectric coefficient of an LB film. First, the sample was mounted on the thermoelectric element, and electrical contacts were made. The chamber was then evacuated by means of a two stage rotary pump, and the sample was maintained under vacuum for approximately 30 minutes. The measurement commenced by

---

\*  $p$  is assumed to be constant over the temperature range of the experiment.

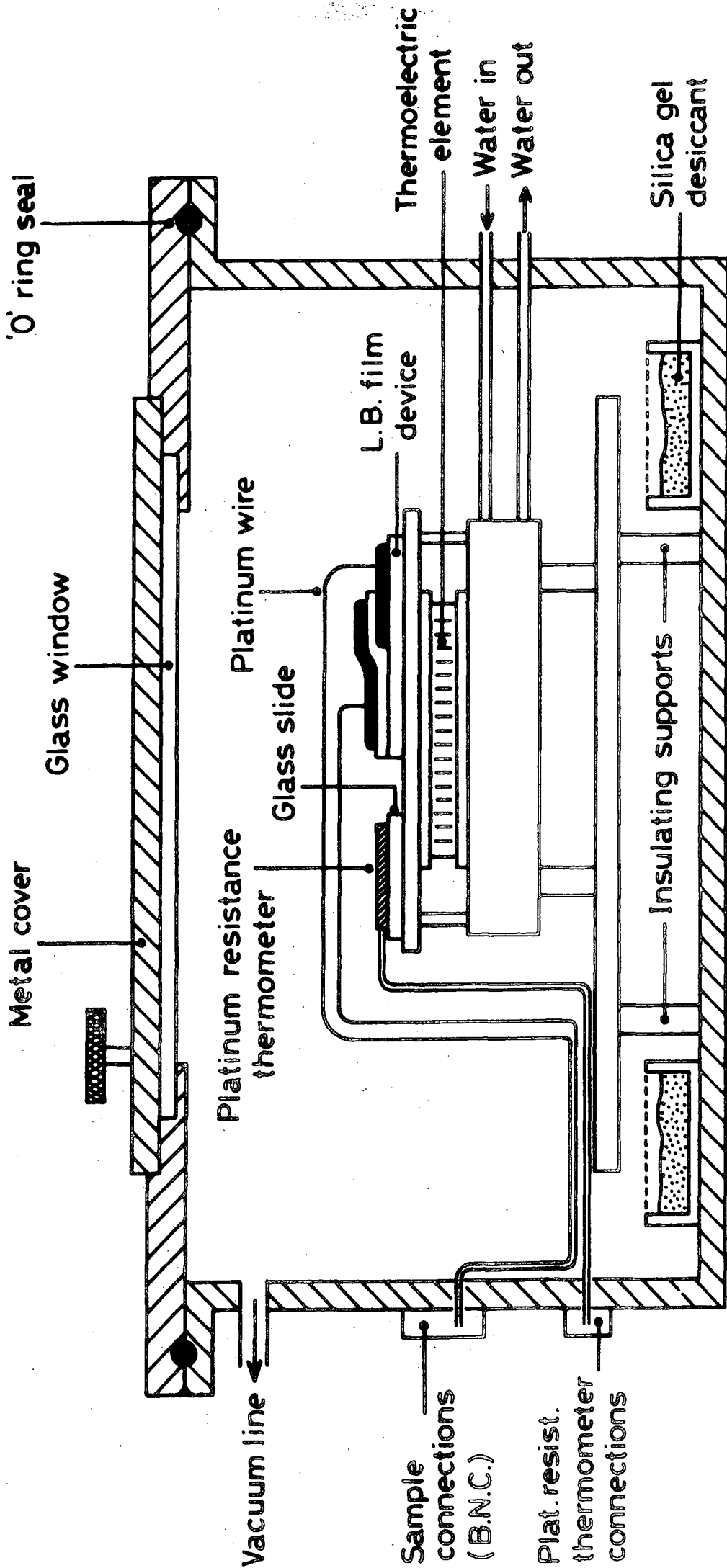


Figure 4.7 Sample chamber used for static pyroelectric detection .

heating the sample through about 10°C and monitoring both the pyroelectric current and the temperature on the chart recorder. The sample was then cooled back to ambient temperature, again monitoring the current and temperature. Since the rate of change of temperature was approximately constant, a trace of the type shown schematically in figure 4.8 was obtained. The rates of change of temperature during heating and cooling were calculated from the gradient of the temperature versus time graph. Two separate values of  $p$  were calculated for the heating and cooling phases of the cycle; an average of these values was then taken.

The static technique was also used to measure the pyroelectric coefficient as a function of temperature. In this case, the sample was mounted in an Oxford Instruments DN 704 gas exchange cryostat, and the current was measured using a Keithley 410A picoammeter. Again, a Rikadenki R-52 chart recorder was used to monitor both current and temperature. The rate of change of temperature was not constant in this case; it was therefore necessary to assume that  $p$  was constant over temperature increments of 5°C, and to take average values of  $dT/dt$  and  $i$  over this range, from which approximate values of  $p$  could be calculated.

#### 4.4.2 Dynamic pyroelectric detection

The dynamic method of Chynoweth [22] was also used to evaluate pyroelectric coefficients, as this represented a more realistic simulation of a thermal imaging system. This technique involved the sample being heated by a black-body source, modulated by a mechanical chopper; the resulting pyroelectric voltage was detected by a phase-sensitive detection (PSD) system, synchronised to the modulation frequency. Pyroelectric coefficients could then be evaluated using equation 3.21 (page 34). The model used in the derivation of equation 3.21 involves approximations concerning the thermal and electrical properties of the structure; the values of  $p$  obtained by this technique are therefore not expected to be as accurate as the static values.

The experimental arrangement is shown in figure 4.9. An incandescent light bulb mounted in an aluminium housing was used as the source of infrared

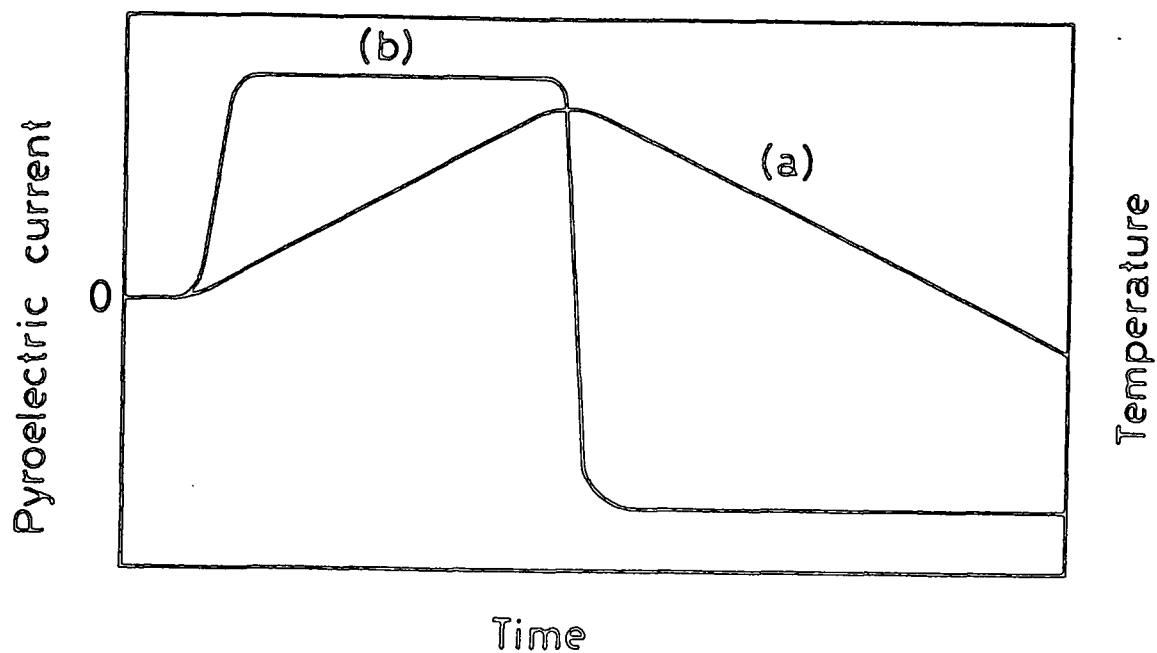


Figure 4.8 Schematic diagram of (a) temperature and (b) pyroelectric current during a heat-cool cycle of a static pyroelectric experiment.

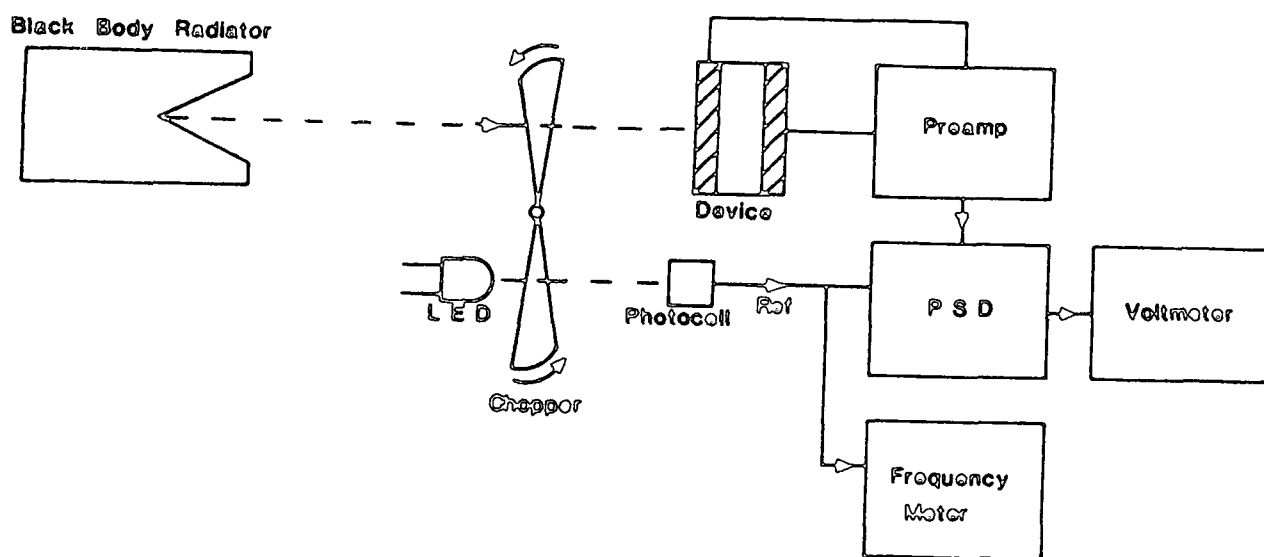


Figure 4.9 Schematic diagram of the experimental arrangement used for dynamic pyroelectric detection.

radiation; this was modulated by a Brookdeal 9479 chopper unit, usually at a frequency of 8 Hz, although some frequency dependent measurements were also made. The devices were mounted in an earthed metal sample chamber in order to reduce background radiation and electrical noise. The system components were mounted on an optical bench to facilitate beam alignment. The voltage output from the device was amplified by a Brookdeal 5006 preamplifier and a Brookdeal 9502 "Ortholoc" two phase lock-in amplifier, and displayed on a voltmeter. The reference signal for the PSD system was derived from the chopper unit, and this signal was also used to display the modulation frequency on a Global Specialties 5001 frequency meter.

In order to calculate pyroelectric coefficients from the measured voltages, it was necessary to evaluate the various parameters in equation 3.21. The dielectric constant,  $\epsilon'_r$ , of the film was calculated from a plot of reciprocal capacitance (at 50 Hz) versus number of monolayers (see section 4.4.4). The thermal conductivities, densities and specific heat capacities ( $K$ ,  $\rho$  and  $c$ ) of the glass substrates were provided by the manufacturers. The incident radiation intensity,  $W$ , was measured using a thermopile. The emissivity,  $\eta$ , of the bismuth was calculated from the pyroelectric voltage generated by a sample of lithium niobate, which had been coated with a layer of the blacking material, and whose pyroelectric coefficient was accurately known.

#### 4.4.3 Surface potential characterisation

In order to assess whether certain samples possessed a permanent polarisation, the Kelvin probe method was used to measure surface potentials [23]. This is an attractive technique, since it is non-destructive of the LB film, and does not require the evaporation of top contacts.

The basic principle of this technique is that a vibrating probe of metal A is positioned just above a substrate of metal B; the metal surfaces can then be thought of as the two electrodes of a parallel plate capacitor. Because the two metals have different work functions, a potential difference will exist between them. If the plates are connected via an external circuit, and the distance between them is changed, there will be a change in the charge on the plates,

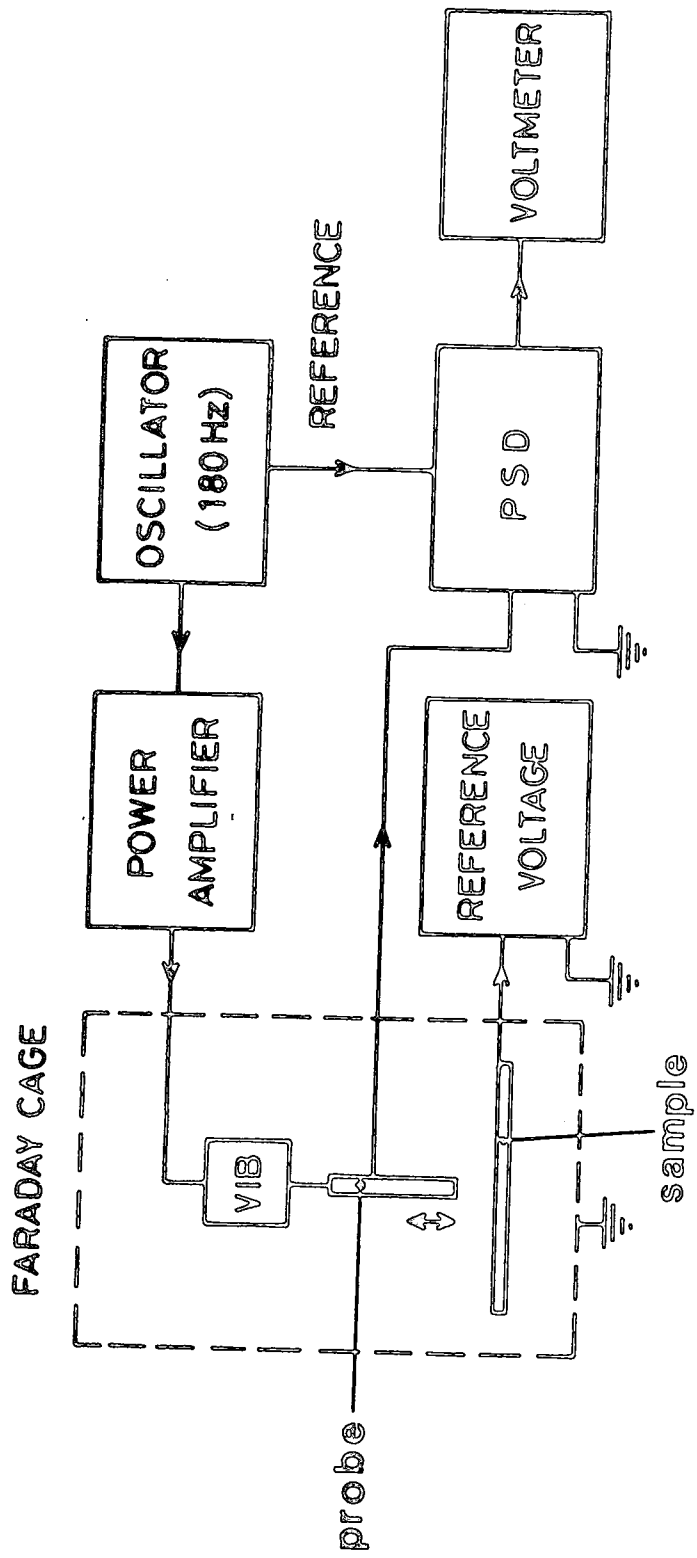


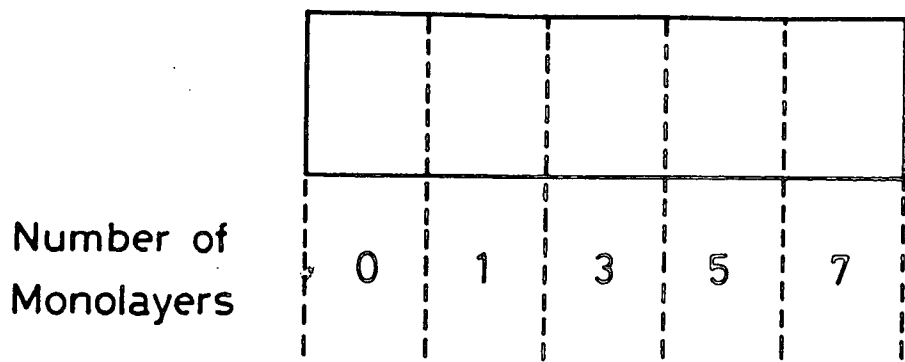
Figure 4.10 Experimental arrangement used for surface potential characterisation.



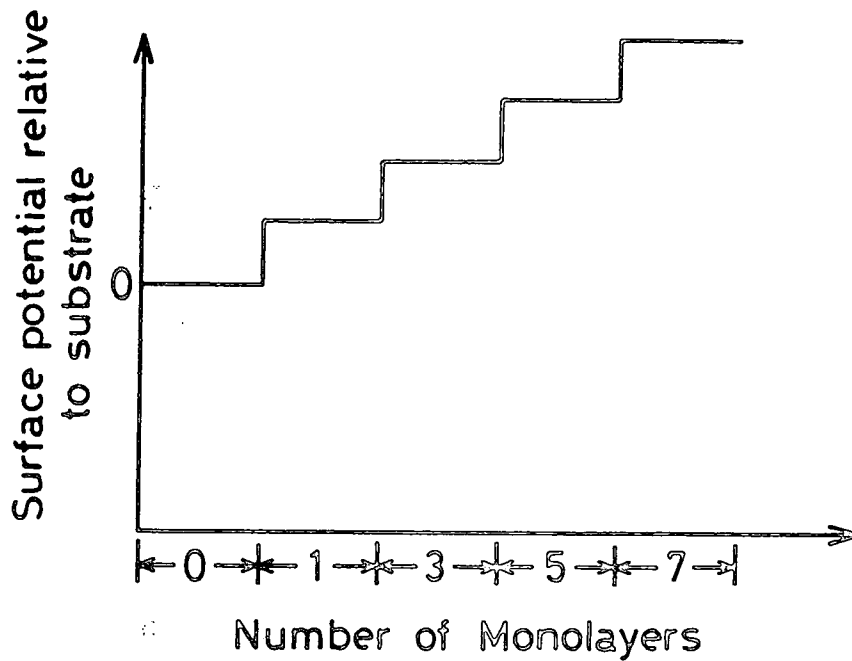
giving rise to a current in the external circuit. If the metal substrate is covered with a layer of a polar LB film, there will be an additional potential barrier to electrons moving out from the surface of the metal (ie. the work function of metal B will have been increased); this will change the potential difference between the plates. On the other hand, if the LB multilayer film is non-polar, the surface potential will be unchanged relative to the clean metal surface.

The system which was used is shown schematically in figure 4.10. The probe consisted of an inner brass electrode of diameter 2 mm, co-axially situated inside a PTFE insulating rod and an outer earthed sleeve; this sleeve served to reduce capacitative coupling between the vibrating electrode and stationary parts of the apparatus at earth potential. The probe was driven by a Gearing and Watson GWV2 vibrator unit at a frequency of 180 Hz. The height of the probe above the sample was variable; however, measurements were performed with a mean separation of about 2 mm. The unit was mounted in an earthed metal chamber (Faraday cage), which could be evacuated using a rotary pump. The a.c. voltage generated by the probe was detected by a Brookdeal 401 lock-in amplifier and displayed on a voltmeter. A null detection technique was employed, whereby a variable d.c. voltage was applied to the specimen using a Time Electronics 2003S voltage calibrator, in order to "back-off" the surface potential. This voltage was adjusted until the voltmeter on the output of the lock-in amplifier gave a zero reading; the applied voltage was then equal and opposite to the surface potential.

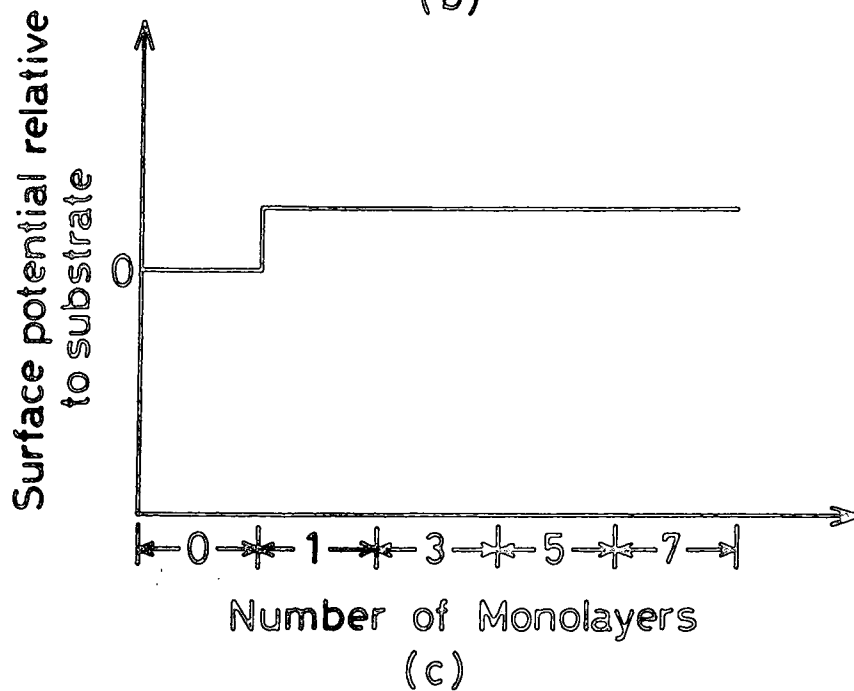
The samples used consisted of aluminised glass slides with different numbers of monolayers deposited in different regions, as shown in figure 4.11a. Initially, the probe was positioned above the clean metal part of the slide, and the surface potential was measured; this value was then taken to be the zero point, relative to which the surface potential of the LB film was measured. The probe was translated horizontally so that the surface potentials of the various regions of the sample could be measured. Figures 4.11b and c show, respectively, the surface potential profiles that would be expected for polar and non-polar multilayer films of the geometry shown in figure 4.11a. Figure 4.11c shows an initial increase in potential on depositing a single monolayer; however, no further increase occurs when additional non-polar bilayers are deposited. In figure 4.11b, on the other



(a)



(b)



(c)

Figure 4.11 (a) A typical sample used for surface potential characterisation. (b) and (c) show schematically the surface potential profiles that would be obtained from a polar and a non-polar film respectively.

hand, the dipoles in successive layers enhance one another, and the surface potential therefore increases as more layers are deposited.

#### 4.4.4 Measurement of relative permittivity

The measured capacitance,  $C_T$ , of an LB film MIM structure consists of a series combination of the capacitance of the LB film,  $C_{LB}$ , and the capacitance of the interfacial oxide layer on the lower aluminium electrode,  $C_{OX}$ . Thus,

$$\frac{1}{C_T} = \frac{1}{C_{LB}} + \frac{1}{C_{OX}}. \quad (4.2)$$

This may be re-written as

$$\frac{1}{C_T} = \frac{Nd}{\epsilon_0 \epsilon'_r A} + \frac{1}{C_{OX}} \quad (4.3)$$

where  $N$  is the number of monolayers,  $d$  is the monolayer thickness,  $\epsilon'_r$  is the real part of the relative permittivity of the LB film (also known as the dielectric constant), and  $A$  is the device area. The two capacitances may therefore be separated out by measuring  $C_T$  for a series of devices containing different numbers of monolayers. If a graph of  $(C_T)^{-1}$  versus  $N$  is plotted, the intercept will be given by  $(C_{OX})^{-1}$  and the gradient by  $d/\epsilon_0 \epsilon'_r A$ . Thus the quantity  $d/\epsilon'_r$  can be calculated from the gradient; this quantity is known as the dielectric thickness. If  $d$  is evaluated from X-ray diffraction, then  $\epsilon'_r$  can be calculated independently.

The MIM capacitors which were used were of the type described in section 4.2.2. For each material, a series of devices comprising different numbers of monolayers was fabricated. The devices were mounted in an earthed metal sample chamber, and electrical contacts were made using platinum wires and silver paste; all measurements were performed under vacuum. The capacitance was measured at 50 Hz, using an ESP 300A auto-ranging capacitance bridge. A graph of  $(C_T)^{-1}$  versus  $N$  was then plotted, from which the dielectric thickness, and ultimately the dielectric constant, was calculated.

Another important measurement was the determination of the frequency dependence of the relative permittivity, as this provides information concerning the various dielectric relaxation processes in the films [24]. These processes arise as a result of four main polarisation mechanisms which occur when an electric

field is applied to a dielectric. Electronic polarisation is due to a displacement between the centres of positive and negative charge within an atom, and occurs in all materials. Ionic polarisation occurs only in ionically bonded materials, and is the result of a shift in the positions of the positive and negative ionic sub-lattices. Dipolar relaxation occurs in materials with a permanent dipole moment, and is due to the tendency of dipoles to align with the electric field. Finally, interfacial polarisation occurs in polycrystalline materials as a result of charge accumulation at grain boundaries or other interfaces.

For each polarisation mechanism, there is a maximum frequency of applied field, above which the mechanism will no longer respond; the response is then said to have relaxed, and it will cease to contribute to the total polarisation. This is manifested by a decrease in the real part of the relative permittivity,  $\epsilon_r'$ , and a peak in the imaginary component,  $\epsilon_r''$ , at the relaxation frequency. Each type of mechanism is associated with a characteristic range of relaxation frequencies, as shown in figure 4.12; thus, a polarisation mechanism can be characterised by the frequency at which its relaxation occurs.

It can be shown [25] that the complex permittivity,  $\epsilon_r$ , of a dielectric in a capacitor at frequency  $\omega$  is given by

$$\epsilon_r = \frac{Gz}{j\omega A\epsilon_0} + \frac{Cz}{A\epsilon_0} \quad (4.4)$$

where  $G$  and  $C$  are the measured a.c. conductance and capacitance,  $z$  is the thickness of the capacitor and  $A$  the area.\* If equation 4.4 is separated into real and imaginary components, then it can be seen that:

$$\epsilon_r' \propto C$$

$$\epsilon_r'' \propto \frac{G}{\omega}$$

Thus, the frequency response of the relative permittivity can be investigated by measuring the capacitance and conductance as functions of frequency.

The experimental arrangement which was used is shown in figure 4.13. The sample was excited by an a.c. voltage of variable frequency. The small a.c. current which resulted was measured by a Brookdeal Ortholoc 9502 two

---

\* Assuming no d.c. conductance.

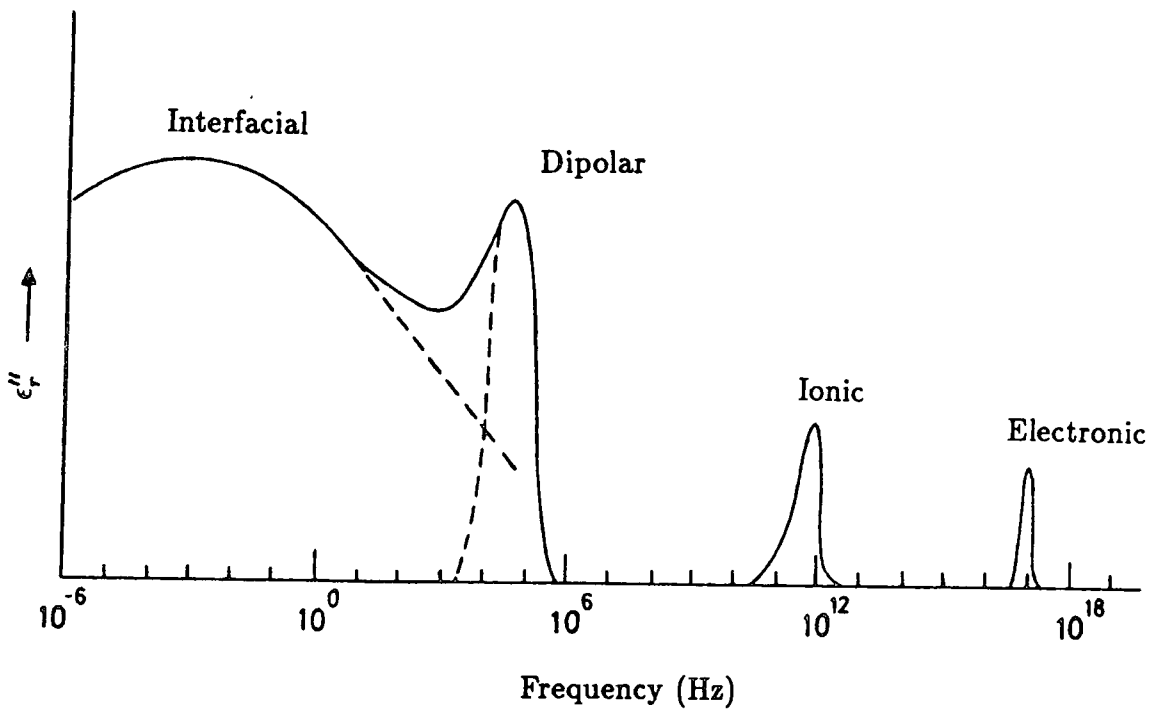
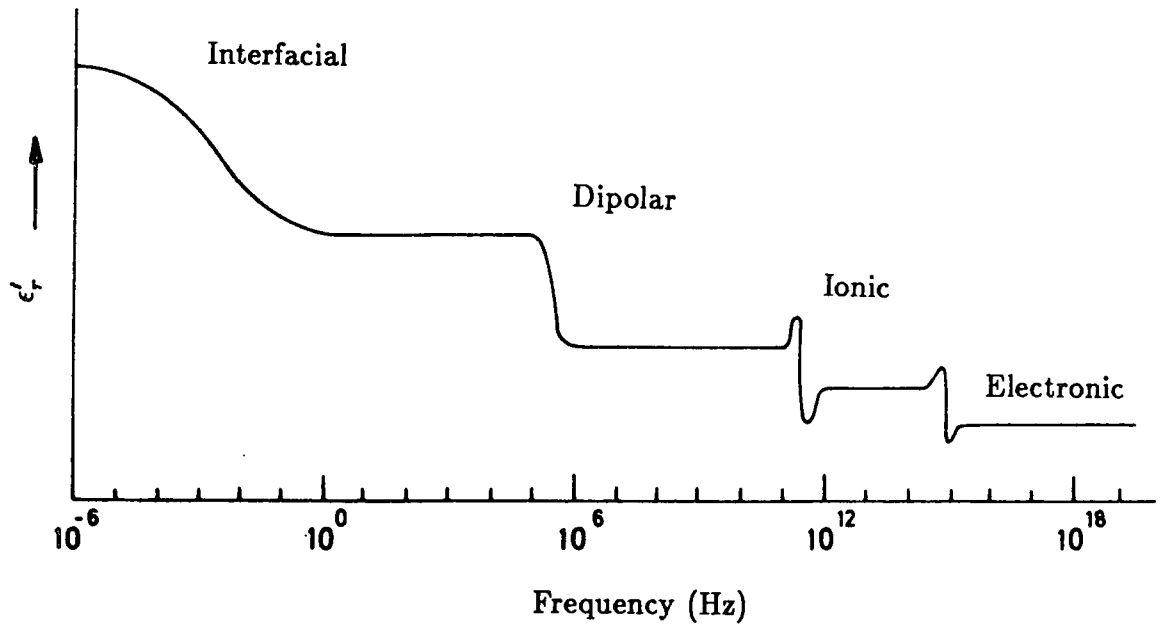


Figure 4.12 Schematic diagram showing the frequency dependence of the real and imaginary parts of the relative permittivity; the various relaxation processes are indicated.

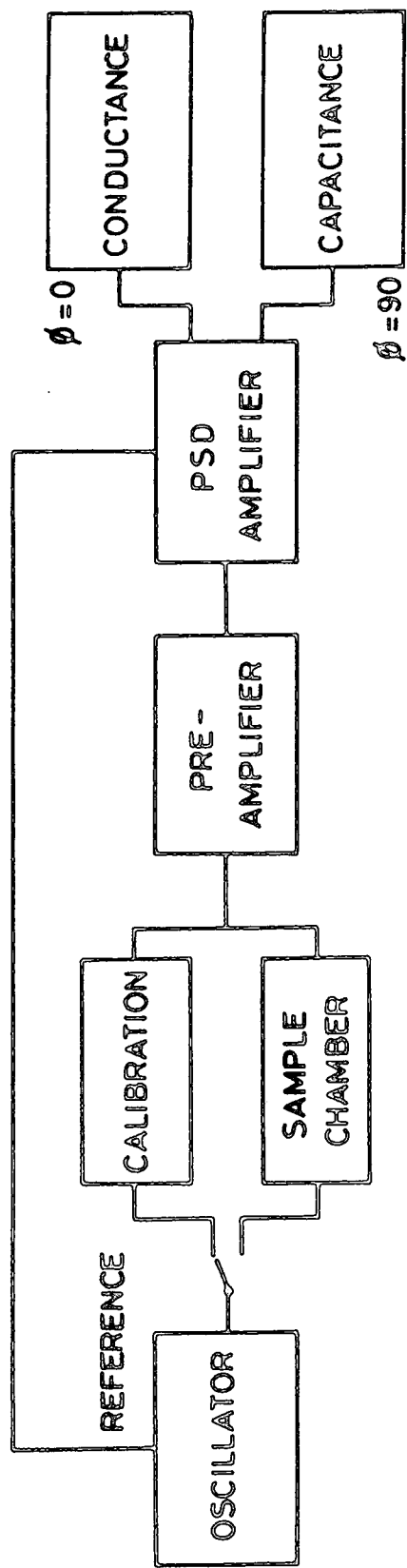


Figure 4.13 Experimental arrangement used for studying the frequency dependence of the relative permittivity.

phase lock-in amplifier; this instrument resolved the current into two components which were in-phase and out-of-phase with the driving signal. These are in turn proportional to the conductance and capacitance. The system was calibrated at each frequency using standard capacitors and resistors.

#### **4.4.5 Thermally stimulated discharge**

If a polar dielectric in the form of a parallel plate capacitor is heated to temperatures approaching its melting point, charge is released due to three principal mechanisms, namely excess charge motion, dipole reorientation and Ohmic conduction. The first of these processes is due to the unintentional incorporation of charges during the production of the device; as the sample is heated, the charges become more mobile and diffuse towards the electrodes, where they can be released into an external circuit. The second process, dipole reorientation is the thermal agitation of the previously well-ordered dipoles in the dielectric; this leads to a decrease in the internal polarisation, and image charges are released at the electrodes. Ohmic conduction is usually negligible in samples of high resistance.

The technique of thermally stimulated discharge (TSD) [26] involves heating a polar dielectric, and monitoring the short-circuit current as a function of temperature. If the discharge mechanisms described above occur, then a series of current peaks will be observed. These peaks may then be analysed and assigned to particular discharge mechanisms [27-31]. The equipment and technique used in the present study were virtually identical to the static pyroelectric detection experiment (section 4.4.1); the only difference being that the samples were heated to much higher temperatures (80°C in some cases). A chart recorder was again used to plot current and temperature as functions of time; these data were then transformed into a graph of TSD current versus temperature.

#### **4.5 SUMMARY**

The fabrication and characterisation of pyroelectric LB film devices have been described. Structural and chemical information concerning the orientation of the molecules and the nature of the bonding within the film can be obtained

using a combination of reflection high energy electron diffraction, Fourier transform infrared spectroscopy and X-ray low angle diffraction.

Static and dynamic detection systems can be used to measure the pyroelectric activity of LB films, and surface potential measurements can reveal the presence of a spontaneous polarisation. The relative permittivity can be measured either by a simple capacitance measurement, or as a function of frequency, using a phase sensitive detection system. Finally, information concerning dipolar orientation and excess trapped charge can be obtained from thermally stimulated discharge experiments.



## CHAPTER 5

### DEPOSITION AND STRUCTURAL CHARACTERISATION OF ACID/AMINE FILMS: RESULTS AND DISCUSSION

#### 5.0 INTRODUCTION

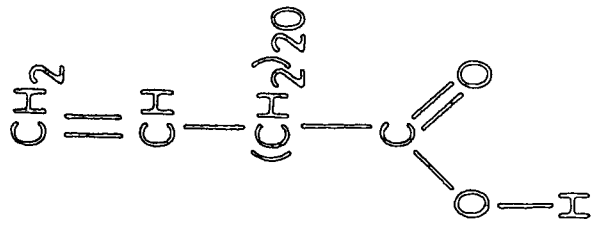
In this chapter and the two following chapters, the results of structural and electrical experiments on three different acid/amine alternate layer systems are presented and discussed. In each case, the acid used was 22-tricosenoic acid; this was alternated with three different amine derivatives. The molecular structures of the four materials are shown in figure 5.1, along with the abbreviations by which they will be known.

Chapter 5 concerns the deposition and structural characterisation of these acid/amine films. Pressure-area isotherms for the various materials, and details of film deposition are presented in section 5.1. In section 5.2 the results of infrared spectroscopic studies are discussed, and related to chemical interactions in the films. Section 5.3 describes RHEED investigations of both single material and alternate layer films. Finally, in section 5.4, X-ray diffraction data, concerning the d-spacing of acid/amine LB films, are presented.

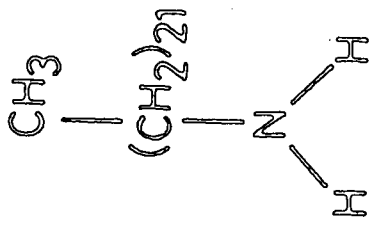
#### 5.1 FILM CHARACTERISATION AND DEPOSITION

##### 5.1.1 Pressure-area isotherms

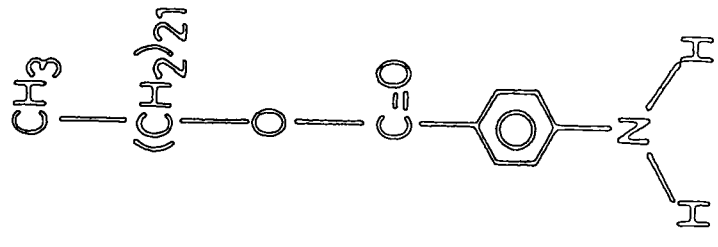
Pressure-area ( $\pi$ - $A$ ) isotherms for 22-tricosenoic acid, 1-docosylamine, docosyl 4-aminobenzoate and 4-octadecylaniline are shown in figures 5.2a, b, c and d, respectively. The isotherms were all recorded with a subphase pH of approximately 5.8, and with a compression rate of around  $2.7 \text{ cm}^2 \text{ s}^{-1}$ . It is clear that all four isotherms conform quite closely to the condensed "classical" shape, with discernible phase transitions occurring in some cases. The molecular area at zero surface pressure was calculated for each material, and compared with the value obtained from measurements on space-filling molecular models; the results are summarised in table 5.1. In each case, the measured area is smaller than the theoretical value, indicating a degree of dissolution into the subphase.



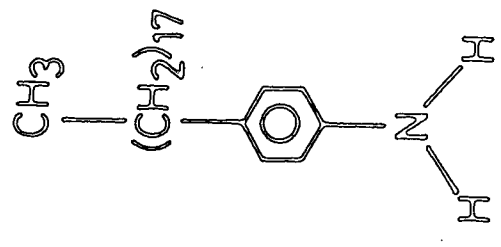
22-tricosenoic acid  
("22-TA")



1-docosylamine  
("docosylamine")

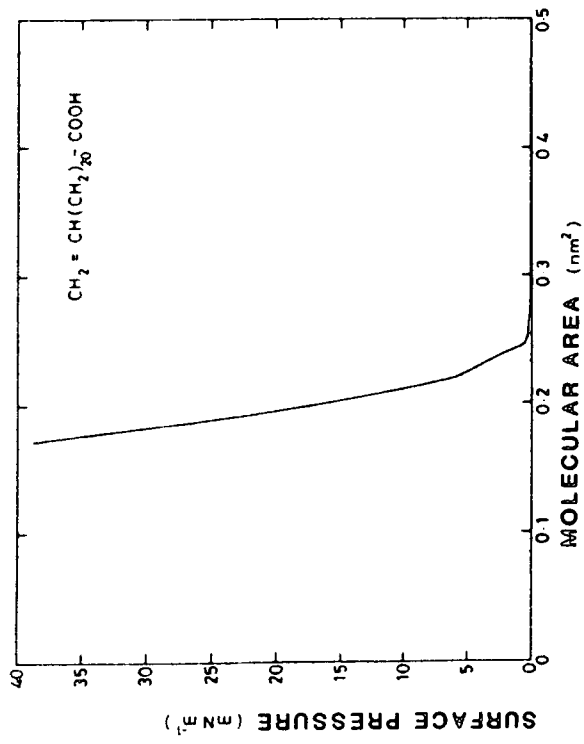


docosyl 4-aminobenzoate  
("aminobenzoate")

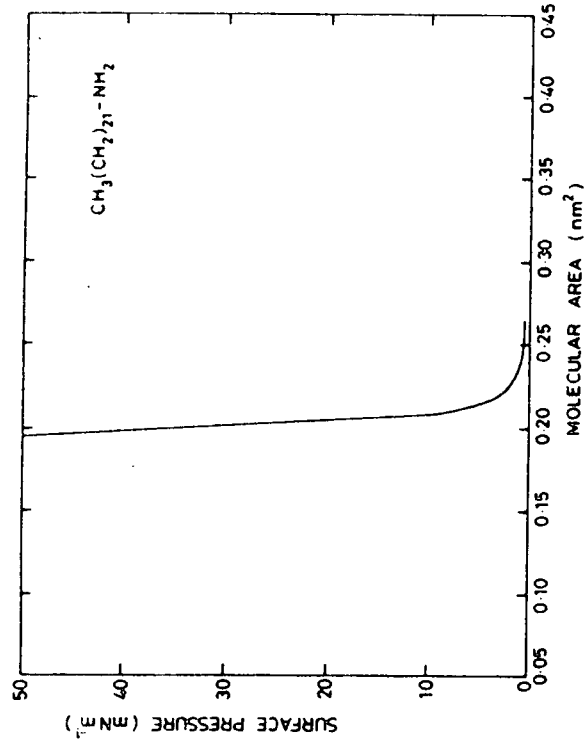


4-octadecylaniline  
("aniline")

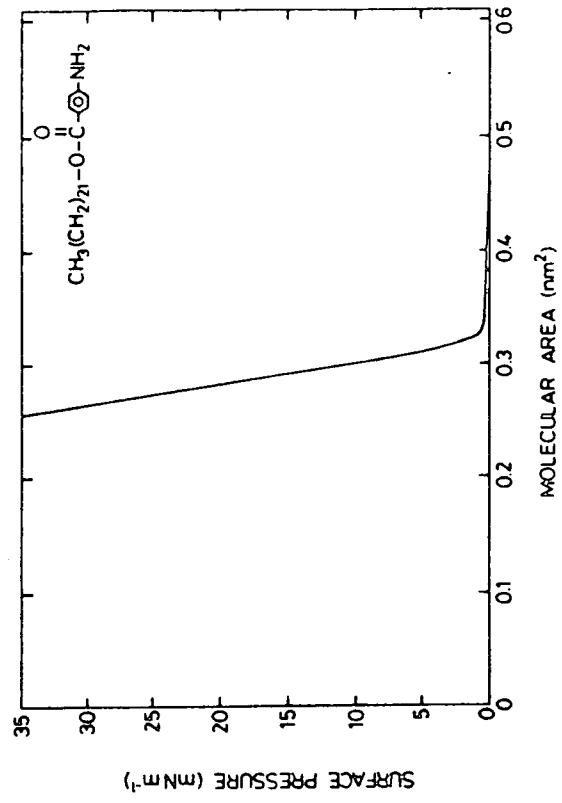
Figure 5.1 Molecular structures of the materials used in this study.



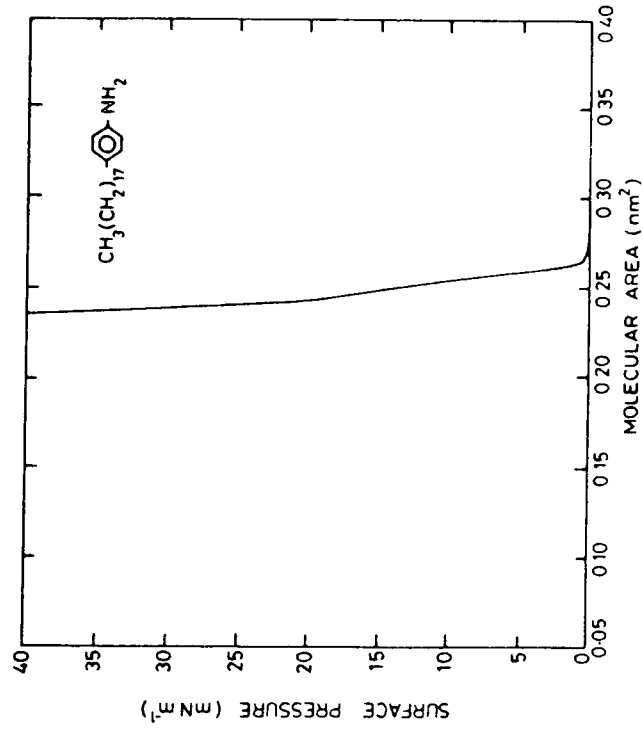
(a)



(b)



(c)



(d)

Figure 5.2 Surface pressure-area isotherms of (a) 22-tricosenoic acid, (b) 1-docosylamine, (c) docosyl 4-aminobenzoate and (d) 4-octadecylaniline.

MATERIAL	MEASURED MOLECULAR AREA (from isotherm) (nm <sup>2</sup> )	THEORETICAL MOLECULAR AREA (from models) (nm <sup>2</sup> )
22-tricosenoic acid	0.22 ± 0.01	0.24 ± 0.03
1-docosylamine	0.21 ± 0.02	0.23 ± 0.03
docosyl 4-aminobenzoate	0.32 ± 0.02	0.33 ± 0.03
4-octadecylamine	0.25 ± 0.01	0.33 ± 0.03

Table 5.1 Measured and theoretical values for molecular areas of the materials used in this study.

For the first three materials, agreement is good; however, for the aniline, the discrepancy is considerable. The reasons for the small measured value of the aniline molecular area are unclear. Dissolution, evaporation or collapse of the monolayer [1] are not the primary causes, since the surface area remained almost constant when the film was maintained at a surface pressure of  $30 \text{ mN m}^{-1}$  for a period of 30 minutes. Previous authors have reported the formation of multilayers on the water surface [2]; however, infrared spectroscopy and X-ray diffraction results, which will be presented in later sections, suggest that a true monolayer is formed in this case. It is possible that the discrepancy is due to impurities in either the aniline solid or in the chloroform solvent.

Based on the results of these isotherm studies and those of previous workers [3], values of surface pressure were chosen for film deposition.  $37 \text{ mN m}^{-1}$  was selected for 22-TA, and  $30 \text{ mN m}^{-1}$  for all of the amines. The stability of each monolayer at the appropriate surface pressure was confirmed by maintaining this pressure for a period of 30 minutes, and monitoring the surface area. All four monolayers were found to be extremely stable; this is illustrated in table 5.2, which gives the percentage decrease in the area occupied by the monolayers during the 30 minute period.

### 5.1.2 Film deposition and device fabrication

It was stated in section 4.1.4 that the first layer was always deposited at a very slow rate, and that this was followed by a 30 minute "draining" period, after which subsequent layers could be deposited faster. The actual substrate speeds employed are given in table 5.3. After deposition of the first layer, 22-TA/docosylamine and 22-TA/aniline films could be deposited at the maximum attainable speed of  $52 \text{ mm min}^{-1}$ ; however, deposition of 22-TA/aminobenzoate had to be performed much more slowly in order to maintain high deposition ratios. In each case, the acid was deposited first, as this was found to produce better quality multilayers than if the amine formed the first layer. Also, the best films were produced by depositing the amine when the substrate was moving into the water and the acid when it was being withdrawn. The deposition ratios were close to unity for all the materials, but were slightly lower for the amine

MATERIAL	SURFACE PRESSURE ( $\text{mN m}^{-1}$ )	% MOLECULES REMAINING AFTER 30 MINUTES
22-TA	37	97
docosylamine	30	98
aminobenzoate	30	98
aniline	30	98

Table 5.2 Results of stability experiments on monolayers of the materials used in this study.

ALTERNATE LAYER SYSTEM	DEPOSITION RATE FOR FIRST LAYER (mm/min)	DEPOSITION RATE FOR SUBSEQUENT LAYERS (mm/min)
22-TA/docosylamine	2	52
22-TA/aminobenzoate	2	5
22-TA/aniline	2	52

Table 5.3 Deposition rates (substrate speeds) for alternate layer LB films.

than for the acid.

During the fabrication of MIM devices, it was found that there was an optimum rate for the thermal evaporation of aluminium top electrodes. Very slow evaporation led to melting of the LB film due to prolonged exposure to the red-hot tungsten source, whilst rapid evaporation also damaged the film because of the high source temperature required. The optimum rate was approximately  $0.4 \text{ nm s}^{-1}$ , and electrodes of thickness 30 nm were deposited in this way. The "stepped evaporation" technique, which has been used by previous workers for the deposition of gold electrodes [4], was found to be unnecessary in this case.

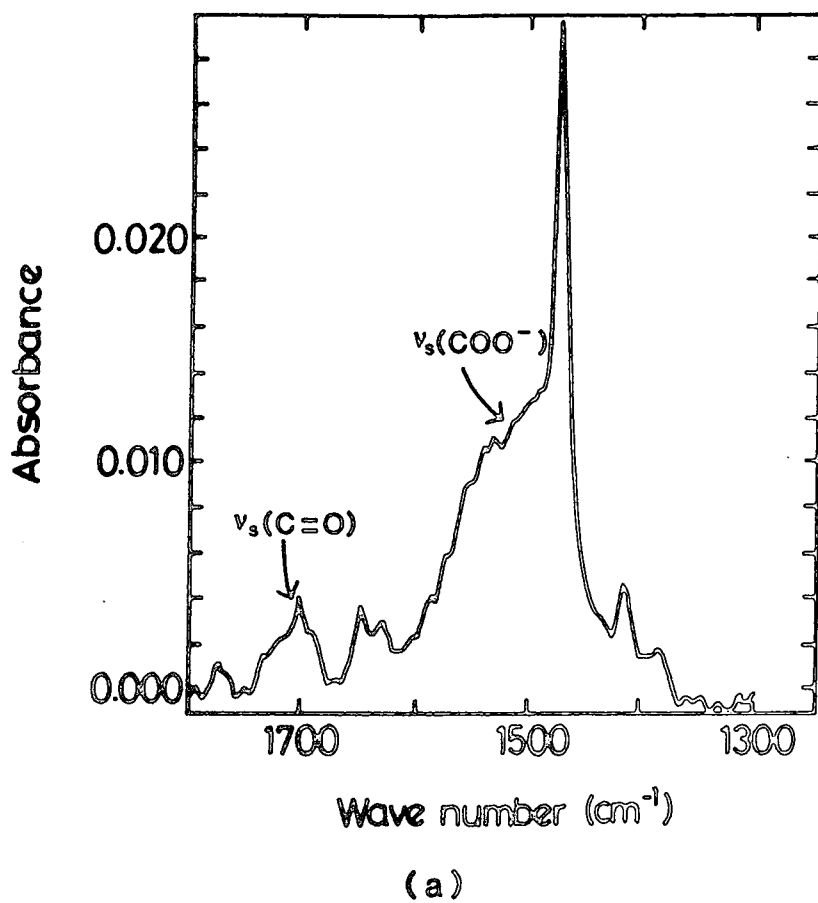
## 5.2 FOURIER TRANSFORM INFRARED SPECTROSCOPY

Detailed pyroelectric data will be presented in chapter 6; however, in order to fully interpret the infrared spectra, it is necessary to state now that no pyroelectric signal was detected in 22-TA/aminobenzoate films, whilst 22-TA/docosylamine and 22-TA/aniline films exhibited pyroelectric activity, with 22-TA/aniline showing the larger pyroelectric coefficient. The infrared spectra of the three systems are described individually in the following sections.

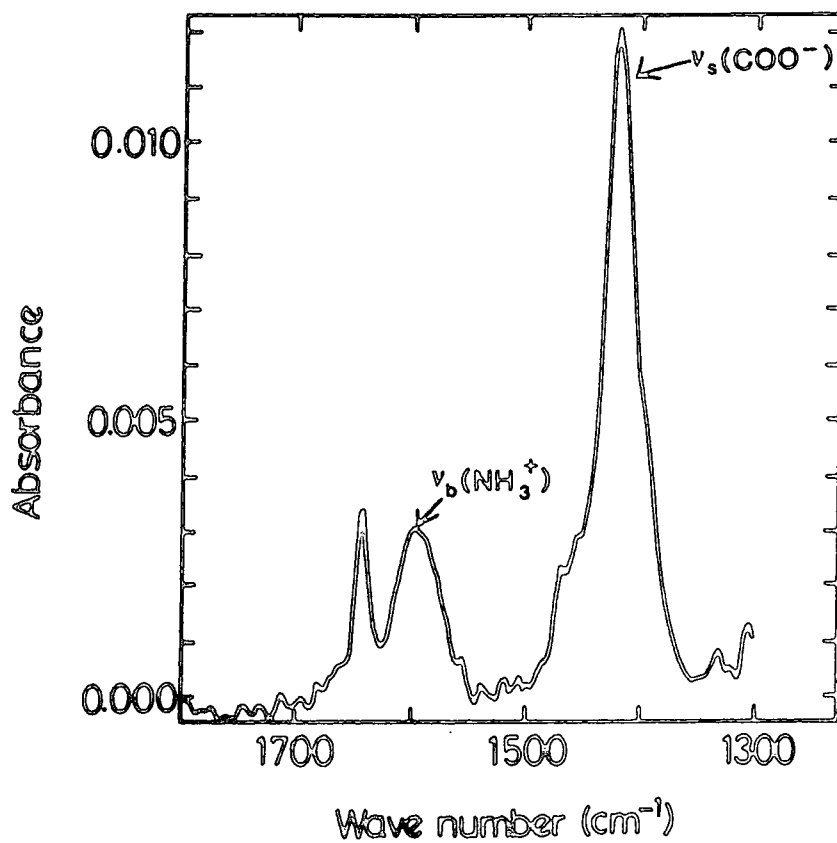
### 5.2.1 22-TA/docosylamine

The transmission and reflection absorption (RAIRS) spectra of 22-TA/docosylamine are shown in figures 5.3a and b, respectively; for comparison, the transmission spectrum of 22-TA is given in figure 5.4. It is clear that, whilst figure 5.4 has a strong absorption in the  $1700 \text{ cm}^{-1}$  region (corresponding to the acid C=O stretching vibration), this band is extremely weak in the 22-TA/docosylamine spectrum of figure 5.3a. This indicates that the acid group (RCOOH) has been largely converted to carboxylate (RCOO<sup>-</sup>), by the transfer of protons to the amine. The very broad and diffuse band in the  $1520\text{--}1580 \text{ cm}^{-1}$  region, which has been observed by previous workers [5], is partly attributable to the COO<sup>-</sup> asymmetric stretch.

The RAIRS spectrum of figure 5.3b confirms the presence of both RCOO<sup>-</sup> ( $\nu_s(\text{COO}^-)$  at  $1420 \text{ cm}^{-1}$ ) and R'NH<sub>3</sub><sup>+</sup> ( $\nu_b(\text{NH}_3^+)$  at  $1597 \text{ cm}^{-1}$ ), where  $\nu_s$  and  $\nu_b$  refer to stretching and bending vibrations, respectively. If it is assumed



(a)



(b)

Figure 5.3 (a) Transmission spectrum of a 60 layer film of 22-TA/docosylamine, (b) RAIRS spectrum of a 29 layer film of 22-TA/docosylamine.



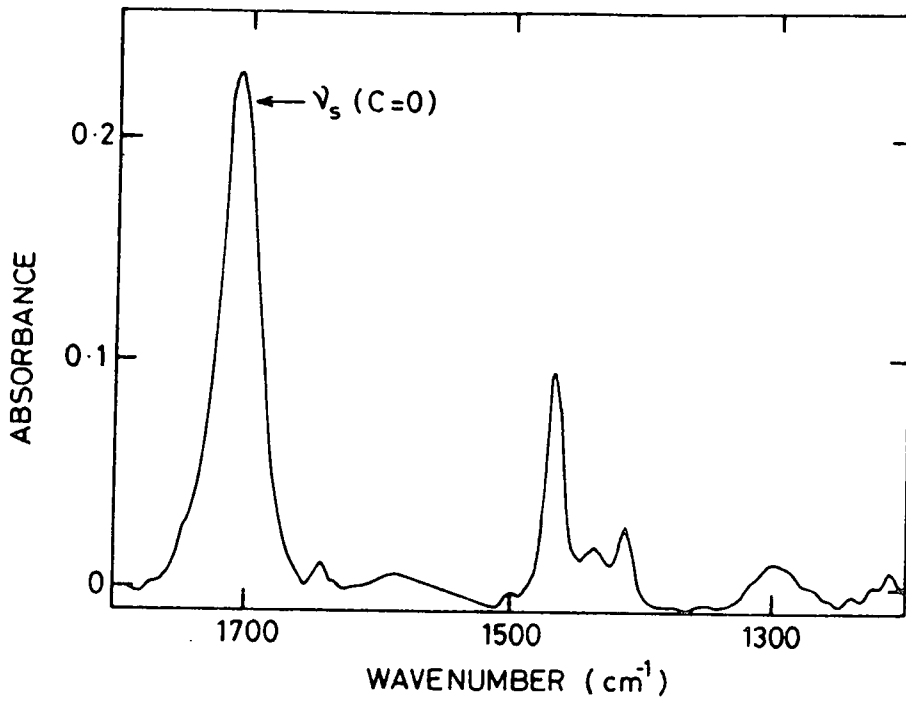


Figure 5.4 Transmission spectrum of a 21 layer film of 22-TA.

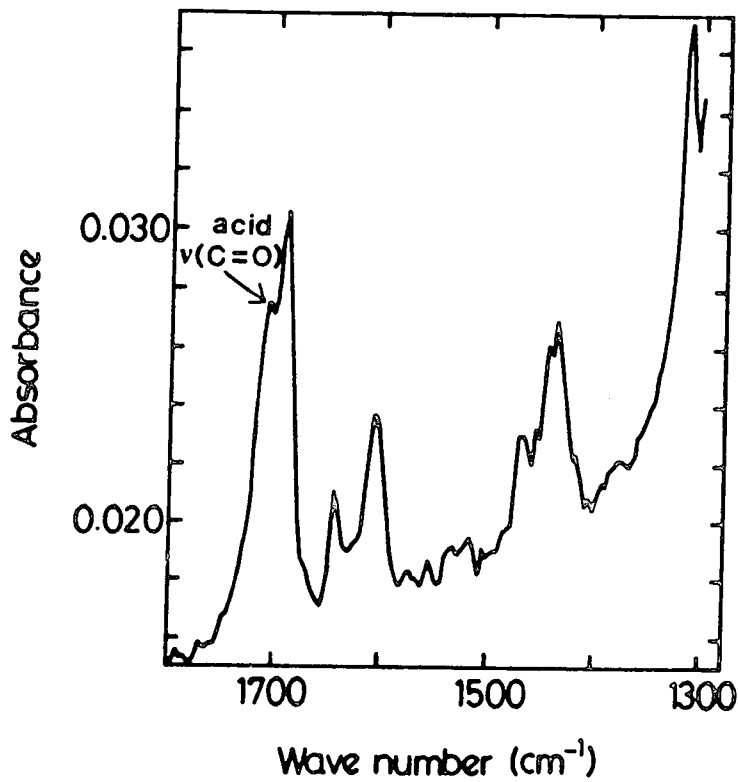


Figure 5.5 RAIRS spectrum of a 25 layer film of 22-TA/aminobenzoate.

that complete proton transfer occurs, resulting in a charge separation of 0.3 nm [5], then the dipole moment associated with the ion formation is 14 D. On the other hand, the dipole moment calculated by summing the individual dipole moments of the acid and the amine [6] is only of the order of 3 D; therefore, the polarisation in the 22-TA/docosylamine films is dominated by the presence of ions. However, it should be noted that pyroelectric activity is dependent not on the magnitude of the polarisation, but on its temperature dependence. The pyroelectric effect might, therefore, be a result of the temperature variation of the small dipole moments of the individual molecules rather than that of the larger dipole moment associated with proton transfer.

### 5.2.2 22-TA/aminobenzoate

The RAIRS spectrum of the 22-TA/aminobenzoate system is shown in figure 5.5, and provides an explanation for the absence of pyroelectric activity in these films. The strong band at  $1696\text{ cm}^{-1}$  is caused by the ester  $\nu(\text{C}=\text{O})$  vibration, but the band of particular interest is that due to the acid  $\nu(\text{C}=\text{O})$  vibration at  $1705\text{ cm}^{-1}$ . Carboxylic acids tend to dimerise through hydrogen bonding, and the geometry of the dimer depends upon the packing of the acid groups. Two types of acid dimer are commonly observed; these are known as "facing" and "sideways" dimers (figure 5.6). The type of dimerisation can be identified from the position of the acid  $\nu(\text{C}=\text{O})$  band in the infrared spectrum, since this absorption occurs around  $1705\text{ cm}^{-1}$  for facing dimers and around  $1728\text{ cm}^{-1}$  for sideways dimers [7]. It is apparent from figure 5.5, therefore, that the acid exists as facing dimers in the 22-TA/aminobenzoate system. This indicates that the molecules must have rearranged in a similar manner to that reported by Barraud *et al* [7] (figure 5.7), restoring a centrosymmetric structure to the layers and precluding pyroelectric activity. In view of the slow dipping speeds which had to be used for this system, it is likely that rearrangement occurred at the point of deposition, rather than at a later time. This reorganisation is analogous to the transformation which occurs when fatty acid salts are constrained to deposit in the X type mode; such films show a tendency to revert to the Y type structure which is adopted by bulk phase fatty acid salts [8].

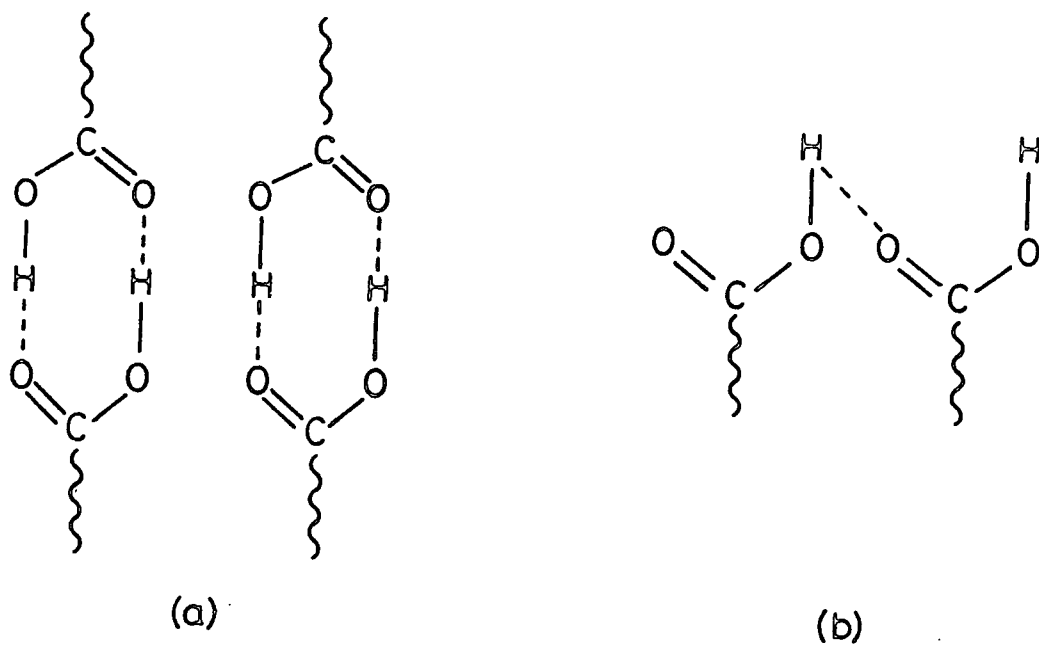


Figure 5.6 Fatty acid dimers: (a) "facing" dimers, (b) "sideways" dimers.

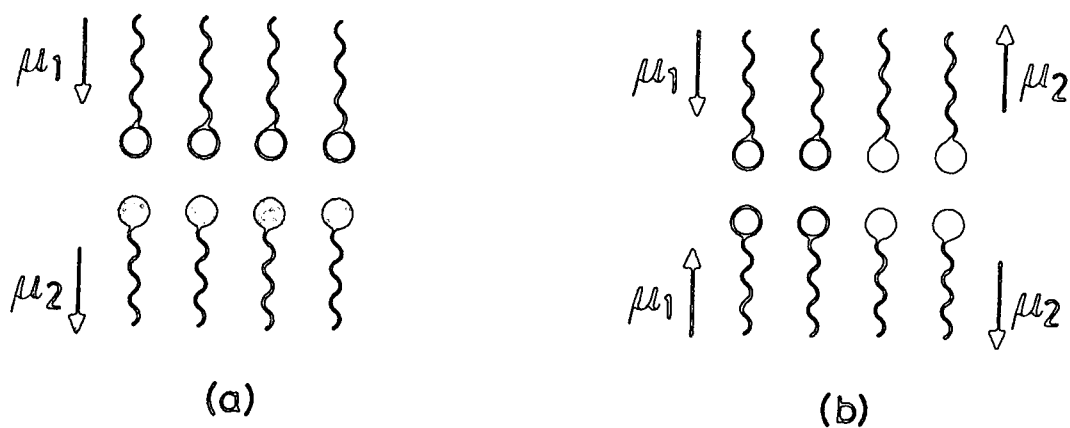


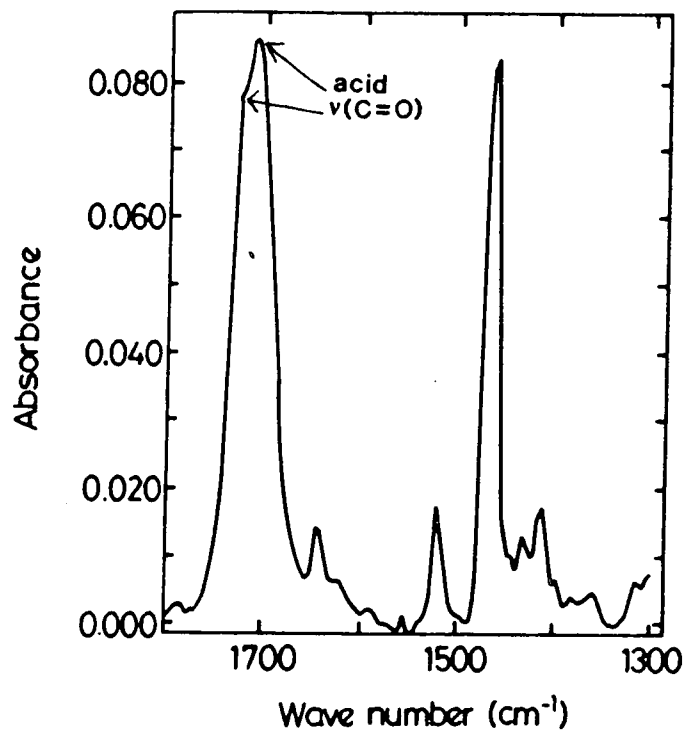
Figure 5.7 Schematic diagram of a 22-TA/aminobenzoate film, (a) before and (b) after rearrangement.  $\mu_1$  and  $\mu_2$  are the dipole moments of the acid and the amine.

### 5.2.3 22-TA/aniline

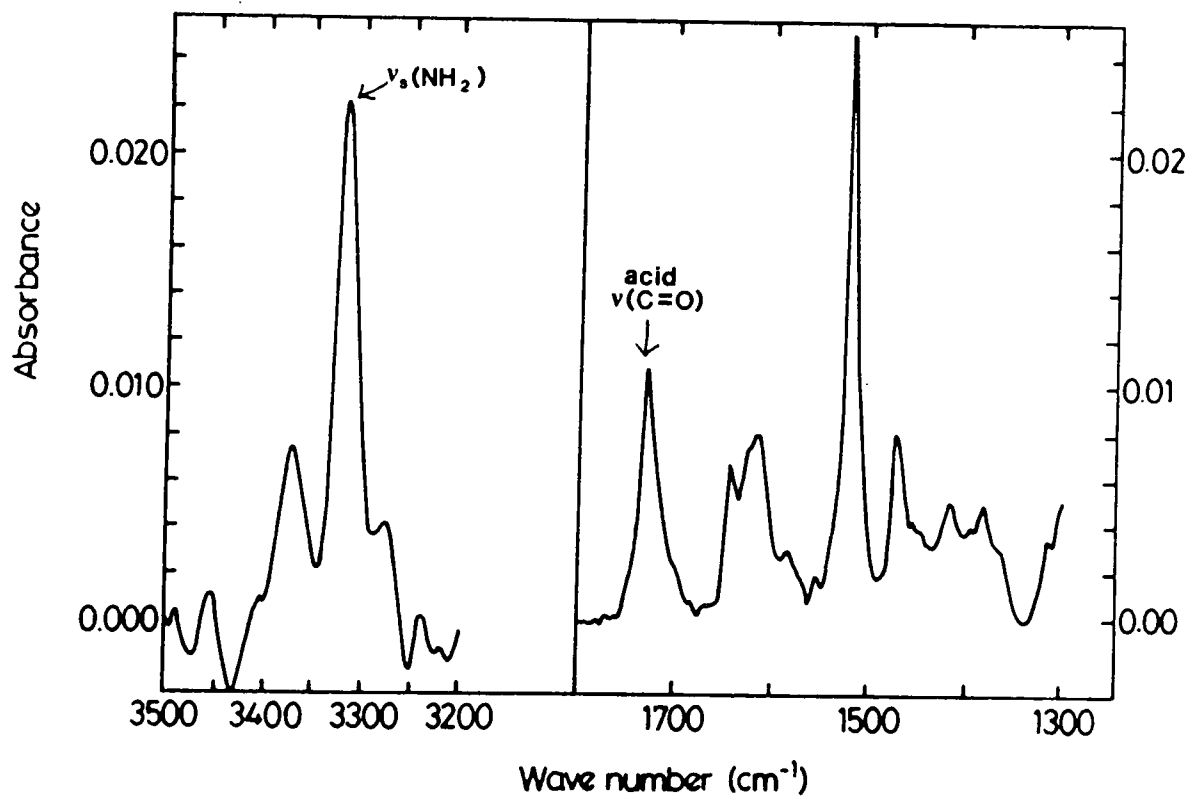
For 22-TA/aniline films, the transmission spectroscopy technique was replaced by attenuated total reflection (ATR) spectroscopy, because of the superior sensitivity and resolution of the latter technique [9]. The ATR and RAIRS spectra are shown in figures 5.8a and b, respectively. No bands assignable to the carboxylate group are present. (The bands at 1520 and 1616  $\text{cm}^{-1}$  are due to the benzene ring of the amine.) In figure 5.8b, the acid  $\nu(\text{C}=\text{O})$  band is at 1728  $\text{cm}^{-1}$ , indicating the presence of sideways dimers. Figure 5.8a, however, shows bands at 1709 and 1728  $\text{cm}^{-1}$ , implying that both sideways and facing dimers are present. The occurrence of facing dimers can be attributed to the presence of two consecutive layers of 22-TA adjacent to the substrate, in order to improve alternate layer deposition onto the ATR crystal [10]. Subtraction of the appropriate spectral density, corresponding to two layers of 22-TA, yielded the isolated 22-TA/aniline sideways dimer spectrum. The results indicate that no proton transfer has occurred, and that the molecules have not rearranged.

The region of figures 5.8a and b corresponding to  $\text{NH}_2$  vibrations contains weak but nevertheless interesting bands. The ATR spectrum of bulk aniline (figure 5.9) exhibits bands at 3372 and 3299  $\text{cm}^{-1}$ , due to the asymmetric and symmetric  $\text{NH}_2$  stretching modes, respectively. In figure 5.8b, the symmetric  $\text{NH}_2$  absorption is shifted to 3318  $\text{cm}^{-1}$ , indicating weaker interactions than in the bulk. The ATR spectrum of figure 5.8a has  $\nu(\text{NH}_2)$  bands at 3390 and 3326  $\text{cm}^{-1}$  (not shown). The cause of these shifts is unclear at present, but may be indicative of an additional hydrogen bonded  $\text{R}'\text{NH}_2$  species, of the type shown in figure 5.10. Such a hydrogen bond may be contributing to the pyroelectric effect in 22-TA/aniline films, in a similar manner to that occurring in KDP (see section 2.4.1).

It is also possible that the larger pyroelectric coefficient of the 22-TA/aniline system, relative to 22-TA/docosylamine, is related to the absence of proton transfer. In the 22-TA/docosylamine system, proton transfer leads to the formation of ions, and the layers are bound to one another by relatively strong ionic forces. In 22-TA/aniline films, on the other hand, the layers are bound only by weak hydrogen bonds, with the result that this system will be more polaris-



(a)



(b)

Figure 5.8 (a) ATR spectrum of an LB film consisting of 2 layers 22-TA and 8 alternate layers of 22-TA/aniline, (b) RAIRS spectrum of a 25 layer film of 22-TA/aniline.

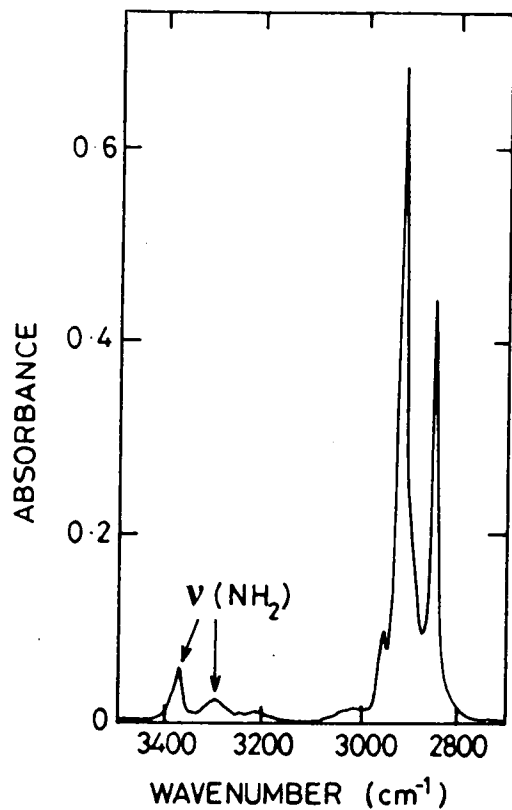


Figure 5.9 ATR spectrum of bulk aniline.

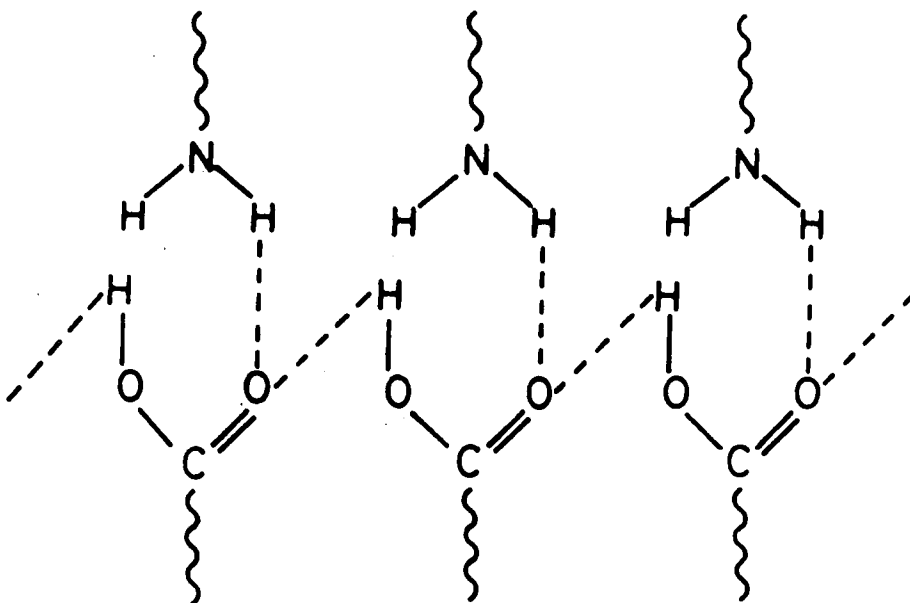


Figure 5.10 Possible hydrogen bonded species in 2,2-TA/aniline films.

able than the 22-TA/docosylamine system. Hence, it might be expected that a change in temperature would produce a larger change in the dipole moment of polarisable 22-TA/aniline films than in ionised 22-TA/docosylamine layers.

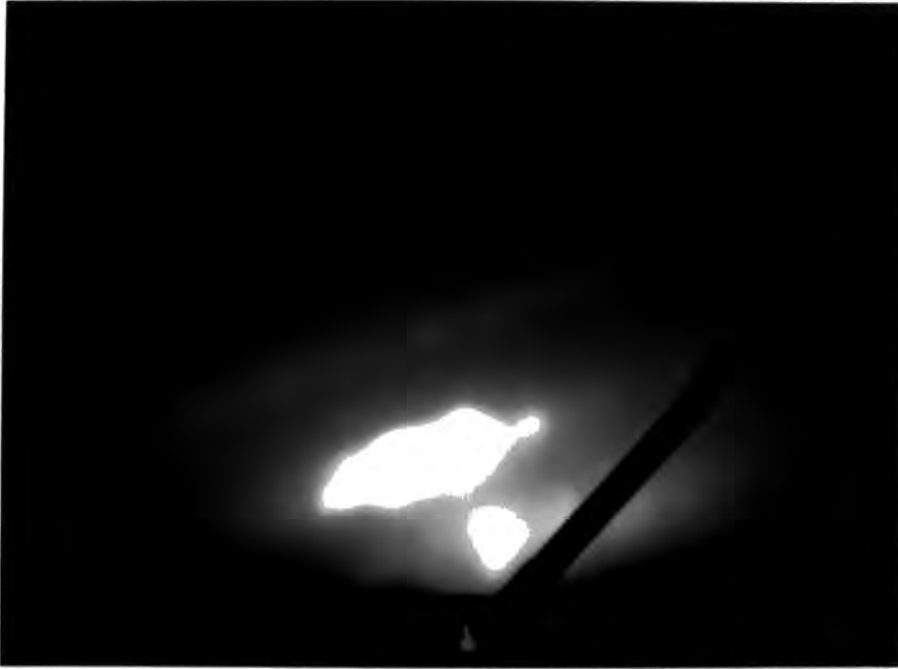
### 5.3 REFLECTION HIGH ENERGY ELECTRON DIFFRACTION

In this section, the results of two RHEED investigations are presented. The first is a general study of ultra-thin LB films comprising one to seven monolayers; 22-TA was chosen as the material for this study, since it is known to produce excellent diffraction patterns [11]. The second investigation concerns the structure of the three different acid/amine systems whose infrared spectra were described above.

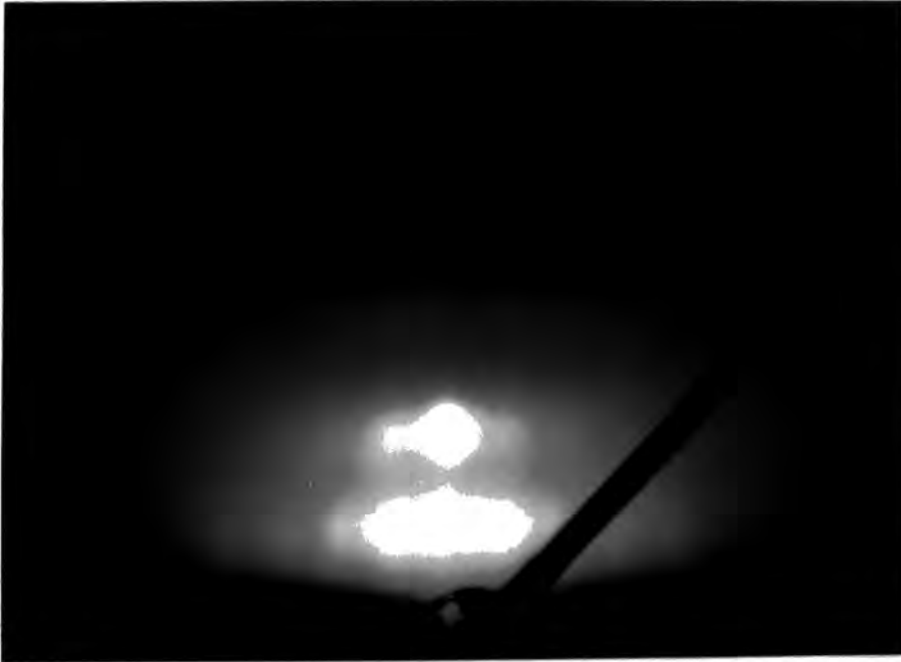
#### 5.3.1 22-tricosenoic acid

In this study, films were deposited onto hydrophilic silicon wafers of either {100} or {111} orientation; films prepared using both vertical and rotary dipping mechanisms were investigated. The RHEED patterns obtained from a seven layer film with the electron beam lying perpendicular and parallel to the direction of dipping are shown in figures 5.11a and b, respectively. The rows of diffraction spots in figure 5.11a are typically tilted at  $\sim 20^\circ$  with respect to the shadow edge of the sample, indicating that the molecular chains are inclined at a similar angle to the substrate normal. The sense of this tilt is upwards for samples dipped in the vertical plane; for rotary dipping, the sense of the tilt is upwards with respect to the substrate normal for the outward stroke. In figure 5.11b, corresponding to the beam parallel to the dipping direction, the rows of reflections are parallel to the shadow edge. This anisotropy with dipping direction has been observed in several previous studies of thicker films of fatty acid materials [12-15].

The RHEED pattern obtained from a three layer film is shown in figure 5.12; similar patterns were produced by one and five layer films. The pattern was found to be invariant as the sample was rotated about the substrate normal, indicating that there was no anisotropy with dipping direction in these very thin films. The patterns exhibit an unusual arrangement of reflections, which



(a)



(b)

Figure 5.11 RHEED patterns from 7 layer film of 22-TA on hydrophilic silicon surface, with the incident electron beam (a) perpendicular and (b) parallel to the direction of dipping.





Figure 5.12 RHEED pattern from 3 layer film of 22-TA on hydrophilic silicon surface.

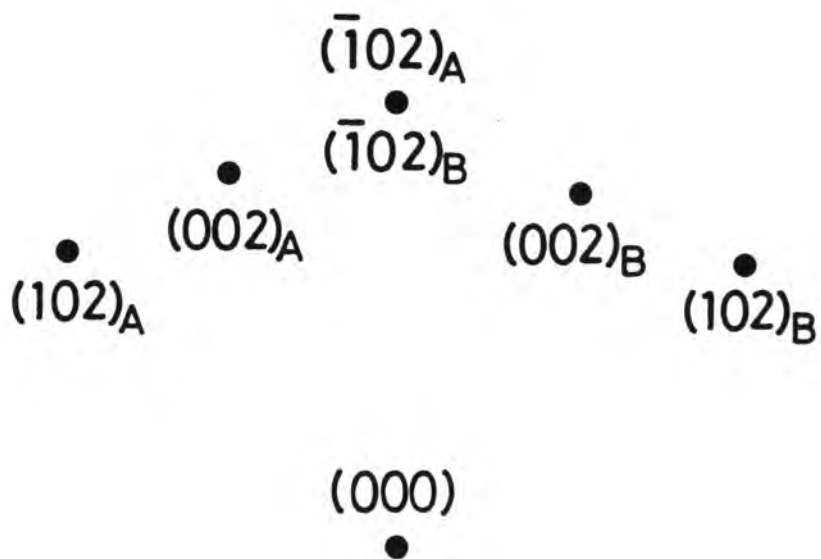


Figure 5.13 The indexing of the RHEED pattern shown in figure 5.12.

is indicative of a structure comprised of grains in which the molecular chains are all inclined at the same angle of about  $20^\circ$  to the substrate normal, but the azimuthal direction of this tilt is random, and varies from grain to grain [16]. It should be noted that the azimuthal angle of the tilt will also vary by a small amount from grain to grain in the thicker films; however, this variation is small in films comprising seven or more monolayers, and the "average" direction of the tilt is  $20^\circ$  upwards from the substrate normal, with respect to the dipping direction. The Miller indices of the most intense reflections are shown in figure 5.13 [16]. The notation used is consistent with that of Peterson and Russell [14], whereby the spots with subscript B are in mirror-image-related positions across the substrate normal to similar reflections with subscript A.

Patterns indicative of an isotropic but tilted structure were obtained from films prepared using both vertical and rotary dipping, and deposited onto both  $\{100\}$  and  $\{111\}$  silicon substrates. It was further observed that when a seven layer film, examined perpendicular to the dipping direction, was tilted so that the electron beam penetrated to a greater depth, the pattern obtained resembled a superposition of figures 5.11a and 5.12. This indicates that the isotropically distributed tilt of the first few monolayers is retained, even though subsequent layers develop a structure in which the molecules within all of the grains are preferentially tilted upwards with respect to the dipping direction.

The effect of the substrate surface on the structure of these very thin films was also investigated. Results obtained from samples dipped onto aluminium substrates showed that, as the film thickness was increased from one to seven layers, there was a progressive increase in the tilting of the molecular chains, to reach a final value of  $\sim 20^\circ$ , and the molecules were always inclined in a single direction, even for monomolecular layers; this is in agreement with the results of Bonnerot *et al* [15]. By using hydrophobic silicon wafers, it was possible to deposit even numbers of monolayers; two and four layer samples of 22-TA prepared in this manner produced RHEED patterns which showed a predominantly single direction of tilt.

Thus, the structure in the first few monolayers is critically dependent upon the chemical nature of the substrate surface. This is almost certainly due to

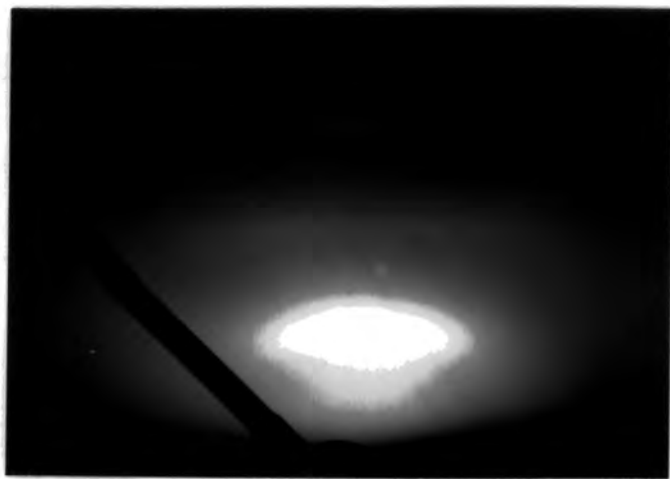
effects occurring in the interface between the substrate and the first monolayer. There is some evidence that, when deposition is such that the polar head-groups in the first monolayer are nearest to the substrate ("head-down"), this layer is chemically bonded to the substrate [17]. Films deposited onto hydrophobic silicon substrates orient in a "head-up" configuration and hence are unlikely to form chemical bonds with the substrate. Films dipped onto aluminium or hydrophilic silicon adopt a head-down arrangement, and will tend to bond to the substrate, but the type of bonds formed will, of course, be different in the two cases. Hence, it is not surprising that the structure of the first monolayer is not the same for each of the three substrates considered. According to the theory of epitaxial development [18], this initial layer will, to a large extent, determine the structure of subsequent layers.

### 5.3.2 Acid/amine alternate layers

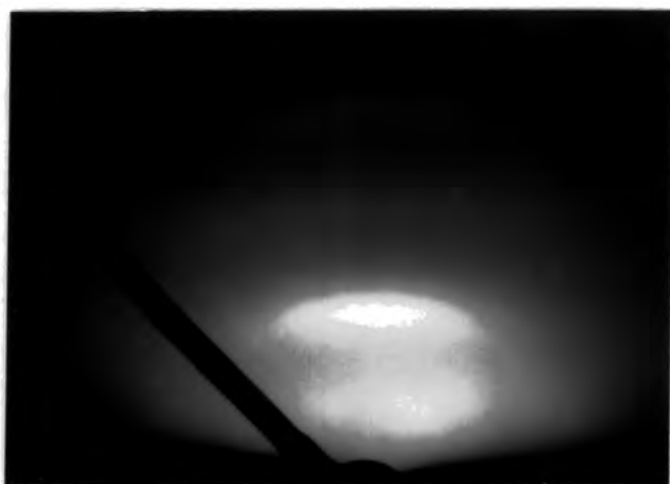
The results presented in the previous section indicate that the structure adopted by the first few monolayers of an LB film can be different from that of subsequent layers; it is therefore necessary to study films comprising at least seven monolayers in order to determine the structure of the "bulk" LB film. However, since the quality of the diffraction pattern deteriorates as the film thickness is increased, due to an accumulation of charge, very thick films cannot be used. It was therefore decided that the optimum thickness for this study of acid/amine alternate layer films would be seven layers.

The RHEED patterns for seven layer films of 22-TA/docosylamine, 22-TA/aminobenzoate and 22-TA/aniline, deposited onto silicon, are shown in figures 5.14a, b and c, respectively. In each case, the incident electron beam was perpendicular to the direction of dipping. The patterns obtained were all independent of whether silicon or aluminium substrates were used, and, in the case of 22-TA/docosylamine, it was confirmed that the structure did not depend upon whether the acid or the amine was deposited first.

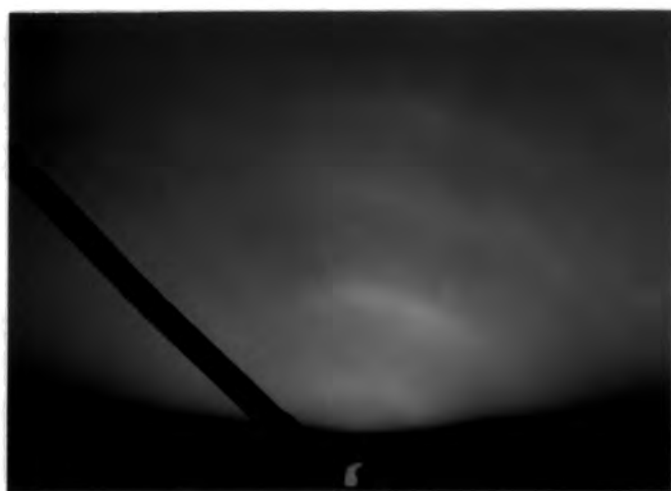
It is clear from figures 5.14a and b that, for films of 22-TA/docosylamine and of 22-TA/aminobenzoate, the molecules are oriented perpendicular to the substrate surface. In both cases, the pattern was invariant as the sample was



(a)



(b)



(c)

Figure 5.14 RHEED patterns from 7 layer films of (a) 22-TA/docosylamine, (b) 22-TA/aminobenzoate and (c) 22-TA/aniline, all on hydrophilic silicon surfaces.

rotated about the substrate normal, indicating isotropy in the substrate plane. The structure of 22-TA/aminobenzoate films will not be discussed further, since it has already been established that these films do not represent true alternate layers. Figure 5.14c shows that in 22-TA/aniline films, the molecules are inclined at  $\sim 20^\circ$  to the substrate normal; as in 7 layer 22-TA films, the sense of this tilt is upwards with respect to the outward stroke of the rotary dipping cycle. The 22-TA/docosylamine and 22-TA/aniline RHEED patterns provide evidence for an apparent relationship between structure and inter-layer bonding in LB films. It has previously been reported that LB films of pure fatty acids, in which the structure is bound together by hydrogen bonds, tend to adopt a triclinic structure, in which the molecules are tilted at  $\sim 20^\circ$  to the substrate normal [19]. However, LB films of fatty acid salts, in which ionic bonds are present, usually pack in an orthorhombic structure, with the molecules perpendicular to the substrate plane. The acid/amine films appear to follow the same pattern, since infrared spectroscopy has shown that 22-TA/docosylamine films are ionically bonded, whilst 22-TA/aniline films are bound together by hydrogen bonds.

#### 5.4 X-RAY LOW ANGLE DIFFRACTION

The X-ray diffractometer traces obtained from various 60 layer LB films are shown in figure 5.15, and the d-spacings calculated from these data are given in table 5.4. For comparison, the chain lengths of the constituent molecules, as determined from molecular models, are listed in table 5.5. The d-spacing of the 22-TA film (5.9 nm) is slightly less than twice the molecular chain length, indicating that bilayers, characteristic of a Y type film, are present, but that the molecules are tilted at a small angle,  $\theta$ , to the substrate normal, as shown in figure 5.16a. It can be shown by simple geometry that  $\theta$  is equal to  $18^\circ$ , which corresponds very closely to the value determined by electron diffraction.

The d-spacing for the 22-TA/docosylamine film (5.9 nm) is also smaller than the sum of the chain lengths of the constituent molecules. In this case, however, the discrepancy cannot be attributed to a tilting of the molecules, since RHEED experiments indicated that the molecular chains are oriented perpendicular to the substrate surface. It is also unlikely that interdigitation of the

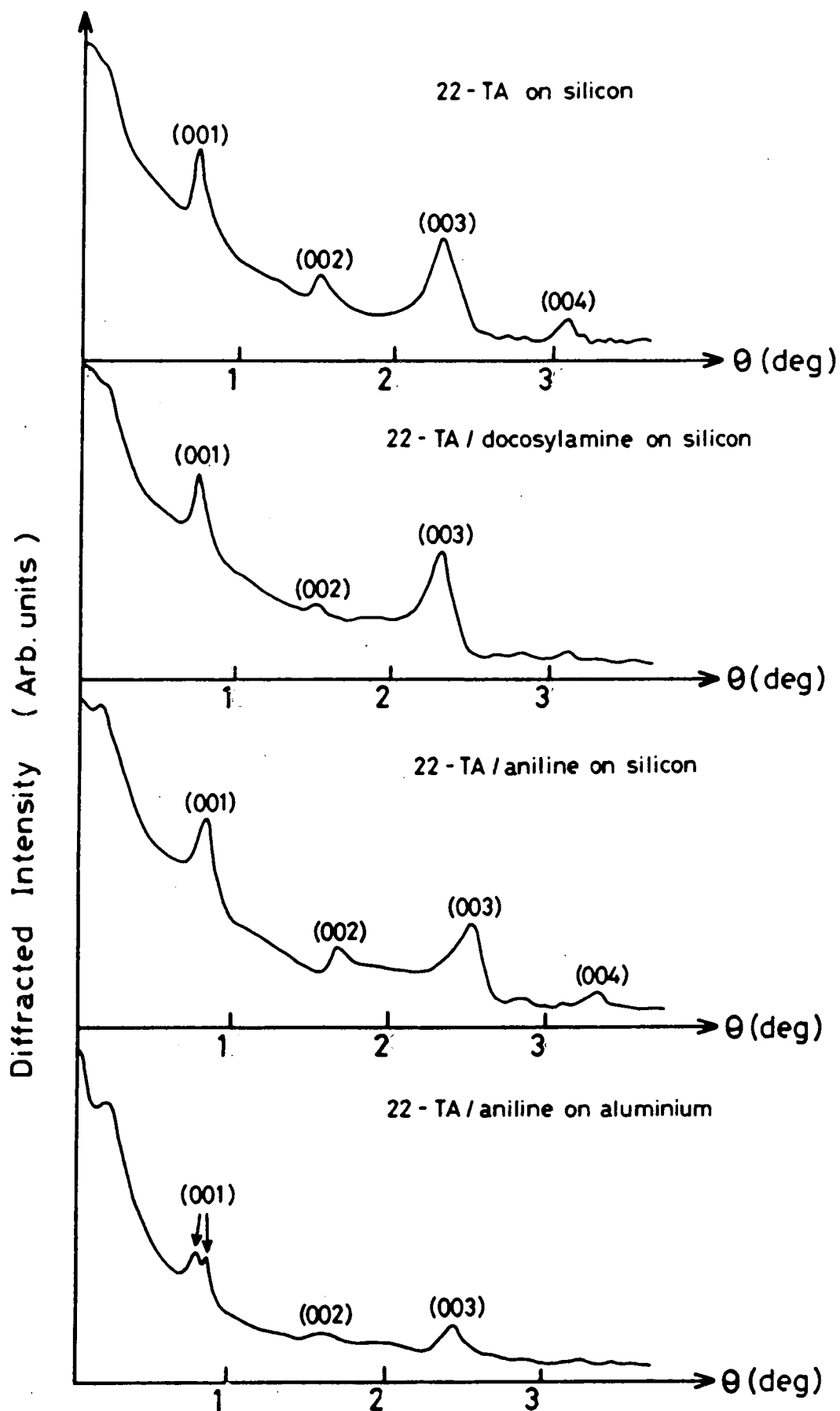


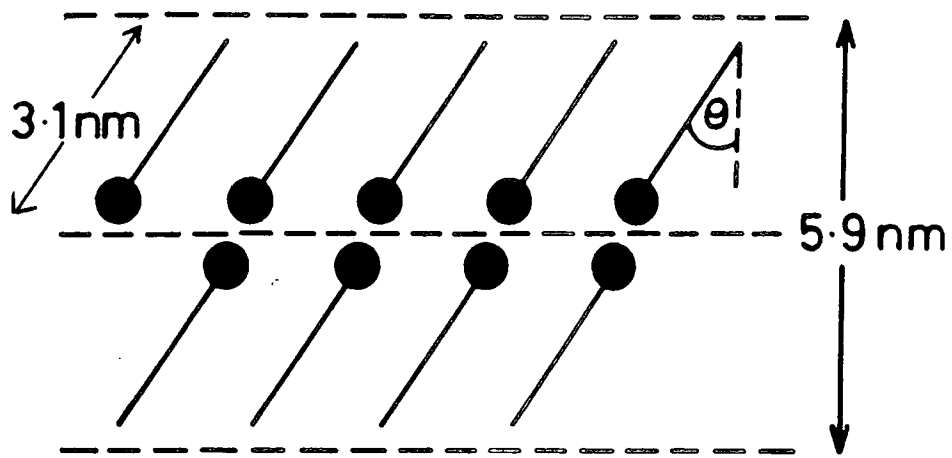
Figure 5.15 X-ray diffractometer traces from 60 layer LB films of 22-TA, 22-TA/ docosylamine and 22-TA/aniline on silicon and aluminium substrates.

MATERIAL	SUBSTRATE	d-SPACING (nm)
22-TA	silicon	$5.9 \pm 0.1$
22-TA/docosylamine	silicon	$5.9 \pm 0.1$
22-TA/aniline	silicon	$5.26 \pm 0.04$
22-TA/aniline	aluminium	$5.7 \pm 0.1$ and $5.27 \pm 0.05$

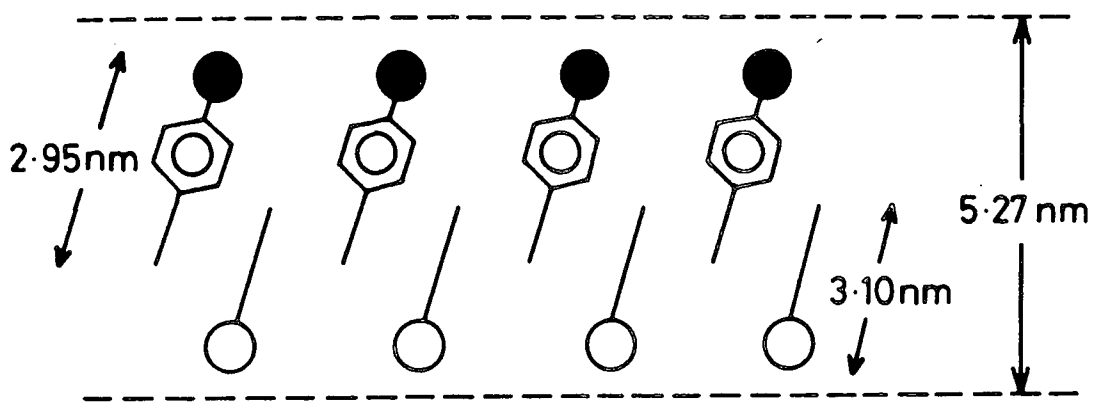
Table 5.4 d-spacings of 60 layer LB films, determined by X-ray low angle diffraction.

MATERIAL	CHAIN LENGTH (nm)
22-TA	3.1
docosylamine	3.0
aniline	2.95

Table 5.5 Molecular chain lengths of the materials used in this study, determined from molecular models.



(a)



(b)

Figure 5.16 (a) Tilting of molecules in 22-TA films; (b) interdigitation of the chains in acid/aniline alternate layer films.



hydrocarbon chains, which has previously been reported in LB films of charge transfer complexes [20], is occurring in these acid/amine films, since the head groups are insufficiently bulky to permit this. A possible explanation is that the formation of positive and negative ions through interaction between the acid and the amine leads to a slight contraction of the head groups and a decrease in the molecular lengths.

22-TA/aniline films deposited on silicon substrates gave a value of 5.26 nm for the d-spacing. However, films deposited on aluminised glass yielded two first order diffraction peaks of approximately equal intensity, corresponding to d-spacings of 5.7 and 5.27 nm. These results imply that the film exists in two different phases on an aluminium substrate, but that only one of these phases is present on a silicon substrate; this indicates again the importance of the substrate surface in determining the final structure of an LB film. RHEED experiments have shown that in 22-TA/aniline films deposited on silicon the molecules are tilted at  $\sim 20^\circ$  to the substrate normal. However, a tilting of  $20^\circ$  cannot account for the difference between the measured d-spacing (5.26 nm) and the sum of the chain lengths (6.05 nm). It is likely, therefore, that there is some chain interdigitation (figure 5.16b), due to the fact that the bulky benzene ring prevents close packing of the hydrocarbon chains. The additional phase which is present in films deposited onto aluminium substrates can be accounted for by molecules oriented at  $20^\circ$  to the substrate normal, but without interdigitation of the chains. For calculations which required a knowledge of the d-spacing in 22-TA/aniline films on aluminium substrates, an average of the values corresponding to the two phases was taken.

## 5.5 SUMMARY

Surface pressure-area isotherms and deposition conditions for three different acid/amine systems have been described. Infrared spectroscopy has shown that chemical interactions between the acid and the amine are different in the three cases: in 22-TA/docosylamine films, protons are transferred from the acid to the amine; in 22-TA/aniline, there is no proton transfer, but there is evidence for hydrogen bonding between the two materials; finally, 22-TA/aminobenzoate

alternate layer films tend to rearrange, producing a centrosymmetric structure, in which pyroelectricity is precluded.

A RHEED study of ultra-thin 22-TA films has shown that the structure in the first few layers of an LB film can be different from that of subsequent layers. It has also been demonstrated that the chemical nature of the substrate surface is of extreme importance in determining the structure adopted by an LB film. RHEED investigations of acid/amine films have revealed that the molecules in 22-TA/docosylamine films are oriented perpendicular to the substrate, whilst those in 22-TA/aniline films are tilted at  $\sim 20^\circ$  to the substrate normal. Finally, XRLAD has shown that there is some evidence for chain interdigitation and for the existence of two different phases in 22-TA/aniline alternate layer films.

## CHAPTER 6

### DIELECTRIC AND PYROELECTRIC CHARACTERISATION OF ACID/AMINE FILMS: RESULTS AND DISCUSSION, PART I

#### 6.0 INTRODUCTION

The results presented in this chapter fall into two main areas, namely, dielectric and pyroelectric characterisation of acid/amine alternate layer films. The dielectric data are presented in section 6.1, and include the measurement of  $\epsilon'_r$ , and of its temperature and frequency dependence, for both 22-TA/docosylamine and 22-TA/aniline films. In section 6.2 the results of static and dynamic pyroelectric experiments on these films are presented, and the effects of film thickness and of substrate thickness and thermal expansion coefficient are discussed.

#### 6.1 DIELECTRIC CHARACTERISATION

##### 6.1.1 Determination of $\epsilon'_r$

Plots of reciprocal capacitance (at 50 Hz) versus number of monolayers for 22-TA/docosylamine and 22-TA/aniline films are shown in figure 6.1. Both graphs comply well with the predicted straight line, indicating the reproducibility of capacitance, and hence of thickness, in successive monolayers. The two graphs intercept the Y-axis at approximately the same point, indicating a common dielectric thickness for the interfacial oxide layer of around 1 nm; this value is in reasonable agreement with those obtained by previous workers [1].

The gradients of the two graphs yield values of 1.05 nm and 0.95 nm for the dielectric thicknesses of the 22-TA/docosylamine and 22-TA/aniline films, respectively. If the values of d-spacing determined by XRLAD are used, these correspond to dielectric constants of 2.8 for the 22-TA/docosylamine and 2.9 for the 22-TA/aniline film. In general, the dielectric constants of LB film amphiphiles decrease as the length of the hydrocarbon chain increases [2], due to the weaker influence of the highly polarisable head group. It might therefore be expected that the relatively long chains of the 22-TA and docosylamine molecules would lead to lower dielectric constants than for films of shorter chain materials

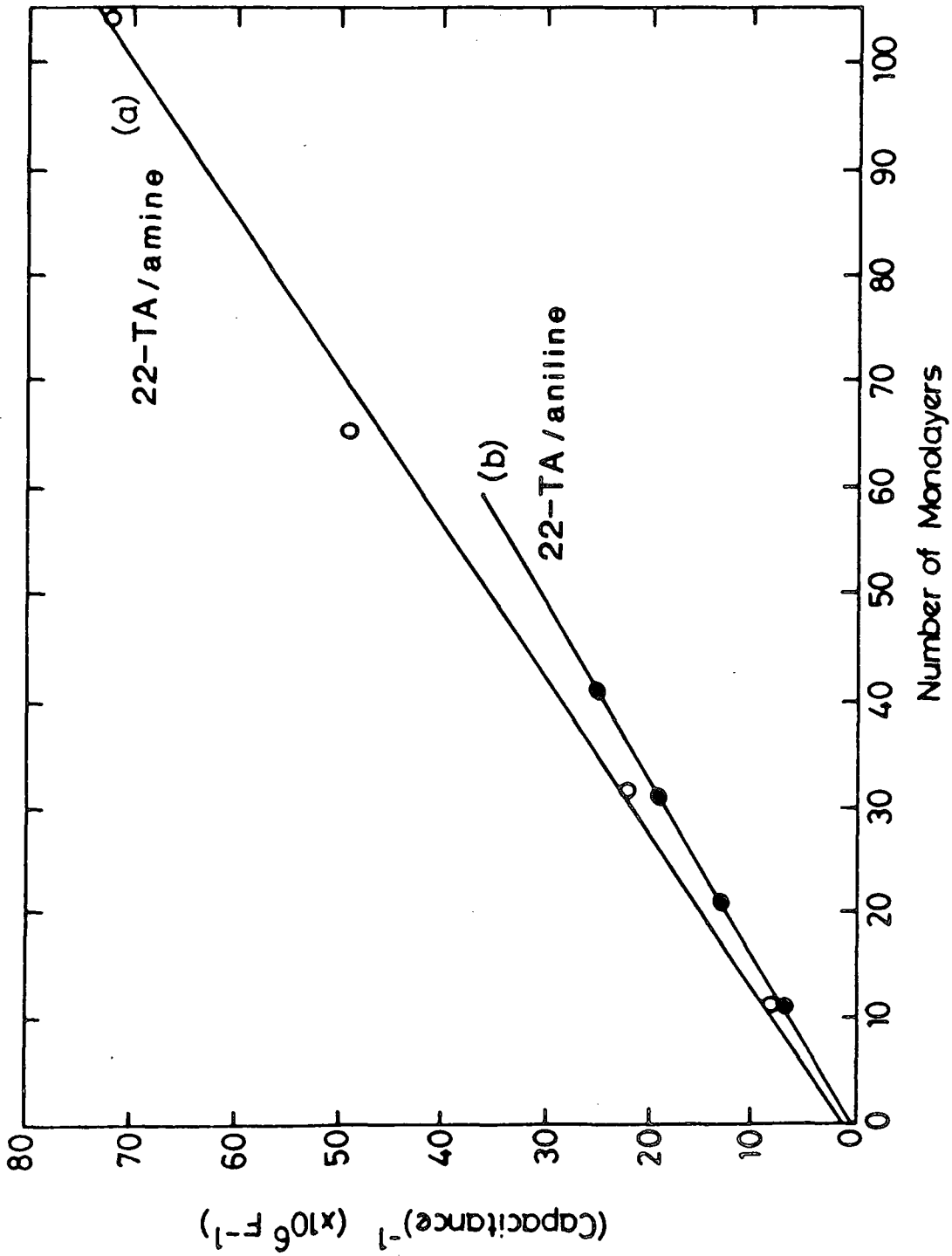


Figure 6.1 Reciprocal capacitance versus number of monolayers plot for (a) 22-TA/  
docosylamine and (b) 22-TA/aniline films.

such as stearic acid. However, the literature value for the dielectric constant of stearic acid is 2.6 [2, 4]. The fact that  $\epsilon'_r$  is greater for the acid/amine films may be indicative of an additional dipolar polarisation mechanism in the non-centrosymmetric alternate layers. However, a wider range of polar and non-polar films will have to be studied before firm conclusions can be reached.

### 6.1.2 Temperature dependence of $\epsilon'_r$

The temperature dependence of the dielectric constant was studied in the range 77–300 K, by measuring the capacitance of the devices as they were heated in a gas exchange cryostat. For both 22-TA/docosylamine and 22-TA/aniline films, the capacitance was constant to within 1% of its room temperature value over the entire temperature range, implying that no structural or chemical phase changes occur within this range. This has important consequences for the pyroelectric evaluation of the films. It was shown in chapter 2 that most conventional pyroelectrics have relatively large dielectric constants, which diverge rapidly near the Curie temperature if the material is also ferroelectric; this results in low values for the pyroelectric figure of merit,  $p/\epsilon'_r$ . The very low dielectric constant of LB films, and the consistency with temperature therefore represent an important advantage of pyroelectric LB films over conventional materials.

### 6.1.3 Frequency dependence of $\epsilon_r$

Although it is possible, in principle, to use the admittance bridge described in section 4.4.4 to measure both capacitance and conductance as functions of frequency; in practice, the conductance of acid/amine films proved to be too small to measure with this system. However, it was possible to measure the relatively large values of capacitance with great precision. The capacitance data were used to calculate the real part of the relative permittivity (*ie.* the dielectric constant) as a function of frequency. Figures 6.2a and b show  $\epsilon'_r$  versus frequency plots for 31 layer films of 22-TA/docosylamine and 22-TA/aniline, respectively. The values of  $\epsilon'_r$  are all slightly higher than those calculated in section 6.1.1; this can be attributed to the fact that the dielectric thickness of the interfacial oxide layer was not subtracted in the present calculations. It is clear

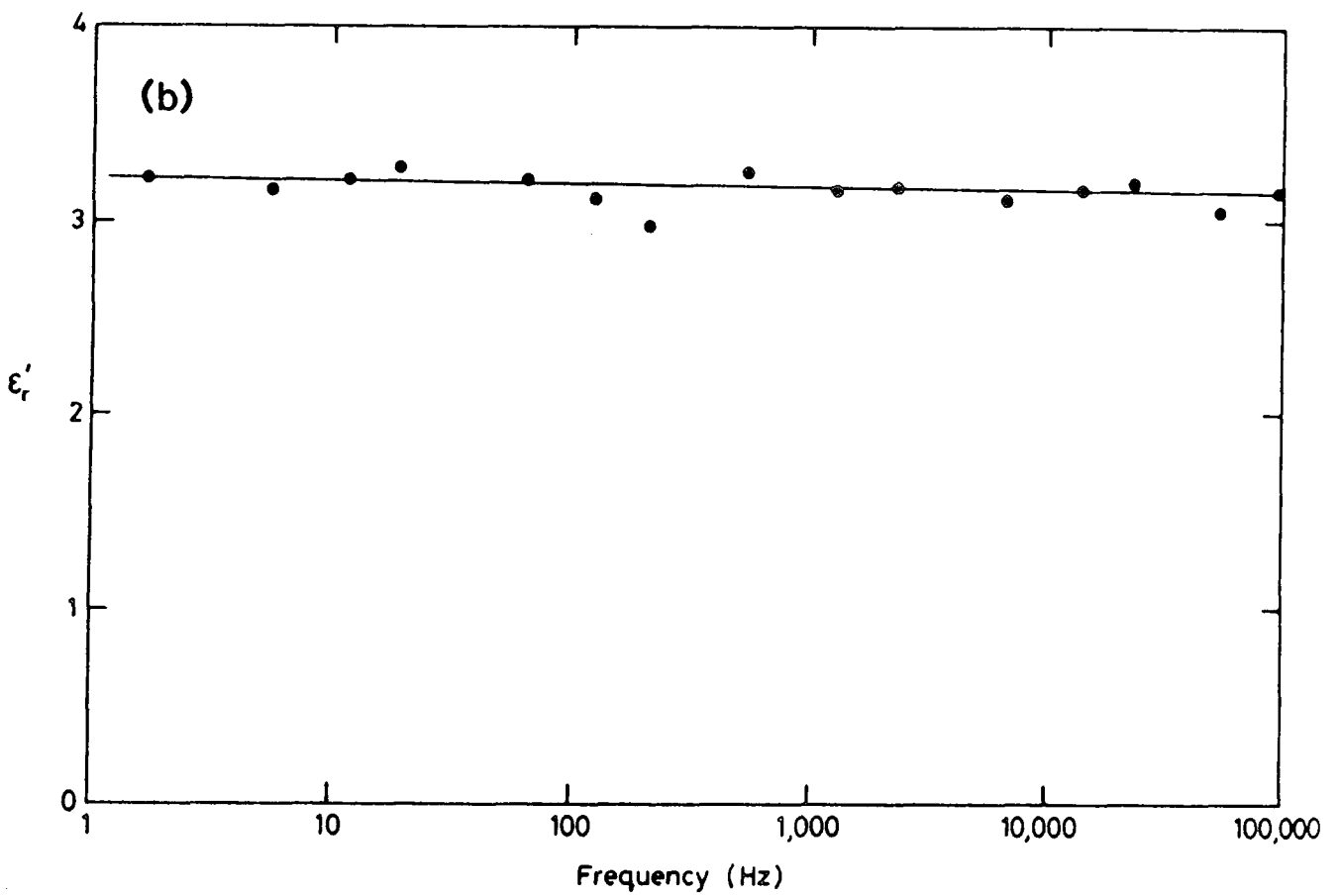
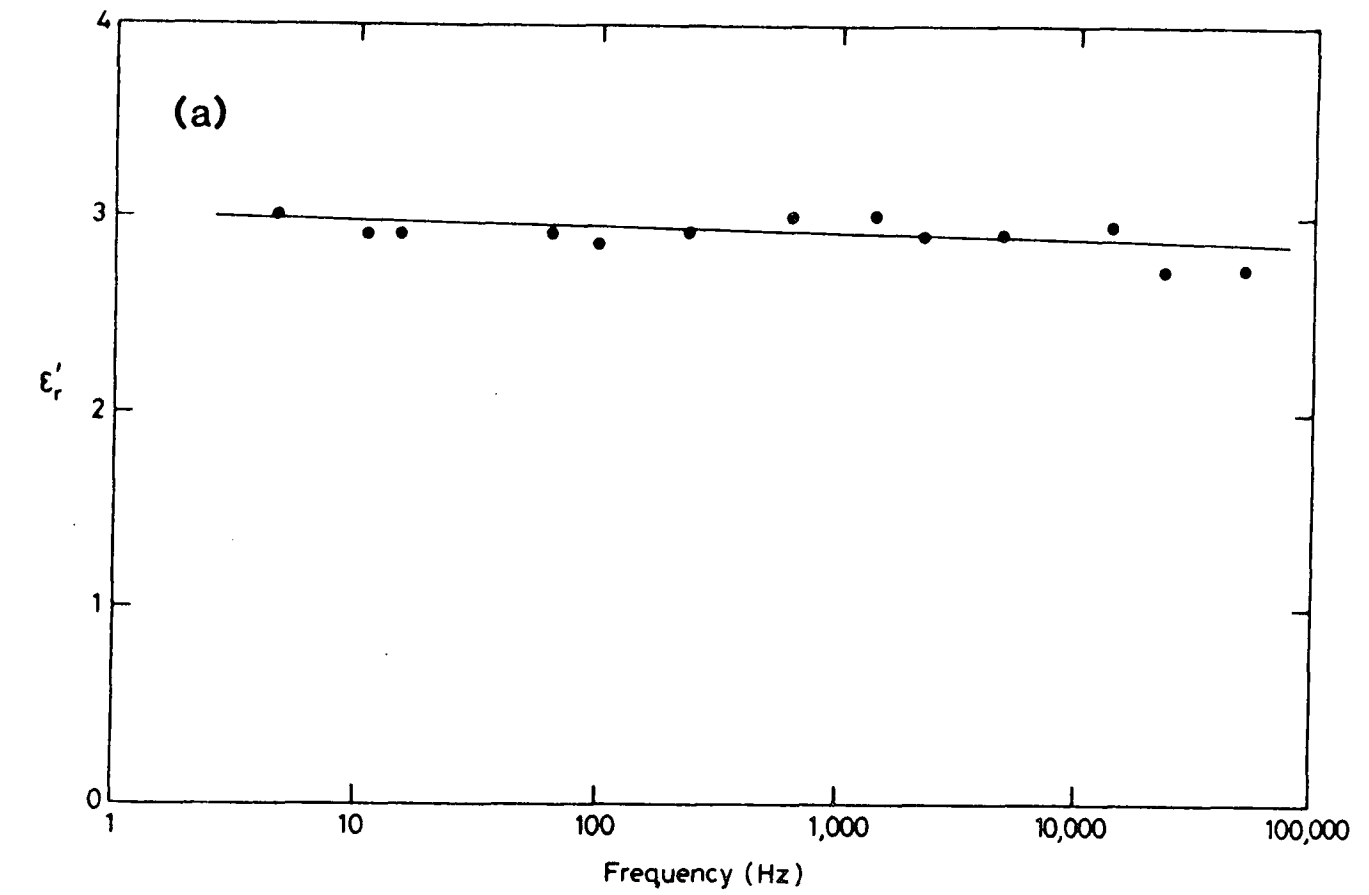


Figure 6.2 Variation of  $\epsilon'_r$  with frequency for 31 layer films of (a) 22-TA/docosylamine and (b) 22-TA/aniline.

that there is very little change in the permittivity over 5 decades of frequency, and there is no evidence for any dielectric relaxation in this frequency régime. Since dipolar relaxations generally occur at frequencies of 1–10 MHz, the only polarisation mechanism which is likely to exhibit a relaxation in the frequency range studied is the interfacial mechanism. The absence of such a relaxation is indicative of a high quality film, with very little charge accumulation at grain boundaries. Thus, it is unlikely that any pyroelectric signal is merely a tertiary effect resulting from inhomogeneous charge distribution. It should be noted, however, that a dielectric relaxation corresponding to interfacial polarisation might occur at frequencies much lower than those attainable with the present system. Indeed, previous workers [5, 6] have reported relaxations in stearic acid LB films at frequencies as low as  $10^{-5}$  Hz.

## 6.2 PYROELECTRIC MEASUREMENTS

### 6.2.1 Static and dynamic measurements

The electrical integrity of every device was assessed by measuring its electrical resistance. Only devices with a resistance in excess of  $10^{11}$   $\Omega$  were used for further experiments. The pyroelectric current obtained from a 99 layer film of 22-TA/docosylamine using the static technique is shown in figure 6.3. It is apparent that the current flows in opposite senses when the sample is heated and when it is cooled, and it can be seen that the current is proportional to the rate of change of temperature, as predicted by equation 2.1. This is strong evidence that the phenomenon observed was, indeed, pyroelectricity. Furthermore, when a control device of 22-TA, which adopts a centrosymmetric structure, was examined, no pyroelectric signal was detected.

In chapter 3, a model was developed to describe the dynamic response of an LB film pyroelectric detector. This model predicted that the measured dynamic pyroelectric voltage,  $v_m$ , is proportional to  $(\omega_0)^{-\frac{1}{2}}$ , where  $\omega_0$  is the angular modulation frequency. The validity of the model was therefore investigated by studying the frequency dependence of  $v_m$ . In figure 6.4  $v_m$  is plotted as a function of  $(\omega_0)^{-\frac{1}{2}}$  for 11 layer and 99 layer films of 22-TA/docosylamine, whilst figure 6.5 shows a similar plot for a 31 layer 22-TA/aniline film. Both graphs

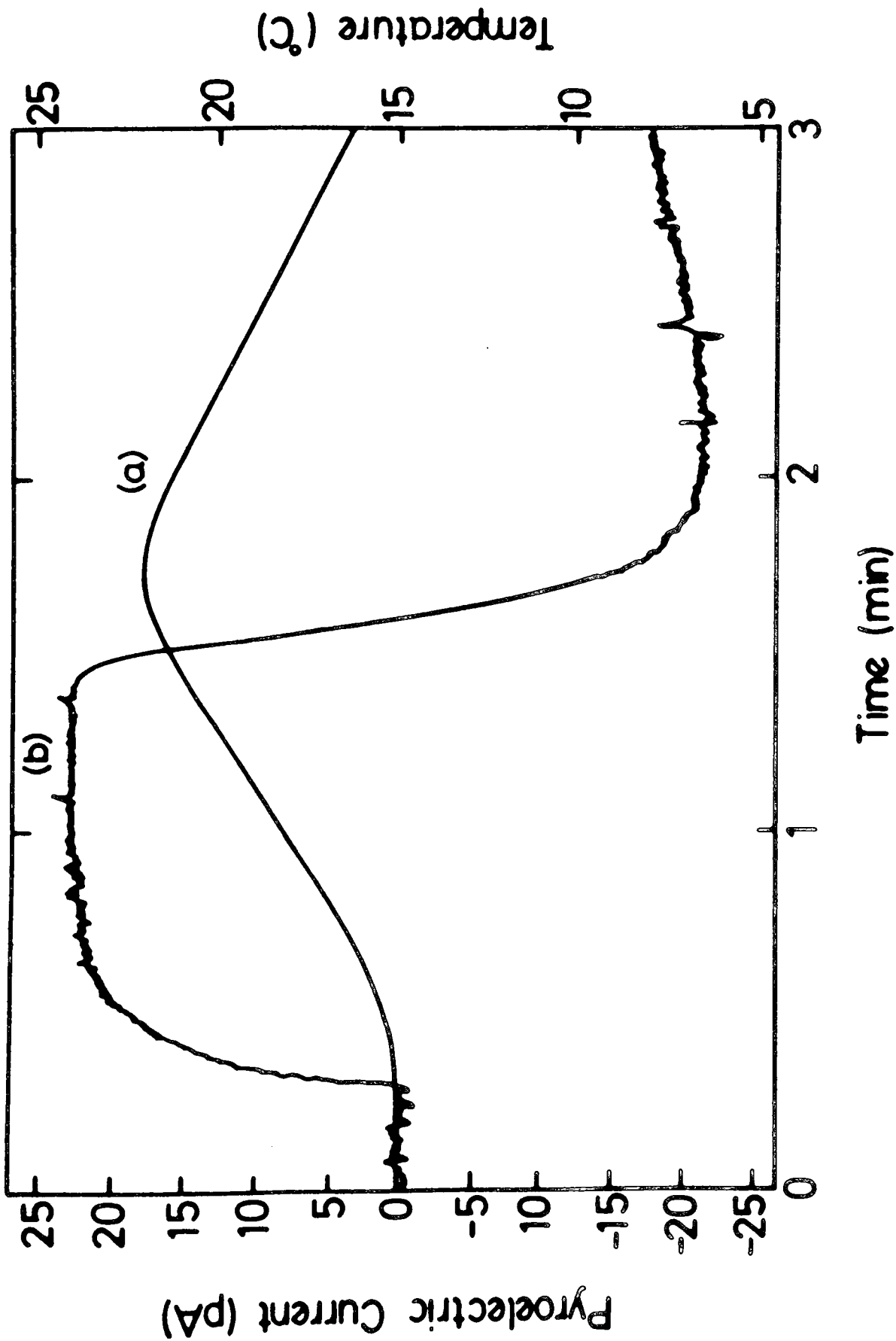


Figure 6.3 The time variation of (a) the temperature and (b) the static pyroelectric current for a 99 layer 22-TA/docosylamine device during a heat-cool cycle.



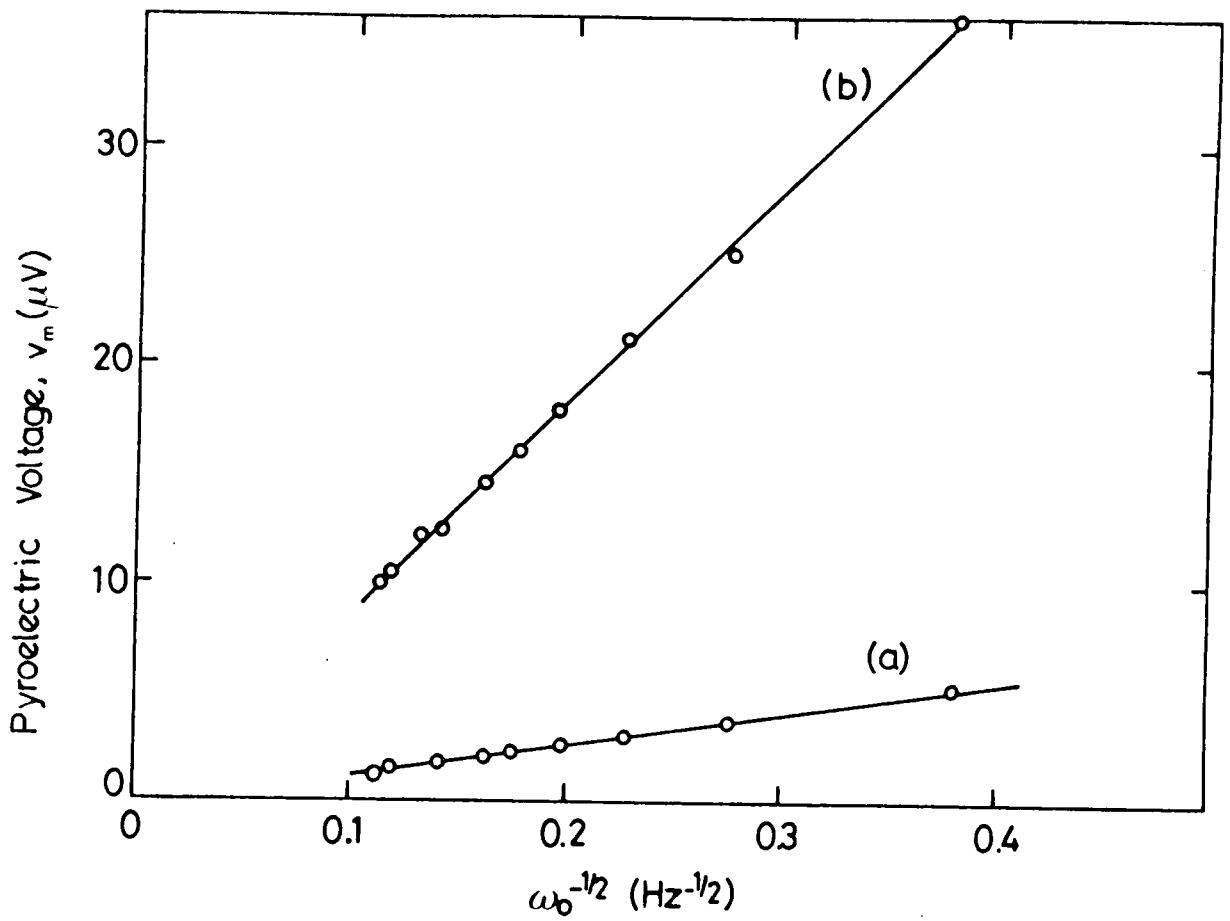


Figure 6.4 Dependence of pyroelectric voltage on (modulation frequency) $^{-1/2}$  for (a) 11 layer and (b) 99 layer 22-TA/docosylamine devices.

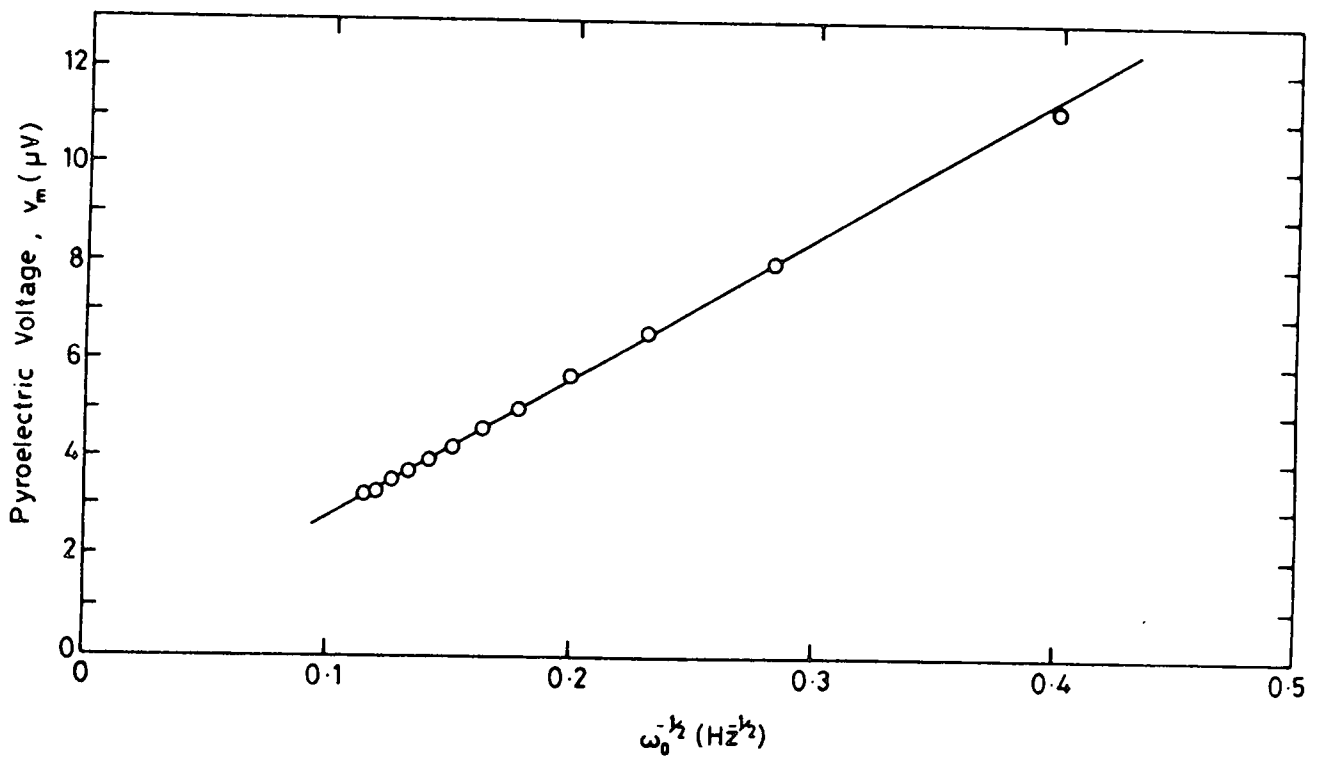


Figure 6.5 Dependence of pyroelectric voltage on (modulation frequency) $^{-1/2}$  for a 31 layer 22-TA/aniline device.

show excellent straight line fits in the frequency range 1–12 Hz, indicating good agreement with equation 3.21. There was some deviation from the straight line for frequencies greater than about 20 Hz; this can be attributed to the low frequency approximation made in the derivation of the theoretical equation.

In order to calculate pyroelectric coefficients from the voltages measured using the dynamic technique, it was necessary to evaluate the various parameters in equation 3.21, using the methods described in section 4.2.2. The dielectric constants of the 22-TA/docosylamine and 22-TA/aniline films were taken to be 2.8 and 2.9, respectively, as discussed in the previous section. For Chance-Propper glass substrates, the values of thermal conductivity, density and specific heat capacity (provided by the manufacturers) were as follows:  $K=0.9 \text{ Wm}^{-1}\text{K}^{-1}$ ,  $\rho = 2.5 \times 10^3 \text{ kg m}^{-3}$ ,  $c = 1 \times 10^3 \text{ J kg}^{-1}\text{K}^{-1}$ . The incident radiation intensity,  $W$ , was measured using a thermopile, and was found to be  $7.5 \text{ Wm}^{-2}$ . The emissivity,  $\eta$ , of the bismuth was calculated from the pyroelectric voltage generated by a blacked sample of  $\text{LiNbO}_3$ , whose pyroelectric coefficient was known; the calculated value for  $\eta$  was 0.8.

Table 6.1 summarises the values of  $p$  measured by the static and dynamic techniques for 31 layer films of 22-TA/docosylamine and 22-TA/aniline; figures of merit ( $p/\epsilon'_r$ ), based on both static and dynamic coefficients are also given. In both cases, the dynamic coefficient ( $p_{\text{dynamic}}$ ) is approximately twice as large as the corresponding static value ( $p_{\text{static}}$ ). As was noted previously, the static coefficients are likely to be the more accurate of the two because of the complexity of the model used in the derivation of the dynamic equation. Also, the calculation of dynamic coefficients involves the determination of many parameters, leading to several possible sources of error. The two prime sources are the measurements of  $W$  and of  $\eta$ , since the value of  $W$  obtained depended critically on the positioning of the thermopile, whilst the value of  $\eta$  was dependent on the “blackness” of the bismuth layer. It was estimated that errors of up to 50% in  $W$  and 25% in  $\eta$  may have been introduced. When a test sample of  $\text{LiNbO}_3$  was examined by the static and dynamic techniques, it was again found that the dynamic coefficient was approximately twice as large as the static coefficient, which was close to its theoretical value.

Type of alternate layer	$P_{\text{static}}$ (nCcm <sup>-2</sup> K <sup>-1</sup> )	$P_{\text{dynamic}}$ (nCcm <sup>-2</sup> K <sup>-1</sup> )	$(p/\epsilon_r)_{\text{static}}$ (nCcm <sup>-2</sup> K <sup>-1</sup> )	$(p/\epsilon_r)_{\text{dynamic}}$ (nCcm <sup>-2</sup> K <sup>-1</sup> )
22-TA/ docosylamine	0.19	0.53	0.07	0.19
22-TA/ aniline	0.65	1.87	0.22	0.64

Table 6.1 Static and dynamic pyroelectric coefficients and figures of merit for acid/amine alternate layer LB films.

It is apparent from table 6.1 that the pyroelectric coefficients for 22-TA/aniline films are approximately three times larger than those for 22-TA/docosylamine films. The pyroelectric coefficient of the 22-TA/aniline system represents the highest reported value, to date, for an LB film, and is of the same order of magnitude as that for PVDF. The large value of  $p$  is, perhaps, somewhat surprising in view of the structural data, which show that two phases are present in 22-TA/aniline films (section 5.4). The mixture of phases may be related to the presence of impurities in the aniline, as indicated by the isotherm (section 5.1.1). If this is the case, then it is likely that the structural order and hence the pyroelectric coefficient might be improved by using purer material.

Although the 22-TA/docosylamine system has a larger spontaneous polarisation than 22-TA/aniline, due to proton transfer, the latter film exhibits the larger pyroelectric coefficient. Since the origin of the pyroelectric effect is likely to be the same for the two types of alternate layer film, it is almost certain that the pyroelectric activity of 22-TA/docosylamine is a result of the temperature dependence of the relatively small dipole moments of the molecular head groups, rather than the larger polarisation resulting from proton transfer and ion formation. The greater pyroelectric activity of 22-TA/aniline films relative to 22-TA/docosylamine is probably a result of the larger polarisability of the former system, due to the presence of the highly delocalised benzene ring. Further enhancement of the pyroelectric effect may therefore be attainable by using molecules containing large delocalised and highly polarisable groups.

The pyroelectric figures of merit compare favourably with those for conventional materials (see table 2.1). If the static coefficients are assumed to represent the true values, then the resultant figure of merit for the 22-TA/aniline film is almost as high as that for PVDF. If the dynamic coefficients are used, then the 22-TA/aniline system has a figure of merit comparable to that of TGS, whilst 22-TA/docosylamine films have values close to those of strontium barium niobate ceramics.

### 6.2.2 Dependence of $p$ on film thickness

In figure 6.6, the measured static and dynamic pyroelectric coefficients of 22-TA/docosylamine films are plotted as a function of the number of monolayers deposited, in curves (a) and (b) respectively. Each point on the graph represents an average of the values obtained from six different devices, and the error bars correspond to the standard error ( $\sigma_{n-1}/n$ ) calculated from these data. The static coefficient is virtually independent of film thickness, whilst the dynamic value, unexpectedly, increases with the number of monolayers. A possible explanation for this observed thickness dependence is that the thermal evaporation of the aluminium top electrodes and the deposition of the blacking layer may have "burnt through" the outermost layers of the film, and hence the values of  $N$  used in equation 3.21 were inaccurate [7]. A series of values for  $p_{\text{dynamic}}$  was therefore recalculated using equation 3.21, but substituting  $N$  with  $N-x$ , where  $x$  is an integer equal in value to the number of layers destroyed by the evaporation process. It was found that the only value of  $x$  for which  $p_{\text{dynamic}}$  became independent of film thickness was  $x = 5$ . The recalculated values are plotted as curve (c) in figure 6.6.

Figure 6.7 shows a plot of the static and dynamic pyroelectric coefficients of 22-TA/aniline films as a function of the number of monolayers deposited. It is interesting to note that in this case both static and dynamic coefficients appear to increase with the number of monolayers in the array. Furthermore, it was not possible to render the dynamic data independent of film thickness by using the  $N-x$  substitution described above. The thickness dependence of the pyroelectric coefficient for 22-TA/aniline films is unexpected, since  $p$  is an intensive variable [8], which should be independent of the amount of material present. Thickness dependent pyroelectric coefficients have been reported for thin films of other materials [9-12], and have been attributed to the predominance of surface effects. In barium titanate, for example, it has been postulated [12] that thin semi-conducting layers exist near the surface of the crystal, with oxygen vacancies acting as donors. In very thin films, charge carriers can penetrate throughout the bulk of the material as a result of diffusion from the surface, and alter the electrical and pyroelectric properties of the crystal. Similar effects have been

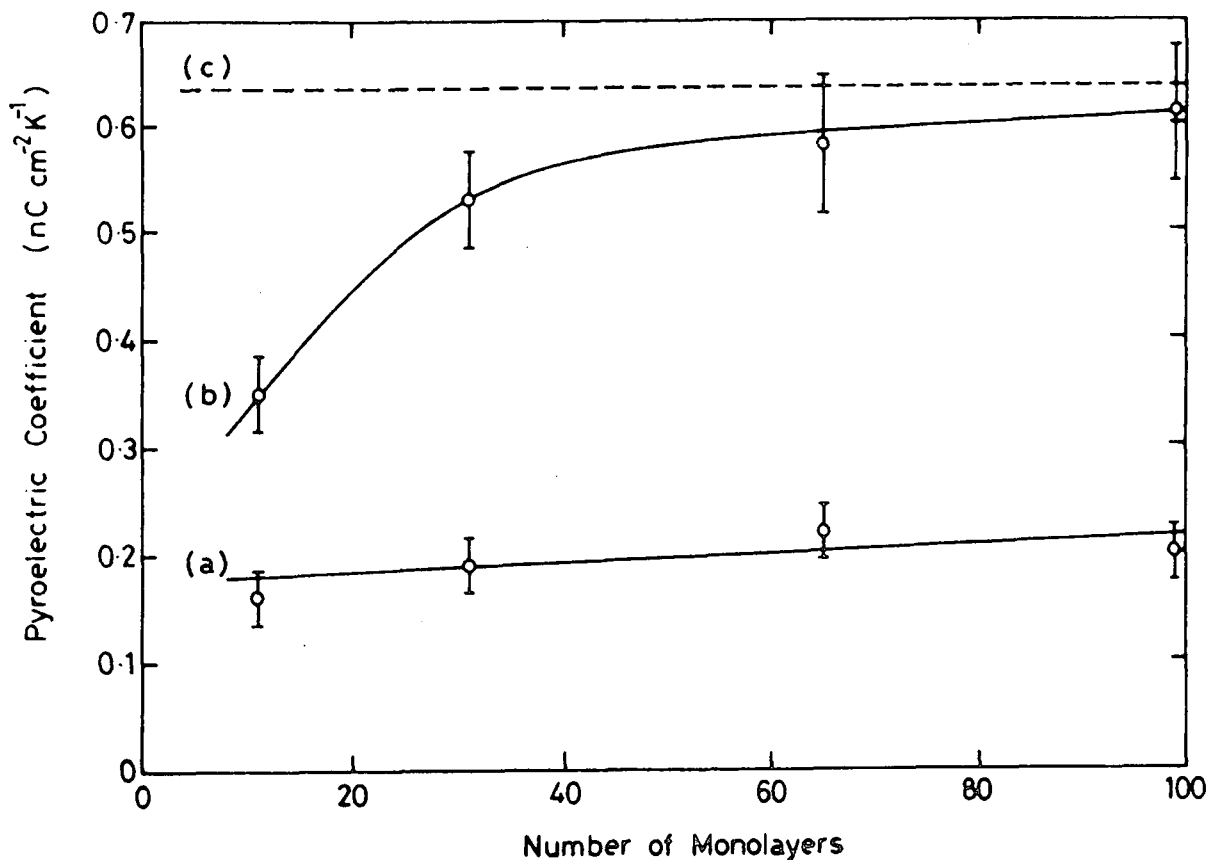


Figure 6.6 Variation of pyroelectric coefficients with number of monolayers for 22-TA/ docosylamine films: (a) measured using the static technique; (b) measured using the dynamic technique; (c) the data of (b) corrected to account for "burning through" 5 layers.

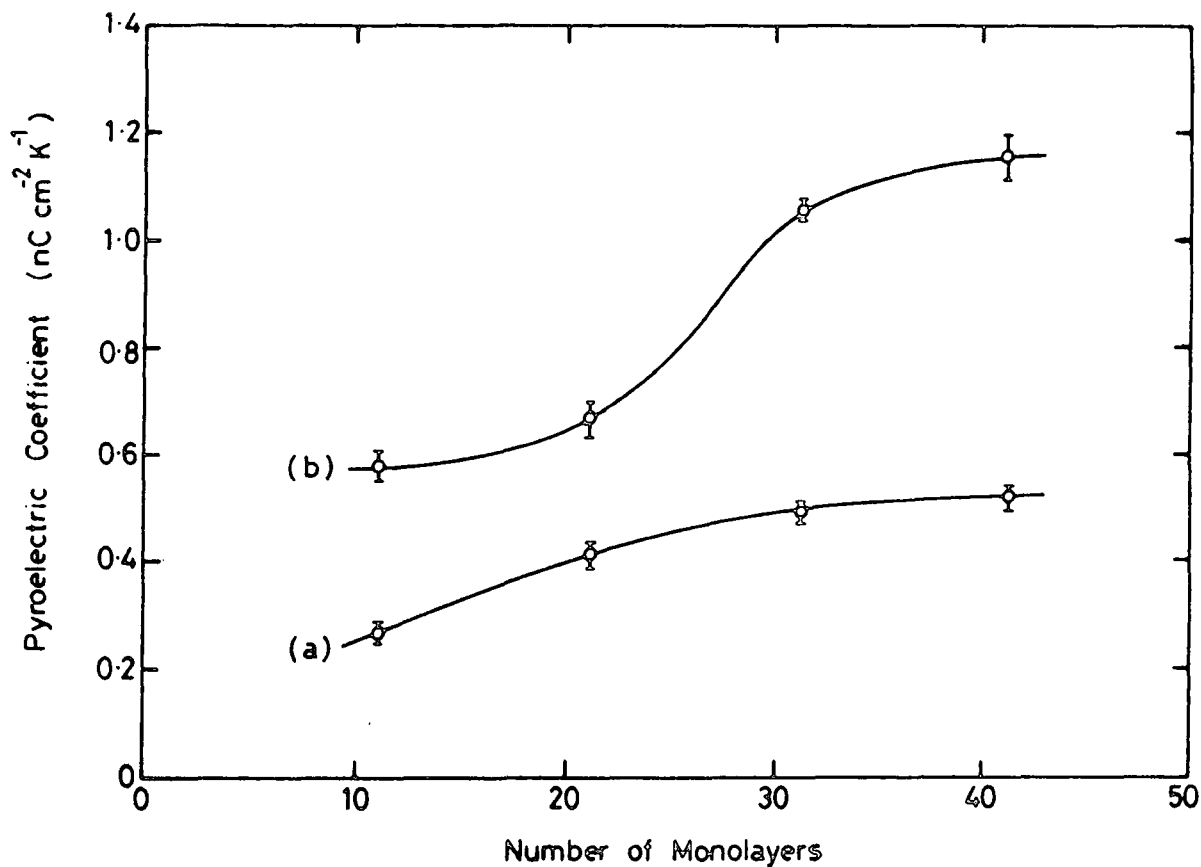


Figure 6.7 Variation of pyroelectric coefficient with number of monolayers for 22-TA/ aniline films: (a) measured using the static technique; (b) measured using the dynamic technique.

observed in organic crystals [11]. It seems likely that surface phenomena are significant in LB films as a result of their extreme thinness, and this may be the cause of the observed thickness dependence of the pyroelectric coefficient for 22-TA/aniline films. A detailed analysis is not yet possible, as there are insufficient data concerning the band structure and surface states of LB films. Although it was stated above that the pyroelectric coefficient of 22-TA/docosylamine films is virtually independent of film thickness, it should be noted that the number of experimental points on the  $p$  versus  $N$  graph is small; the slight increase in  $p$  may therefore be significant, indicating the predominance of surface effects in these films.

### 6.2.3 Dependence of $p$ on substrate thickness

It was predicted in chapter 3 that the heat sinking effect of the substrate can be reduced by using a thinner substrate. Indeed, previous workers have improved the pyroelectric response of LB film devices by using thin polymer film substrates [13]. In the present study, microscope cover slips, made of the same glass as the Chance-Propper microscope slides, were used; this ensured that all other parameters were maintained constant, the only variable being the thickness of the substrate. It was found that the dynamic pyroelectric voltages generated by 31 layer 22-TA/docosylamine films on the two substrates were as follows:

Microscope slide (thickness=1100  $\mu\text{m}$ ):  $v_m=3.2 \mu\text{V}$

Cover slip (thickness= 210  $\mu\text{m}$ ):  $v_m=7.2 \mu\text{V}$ .

Thus it can be seen that, as predicted, the pyroelectric voltage responsivity of an LB film detector can be improved by using a thinner substrate. As was noted in section 3.4, reducing the thickness of the substrate tends to decrease the total thermal admittance of the device, and hence increase the excess temperature of the device above ambient. This in turn produces a larger voltage per unit incident radiation power.

#### 6.2.4 Dependence of $p$ on $\alpha_{1s}$

In chapter 3, the general thermodynamic model for a pyroelectric crystal was applied to an LB film whose polar axis is perpendicular to the substrate plane (section 3.3.1). It was shown that the so-called partially clamped pyroelectric coefficient,  $p_3^{pc}$ , measured in such a case is given by

$$p_3^{pc} = p_3^\sigma - \frac{2d_{31}(\alpha_1 - \alpha_{1s})}{s_{11} + s_{12}}, \quad (6.1)$$

where  $p_3^\sigma$  is the total pyroelectric coefficient for the free crystal;  $\alpha_1$  and  $\alpha_{1s}$  are the thermal expansion coefficients, in the substrate plane, of the LB film and the substrate, respectively;  $d_{31}$ ,  $s_{11}$  and  $s_{12}$  are components of the piezoelectric and elastic compliance tensors, as discussed in chapters 2 and 3. If we let

$$c = \frac{2d_{31}}{s_{11} + s_{12}},$$

then equation 6.1 simplifies to

$$p_3^{pc} = p_3^\sigma - c(\alpha_1 - \alpha_{1s}). \quad (6.2)$$

The primary pyroelectric contribution to the overall pyroelectric coefficient is contained entirely in the  $p_3^\sigma$  term, whilst any secondary effect contributes both to  $p_3^\sigma$  and to  $c$  (since  $c$  is a function of the piezoelectric coefficient). Therefore, the occurrence of a significant secondary contribution will result in a non-zero value of  $c$ , and this will lead to a measured pyroelectric coefficient,  $p_3^{pc}$ , which is dependent upon the thermal expansion coefficient of the substrate,  $\alpha_{1s}$ . The presence of a secondary contribution was therefore investigated by measuring the pyroelectric coefficients of films deposited onto a series of different aluminised glasses. The thermal expansion coefficients of these glasses are given below:

Silica	$\alpha_{1s} = 0.5 \times 10^{-6} \text{ K}^{-1}$
Pyrex	$\alpha_{1s} = 3.2 \times 10^{-6} \text{ K}^{-1}$
Corning 7059	$\alpha_{1s} = 4.6 \times 10^{-6} \text{ K}^{-1}$
Chance – Propper	$\alpha_{1s} = 7.87 \times 10^{-6} \text{ K}^{-1}$

The thermodynamic model developed in section 3.3.1 assumes that the polar axis of the LB film is perpendicular to the plane of the substrate. Since this



is not the case for 22-TA/aniline films, the present investigation was performed using 22-TA/docosylamine layers. A series of 31 layer devices was fabricated on each type of substrate, and the pyroelectric coefficients were measured using both static and dynamic techniques.

In figure 6.8, the static and dynamic coefficients are plotted as a function of the substrate thermal expansion coefficient. This shows that the measured pyroelectric coefficient tends to decrease as  $\alpha_{1s}$  increases, indicating that piezoelectrically induced secondary effects are making a significant contribution to the overall pyroelectric coefficient. Unfortunately, it is not possible, on the basis of these results, to totally separate the primary and secondary effects, since the  $p_3^\sigma$  term contains both primary and secondary contributions. In the next chapter, a different approach will be taken in order to separate the primary and secondary pyroelectric terms. The fact that  $p_3^{pc}$  decreases as  $\alpha_{1s}$  increases implies that the secondary contribution is a negative one, which serves to decrease the pyroelectric coefficient which would be observed if only the primary effect were occurring. The secondary effect is therefore undesirable, and should be reduced as far as possible by using a substrate with a small thermal expansion coefficient.

The effect of the substrate thermal expansion coefficient on the static measurement is much smaller than that occurring for the dynamic technique. The explanation for this can be seen by referring back to section 3.3.1. It was shown in equation 3.4 (page 31) that the pyroelectric coefficient,  $p_3^{pc}$ , for a partially clamped film is given by

$$p_3^{pc} = p_3^\sigma + 2d_{31} \frac{d\sigma_1}{dT}, \quad (6.3)$$

where  $p_3^\sigma$  is the pyroelectric coefficient for the free crystal,  $d_{31}$  is a component of the piezoelectric tensor,  $T$  is the temperature, and  $\sigma_1$  is the mechanical stress in the plane of the substrate. In the static experiment, the device is essentially uniformly heated at a very slow rate, and the stresses in the substrate plane are therefore expected to be much smaller than those occurring with the dynamic technique. Hence, the effect of partial clamping will be greater for a dynamic measurement than for a static measurement, and the pyroelectric coefficient measured using the former technique will show a much stronger dependence on

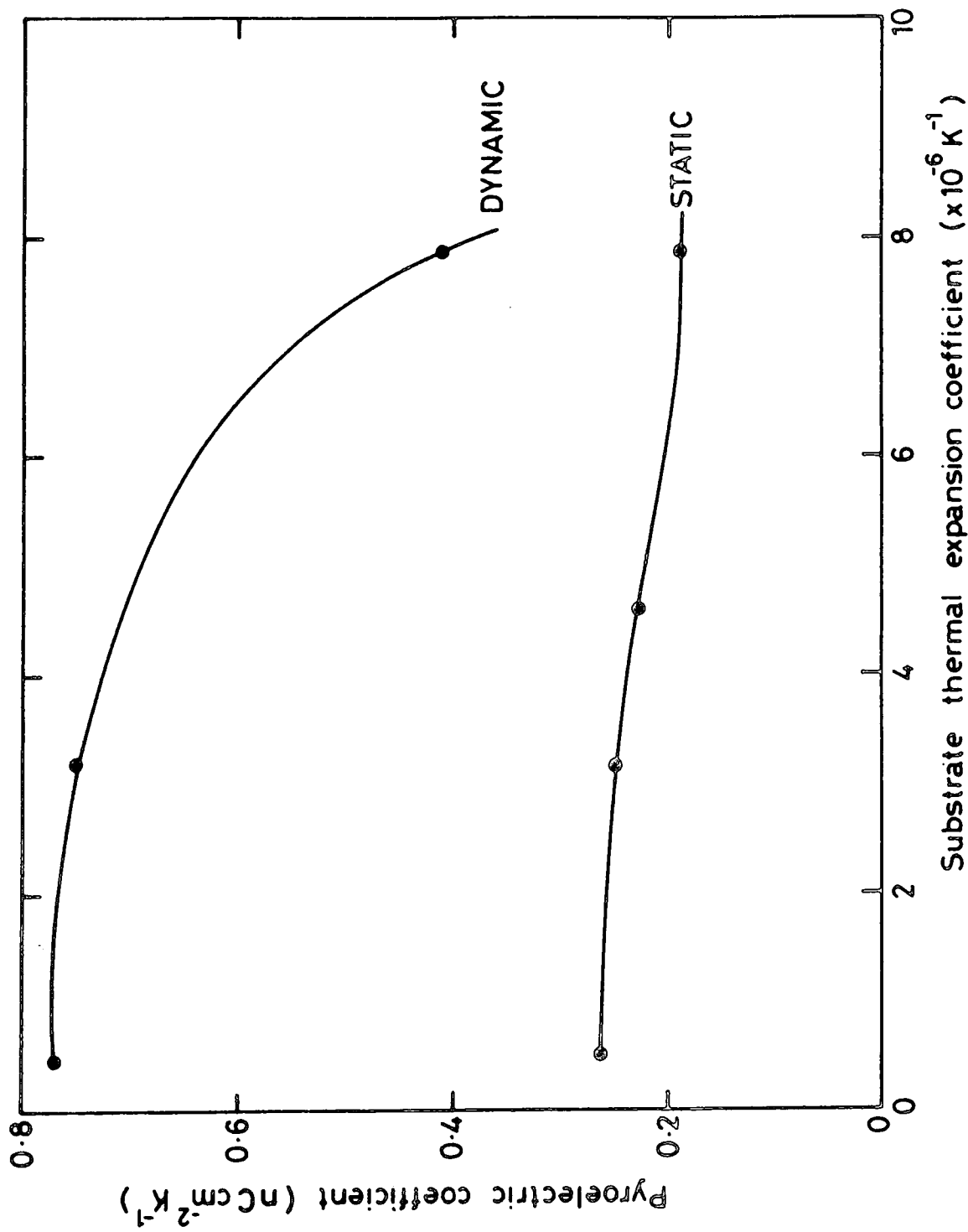


Figure 6.8 Dependence of the pyroelectric coefficient on the thermal expansion coefficient of the substrate for 31 layer films of 22-TA/docosylamine.

the thermal expansion coefficient of the substrate.

These results are in contrast to those of Blinov *et al* [14], who have postulated that the pyroelectric activity observed in LB films of azo dyes is predominantly a primary effect; this theory is based on a comparison between experimental and literature values for the temperature dependence of the dipole moments of the materials. Smith *et al* [15], however, have attributed the pyroelectric effect in alternate layer films consisting of stearylamine with a variety of fatty acids to secondary phenomena, on the basis of the low values of the pyroelectric coefficient ( $\sim 0.03\text{--}0.11 \text{ nCcm}^{-2}\text{K}^{-1}$ ), which resulted from a relatively large polarisation.

### 6.3 SUMMARY

Dielectric constants of 2.8 and 2.9 have been measured for 22-TA/ docosylamine and 22-TA/aniline films, respectively; these values are virtually independent of either temperature or frequency. Pyroelectric coefficients have been measured using static and dynamic techniques, and values of  $0.19 \text{ nCcm}^{-2}\text{K}^{-1}$  for 22-TA/docosylamine and  $0.65 \text{ nCcm}^{-2}\text{K}^{-1}$  for 22-TA/aniline have been obtained from the static method. Coefficients measured using the dynamic technique are approximately twice as large; however, the static values are considered to be the more accurate of the two. The figures of merit calculated from these measurements of  $p$  and of  $\epsilon_r$  compare favourably with those for conventional pyroelectric materials such as PVDF and TGS.

As predicted in chapter 3, it has been found that the thermal clamping effect of the substrate can be reduced by using a thinner substrate; this leads to an enhanced voltage responsivity. Mechanical clamping has also been investigated by using substrates of different thermal expansion coefficient,  $\alpha_{1s}$ . It has been found that the pyroelectric coefficient decreases as  $\alpha_{1s}$  increases; this implies that the secondary pyroelectric contribution is a negative one, which reduces the pyroelectric coefficient relative to that which would be observed if only the primary effect were occurring.

## CHAPTER 7

### DIELECTRIC AND PYROELECTRIC CHARACTERISATION OF ACID/AMINE FILMS: RESULTS AND DISCUSSION, PART II

#### 7.0 INTRODUCTION

In the preceding chapter the results of some fundamental pyroelectric and dielectric studies of acid/amine films were presented. Chapter 7 is concerned with more sophisticated investigations of these alternate layer films. Section 7.1 describes the results of a study of the temperature dependence of the pyroelectric coefficient, and attempts to correlate the experimental data with theoretical models. In section 7.2, thermally stimulated discharge of polar LB films is discussed, and a model is proposed to account for the observed thermograms. Both investigations provide further insight into the nature of the spontaneous polarisation and the pyroelectric effect in acid/amine LB films.

#### 7.1 TEMPERATURE DEPENDENCE OF $p$

The theoretical temperature dependence of  $p$  has been debated for many years. One of the earliest treatments was performed by Boguslawski in 1914 [1-3], using an Einstein model of independent linear oscillators. In this model the crystal is assumed to consist of an array of atoms, all undergoing simple harmonic oscillations at the same frequency. The Einstein model gave a good fit to the experimental data obtained by Ackermann [4] at high temperatures, but there was considerable deviation at lower temperatures. Boguslawski also obtained moderate success using a Debye model of coupled oscillators, in which the atoms are assumed to oscillate at a range of frequencies, whose distribution is given by Bose-Einstein statistics. However, this theory predicted a low temperature relationship of the form  $p \propto T^3$ , whilst experiments showed that  $p \propto T$ .

The problem was largely resolved by Born [5], who acknowledged the need to distinguish between primary and secondary pyroelectricity. Born postulated that, since the piezoelectric coefficient is virtually independent of temperature, the secondary contribution should follow the same temperature dependence as

the thermal expansion coefficient; that is, a  $T^3$  dependence at low temperatures. Born also introduced a quantum mechanical correction to account for the deformation of the electronic clouds surrounding the nuclei of the atoms, and hence derived a function to describe the primary pyroelectric coefficient. This expression indeed followed the observed linear dependence on temperature for small  $T$ .

It has subsequently been proposed by Lang [6], that the Born function is an adequate description of the primary pyroelectric coefficient at temperatures sufficiently low that only acoustic phonons are excited, but that at higher temperatures optical phonon vibrations contribute a series of Einstein functions to the pyroelectric effect. Thus, the primary pyroelectric coefficient,  $p^\epsilon$ , is given by

$$p^\epsilon = a B \left( \frac{\Theta_D}{T} \right) + \sum_{i=1}^n b_i E \left( \frac{\Theta_{E_i}}{T} \right) \quad (7.1)$$

where  $a$  and  $b_i$  are constants of proportionality,  $\Theta_D$  and  $\Theta_{E_i}$  are the characteristic Debye and Einstein temperatures of the crystal [7], and  $B(x)$  and  $E(x)$  are the Born and Einstein functions. Lang illustrated the validity of this model by empirically fitting the temperature dependent primary pyroelectric coefficient of lithium sulphate monohydrate (LSM) to an expression consisting of a Debye temperature and five Einstein temperatures. Russian scientists [8] have performed similar analyses on a much wider range of materials, and have concluded that the primary pyroelectric coefficient in ferroelectric crystals is defined mainly by optical phonon modes, whilst non-ferroelectric pyroelectrics exhibit mainly acoustic modes.

Figure 7.1 shows the temperature dependence of the pyroelectric coefficient for 31 layer films of 22-TA/docosylamine and 22-TA/aniline deposited onto Chance-Propper glass substrates. For both films there is an initial increase in pyroelectric coefficient, reaching a maximum at around 245 K for 22-TA/docosylamine and around 270 K for 22-TA/aniline films. At higher temperatures the pyroelectric coefficient begins to decrease quite rapidly. The low temperature data were fitted to an empirical power law by plotting  $\log_{10} p$  versus  $\log_{10} T$ ; the results are shown in figure 7.2. Both graphs show good fits to straight lines, indicating a relationship of the form  $p \propto T^n$ . For the 22-TA/docosylamine film  $n=2.3$ ; whilst, for the 22-TA/aniline film, the graph has

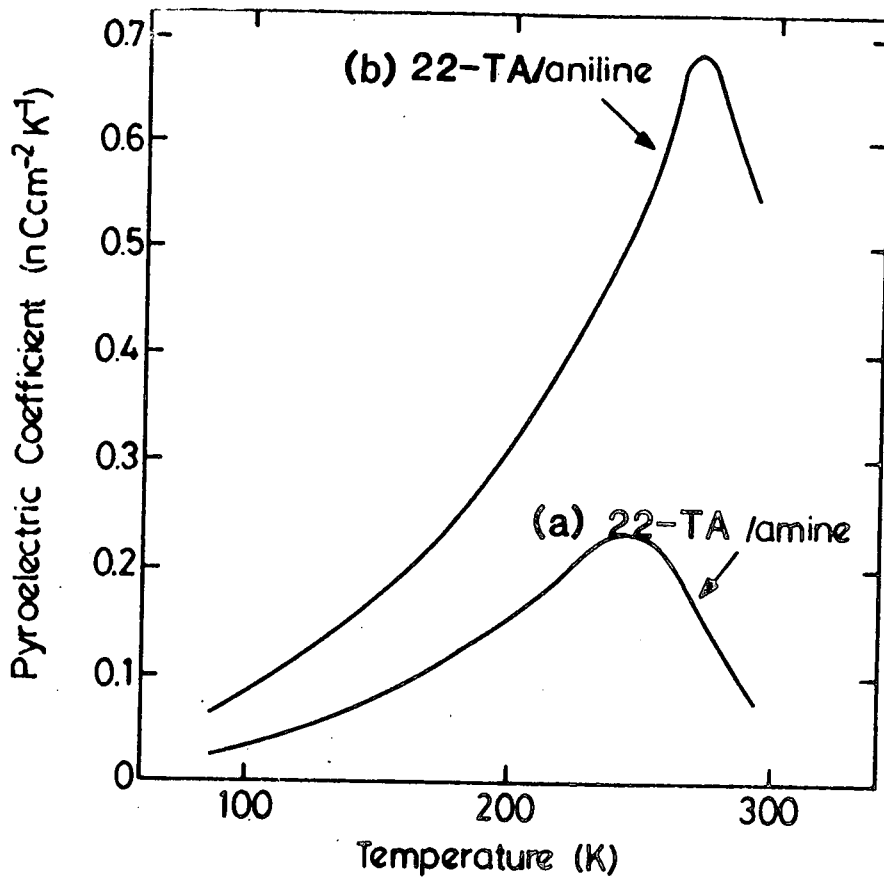


Figure 7.1 Temperature dependence of the pyroelectric coefficient for 31 layer films of (a) 22-TA/docosylamine and (b) 22-TA/aniline on Chance-Propper glass substrates. (Static measurement)

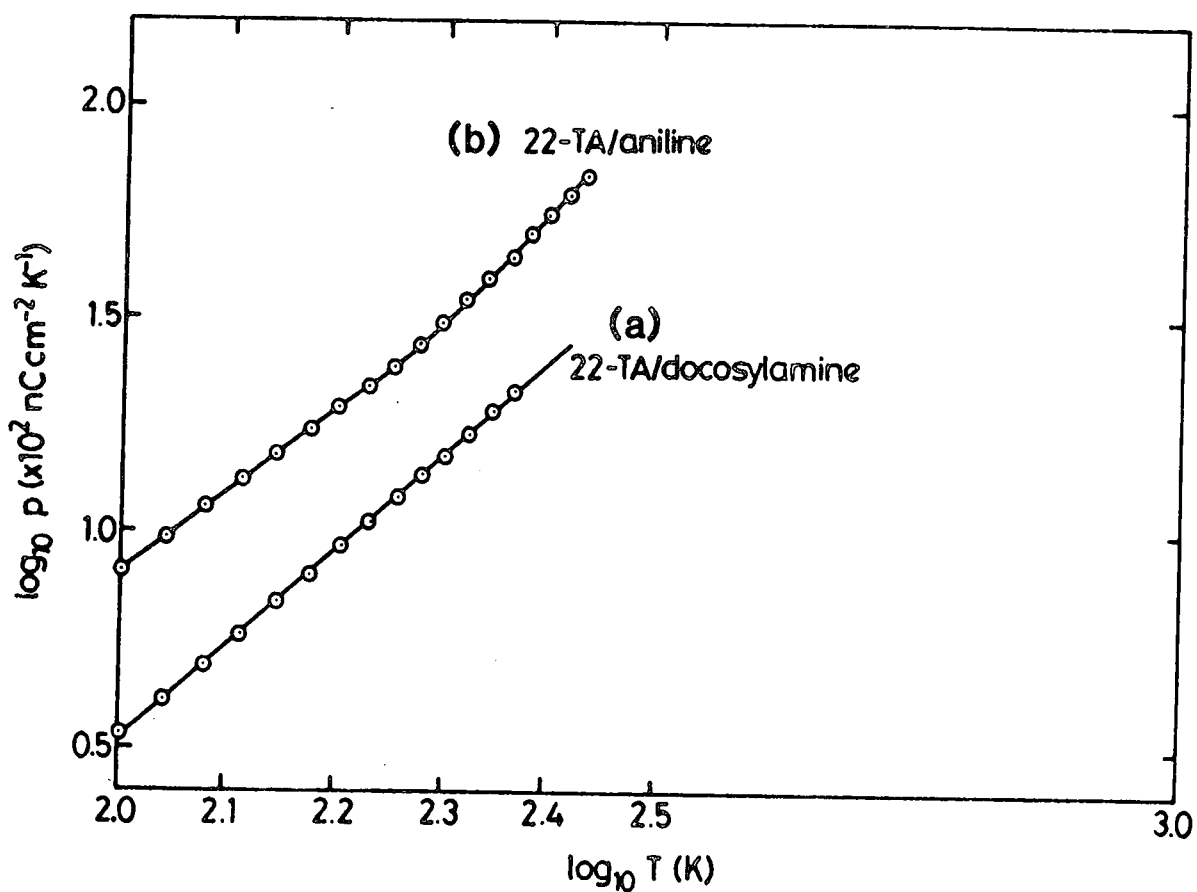


Figure 7.2 Log-log plot of the temperature dependence of the pyroelectric coefficient for (a) 22-TA/docosylamine and (b) 22-TA/aniline films (low temperature régime).

two straight line regions corresponding to  $n=1.9$  for  $100 \text{ K} < T < 190 \text{ K}$  and  $n=2.6$  for  $190 \text{ K} < T < 260 \text{ K}$ .

The interpretation of the LB film data in terms of a detailed lattice dynamic model would be almost impossible for two reasons; firstly, the complexity of the unit cell will give rise to a very large number of optical phonon modes; and secondly, the simple  $T^3$  dependence of the secondary pyroelectric effect will be complicated by the partial clamping effect of the substrate. Nevertheless, it is possible to make some qualitative observations from the results.

The decrease in pyroelectric coefficient of the two systems above a certain temperature might be due to two possible effects; namely, a phase change or competition between primary and secondary pyroelectric effects [6]. Since the dielectric constant is a well-behaved function of temperature in both cases, a phase change is unlikely. The possibility of competing primary and secondary effects was investigated by repeating the measurement using a 31 layer film of 22-TA/docosylamine deposited onto Corning 7059 glass. Since this material has a lower thermal expansion coefficient than Chance-Propper glass, the secondary pyroelectric contribution should be different from that observed previously.

The  $p$  versus  $T$  graphs obtained using the two different substrates are shown in figure 7.3. The graphs are virtually identical at low temperatures, but the pyroelectric coefficient of the sample deposited on Corning glass continues to rise up to a temperature of approximately 260 K, and reaches a greater maximum value. It was shown in section 6.2.4 that the primary and secondary contributions to the total pyroelectric effect are opposite in sign, and that a larger secondary contribution tends to give a smaller total pyroelectric coefficient. Since only the secondary contribution will be affected by changing the substrate material, this suggests that the pyroelectric effect is predominantly primary at low temperatures, and secondary phenomena only begin to dominate at around 240–260 K, depending on the thermal expansion coefficient of the substrate.

Although there are insufficient data to totally separate the primary and secondary contributions, figure 7.4 shows qualitatively their deduced temperature dependences. The absence of any significant secondary contribution at low

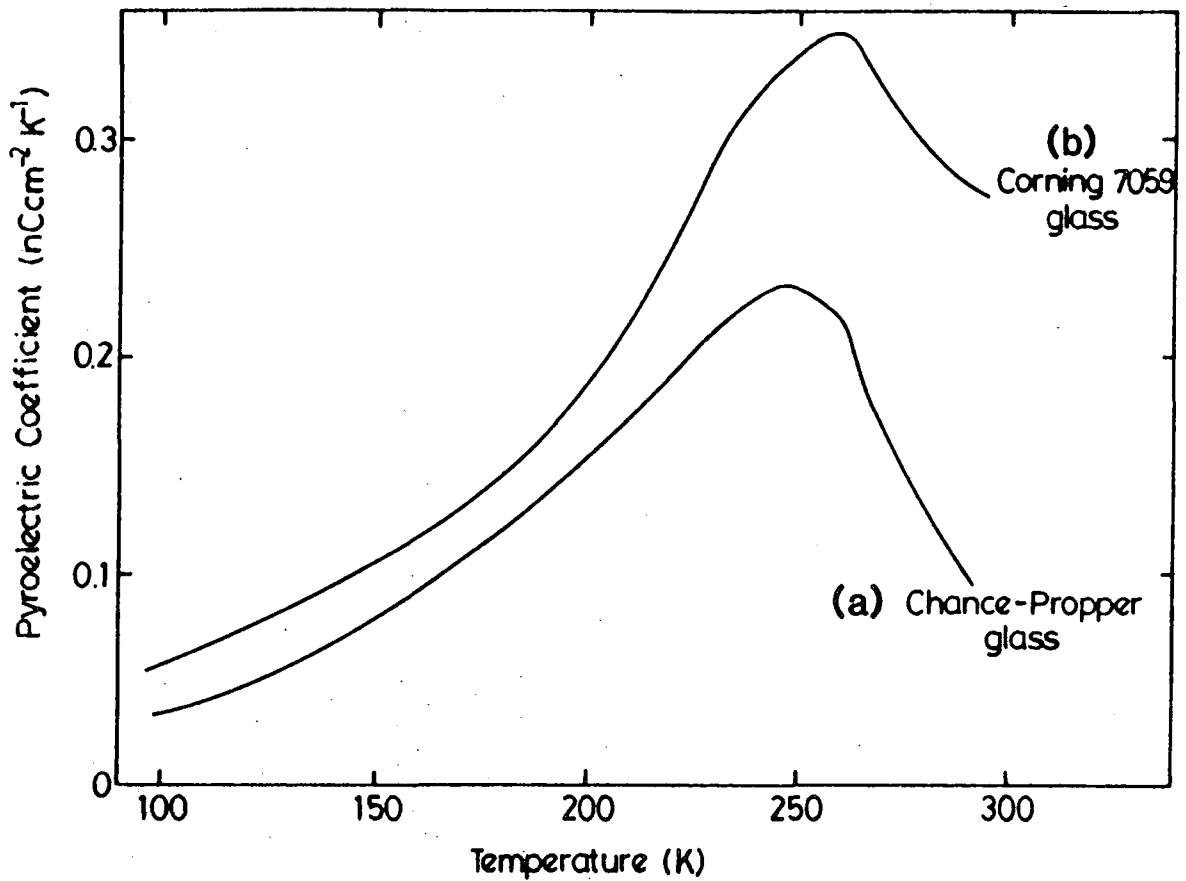


Figure 7.3 Temperature dependence of the pyroelectric coefficient for 31 layer films of 22-TA/docosylamine deposited onto (a) Chance-Propper glass and (b) Corning 7059 glass substrates.

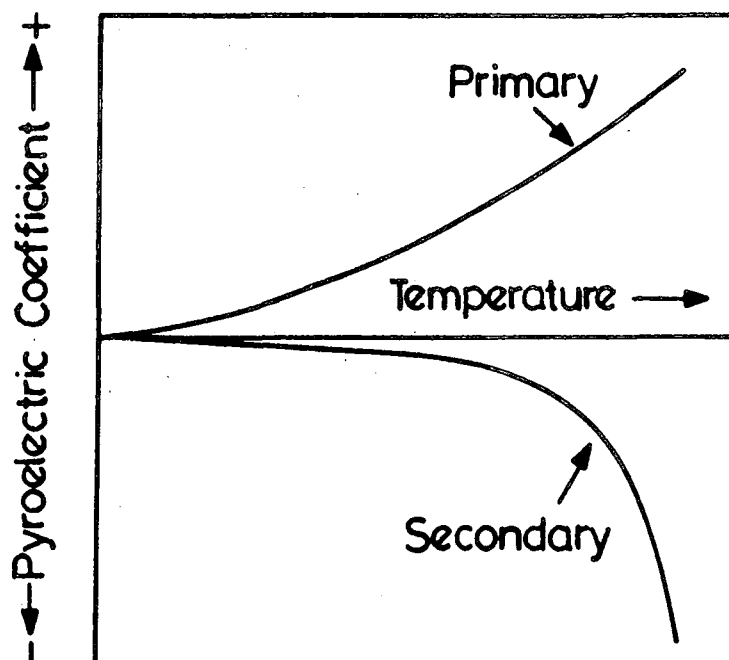


Figure 7.4 Schematic diagram of the temperature dependences of the primary and secondary pyroelectric coefficients.



temperatures, which is in apparent contradiction to the predicted  $T^3$  dependence, has been observed in bulk crystals [8], and has been attributed to the temperature dependence of the constant of proportionality of the secondary pyroelectric coefficient. A full analysis for the LB film samples is not yet possible, as there is insufficient information concerning the temperature dependence of partial clamping.

The preceding discussion indicates that, at temperatures below about 240 K, the pyroelectric effect is predominantly primary in origin, and should therefore obey equation 7.1. However, at present, there are too many unknown parameters to determine whether the observed temperature dependences fit this theoretical relationship. The abrupt change in gradient of the logarithmic plot for the 22-TA/aniline film at 190 K suggests a radical change in the contributions from the various phonon modes at this temperature. In order to gain further insight into these phonon vibrations, and evaluate some of the parameters in equation 7.1, low frequency infrared studies ( $100\text{--}500\text{ cm}^{-1}$ ) were performed on the acid/amine films. Radiation of this frequency is insufficiently energetic to excite most bond vibrations, but instead excites whole lattice vibrations (phonon modes). Born, Einstein or Debye temperatures,  $\Theta$ , can be calculated from the frequencies at which infrared absorption occurs, using the relationship

$$\bar{\nu} = \frac{k\Theta}{hc} \quad (7.2)$$

where  $\bar{\nu}$  is the wavenumber and  $k$ ,  $h$  and  $c$  have their usual meanings. Unfortunately, the existing system proved insufficiently sensitive to detect the relatively weak far infrared bands above the high level of background noise. However, it is likely that, in the future, far infrared studies may become possible, using a liquid helium cooled detector.

## 7.2 THERMALLY STIMULATED DISCHARGE

The basic principles of thermally stimulated discharge (TSD) were described in section 4.4.5. Previous TSD studies [9–15] have been almost exclusively concerned with polymer electrets. These structures are usually formed by a thermal process, in which the polymer is heated to a temperature above its glass transition point, such that the dipolar side groups and free charges are mobilised. An

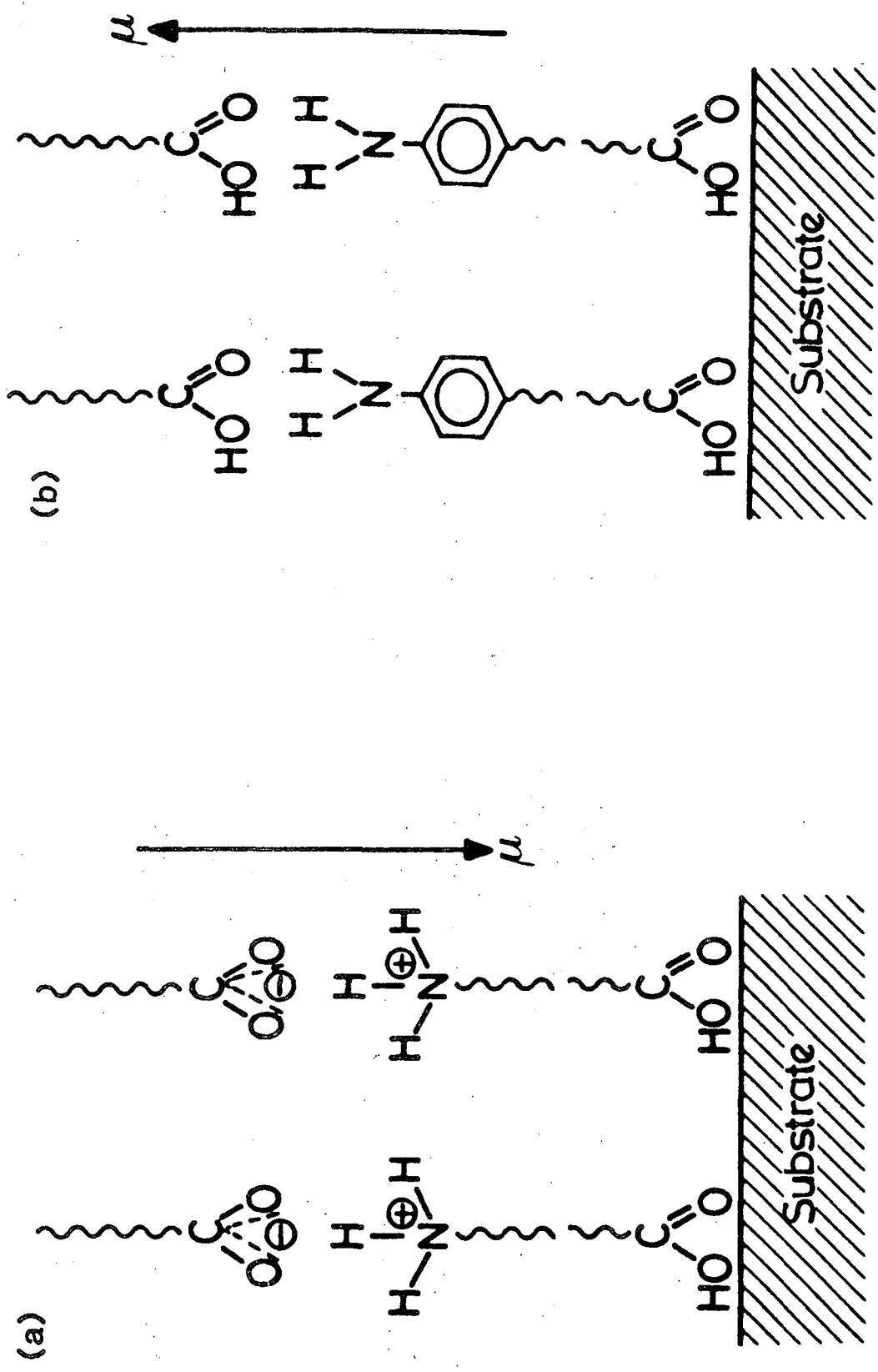


Figure 7.5 Schematic diagram showing the spontaneous polarisation of (a) 22-TA/  
docosylamine and (b) 22-TA/aniline LB films.

electric field of the order of  $10^4 \text{ V cm}^{-1}$  is then applied, causing an alignment of the dipoles and a drift of free charges to the electrodes. After a period of time, the charged polymer is cooled back to room temperature, and the polymer chains are immobilised, freezing in the polarisation. When the applied field is subsequently removed, the polymer is in a state of permanent polarisation. This is a non-equilibrium state, and the polarisation will therefore tend to decay; however, this happens only very slowly at room temperature. In order to make realistic studies of the discharge, the process must therefore be accelerated by increasing the mobility of the frozen-in dipoles and charges; this can be achieved using TSD. Polar LB films differ from polymer electrets, in that their permanent polarisation constitutes an equilibrium state. The TSD current versus temperature "thermogram" of a polar LB film is therefore expected to be dominated, not by the decay of the built-in polarisation, but by other processes [16, 17].

It was determined in section 5.2 that the spontaneous polarisation in 22-TA/docosylamine films is predominantly due to the large dipole moment resulting from proton transfer and ion formation [18]. In 22-TA/aniline films, however, no proton transfer occurs, and the only component of the polarisation is that due to the head groups of the constituent molecules. Since these two contributions to the polarisation are in opposite directions with respect to the substrate, the resultant spontaneous polarisation of a 22-TA/docosylamine film is therefore in the opposite sense to that of a 22-TA/aniline film (figure 7.5). In the present study, both 22-TA/docosylamine and 22-TA/aniline films were studied.

### 7.2.1 Results of TSD experiments

Figures 7.6a and b show the current versus temperature thermograms obtained from 31 layer 22-TA/docosylamine and 22-TA/aniline films respectively. The dashed lines indicate the data obtained on re-heating the samples. For comparison figure 7.7 shows the corresponding TSD curves obtained from a 31 layer film of 22-TA. All samples were heated at a constant rate of approximately  $1^\circ\text{C s}^{-1}$ . The data shown in figures 7.6 and 7.7 were found to be reproducible for a number of samples fabricated under similar conditions.

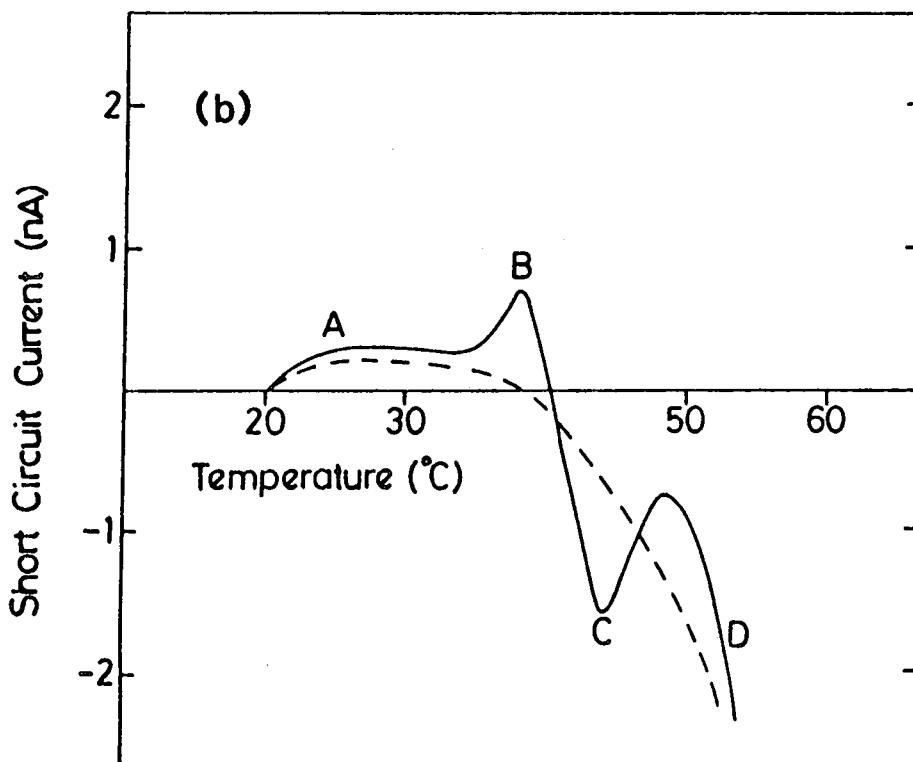
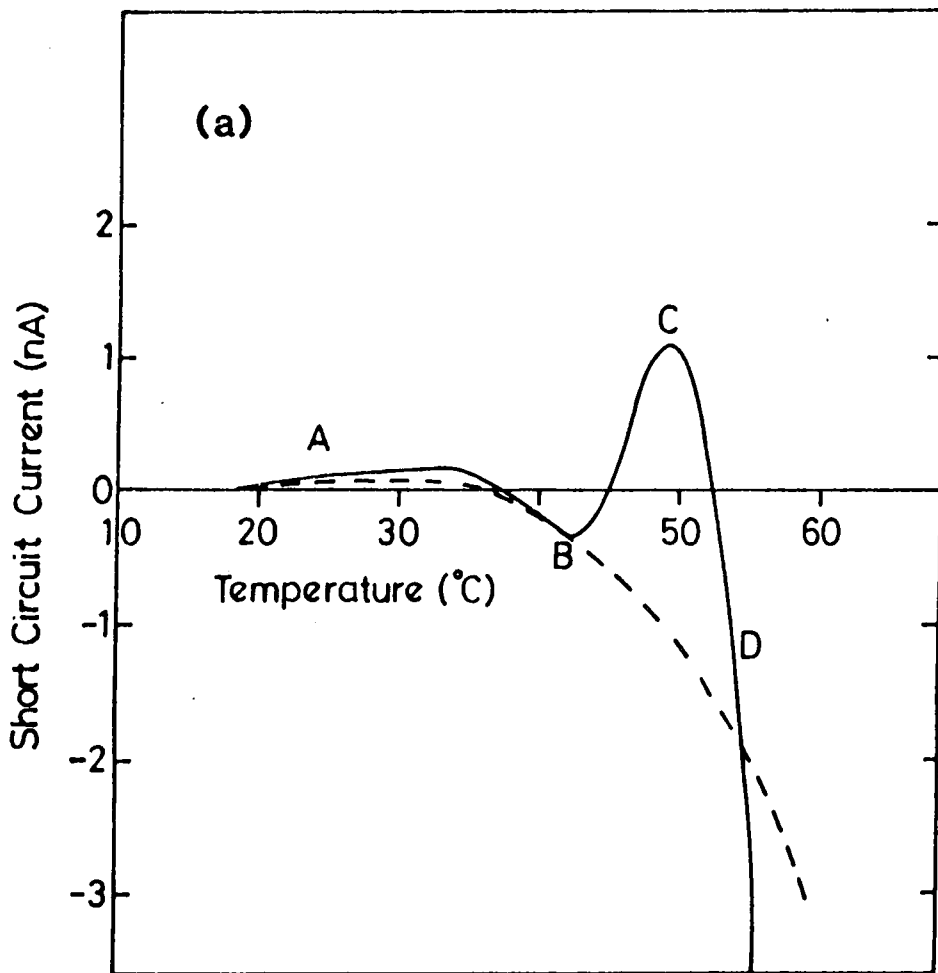


Figure 7.6 TSD thermograms from 31 layer samples of (a) 22-TA/docosylamine and (b) 22-TA/aniline. The dashed lines show the data obtained on re-heating the samples.

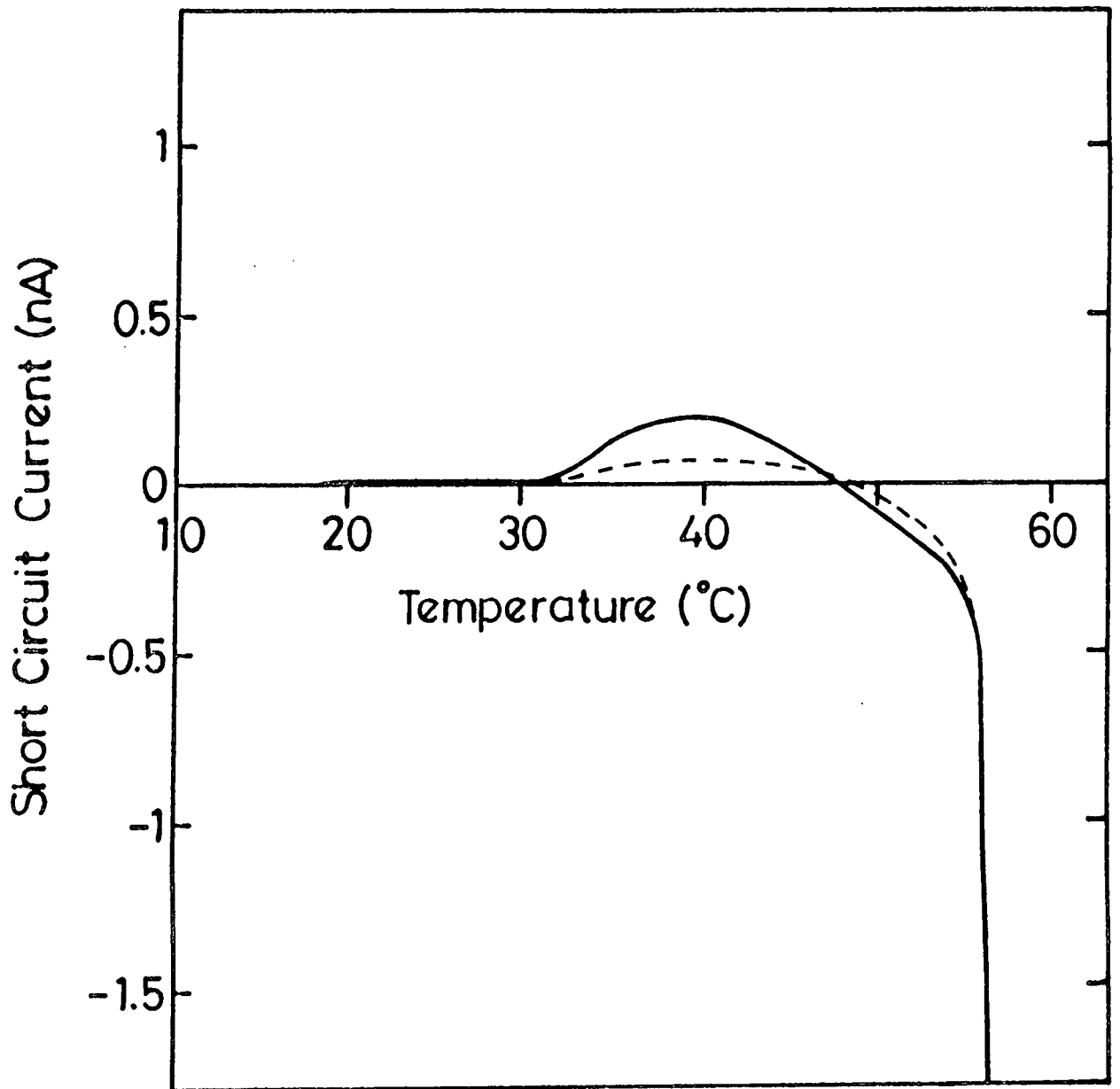


Figure 7.7 TSD thermogram from a 31 layer sample of 22-TA. The dashed line shows the data obtained on re-heating the sample.

The thermograms for the initial heating of both alternate layer structures consist of four distinct features: a small, approximately constant, current at low temperatures, followed by two more distinct peaks, and finally a rapidly decreasing current at around 55°C. The evidence which will be presented in the following sections suggests that the origins of these four features are essentially the same for the two materials, and they have therefore been designated A, B, C and D in both cases. For the 22-TA/aniline data of figure 7.6b, C has been assigned to the current minimum at  $\sim 43^\circ\text{C}$ , rather than to the current maximum at  $\sim 48^\circ\text{C}$ , because the former lies below the dashed reheating curve, and hence represents a genuine current peak. Thus the current flow corresponding to features A and D is in the same direction in the 22-TA/docosylamine and 22-TA/aniline films; however for peaks B and C the flow of the current is in opposite senses in the two types of film. When the samples are heated for the second time, features A and D remain (although the magnitude of A has decreased), but B and C are absent. The data for 22-TA (figure 7.7) simply reveal a small peak at  $\sim 40^\circ\text{C}$  (note the expanded ordinate scale in this diagram), followed by a rapid decrease in current.

### 7.2.2 Feature A

Feature A is almost certainly a pyroelectric current, since the effect is not observed in the centrosymmetric 22-TA film. Moreover, the pyroelectric coefficients calculated from the magnitude of the current correspond closely to the values obtained using the static and dynamic measurement techniques. It is interesting to note that the pyroelectric current flows in the same sense in the two types of alternate layer film, despite the fact that the overall polarisation is in opposite directions (figure 7.5). This leads to the important result that pyroelectricity in 22-TA/docosylamine layers is related to the temperature dependence of the relatively small dipole moments associated with the head groups, rather than to the larger polarisation resulting from proton transfer and ion formation. This is in agreement with the theory that pyroelectric activity is related to molecular polarisability.

### 7.2.3 Feature D

The slight decrease in pyroelectric activity for both types of alternate layer film after the initial heating process indicates that some degree of disorder has been introduced into the LB assembly. This is the most likely origin of the rapidly decreasing current at high temperatures, which occurs in both alternate layer systems (feature D) and also in the 22-TA film. The temperature at which the rapid current decrease begins seems to be related to the melting points of the three types of film investigated. Approximate values for the melting points were obtained by continuing the heating process, and noting the temperature,  $T_m$ , at which the film acquired an "amorphous" appearance. The measured values were as follows:

22-TA	$T_m = 55^\circ \text{C}$
22-TA/docosylamine	$T_m = 80^\circ \text{C}$
22-TA/aniline	$T_m = 57^\circ \text{C}$

As expected, the highest melting point occurs for the 22-TA/docosylamine film, which contains ionic bonds. Previous workers [19–21] have reported on the thermal disordering of fatty acid LB films. Naselli *et al* [19] have attributed their infrared spectroscopy results to a two step process in the organic layer: in the first stage the head groups of the molecules remain static, but the hydrocarbon chains begin to move and adopt random configurations relative to the substrate surface; at higher temperatures the head groups also become disordered, and the film melts.

The possibility of similar processes occurring in the alternate layer films was investigated by measuring the infrared spectrum of a 22-TA/docosylamine film both before and after heating to  $60^\circ\text{C}$  (approximately  $20^\circ\text{C}$  below the melting point). Figure 7.8 shows the region of the spectrum corresponding to  $\text{CH}_2$  and  $\text{CH}_3$  absorptions. It is evident that there is a change in the relative intensities of the bands on heating the sample, indicating a change in the orientation of the molecular chains relative to the substrate surface. The data are very similar to those obtained by Naselli *et al* for multilayers of cadmium stearate [19]. It is likely, therefore, that the decrease in current noted for all the present samples above  $50^\circ\text{C}$  (feature D) is associated with a pre-transitional disordering

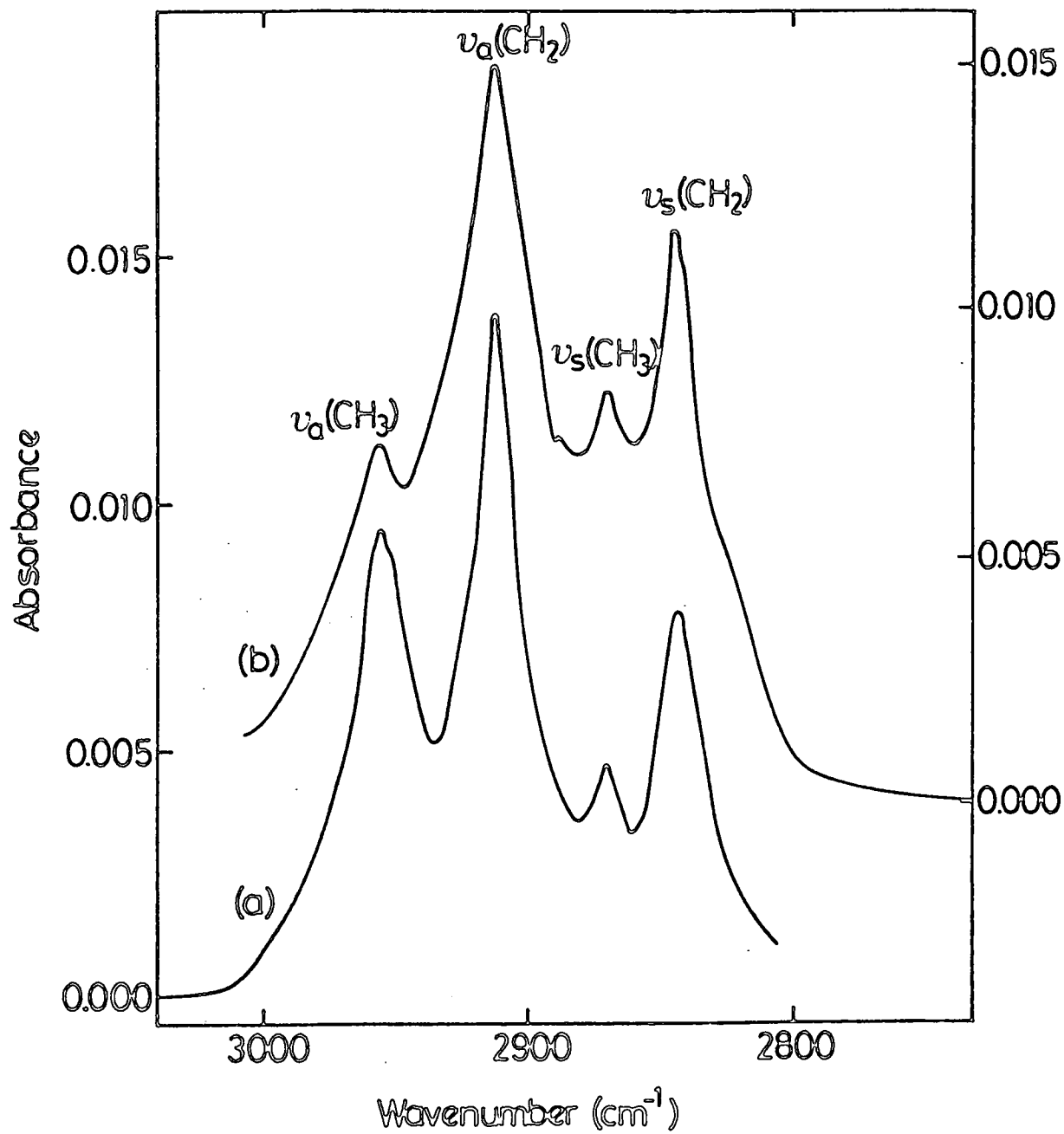


Figure 7.8 Part of the infrared spectrum of a 31 layer film of 22-TA/docosylamine, (a) before and (b) after heating to 60°C.



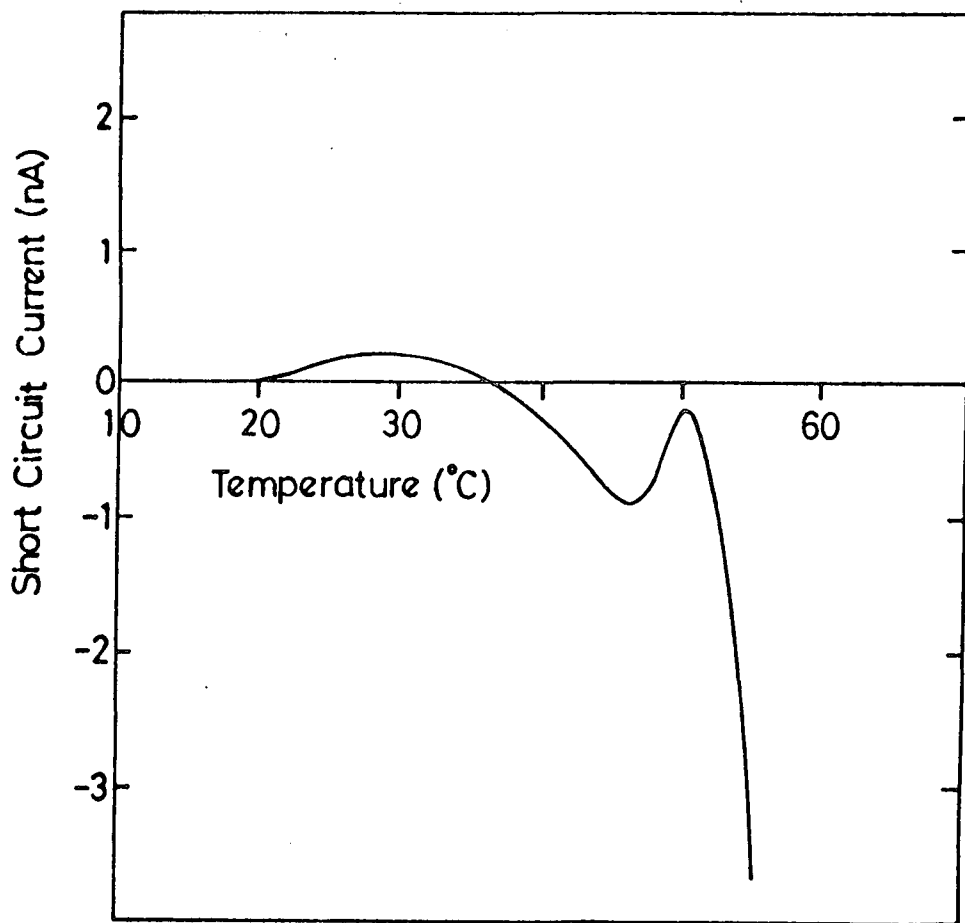


Figure 7.9 TSD thermogram of a 31 layer sample of 22-TA/docosylamine which was short-circuited for 24 hours before performing the experiment.

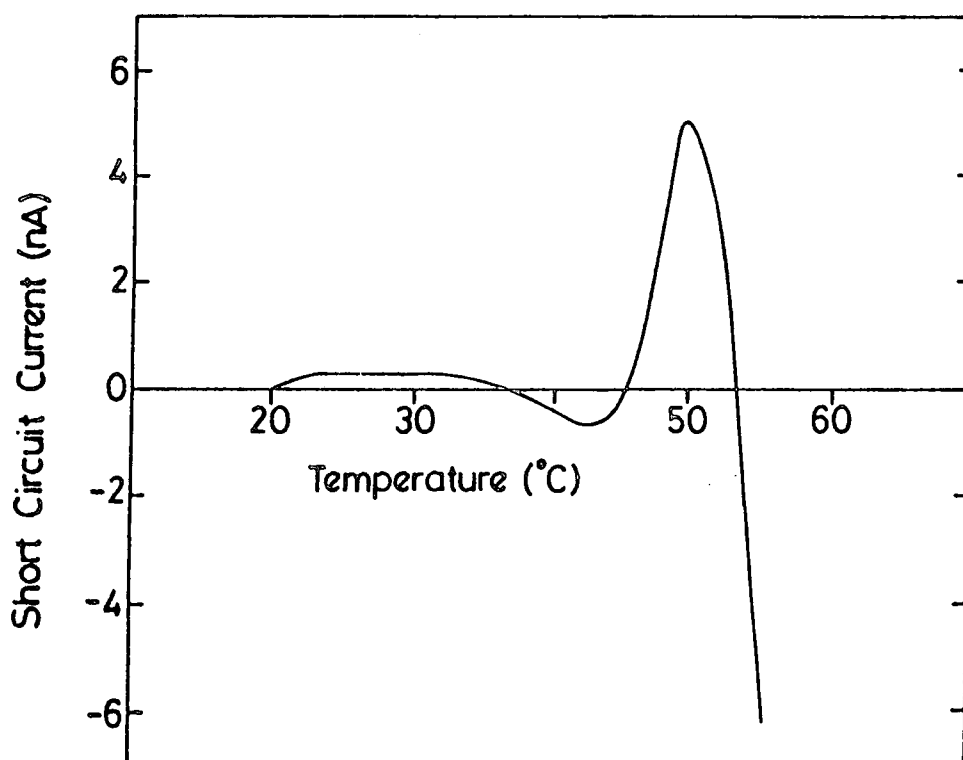


Figure 7.10 TSD thermogram of a 15 layer sample of 22-TA/docosylamine.

C has the opposite polarity in 22-TA/docosylamine and 22-TA/aniline samples implies that the internal polarisation in the alternate layer structures is the main driving force.

In a similar experiment it was found that the small current peak at approximately 40°C in the 22-TA structure (figure 7.7) could be significantly reduced in magnitude by short-circuiting the structure before performing the TSD experiment. This peak is therefore also attributed to the movement of excess charges. The driving force for the release of this charge is probably derived from some slight asymmetry in the device structure; possible sources include the unpaired dipole resulting from the deposition of an odd number of monolayers, or the presence of an interfacial oxide layer on the lower electrode. The small dipole associated with the terminal double bond in the hydrocarbon chain is almost certainly not the driving force, since very similar results were obtained from a 31 layer film of the saturated analogue, tricosanoic acid.

The second additional experiment involved studying the dependence of the TSD current on the number of monolayers in the array. Figure 7.10 shows the thermogram obtained for a 15 layer 22-TA/docosylamine sample. For this device, peak B is of a similar magnitude to that observed in the 31 layer sample of figure 7.6a, whilst peak C has increased significantly in magnitude. The TSD currents associated with dipole reorientation have an efficiency of 100% [9]; this is because each unit change in polarisation of the sample will release a corresponding image charge from the electrodes, which can then flow around the external circuit. However, for decay processes involving the release of space charges, only part of the charge originally stored may be recovered. In the latter case the efficiency of the process will depend on recombination both within the specimen and at the electrodes. Thus, changes in properties such as the sample thickness are expected to directly effect the components of the TSD current which are due to trapped charge. The data shown in figure 7.10 therefore appear to confirm the theory that peak B is due to dipole reorientation and C is due to release of trapped charges.

### 7.2.5 Origins of excess charges and dipoles

The TSD experiment cannot, of course, identify directly the origins of the charges and dipoles that produce the current maxima. Nevertheless, the features observed in these studies require some comment. The dipoles that are responsible for peak B cannot be those directly associated with the head groups of the alternate layer structures. If this were the case, heating the samples to approximately 50°C (*ie.*, above peak B) would eliminate the pyroelectric effect. However, the dipoles concerned must be oriented in the same direction as the overall polarisation in the specimens (figure 7.5); this is necessary to account for the fact that peak B is of opposite polarity in the 22-TA/docosylamine and 22-TA/aniline structures. A tentative explanation is that B is due to the reorientation of water molecules which have been incorporated into the film during deposition. Such polar molecules will tend to align themselves with the internal electric field in the multilayer assembly, and may become tightly bound within the film structure; thus they may not be removed by the room temperature desiccation procedure. However, when the sample is heated, the water molecules will first gain thermal energy and reorient into random configurations, accounting for peak B, and ultimately be expelled from the multilayer assembly, possibly by diffusion to grain boundaries where they are free to evaporate. Other workers have attributed low frequency dielectric dispersions in LB films to trapped water [23, 24], and have speculated that, in some cases, the electrical properties of LB films can be heavily dominated by the presence of small amounts of water.

The presence of charges in multilayer systems has also been postulated by earlier researchers [25-27]. For example, it has been suggested that trapped charges can account for the change in Schottky barrier height observed when an LB layer is sandwiched between a metal and a semiconductor [26]. A detailed study by Evans [27] has revealed the presence of two types of charge in symmetric LB arrays. By monitoring the capacitance-voltage characteristics of metal-insulator-semiconductor (MIS) devices incorporating LB layers of 22-tricosenoic acid, Evans concluded that a positive charge is associated with the deposition of the first monolayer; however, negative charge is introduced into the system with each subsequent monolayer coated onto the device. In the present

study, peak C is more likely to originate from bulk trapped charges than from surface charges, which would probably be neutralised by the electrodes [9].

The mechanisms of charge storage in electrets have been reviewed by Perlman [12]. The trapping of excess charges can occur on three structural levels, known as primary, secondary and tertiary. At the primary level, the traps are on the molecular chains themselves, and charge is stored at atomic sites; such charge may be released by individual atomic motions. At the secondary level, electrons become caged within groups of atoms in neighbouring molecules, and can be released only by the cooperative motion of atomic groups. At the tertiary level, charge is stored at grain boundaries, dislocations and other defects. In all of the LB film samples, peak C occurs at a temperature just below that at which the hydrocarbon chains begin to move. It therefore seems likely that charge is stored at either the secondary or the tertiary level, rather than on the molecular chains.

### 7.3 SUMMARY

The temperature dependence of the pyroelectric coefficients of 22-TA/docosylamine and 22-TA/aniline films has been investigated. Both types of film show a relationship of the form  $p \propto T^n$ : for 22-TA/docosylamine,  $n=2.3$ ; whilst for 22-TA/aniline,  $n=1.9$  for  $100 \text{ K} < T < 190 \text{ K}$ , and  $n=2.6$  for  $190 \text{ K} < T < 260 \text{ K}$ . The results of experiments using different substrate materials indicate that at low temperatures the pyroelectric effect is predominantly primary in origin, but that secondary phenomena begin to dominate at temperatures above about 250 K. At this stage, it is not possible to fully interpret the results in terms of lattice dynamical models; however, it is hoped that future far infrared data will lead to a greater understanding of the relationship between pyroelectricity and phonon modes in LB films.

In TSD experiments, four distinct features have been identified in the current versus temperature thermograms of 22-TA/docosylamine and 22-TA/aniline alternate layer films. The precise origins of these features cannot be determined conclusively from the present experimental data. However, it seems likely that they result from the pyroelectric effect, the reorientation of dipoles,

the release of excess charge, and the thermal disordering of the structure. The polarities of the current peaks which are due to the pyroelectric effect indicate that pyroelectricity in 22-TA/docosylamine films is related to the small dipole moments of the constituent molecules, rather than the larger polarisation resulting from proton transfer and ion formation.

## CHAPTER 8

### OTHER MATERIALS: RESULTS AND DISCUSSION

#### 8.0 INTRODUCTION

The results presented so far have concentrated on two specific alternate layer films, namely 22-TA/docosylamine and 22-TA/aniline. However, during the course of this work, a wide range of other materials was assessed for LB film forming ability and pyroelectric activity. The results of these studies are presented in this chapter, and have been divided into three categories: section 8.1 describes studies of other alternate layer systems; in section 8.2 the results of an investigation into the use of ionically terminated polymers are presented; finally, section 8.3 discusses pyroelectric and surface potential studies of some stearic acid esters.

It should be noted that the dynamic pyroelectric coefficients quoted in this chapter are only approximate. This is because it would have been an extremely time-consuming process to measure the d-spacing and dielectric constant of every material; therefore, the values of these parameters measured for 22-TA/docosylamine have been used throughout the chapter.

#### 8.1 OTHER ALTERNATE LAYER SYSTEMS

In addition to the acid/amine systems described in the preceding chapters, a range of other alternate layer films was evaluated for pyroelectric activity. These studies are described in the following sections, and have been classified into three groups: highly polarisable systems, systems possessing a large dipole moment, and other systems.

##### 8.1.1 Highly polarisable systems

Recently, the Langmuir-Blodgett technique has been successfully applied in the field of non-linear optics, and phenomena such as the Pockel's effect and second harmonic generation have been observed in LB films of dye materials [1-6]. It has been noted by Lines and Glass [7] that the residual non-linear

susceptibility,  $\chi^{(NL)}$ , of a crystal is directly proportional to the pyroelectric coefficient,  $p$ . It is therefore expected that those materials which exhibit non-linear optical effects should also be pyroelectric. The largest non-linear susceptibilities have been observed in non-centrosymmetric films of chromophoric materials, in which donor and acceptor groups are separated by a conjugated system. In such materials, charge transfer occurs along the conjugated group, resulting in a large dipole moment. It is immediately apparent that these properties of non-centrosymmetry and a large dipole moment are identical to the requirements for pyroelectricity. Furthermore, as was noted in chapters 5 and 6, a large polarisability is desirable for enhanced pyroelectric activity. It would seem, therefore, that alternate layer structures incorporating chromophoric molecules are ideal candidates for the observation of pyroelectricity.

A range of different chromophoric alternate layer systems was investigated, and the experimental conditions and results are summarised in table 8.1. The pyridinium salt and diacetylene derivative in systems A4 and A7 are not, strictly speaking, chromophores, but were nevertheless used because of their highly polarisable functional groups. With the exception of system A6, the films consisted of an "active" component (the chromophoric material) and a "passive" component, which was a fatty acid or a fatty amine. The role of the passive material was to prevent cancellation of the dipole moments in successive layers of the active component. In system A6, both components were active, as it was hoped that this would lead to further enhancement of the pyroelectric effect [4].

The dipping conditions used, which were in accordance with those of previous workers [8-10], are summarised in the fourth column of table 8.1;  $\pi_A$  and  $\pi_B$  refer to the surface pressures of the two monolayers. Unless otherwise indicated, all films were deposited from a nominally pure water subphase of pH 5.8. In every case, the dipping speed was  $2.5 \text{ mm min}^{-1}$ , and a total of 31 layers was deposited. The film quality was assessed qualitatively from observation of the deposition ratios and visual inspection of the deposited layer. In two cases (A6 and A7) it proved impossible to deposit multilayers of the materials.

The pyroelectric results are somewhat disappointing, since only systems A3 and A5 showed any pyroelectric activity, and the coefficients in both cases are

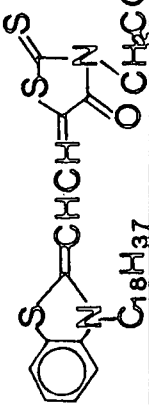
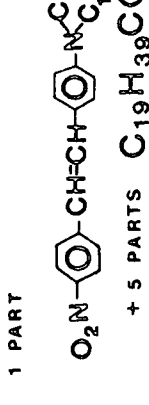
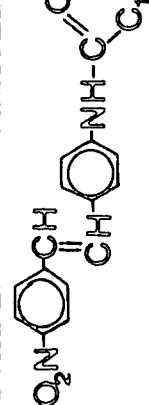
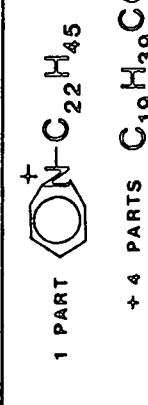
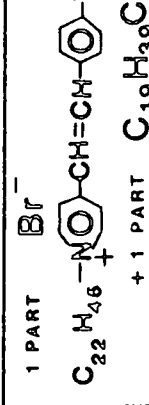
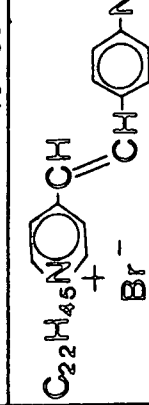
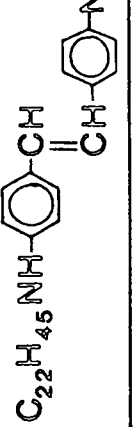
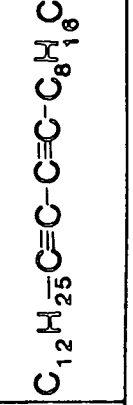
REF. NO.	MATERIAL A	MATERIAL B	DIPPING CONDITIONS	FILM QUALITY	PYROELECTRIC ACTIVITY
A1	 $C_{18}H_{13}N_2S_2O_2$	$C_{19}H_{39}COOH$	$\pi_A = 25 \text{ mN m}^{-1}$ $\pi_B = 30 \text{ mN m}^{-1}$ $Cd^{2+}$ present	Very good	No signal detected
A2	 $C_{19}H_{39}N_2S_2O_2$	$C_{19}H_{39}COOH$	$\pi_A = 30 \text{ mN m}^{-1}$ $\pi_B = 30 \text{ mN m}^{-1}$ $Cd^{2+}$ present	Fair	No signal detected
A3	 $C_{17}H_{35}N_2S_2O_2$	$CH_2=CHC_{20}H_{40}COOH$	$\pi_A = 32 \text{ mN m}^{-1}$ $\pi_B = 37 \text{ mN m}^{-1}$	Good	Pydynamic $\approx 0.04 \text{ nCcm}^{-2}K^{-1}$
A4	 $C_{22}H_{45}N_2S_2O_2$	$CH_2=CHC_{20}H_{40}COOH$	$\pi_A = 30 \text{ mN m}^{-1}$ $\pi_B = 37 \text{ mN m}^{-1}$	Poor	No signal detected
A5	 $C_{19}H_{39}N_2S_2O_2$	$C_{19}H_{39}COOH$	$\pi_A = 30 \text{ mN m}^{-1}$ $\pi_B = 30 \text{ mN m}^{-1}$ $Cd^{2+}$ present	Good	Pydynamic $\approx 0.03 \text{ nCcm}^{-2}K^{-1}$
A6	 $C_{22}H_{45}N_2S_2O_2$	 $C_{22}H_{45}N_2S_2O_2$	$\pi_A = 35 \text{ mN m}^{-1}$ $\pi_B = 30 \text{ mN m}^{-1}$ $Cd^{2+}$ present, pH = 9	Would not form multilayers	—
A7	 $C_{12}H_{25}N_2S_2O_2$	$C_{22}H_{45}NH_2$	$\pi_A = 15 \text{ mN m}^{-1}$ $\pi_B = 30 \text{ mN m}^{-1}$	Would not form multilayers	—

Table 8.1 Experimental conditions and results for the deposition and pyroelectric characterisation of alternate layer films containing highly polarisable groups.



extremely small. The reasons for the poor pyroelectric response of materials containing delocalised groups are unclear in view of the large non-linear susceptibilities of these materials [9]. In the cases where the film quality was not very good, this may be attributable to poor structural order; however, this is certainly not the case for films such as A1, A3 and A5. A possible explanation lies in the fact that non-linear optical studies have generally been performed on small (1-7) numbers of monolayers, whilst much thicker films were used in the present pyroelectric study. It is conceivable that, as more layers are deposited, the structure changes, and reorganises to give a centrosymmetric film. A similar effect was reported in 22-TA/aminobenzoate films in chapter 5, and it would be very interesting to perform infrared spectroscopic studies of the chromophore containing films, in order to ascertain whether structural reorganisation is occurring.

It is interesting to note that the pyroelectric acid/amine films discussed in the preceding chapters are expected to exhibit non-linear optical effects. 10 layer samples of 22-TA/docosylamine and 22-TA/aniline, deposited onto quartz substrates, were therefore sent to Plessey, Caswell for measurement of second harmonic intensity. No signal was detected from the 22-TA/docosylamine film, but a small signal, equivalent to  $\frac{1}{5}$  that of a monolayer of hemicyanine (material A of system A6 in table 8.1), was generated by 22-TA/aniline films.

### 8.1.2 Systems with large dipole moments

In addition to the acid/amine films already described, a range of other alternate layers, in which the constituent molecules possessed dipole moments in opposite senses with respect to the hydrocarbon chain, was investigated. The experimental details and results are summarised in table 8.2. All materials were deposited from a nominally pure water subphase of pH 5.8; the surface pressures and dipping speeds employed in each case are indicated.

Several of the systems investigated would not form multilayer films; this may be attributable to the very weak interactions between the head groups of the two materials. However, all of the films which did form multilayers gave pyroelectric signals. The pyroelectric coefficient of the acid/amide system (B4)

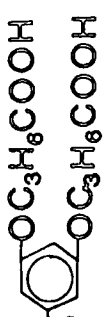
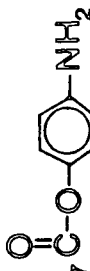
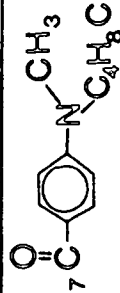

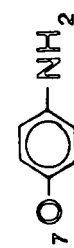
REF. NO.	MATERIAL A	MATERIAL B	DIPPING CONDITIONS	FILM QUALITY	PYROELECTRIC ACTIVITY
B1	$C_{18}H_{37}CN$	$C_{22}H_{45}NH_2$	$\pi_A = 25 \text{ mN m}^{-1}$ $\pi_B = 30 \text{ mN m}^{-1}$ Speed = 2.5 mm min <sup>-1</sup>	Would not form multilayers	—
B2	$CH_2=CHC_{20}H_{40}COOH$	$C_{18}H_{37}OH$	$\pi_A = 37 \text{ mN m}^{-1}$ $\pi_B = 30 \text{ mN m}^{-1}$ Speed = 2.5 mm min <sup>-1</sup>	Would not form multilayers	—
B3	$C_{14}H_{29}$  $OC_3H_6COOH$ $OC_3H_6COOH$	$C_{22}H_{45}NH_2$	$\pi_A = 30 \text{ mN m}^{-1}$ $\pi_B = 30 \text{ mN m}^{-1}$ Speed = 2.5 mm min <sup>-1</sup>	Would not form multilayers	—
B4	$CH_2=CHC_{20}H_{40}COOH$	$C_{21}H_{43}C(=O)NH_2$	$\pi_A = 37 \text{ mN m}^{-1}$ $\pi_B = 30 \text{ mN m}^{-1}$ Speed = 50 mm min <sup>-1</sup>	Very good	Dynamic $\approx 0.55 \text{ nCcm}^{-2}K^{-1}$ Potatic $\approx 0.15 \text{ nCcm}^{-2}K^{-1}$
B5	$C_{22}H_{45}COOH$	$C_{22}H_{45}NH_2$	$\pi_A = 33 \text{ mN m}^{-1}$ $\pi_B = 30 \text{ mN m}^{-1}$ Speed = 50 mm min <sup>-1</sup>	Fair	Dynamic $\approx 0.32 \text{ nCcm}^{-2}K^{-1}$ Potatic $\approx 0.05 \text{ nCcm}^{-2}K^{-1}$
B6	$CH_2=CHC_{20}H_{40}COOH$	$C_{18}H_{37}C(=O)O$ 	$\pi_A = 37 \text{ mN m}^{-1}$ $\pi_B = 30 \text{ mN m}^{-1}$ Speed = 50 mm min <sup>-1</sup>	Good	Dynamic $\approx 0.13 \text{ nCcm}^{-2}K^{-1}$
B7	$C_{18}H_{37}C(=O)N(CH_3)C_4H_8COOH$ 	$C_{18}H_{37}$ 	$\pi_A = 35 \text{ mN m}^{-1}$ $\pi_B = 30 \text{ mN m}^{-1}$ Speed = 20 mm min <sup>-1</sup>	Would not form multilayers	—
B8	$CH_2=CHC_{20}H_{40}COOH$	$C_{18}H_{37}O$ 	$\pi_A = 37 \text{ mN m}^{-1}$ $\pi_B = 30 \text{ mN m}^{-1}$ Speed = 5 mm min <sup>-1</sup>	Good	Dynamic $\approx 0.28 \text{ nCcm}^{-2}K^{-1}$

Table 8.2 Experimental conditions and results for the deposition and pyroelectric characterisation of alternate layer films possessing large dipole moments.

is approximately equal to that of 22-TA/docosylamine (see table 6.1). The similarity in the pyroelectric coefficients of these two films suggests that proton transfer may have occurred in the acid/amide film, in a similar manner to that occurring in 22-TA/docosylamine. It would therefore be of interest to study infrared spectra of acid/amide films in order to further investigate this phenomenon. System B5 is very similar to 22-TA/docosylamine, but with the acid replaced by its saturated analogue, tricosanoic acid. The reduced pyroelectric coefficient of B5 is probably not related to the absence of the terminal double bond, but is more likely to be a result of the poorer quality of the film.

Systems B6 and B8 are both based on 22-TA/aniline films, but with additional electron accepting groups between the benzene ring and the hydrocarbon chain of the aniline molecule. The pyroelectric coefficient of both films is significantly lower than that of the simple 22-TA/aniline system. This implies a reduction in polarisability due to the presence of the acceptor group. It is worth noting that, although B7 would not form multilayers, this is potentially a very interesting system, since the aniline and the acid terminated dye represent the two best reported materials in terms of attaining large pyroelectric coefficients [11, 12]. It would therefore be worthwhile, in the future, experimenting with different deposition conditions in an attempt to deposit alternate layers of these two materials.

### 8.1.3 Other alternate layer systems

The alternate layers reported in this section were investigated for a variety of reasons. The experimental details and results are given in table 8.3. In the first three cases (C1, C2 and C3), material B is a "passive" component, whilst material A possesses a specific property which it was intended to exploit. In system C1, the active material was chosen because it has a chiral centre, and possesses a structure similar to many ferroelectric liquid crystals [13]. However, the measured pyroelectric coefficients are extremely small, and it seems, therefore, that the properties of the liquid crystalline phase are not applicable to the material in LB film form. In system C2, the active material is a bisubstituted benzene derivative, and it was hoped that such a material would show similar

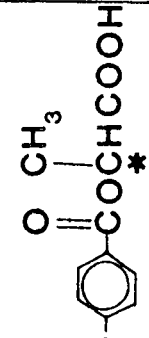
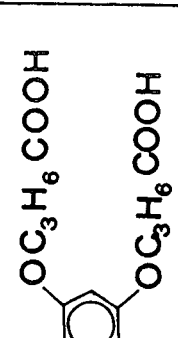
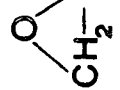

REF. NO.	MATERIAL A	MATERIAL B	DIPPING CONDITIONS	FILM QUALITY	PYROELECTRIC ACTIVITY
C1	$C_{13}H_{27}O$  $CH_2CHC(=O)CH_2COOH$	$CH_2CHC(=O)CH_2COOH$	$\pi_A = 30 \text{ mN m}^{-1}$ $\pi_B = 37 \text{ mN m}^{-1}$ Speed = 5 mm min <sup>-1</sup>	Good	$P_{dynamic} \approx 0.03 \text{ nCcm}^{-2}K^{-1}$ $P_{static} \approx 0.01 \text{ nCcm}^{-2}K^{-1}$
C2	$C_{14}H_{29}$  $CH_2CHC(=O)H$	$CH_2CHC(=O)H$	$\pi_A = 30 \text{ mN m}^{-1}$ $\pi_B = 37 \text{ mN m}^{-1}$ Speed = 2.5 mm min <sup>-1</sup>	Would not form multilayers	—
C3	$C_{18}H_{36}$  $CH_2CHC(=O)H$	$C_{22}H_{45}NH_2$	$\pi_A = 30 \text{ mN m}^{-1}$ $\pi_B = 30 \text{ mN m}^{-1}$ Speed = 50 mm min <sup>-1</sup>	Good	No signal detected
C4	$C_{18}H_{37}$  $CH_2CHC(=O)H$	$C_{22}H_{45}NH_2$	$\pi_A = 28 \text{ mN m}^{-1}$ $\pi_B = 30 \text{ mN m}^{-1}$ Speed = 50 mm min <sup>-1</sup>	Fair	$P_{dynamic} \approx 0.25 \text{ nCcm}^{-2}K^{-1}$

Table 8.3 Experimental conditions and results for the deposition and pyroelectric characterisation of some miscellaneous alternate layer films.

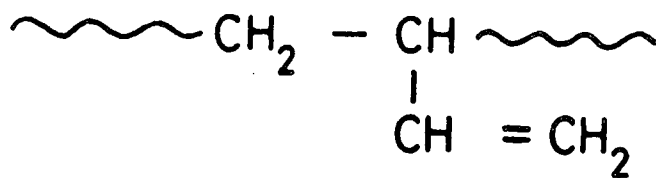
temperature dependent behaviour to m-DNB (see section 2.4.3). Unfortunately, the two materials would not form alternate multilayer films; this is probably attributable to the large difference in cross-sectional area of the two molecules. The active epoxide of system C3 contains a highly strained cyclic group, whose bond angles, and hence polarisation, should be strongly temperature dependent. Although the quality of film C3 was good, no pyroelectric signal was detectable. This is surprising in view of the fact that acid and amine groups are present, and may be indicative of a structural rearrangement.

The phenol/amine system (C4) was selected as it represents a weak acid/strong base system, and it was hoped that the degree of proton transfer in such a film might be intermediate between the total transfer occurring in 22-TA/docosylamine and the complete lack of proton transfer in 22-TA/aniline. If this were the case, it is likely that the degree of proton transfer would be a function of temperature, and hence might contribute to the pyroelectric effect. In fact, the measured pyroelectric coefficient is very much smaller than that of 22-TA/aniline films. This is almost certainly attributable to the poorer quality of the C4 films.

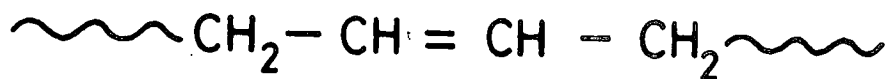
In summary, then, attempts to improve on the pyroelectric activity of acid/amine films have been largely unsuccessful, and the 22-TA/aniline system remains the best reported alternate layer LB film pyroelectric system.

## 8.2 IONICALLY TERMINATED POLYMERS

An alternative approach to creating the non-centrosymmetric films necessary for observation of the pyroelectric effect is to use materials which deposit in the X or Z type modes (figure 3.4). One such class of materials is the ionically terminated polybutadienes (PBD's). The repeat unit in the PBD chain is  $C_4H_6$ , but the structure has two isomeric variants, referred to as 1,2-PBD and 1,4-PBD, as shown in figure 8.1. Previous workers [14] have built up X type multilayer structures of low ( $\sim 600$ ) molecular weight 1,2-PBD, terminated by a quaternary ammonium salt,  $-N(CH_3)_3^+ Br^-$ , which acts as the hydrophilic head group for LB film deposition. The process used in depositing multilayers involves irradiating the deposited film with ultraviolet light after deposition of



(a)



(b)

Figure 8.1 The structural isomers of polybutadiene: (a) 1,2-PBD; (b) 1,4-PBD.

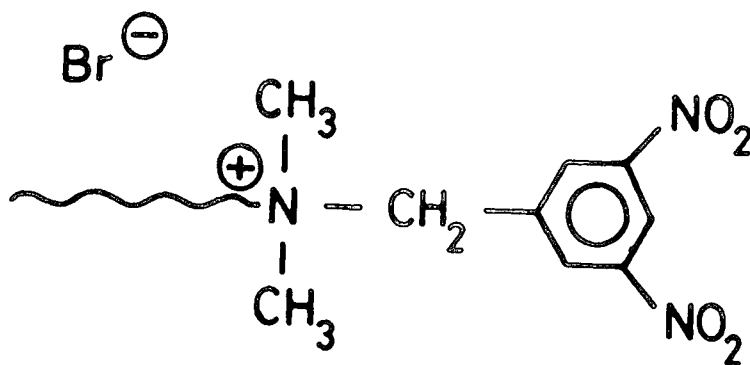


Figure 8.2 The molecular structure of m-DNB terminated PBD.

each monolayer, in order to initiate cross-linking of the polymer chains and so stabilise the structure.

In the present study, a range of PBD's of both 1,2 and 1,4 configurations and possessing various terminal groups and molecular weights was studied.

### 8.2.1 Ammonium terminated PBD

Initially, the work of Christie *et al* [14] was repeated, using the quaternary ammonium terminated 1,2-PBD of molecular weight 600. The cross-linking process was performed by irradiating the sample in an EPROM eraser for 50 minutes after deposition of each monolayer. Devices prepared in this manner did not exhibit pyroelectricity, in agreement with the results obtained by Christie *et al*. Since it has been shown [15], using the surface potential technique, that the PBD films possess a permanent polarisation, the absence of pyroelectric activity cannot be attributed to reorganisation, yielding a centrosymmetric structure. An alternative explanation is that the film, which is already partially clamped in two directions by the substrate, is rendered fully clamped by the cross-linking of the polymer chains. The total absence of pyroelectricity implies that any pyroelectric activity in "unclamped" PBD is almost entirely secondary in origin, and that mechanical constraints remove this piezoelectrically induced effect.

A sample of ammonium terminated PBD of the 1,4 configuration was also studied. As with the 1,2 material, it was found that multilayers could not be deposited in the absence of ultraviolet radiation. However, in this case, even after irradiating the samples for 90 minutes, it was not possible to deposit more than one monolayer. This can be explained by the fact that irradiation of 1,4-PBD does not initiate cross-linking, but rather causes chain fission [16].

### 8.2.2 Boron terminated PBD

Several batches of 1,2-PBD terminated by various boron containing groups and with a range of molecular weights were studied. The terminal groups used were:  $-\text{B}(\text{C}_2\text{H}_5)_3^- \text{Li}^+$ ,  $-\text{B}(\text{C}_4\text{H}_9)_3^- \text{Li}^+$  and  $-\text{B}(\text{C}_6\text{H}_5)_3^- \text{Li}^+$ . In every case, the material reacted with the atmosphere within hours of being dissolved in the chloroform solvent, forming a white or blue precipitate. The reaction was

thought to be due to elimination of the polar group via a hydrolysis or oxidation reaction. It was therefore not possible to form LB films of these boron terminated PBD's.

### 8.2.3 Ammonium terminated polystyrene

Low ( $\sim 1500$ ) molecular weight ammonium terminated polystyrene was also investigated, in the hope that it would exhibit X type deposition without the constraint of cross-linking encountered with PBD. Unfortunately, the spread monolayer was so rigid that material could not flow to counter the effect of removing the monolayer from the surface. Attempts were made to overcome this difficulty by mixing the spreading solution with arachidic acid, and by using a mixed solvent of chloroform and mesitylene, as described by Baker [17], but no significant improvement was observed.

### 8.2.4 Acid terminated PBD

A study of carboxylic acid terminated 1,2-PBD of molecular weight 800 yielded the interesting result that the deposition mode, after ultraviolet irradiation, was Y type. This suggests that the X type deposition observed for the ammonium terminated material was not directly related to cross-linking, as had previously been thought, but rather to the nature of the polar group.

Since this material deposited in a centrosymmetric structure, attempts were made to dip alternate layers of acid terminated and quaternary ammonium terminated PBD. Unfortunately, multilayers could not be deposited using the conventional alternate layer technique; however, it is possible that exposing the film to ultraviolet radiation after deposition of each bilayer might enable the dipping of PBD acid/amine alternate layer films.

### 8.2.5 m-DNB terminated PBD

The pyroelectric properties of m-DNB were discussed in section 2.4.3. This group was incorporated into an LB film by using a novel m-DNB terminated PBD, which is shown in figure 8.2. The PBD was of the 1,2 configuration, and of molecular weight 700. The  $\pi$ -A isotherm of this material is shown in figure



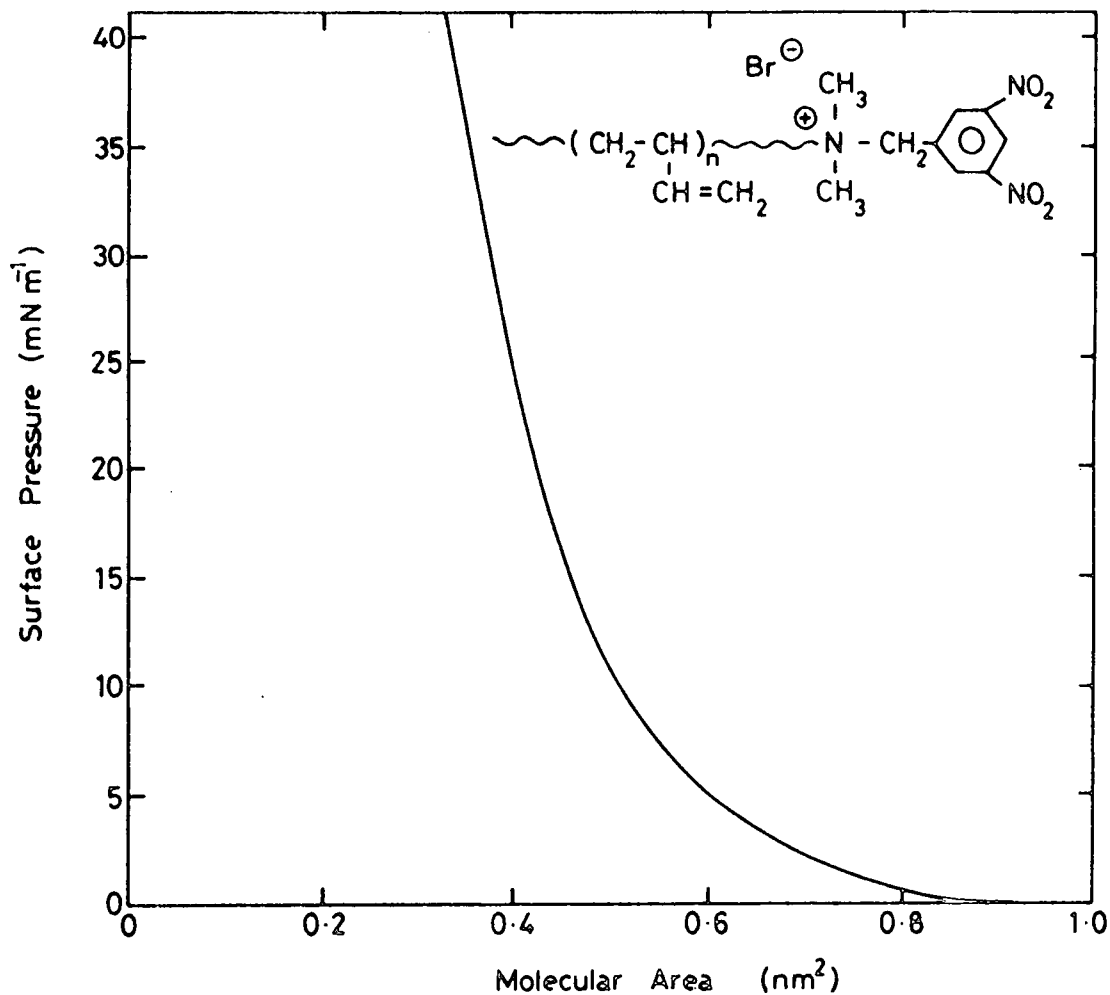


Figure 8.3 Surface pressure-area isotherm of m-DNB terminated PBD.

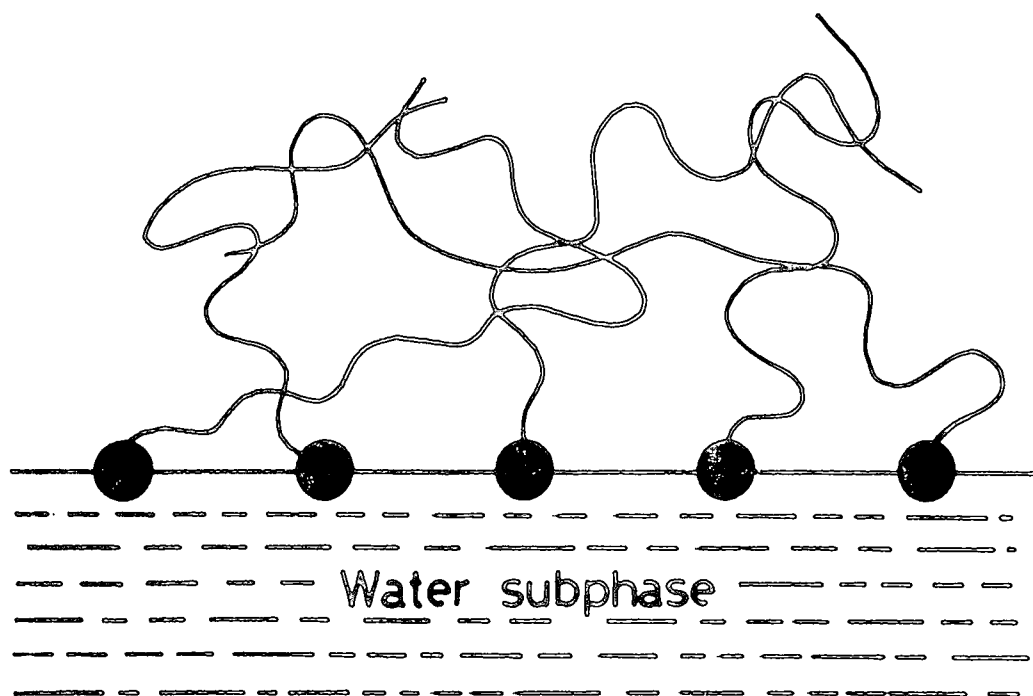


Figure 8.4 Schematic diagram showing the structure of an expanded monolayer on the water surface.

8.3, and is of the "expanded" type. As with most expanded isotherms, the measured molecular area of  $0.49 \text{ nm}^2$  is considerably greater than that calculated from molecular models ( $\sim 0.35 \text{ nm}^2$ ); Gaines [18] has attributed this observation to a monolayer which is liquid-like, with the polar groups anchored in the air-water interface, but the chains randomly intertwined (figure 8.4). Using a surface pressure of  $35 \text{ mN m}^{-1}$ , a dipping speed of  $7 \text{ mm min}^{-1}$ , and by irradiating the sample for 5 minutes after deposition of each monolayer, it was possible to build up X type multilayers of m-DNB terminated PBD; however, no pyroelectric signal was detected from these films. As with the other PBD's, it was expected that the cross-linking process would remove the secondary component of the pyroelectric effect; however, the primary contribution from the m-DNB group was still expected. The absence of such a contribution suggests that the anharmonic vibrations of the nitro groups are precluded by the packing arrangement in the LB film.

An alternative packing arrangement was achieved by depositing alternate layers of m-DNB terminated PBD and 22-TA. It was found that such films could be formed without irradiating the sample; however, films prepared in this manner could not withstand the evaporation of top electrodes. This is not surprising in view of the liquid-like properties of non-cross-linked PBD. The problem was overcome in two ways: the first method involved depositing 31 alternate layers, and then irradiating the film for 50 minutes; whilst the second technique consisted of depositing 31 alternate layers, followed by 20 layers of pure 22-TA. Both methods enabled high resistance devices to be fabricated, and devices prepared using both techniques showed a small degree of pyroelectric activity; the measured pyroelectric coefficients are given in table 8.4. These very small coefficients are unlikely to be due to the large primary pyroelectric effect expected to result from the m-DNB group. It is more likely that the observed effect is a result of the asymmetry of the lattice, and that anharmonic vibrations of the m-DNB group are again restricted by the packing arrangement.

SYSTEM	P <sub>static</sub> (nCcm <sup>-2</sup> K <sup>-1</sup> )	P <sub>dynamic</sub> (nCcm <sup>-2</sup> K <sup>-1</sup> )
31 alternate layers - irradiated	0.03	0.06
31 alternate layers + 20 layers 22-TA	0.02	0.03

Table 8.4 Pyroelectric coefficients of alternate layer films of m-DNB terminated PBD and 22-TA.

### 8.3 ESTERS OF STEARIC ACID

X type deposition has been widely reported [19–22] in the esters of stearic acid. In contrast to fatty acid multilayers [23], these X type structures do not undergo rearrangement, but retain their overall polarisation. The following sections describe investigations of two such esters, namely ethyl stearate and vinyl stearate.

#### 8.3.1 Ethyl stearate

Ethyl stearate ( $C_{17}H_{35}COOC_2H_5$ ) was found to form stable monolayers, giving a condensed isotherm (figure 8.5), and a molecular area of  $0.25 \text{ nm}^2$ , in agreement with the work of Fukuda and Shiozawa [21]. However, the collapse pressure of  $40 \text{ mN m}^{-1}$  was considerably higher than that measured by previous workers; this may be attributable to the low (99%) purity of the material. Although it was possible to deposit X type multilayers of ethyl stearate, deposition ratios were only around 0.3. The poor quality of the films, which was apparent from a visual inspection, meant that top electrodes could not be deposited without short-circuiting the device. It was therefore not possible to test ethyl stearate multilayers for pyroelectric activity.

#### 8.3.2. Vinyl stearate

The  $\pi$ - $A$  isotherm of vinyl stearate ( $C_{17}H_{35}COOCH=CH_2$ ) is shown in figure 8.6, and resembles two superimposed "classical" type isotherms, occurring for different degrees of compression of the monolayer. The most probable interpretation of this isotherm is that a phase change occurs at a molecular area of around  $0.19 \text{ nm}^2$ , and the regions on either side of this value correspond to the  $\pi$ - $A$  isotherms of the two different phases. The molecular areas at zero surface pressure for the two regions of the isotherm are  $0.15 \text{ nm}^2$  and  $0.20 \text{ nm}^2$ . Vinyl stearate can be constrained to deposit in either the X or Y type modes, depending on the surface pressure employed; however, X-ray measurements [21] have shown that Y type films rearrange to give an ultimate structure which is identical to that of films deposited in the X type mode. An experiment was devised to illustrate this phenomenon by surface potential measurements, and

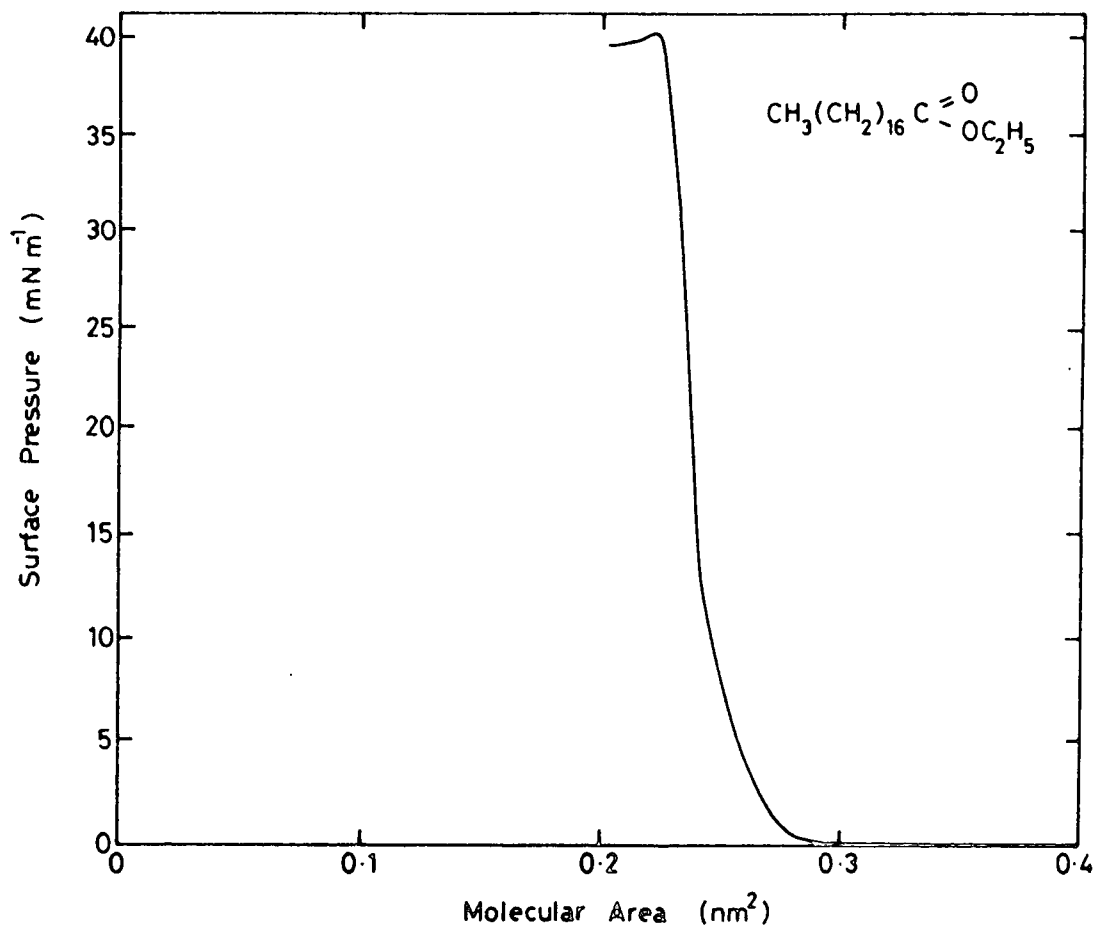


Figure 8.5 Surface pressure-area isotherm of ethyl stearate.

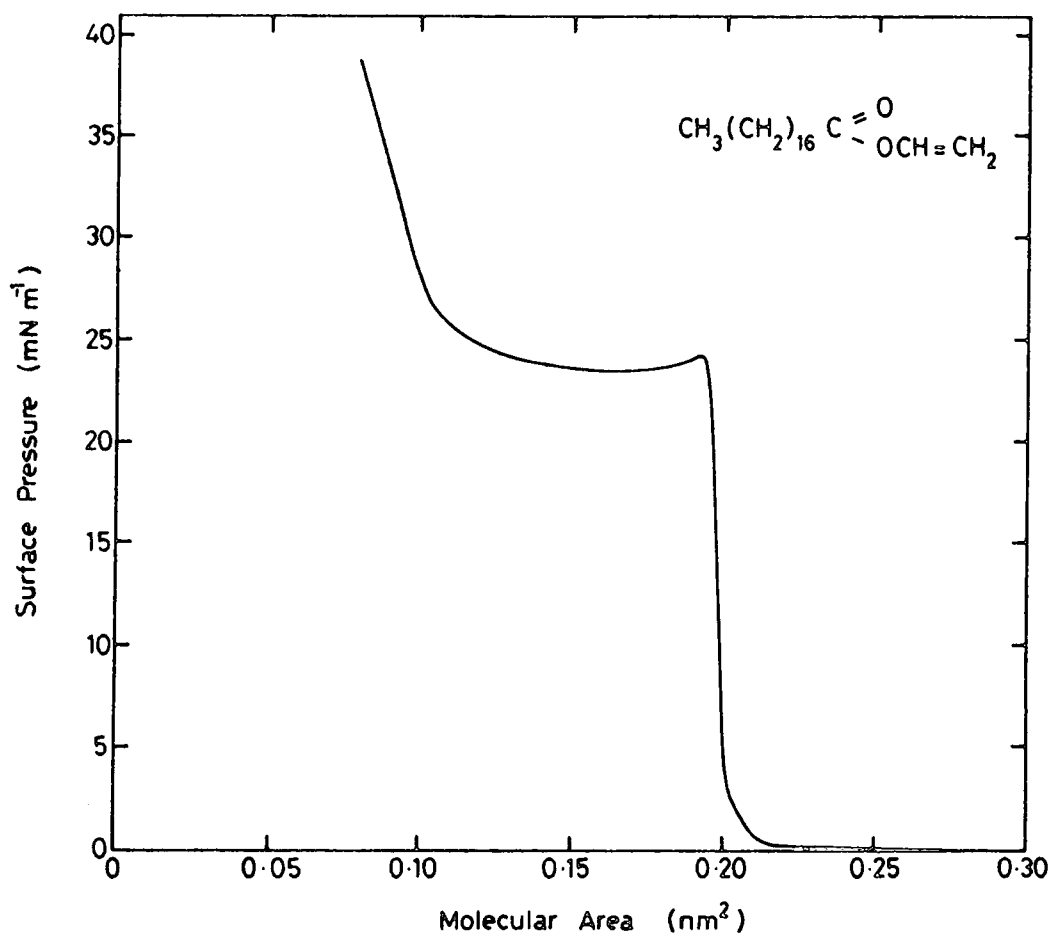


Figure 8.6 Surface pressure-area isotherm of vinyl stearate.

is described below.

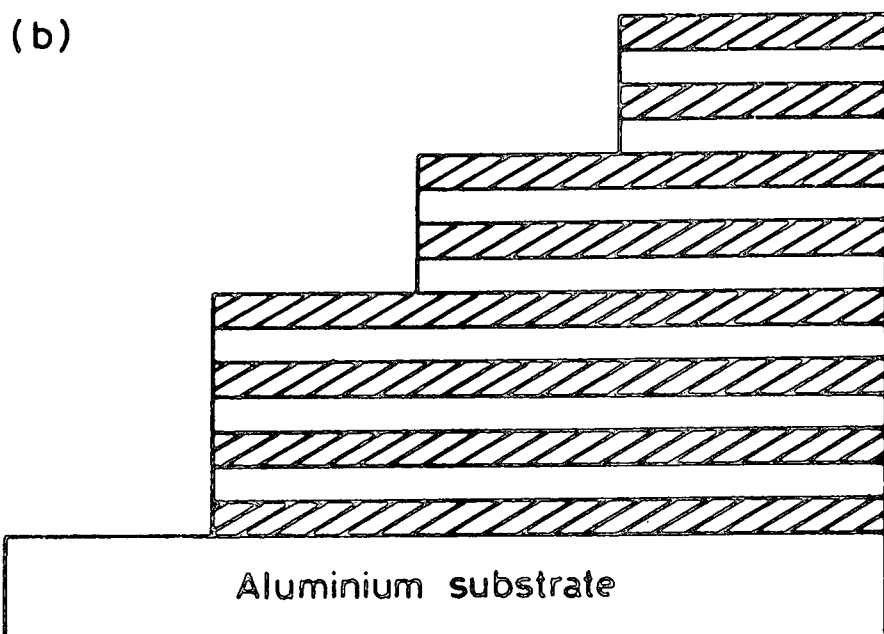
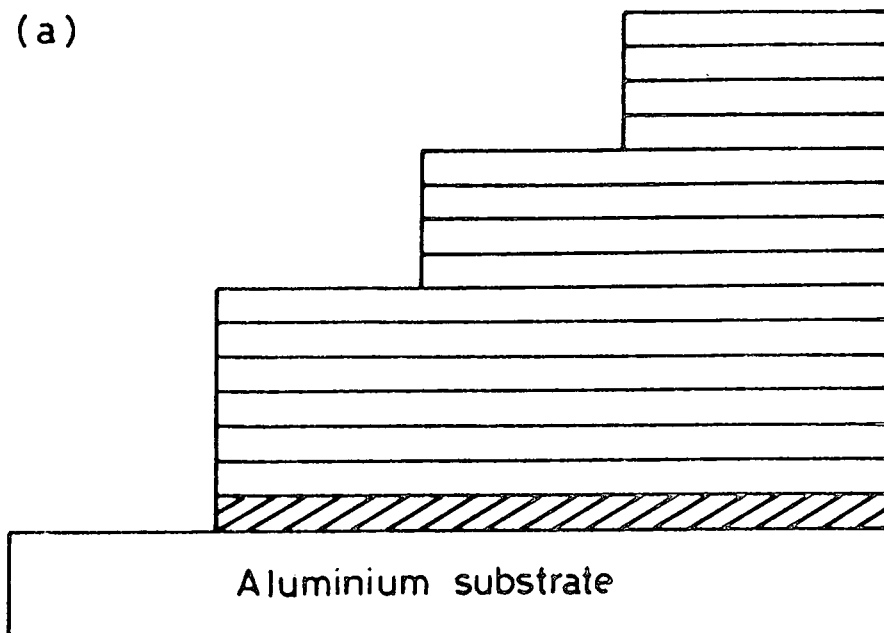
It was found that the hydrophilic nature of the aluminium substrate led to the first layer always being deposited on the initial withdrawal of the substrate through the floating monolayer. Subsequently, an X type film could be prepared by dipping at a surface pressure of  $10 \text{ mN m}^{-1}$  or a Y type sample by dipping at  $28 \text{ mN m}^{-1}$ . The two samples consisted of regions of different film thickness, and were of such a geometry that rearrangement of the Y type device would result in a structure identical to that of the X type device; this is illustrated in figure 8.7. Figures 8.8a and b show, respectively, the results of surface potential measurements on the X and Y type samples. The error bars on the horizontal scale, which have been shown as an inset for clarity, correspond to the diameter of the vibrating probe.

It should be noted that a dipole in the “down” direction (positive pole away from substrate) will cause an increase in surface potential, whilst an “upward” pointing dipole (positive pole towards substrate) will cause a decrease in potential relative to the clean aluminium surface. The X type sample is therefore expected to have a surface potential which increases in a step-wise fashion corresponding to the different film thicknesses. Figure 8.8a does indeed show an increase in surface potential along the film, but the increase occurs in a gradual rather than a stepped fashion. The most likely explanation for this is associated with the incorporation of charges in the film [24].

As the substrate is repeatedly passed through the water subphase during the deposition process, ions may be adsorbed by the film, and some of the ions may remain attached on withdrawal of the substrate from the water, producing a surface charge. If there are  $n$  elementary charges,  $+e$ , per unit area on the surface of a film of thickness  $t$  and dielectric constant  $\epsilon'_r$ , then there will be an induced charge  $-ne$  on the surface of the underlying metal, and an apparent surface potential,  $V_S$ , given by

$$V_S = \frac{net}{\epsilon_0 \epsilon'_r}. \quad (8.1)$$

During the deposition process, such surface charges may be covered by subsequent layers, so that internal volume charges are built into the film. The potential which results from these internal charges may be calculated using the





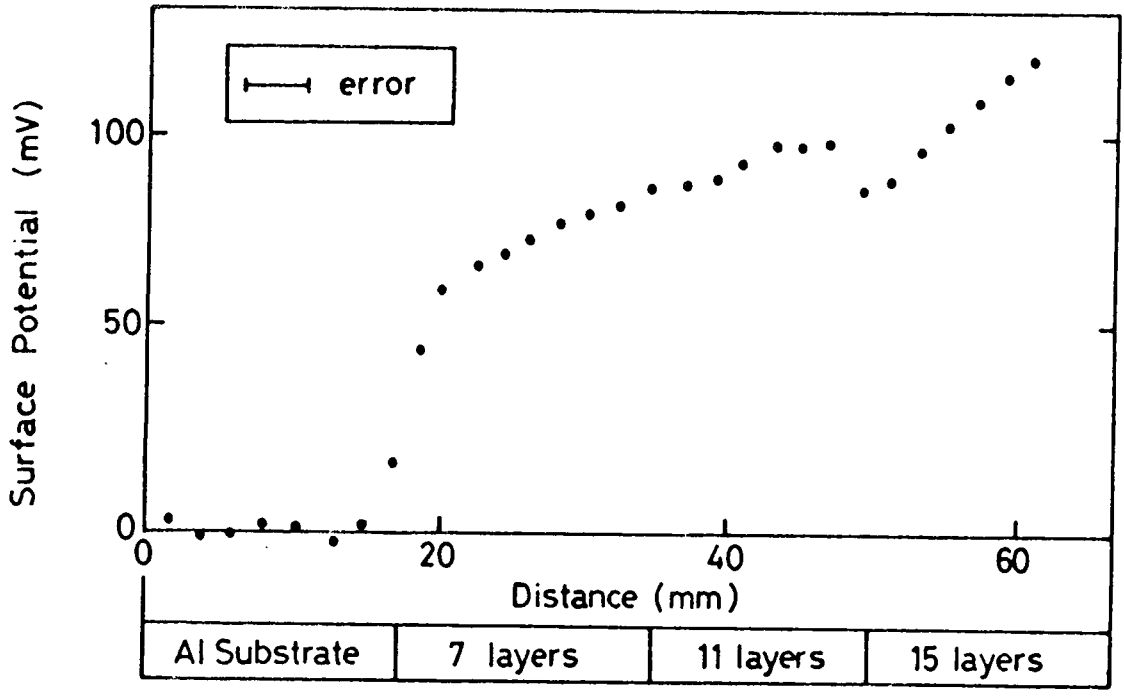
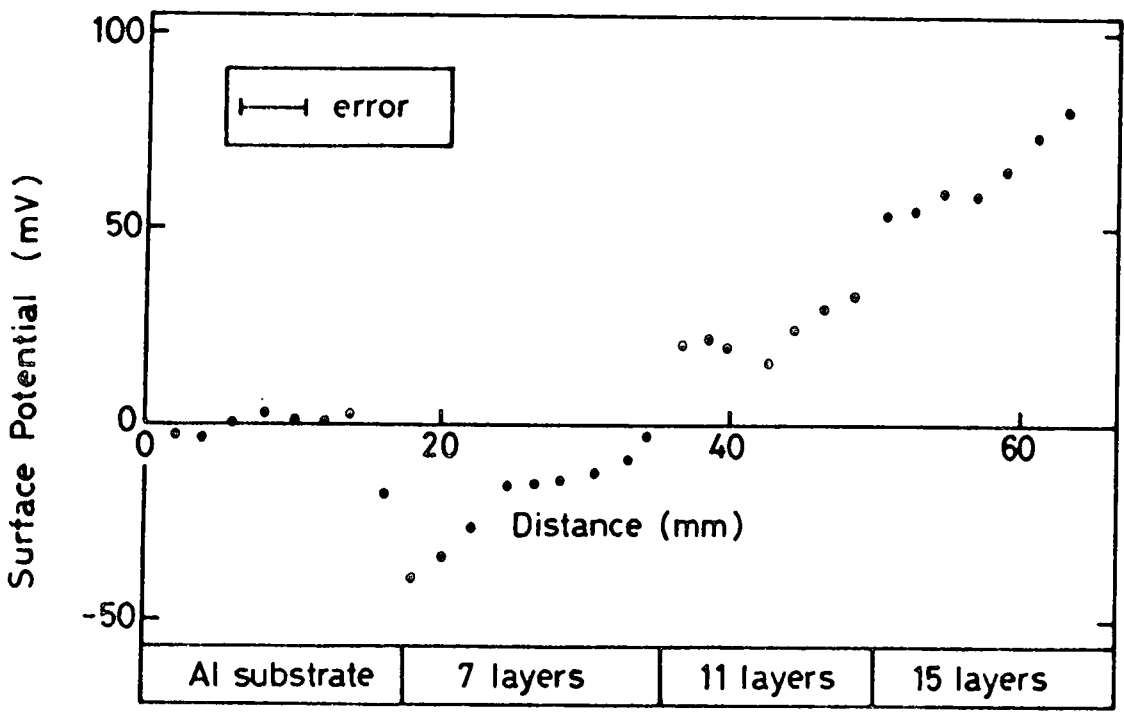
 = dipole in  $\downarrow$  direction  
 = dipole in  $\uparrow$  direction

Figure 8.7 Schematic diagram of the stepped thickness vinyl stearate samples used for surface potential measurements: (a) X type sample; (b) Y type sample.



(a)



(b)

Figure 8.8 Results of surface potential measurements on vinyl stearate films deposited in (a) the X type mode, and (b) the Y type mode.



Poisson equation. The accumulation of surface and volume charges is expected to be greatest for those parts of the sample which have been immersed in the water for the longest period of time. Hence, the gradual increase in surface potential can be accounted for by the incorporation of spurious surface and volume charges in the film. This indicates that the surface potential technique is not always a reliable method for revealing a spontaneous polarisation, and the results should be treated with great caution.

If the predicted rearrangement of the Y type sample occurs, then the surface potential should vary in an identical manner to that of the X type sample. On the other hand, if no rearrangement occurs, there should be a small decrease in potential corresponding to the first step (due to the unpaired dipole of the first layer), and no subsequent variation along the rest of the sample. Figure 8.8b shows an initial decrease in surface potential, which may be due to spurious effects at the edge of the film. The remainder of the 7 layer region shows an almost constant value of surface potential, slightly lower than that of the clean surface; this suggests that the Y type structure is retained in the first few layers of the film. For greater film thicknesses there is a gradual increase in surface potential, with discernible steps at the boundaries between the regions of different film thickness. This suggests that the predicted rearrangement has occurred, and the fact that there are clear potential steps indicates that there is less charge accumulation in the Y type film than in the X type.

Although the surface potential measurements were inconclusive in indicating whether vinyl stearate films possess a permanent polarisation, it was decided to examine an X type device of this material using the dynamic pyroelectric technique. The measured pyroelectric coefficient was approximately  $0.06 \text{ nCcm}^{-2}\text{K}^{-1}$ , indicating that vinyl stearate films are only weakly pyroelectric.

#### 8.4 SUMMARY

Several alternate layer LB film systems have exhibited pyroelectric activity; however, the 22-TA/aniline system remains the best pyroelectric LB film reported, to date. The X type deposition approach to producing pyroelectric films has been largely unsuccessful. X type films of ionically terminated polymers

were not pyroelectric, probably because of the mechanical constraints placed on the film by molecular packing and cross-linking of the chains. A small pyroelectric signal was detected from vinyl stearate multilayers, but attempts to detect directly the spontaneous polarisation in such films using the surface potential method were unsuccessful, because of the presence of trapped charge.

## CHAPTER 9

### CONCLUSIONS AND SUGGESTIONS FOR FURTHER WORK

#### 9.1 SUMMARY

The LB technique has been successfully used to fabricate ultra-thin organic films which exhibit the pyroelectric effect. The work presented in this thesis has concentrated mainly on two specific acid/amine alternate layer systems, namely 22-TA/docosylamine and 22-TA/aniline. The latter type of film has exhibited the largest reported pyroelectric coefficient, to date, for an LB film, and possesses a figure of merit ( $p/\epsilon_r'$ ) comparable with those of commercially available materials.

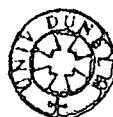
In view of the close relationship between structure and pyroelectric activity, three complementary structural studies of the films were undertaken. RHEED experiments showed that the molecules are oriented with their chain axes perpendicular to the substrate plane in 22-TA/docosylamine films, but that the molecules are tilted at approximately  $20^\circ$  to the substrate normal for 22-TA/aniline. A more general investigation of ultra-thin LB films demonstrated the importance of the substrate surface in determining the structure adopted by a film. The second structural technique to be used was FTIR spectroscopy. This method revealed that ionic bonding occurs in 22-TA/docosylamine films as a result of proton transfer from the acid to the amine. In 22-TA/aniline, however, the electron withdrawing nature of the benzene ring reduces the basicity of the amine to such an extent that no proton transfer occurs, and the layers in such films are bound together by weaker hydrogen bonds. The results suggest a possible link between polarisability and pyroelectric activity. FTIR also revealed that the absence of pyroelectric activity in 22-TA/aminobenzoate films can be attributed to a rearrangement of the film, producing a centrosymmetric structure. It was shown by X-ray diffraction that the d-spacing of 22-TA/aniline films is considerably less than expected, and this has been interpreted in terms of an interdigitation of the hydrocarbon chains in adjacent layers.

A detailed study of the dielectric and pyroelectric properties of acid/amine films has been undertaken. The dielectric constants of 22-TA/docosylamine and 22-TA/aniline films are 2.8 and 2.9 respectively, and show very little variation with either temperature (in the range 77–300 K) or frequency (in the range 1 Hz–100 kHz). The low values of dielectric constant represent an important advantage of LB films over most conventional pyroelectric materials.

The pyroelectric coefficients of 31 layer films, measured using the static technique, are approximately  $0.19 \text{ nCcm}^{-2}\text{K}^{-1}$  for 22-TA/docosylamine and  $0.65 \text{ nCcm}^{-2}\text{K}^{-1}$  for 22-TA/aniline. These correspond to figures of merit ( $p/\epsilon_r'$ ) of  $0.07 \text{ nCcm}^{-2}\text{K}^{-1}$  and  $0.22 \text{ nCcm}^{-2}\text{K}^{-1}$ , respectively. The latter figure compares favourably with those for conventional materials; for example,  $p/\epsilon_r'$  is equal to  $0.14 \text{ nCcm}^{-2}\text{K}^{-1}$  for strontium barium niobate and  $0.3 \text{ nCcm}^{-2}\text{K}^{-1}$  for PVDF. The pyroelectric coefficients measured using the dynamic technique are consistently higher than the static values, indicating some degree of inaccuracy in either the model used to describe the pyroelectric response or in the measurement of the various parameters. However, studies of the frequency dependence of the pyroelectric voltage have demonstrated the validity of the theoretically derived relationship,  $v_m \propto \omega_0^{-\frac{1}{2}}$ .

The effect of the substrate has been studied in detail, and it has been shown by a combination of theoretical and experimental techniques that the substrate causes both thermal and mechanical clamping effects. Thermal clamping is a result of the heat sinking effect of the substrate, and a novel theoretical model has been proposed to describe this. Mechanical clamping refers to the reduction in the secondary pyroelectric effect due to a mis-match in the thermal expansion coefficients of the LB film and the substrate. Studies of films deposited onto different substrates have revealed that there is a significant piezoelectrically induced secondary contribution to the overall pyroelectric coefficient. Furthermore, this secondary component is a negative one, which serves to decrease the pyroelectric coefficient relative to that which would be observed if only the primary effect were occurring.

The temperature dependence of the pyroelectric coefficient has been investigated. For both types of acid/amine film there is an initial increase in pyroelec-



tric coefficient, reaching a maximum at around 245 K for 22-TA/docosylamine and around 270 K for 22-TA/aniline films. At higher temperatures, the pyroelectric coefficients begin to decrease again. The low temperature data have been fitted to an empirical power law of the form  $p \propto T^n$ , and the results have been compared with theoretical lattice dynamical models. Experiments using different substrate materials indicate that the pyroelectric effect is predominantly primary at low temperatures, but that secondary phenomena begin to dominate at around 240–260 K.

In TSD experiments, four features have been identified in the current versus temperature thermograms. Two of these are almost certainly attributable to the pyroelectric effect and to a pre-transitional disordering of the hydrocarbon chains prior to melting. The sense of the pyroelectric current indicates that the pyroelectric effect in 22-TA/docosylamine films is due to the temperature dependence of the small dipole moments of the constituent molecules, rather than of the larger polarisation resulting from proton transfer and ion formation. The origins of the other two peaks are less clear, but there is evidence that these result from the release of trapped space charge, and the reorientation of dipolar groups (possibly water molecules.)

In addition to the acid/amine systems, a large range of other films has been investigated. Other alternate layer films were generally unsuccessful compared with the acid/amines; many materials would not form alternate layers, and a large proportion of those which did were of poor structural quality. As an alternative approach to producing polar films, X type layers of ionically terminated polybutadienes were investigated. In general, it was necessary to irradiate these films with ultraviolet light after deposition of each monolayer, in order to initiate cross-linking of the polymer chains and form a stable base for deposition of the next layer. Little or no pyroelectric activity was observed in such films, and this has been attributed to the mechanical clamping effect of the rigid polymer matrix. A small pyroelectric effect was observed in X type multilayers of vinyl stearate; however, surface potential measurements on these films were inconclusive due to the effects of trapped space charge.

## 9.2 SUGGESTIONS FOR FURTHER WORK

As a result of the present work, comparatively large pyroelectric figures of merit have been attained in alternate layer LB films. The origins of the pyroelectric effect and the influence of such parameters as the substrate thickness and thermal expansion coefficient are now reasonably well understood. However, there remain some areas in which further basic research is required in order to understand the physical processes involved. In particular, it is anticipated that infrared spectroscopic studies will be of extreme importance in gaining further insight into the microscopic origins of pyroelectricity. Recent infrared investigations have revealed changes in the interlayer hydrogen bonding of 22-TA/aniline films as a function of temperature; this may indicate that hydrogen bonds play an important role in the mechanism of the pyroelectric effect. Infrared spectroscopy may also prove useful as a tool for observing phonon vibrations, and hence lead to an understanding of the lattice dynamics of LB films.

Although the pyroelectric figure of merit for 22-TA/aniline is comparable with those of commercially available materials, this type of film has a low melting point ( $\sim 57^{\circ}\text{C}$ ), and hence is unlikely to be useful in a practical thermal imaging device. It is therefore desirable that new materials are found which, not only possess large pyroelectric figures of merit, but are also more stable with respect to temperature. Another drawback of the present alternate layer films is the relative importance of secondary pyroelectricity at room temperature. The maximum attainable sensitivity in devices based on such films may ultimately be determined by the substrate rather than the LB film. New materials, whose pyroelectric effect is predominantly primary at room temperature, must therefore be sought.

In addition to investigating new materials and studying the origins of pyroelectricity, future work should concentrate on the incorporation of LB films into efficient thermal imaging devices. In particular, it is essential that ultra-thin substrates are developed in order to reduce thermal clamping and improve the voltage responsivity. This might be achieved using "pellicles" of silicon oxide or silicon nitride, fabricated by growing a surface insulating layer on a silicon wafer, and etching away the semiconductor from the back. An array of pixels could be

defined in this way, and the amplifying circuitry could also be accommodated on the same wafer.

Another component of the device requiring considerable further research is the electrodes. Metal electrodes are incompatible with organic materials; in particular, the highly energetic evaporation of top electrodes will inevitably result in some damage to the LB film. It would therefore be desirable to use conducting organic materials as electrodes. There is a great deal of current interest in producing conducting LB films [1-3], and preliminary experiments in this laboratory have suggested that "MIM" devices composed entirely of LB films can be fabricated. Structures such as these would represent the first step towards a new generation of electronic devices based entirely on organic materials.

### 9.3 CONCLUSIONS

In this section the results reported in this thesis will be evaluated, and LB films will be compared with other materials which are used for pyroelectric detection. The precisely defined symmetry of LB films has enabled the creation of structures which are inherently polar, and hence do not need poling. This is in contrast to polymers and ceramics, both of which must be subjected to a poling process in order to render them pyroelectric. Although the pyroelectric coefficients of the LB films are small compared with most polar single crystals and ceramics, the very low dielectric constants compensate for this, making the values of  $p/\epsilon_r'$  comparable with those for many commercially available materials.

It is important to note that a wide variety of chemical groups can easily be incorporated into LB film forming molecules. Therefore, as the basic physical processes responsible for the pyroelectric effect become clearer, it will be possible to design and synthesise new LB film materials with enhanced pyroelectric properties. New materials must also be investigated with a view to improving the stability of pyroelectric LB films; it is particularly important that materials with a greater thermal stability are found if LB films are to compete with inorganic crystals and ceramics.

Possibly the greatest drawback of using LB films is the reduction of the py-

roelectric response by the substrate, through thermal and mechanical clamping effects. However, it is anticipated that this problem might be partially overcome by using ultra-thin substrates, such as silicon oxide pellicles. If an array of these pellicles could be fabricated on a silicon wafer, then there would be a possibility of incorporating the amplifying circuitry into the same wafer. It should be noted that ferroelectric liquid crystals also suffer from the constraints of thermal clamping, since they must be incorporated into glass cells.

As the size of microelectronic components is further reduced, it is anticipated that organic materials will become increasingly important for a wide range of electronics applications. The LB technique represents an elegant and convenient method for fabricating organic structures with the required electrical, optical or structural properties. If the two principal problems of thermal stability and clamping by the substrate can be overcome, then it seems very likely that LB films will compete favourably with the current generation of pyroelectric materials, and may be exploited on a commercial basis.



## REFERENCES

### CHAPTER 1

1. Report of the Molecular Electronics Advisory Group to the SERC (1985).
2. N. J. Thomas, G. G. Roberts and M. C. Petty, "Switching characteristics for GaAs/LB film MISS devices", *Insulating Films on Semiconductors*, 71 (1986).
3. D. B. Neal, M. C. Petty, G. G. Roberts, M. M. Ahmad, W. J. Feast, I. R. Girling, N. A. Cade, P. V. Kolinsky and I. R. Peterson, "Langmuir-Blodgett films for non-linear optics", *Proc. IEEE International Symposium on the Applications of Ferroelectrics*, 89 (1986).
4. S. Baker, G. G. Roberts and M. C. Petty, "Phthalocyanine Langmuir-Blodgett film gas detectors", *Proc. IEE I*, 130, 260 (1983).
5. D. Long and J. L. Schmitt, "Mercury cadmium telluride and closely related alloys", in *Semiconductors and Semimetals*, vol. 5, ed. Willardson and Beer, Academic Press (1970).
6. S. G. Porter, "A brief guide to pyroelectric detectors", *Ferroelectrics*, 33, 193 (1981).
7. M. E. Lines and A. M. Glass, "Principles and applications of ferroelectrics and related materials", Oxford University Press (1977).
8. J. C. Joshi and A. L. Dawar, "Pyroelectric materials: their properties and applications", *Phys. Stat. Sol. a*, 70, 353 (1982).
9. P. Pantelis, "Properties and applications of piezoelectric polymers", *Phys. Technol.*, 15, 239 (1984).
10. G. G. Roberts, "An applied science perspective of Langmuir- Blodgett films", *Advances in Physics*, 34, 475 (1985).

### CHAPTER 2

1. S. B. Lang, "Pyroelectricity: a 2300-year history", *Ferroelectrics*, 7, 231 (1974).
2. E. R. Caley and J. F. C. Richards, "Theophrastus on stones", The Ohio State University, Columbus (1956).

3. J. Bostock and H. T. Riley, "The natural history of Pliny", Henry Bohn, London (1857).
4. "Hortus sanitatis major", J. Prüss, Strasbourg (1497). In Blacker-Wood library, McGill University, Canada.
5. L. Lemery, "Diverses observations de physique générale", Histoire de l'Académie Royale des Sciences, Paris, 7 (1717).
6. F. U. T. Aepinus, "Mémoires concernant quelques nouvelles expériences électriques remarquables", Histoire de l'Académie Royale des Sciences et Belles Lettres, Berlin, 12, 105 (1756).
7. J. Canton, "Electrical properties of the tourmalin", Gentleman's Magazine, 29, 424 (1759).
8. "The complete works of Benjamin Franklin", vol. V, ed. J. Bigelow, Putnam, New York.
9. D. Brewster, "Observations on the pyro-electricity of minerals", Edinburgh J. Sci., 1, 208 (1824).
10. W. Thomson (Lord Kelvin), "On the thermoelectric, thermomagnetic and pyroelectric properties of matter", Phil. Mag., 5, 4 (1878).
11. W. Thomson (Lord Kelvin), "On the theory of the pyroelectricity and piezoelectricity of crystals", Phil. Mag., 36, 453 (1893).
12. G. Lippman, "Principe de la conservation de l'électricité", Ann. Chim. Phys., 24, 145 (1881).
13. J. Curie and P. Curie, "Développement par pression de l'électricité polaire dans les cristaux hémihédres à faces inclinées", C. R. Acad. Sci., 91, 294 (1880).
14. E. Schrödinger, "Kinetics of dielectrics: melting point, pyroelectricity and piezoelectricity", Akad. Wiss. Wien., Berlin, 121, 1937 (1912).
15. M. Born, "Pyroelectricity, temperature and the lattice theory", Phys. Z., 23, 125 (1922).
16. Y. Ta, "Action of radiations on pyroelectric crystals", C. R. Acad. Sci., 207, 1042 (1938).
17. L. J. Sivian, "Energy translation utilizing pyroelectricity", U. S. Patent 2299760 (1942).

18. A. G. Chynoweth, "Dynamic method for measuring the pyroelectric effect with special reference to barium titanate", *J. Appl. Phys.*, **27**, 78 (1956).
19. Third International Meeting on Ferroelectricity, Edinburgh, Sept. 1973, published in *Ferroelectrics*, **7** and **8** (1974).
20. Third European Meeting on Ferroelectricity, Zurich, Sept. 1975, published in *Ferroelectrics*, **12**, **13** and **14** (1976).
21. IEEE International Symposium on the Applications of Ferroelectrics, Bethlehem, USA, June 1986.
22. *Ferroelectrics*, published by Gordon and Breach, New York, 1970 to present.
23. S. B. Lang, "Literature guide to pyroelectricity", published annually in *Ferroelectrics*, commencing *Ferroelectrics*, **5**, 125 (1973).
24. IEEE standard definitions of primary ferroelectric terms, IEEE, New York (1986).
25. A. J. Goss, R. D. Nixon, R. Watton and W. M. Wreathall, "Infrared television using the pyroelectric vidicon", *GEC Journal of Research*, **2**, 198 (1984).
26. A. M. Glass, J. S. Patel, D. H. Olson and J. M. Geary, "Pyroelectric detection with smectic liquid crystals", *J. Appl. Phys.*, **60**, 2778 (1986).
27. H. M. Al-Allak, Ph. D. thesis, University of Wales, Cardiff (1983).
28. J. Fousek and L. Lejcek, "Ferroelectric liquid crystals: properties of real structures", *Proc. IEEE International Symposium on the Applications of Ferroelectrics*, 199 (1986).
29. V. F. Kosorotov, L. S. Kremenchugskii, L. V. Levash and L. V. Shchedrina, "Investigation of the pyroelectric effect under temperature gradient conditions", *Sov. Phys. Solid State*, **26**, 540 (1984).
30. L. M. Blinov, S. V. Ermakov and L. M. Korolev, "Surface pyroelectric effect in insulating films", *Sov. Phys. Solid State*, **14**, 3073 (1973).
31. J. F. Nye, "Physical properties of crystals", Oxford University Press (1957).
32. K. Nassau, "Ferroelectricity", ed. E. F. Weller, Elsevier (1967).
33. A. D. Franklin, "Ferroelectricity of barium titanate single crystals", *Progr. Dielec.*, **1**, 17 (1959).

34. A. W. Hewat, "Cubic-tetragonal-orthorhombic-rhombohedral ferroelectric transitions in perovskite potassium niobate", *J. Phys. C*, **6**, 2559 (1973).
35. G. Shirane, R. Pepinsky and B. C. Frazer, "X-ray and neutron diffraction study of ferroelectric  $\text{PbTiO}_3$ ", *Acta Crystallog.*, **9**, 131 (1956).
36. A. Avogadro, G. Bonera, F. Borsa and A. Rigamonti, "Static and dynamic properties of the structural phase transitions in  $\text{NaNbO}_3$ ", *Phys. Rev. B*, **9**, 3905 (1973).
37. D. G. Demurov and Y. N. Venevtsev, "Character of phase transition of ferroelectric  $\text{KTaO}_3$ ", *Sov. Phys. Solid State*, **13**, 553 (1971).
38. S. C. Abrahams, E. Buehlov, W. C. Hamilton and S. J. Laplaca, "Ferroelectric lithium tantalate - temperature dependence of the structure in the ferroelectric phase and the paraelectric structure at 940 K", *J. Phys. Chem. Solids*, **34**, 521 (1973).
39. M. H. Francombe, "The relation between structure and ferroelectricity in lead barium and barium strontium niobates", *Acta Crystallog.*, **13**, 131 (1960).
40. G. E. Bacon and R. S. Pease, "A neutron diffraction study of the ferroelectric transition of potassium dihydrogen phosphate", *Proc. R. Soc. Lond. A*, **230**, 259 (1955).
41. S. Sawada, S. Nomura, S. Fujii and I. Yoshida, "Ferroelectricity in  $\text{NaNO}_2$ ", *Phys. Rev. Lett.*, **1**, 320 (1958).
42. R. Nitsche and W. J. Merz, "Photoconduction in ternary V-VI-VII compounds", *J. Phys. Chem. Solids*, **13**, 154 (1960).
43. M. E. Lines and A. M. Glass, "Principles and applications of ferroelectrics and related materials", Oxford University Press (1977).
44. B. Jaffe, W. R. Cook and H. Jaffe, "Piezoelectric ceramics", Academic Press, London (1971).
45. V. V. Gagulin and B. A. Chayanov, "Ferroelectric and pyroelectric organic materials", *Izvestiya Akademii Nauk SSSR, Neorganicheskie Materialy*, **18**, 1667 (1982).
46. S. Hoshino, Y. Okaya and R. Pepinsky, "Crystal structure of the ferroelectric phase of  $(\text{glycine})_3 \text{H}_2\text{SO}_4$ ", *Phys. Rev.*, **115**, 323 (1959).

47. M. I. Kay and R. Kleinberg, "The crystal structure of triglycine sulfate", *Ferroelectrics*, **5**, 45 (1973).
48. K. Itoh and T. Mitsui, "Studies of the crystal structure of triglycine sulfate in connection with its ferroelectric phase transition", *Ferroelectrics*, **5**, 235 (1973).
49. T. Asaji and A. Weiss, "Pyroelectricity of molecular crystals: benzene derivatives", *Z. Naturforsch.*, **40a**, 567 (1985).
50. A. V. Bobrov, J. P. Mathieu and H. Poulet, *J. Raman. Spectr.*, **2**, 381 (1974).
51. J. Giermenska, R. Nowak and J. Sworakowski, "Piezo- and pyroelectric properties of m-dinitrobenzene single crystals", *Materials Science*, **10**, 77 (1984).
52. J. C. Burfoot and G. W. Taylor, "Polar dielectrics and their applications", Macmillan Press (1979).
53. W. P. Mason, "Piezoelectric crystals and their application to ultrasonics", Van Nostrand, New York (1950).
54. C. F. Pulvari, "An improved field-controlled polarization-transfer device", *IEEE Trans. Electron Devices*, **16**, 580 (1969).
55. M. Kahn and R. Ford, "Positive temperature coefficient resistors as high power pulse switches", *Proc. IEEE International Symposium on the Applications of Ferroelectrics*, 669 (1986).
56. J. E. Geusic, H. J. Levinstein, S. Singh, R. G. Smith and L. G. Van Uitert, "Continuous 0.532  $\mu$  solid state source using  $Ba_2NaNb_5O_{15}$ ", *Appl. Phys. Lett.*, **12**, 306 (1968).
57. D. Long and J. L. Schmitt, "Mercury cadmium telluride and closely related alloys", in *Semiconductors and Semimetals*, vol. 5, ed. Willardson and Beer, Academic Press (1970).
58. E. H. Putley, "The pyroelectric detector", in *Semiconductors and Semimetals*, vol. 5, ed. Willardson and Beer, Academic Press (1970).
59. S. T. Liu and D. Long, "Pyroelectric detectors and materials", *Proc. IEEE*, **66**, 14 (1978).

60. S. G. Porter, "A brief guide to pyroelectric detectors", *Ferroelectrics*, **33**, 193 (1981).
61. L. E. Garn and E. J. Sharp, "Pyroelectric vidicon target materials", *IEEE Trans. PHP*, **10**, 208 (1974).
62. R. Watton, "Pyroelectric materials: operation and performance in thermal imaging camera tubes and detector arrays", *Ferroelectrics*, **10**, 91 (1976).
63. R. Watton, D. Burgess and P. Nelson, "The thermal behaviour of reticulated targets in the pyroelectric vidicon", *Infrared Phys.*, **19**, 683 (1979).
64. P. A. Schlosser and D. D. Glower, "A self-scanned ferroelectric image sensor", *IEEE Trans. Sonics and Ultrasonics*, **19**, 257 (1972).
65. R. J. Phelan and A. R. Cook, "Electrically calibrated pyroelectric optical radiation detector", *Appl. Opt.*, **12**, 2494 (1973).
66. A. Hadni, "Applications of the pyroelectric effect", *J. Phys. E*, **14**, 1233 (1981).
67. S. B. Lang and F. Steckel, "Study of the ultrasensitive pyroelectric thermometer", *Rev. Sci. Instrum.*, **36**, 1817 (1965).
68. J. C. Joshi and A. L. Dawar, "Pyroelectric materials, their properties and applications", *Phys. Stat. Sol. a*, **70**, 353 (1982).
69. J. A. Gonzalo, "Ferroelectric materials as energy convertors", *Ferroelectrics*, **11**, 423 (1976).

### CHAPTER 3

1. S. G. Porter, "A brief guide to pyroelectric detectors", *Ferroelectrics*, **33**, 193 (1981).
2. J. C. Joshi and A. L. Dawar, "Pyroelectric materials, their properties and applications", *Phys. Stat. Sol. a*, **70**, 353 (1982).
3. S. C. Li, "The optimum of a thin pyroelectric film on a substrate", *Ferroelectrics*, **46**, 209 (1983).
4. M. H. Francombe, "Research status and device potential of ferroelectric thin films", *Ferroelectrics*, **3**, 199 (1972).
5. H. Kawai, "The piezoelectricity of polyvinylidene fluoride", *Japan. J. Appl. Phys.*, **8**, 975 (1969).

6. H. R. Gallantree, "A review of the transducer applications of polyvinylidene fluoride", *Proc. IEE I*, **130**, 219 (1983).
7. P. Pantelis, "Properties and applications of piezoelectric polymers", *Phys. Technol.*, **15**, 239 (1984).
8. P. D. Southgate, "Room temperature poling and morphology changes in pyroelectric polyvinylidene fluoride", *Appl. Phys. Lett.*, **28**, 250 (1976).
9. K. Tashiro, K. Takano, M. Kobayashi, Y. Chatani and H. Tadokoro, "Structural study on ferroelectric phase transition of vinylidene fluoride-trifluoroethylene random copolymers", *Polymer*, **22**, 1312 (1981).
10. A. J. Lovinger, T. Furukawa, G. T. Davis and M. G. Broadhurst, "Crystalline forms in a copolymer of vinylidene fluoride and trifluoroethylene", *Macromolecules*, **15**, 323 (1982).
11. A. J. Lovinger, T. Furukawa, G. T. Davis and M. G. Broadhurst, "Crystallographic changes characterizing the Curie transition in three ferroelectric copolymers of vinylidene fluoride and trifluoroethylene", *Polymer*, **24**, 1225 (1983).
12. T. Furukawa, J. X. Wen, K. Suzuki, Y. Takashina and M. Date, "Piezoelectricity and pyroelectricity in vinylidene fluoride/trifluoroethylene copolymers", *J. Appl. Phys.*, **56**, 829 (1984).
13. R. B. Meyer, L. Liebert, L. Strzelecki and P. Keller, "Ferroelectric liquid crystals", *J. Physique Lett.*, **36**, L69 (1975).
14. J. W. Goodby, "Synthesis, properties and applications of ferroelectric liquid crystals", *Ferroelectrics*, **49**, 275 (1983).
15. J. Fousek and L. Lejcek, "Ferroelectric liquid crystals: properties of real structures", *Proc. IEEE International Symposium on the Applications of Ferroelectrics*, 199 (1986).
16. A. M. Glass, J. S. Patel, J. W. Goodby, D. H. Olson and J. M. Geary, "Pyroelectric detection with smectic liquid crystals", *J. Appl. Phys.*, **60**, 2778 (1986).
17. A. J. Goss, R. D. Nixon, R. Watton and W. M. Wreathall, "Infrared television using the pyroelectric vidicon", *GEC Journal of Research*, **2**, 198 (1984).

18. G. Durand and P. Martinot-Lagarde, "Physical properties of ferroelectric liquid crystals", *Ferroelectrics*, **24**, 89 (1980).
19. K. B. Blodgett, "Films built by depositing successive monomolecular layers onto a solid surface", *J. Am. Chem. Soc.*, **57**, 1007 (1935).
20. E. Stenhagen, "Built-up films of esters", *Trans. Faraday Soc.*, **34**, 1328 (1938).
21. A. Cemel, T. Fort and J. B. Lando, "Polymerization of vinyl stearate multilayers", *J. Polym. Sci. A1*, **10**, 2061 (1972).
22. C. Holley, "X-ray and optical properties of barium copper stearate films", *Phys. Rev.*, **53**, 534 (1938).
23. S. Baker, M. C. Petty, G. G. Roberts and M. V. Twigg, "The production and properties of stable metal-free phthalocyanine Langmuir-Blodgett films", *Thin Solid Films*, **99**, 53 (1983).
24. P. Christie, M. C. Petty, G. G. Roberts, D. H. Richards, D. Service and M. J. Stewart, "The preparation and dielectric properties of polybutadiene Langmuir-Blodgett films", *Thin Solid Films*, **134**, 75 (1985).
25. S. T. Liu and D. Long, "Pyroelectric detectors and materials", *Proc. IEEE*, **66**, 14 (1974).
26. L. M. Blinov, N. N. Davydova, V. V. Lazarev and S. G. Yudin, "Spontaneous polarization of Langmuir multimolecular films", *Sov. Phys. Solid State*, **24**, 1523 (1982).
27. L. M. Blinov, L. V. Mikhnev, E. B. Sokolova and S. G. Yudin, "Pyroelectric effect in one and several monomolecular layers", *Sov. Tech. Phys. Lett.*, **9**, 640 (1983).
28. L. M. Blinov, N. V. Dubinin, L. V. Mikhnev and S. G. Yudin, "Polar Langmuir-Blodgett films", *Thin Solid Films*, **120**, 161 (1984).
29. L. M. Blinov, L. V. Mikhnev and S. G. Yudin, "A study of molecular orientation in a sequence of Langmuir layers", *Phys. Chem. Mech. Surfaces*, **3**, 2919 (1985).
30. A. Barraud, J. Leloup, A. Gouzerh and S. Palacin, "An automatic trough to make alternate layers", *Thin Solid Films*, **133**, 117 (1985).



31. M. F. Daniel, J. C. Dolphin, A. J. Grant, K. E. N. Kerr and G. W. Smith, "A trough for the fabrication of non-centrosymmetric Langmuir-Blodgett films", *Thin Solid Films*, **133**, 235 (1985).
32. B. Holcroft, M. C. Petty, G. G. Roberts and G. J. Russell, "A Langmuir trough for the production of organic superlattices", *Thin Solid Films*, **134**, 83 (1985).
33. C. A. Jones, M. C. Petty, G. H. Davies, J. Yarwood, N. M. Ratcliffe and J. W. Barton, "Infrared studies of pyroelectric Langmuir-Blodgett films" *Thin Solid Films*, in the press.
34. G. W. Smith, M. F. Daniel, J. W. Barton and N. Ratcliffe, "Pyroelectric activity in non-centrosymmetric Langmuir-Blodgett multilayer films", *Thin Solid Films*, **132**, 125 (1985).
35. P. Christie, G. G. Roberts and M. C. Petty, "Spontaneous polarization in organic superlattices", *Appl. Phys. Lett.*, **48**, 1101 (1986).
36. V. S. Lysenko and A. F. Mal'nev, "Optical characteristics of metal blacks", *Zhurnal Prikladnoi Spektroskopii*, **10**, 838 (1969).
37. J. D. Zook and S. T. Liu, "Pyroelectric effects in thin films", *J. Appl. Phys.*, **49**, 4604 (1978).
38. B. R. Holeman, "Sinusoidally modulated heat flow and the pyroelectric effect", *Infrared Phys.*, **12**, 125 (1972).
39. A. Van der Ziel, "Pyroelectric response and  $D^*$  of thin pyroelectric films on a substrate", *J. Appl. Phys.*, **44**, 546 (1973).
40. H. Blackburn and H. C. Wright, "Thermal analysis of pyroelectric detector", *Infrared Phys.*, **10**, 191 (1970).
41. A. G. Chynoweth, "Dynamic method for measuring the pyroelectric effect with special reference to barium titanate", *J. Appl. Phys.*, **27**, 78 (1956).
42. P. Christie, C. A. Jones, M. C. Petty and G. G. Roberts, "Dynamic pyroelectric response of Langmuir-Blodgett film infrared detectors", *J. Phys. D*, **19**, L167 (1986).
43. E. H. Putley, "The pyroelectric detector", in *Semiconductors and Semimetals*, vol. 5, ed. Willardson and Beer, Academic Press (1970).

## CHAPTER 4

1. K. B. Blodgett and I. Langmuir, "Built-up films of barium stearate and their optical properties.", *Phys. Rev.*, **51**, 964 (1937).
2. G. G. Roberts, W. A. Barlow and P. S. Vincett, "Technological applications of Langmuir-Blodgett films", *Phys. in Technol.*, **12c**, 69 (1981).
3. N. Carr, "The concentration of particulate matter in the Langmuir-Blodgett aqueous subphase and implications for high optical quality multilayers", *Chemtronics*, **1**, 167 (1986).
4. B. Holcroft, M. C. Petty, G. G. Roberts and G. J. Russell, "A Langmuir trough for the production of organic superlattices", *Thin Solid Films*, **134**, 83 (1985).
5. P. Christie, M. C. Petty, G. G. Roberts, D. H. Richards, D. Service and M. J. Stewart, "The preparation and dielectric properties of polybutadiene Langmuir-Blodgett films", *Thin Solid Films*, **134**, 75 (1985).
6. G. L. Gaines, Jr., "Insoluble monolayers at liquid-gas interfaces", Interscience, New York (1966).
7. V. S. Lysenko and A. F. Mal'nev, "Optical characteristics of metal blacks", *Zhurnal Prikladnoi Spektroskopii*, **10**, 838 (1969).
8. L. H. Germer and K. H. Storks, "Arrangement of molecules in a single layer and in multiple layers", *J. Chem. Phys.*, **6**, 280 (1938).
9. I. R. Peterson, G. J. Russell and G. G. Roberts, "A new model for the deposition of  $\omega$ -tricosenoic acid LB film layers", *Thin Solid Films*, **109**, 371 (1983).
10. G. J. Russell, M. C. Petty, I. R. Peterson, G. G. Roberts, J. P. Lloyd and K. K. Kan, "A RHEED study of cadmium stearate Langmuir-Blodgett films", *J. Mat. Sci.*, **3**, 25 (1984).
11. I. R. Peterson and G. J. Russell, "An electron diffraction study of  $\omega$ -tricosenoic acid Langmuir-Blodgett films", *Phil. Mag. A*, **49**, 463 (1984).
12. I. R. Peterson and G. J. Russell, "Deposition mechanisms in Langmuir-Blodgett films", *Brit. Polym. J.*, **17**, 364 (1985).
13. I. R. Peterson and G. J. Russell, "The deposition and structure of LB films of long chain fatty acids", *Thin Solid Films*, **134**, 143 (1985).

14. A. Bonnerot, P. A. Chollet, H. Frisby and M. Hoclet, "Infrared and electron diffraction studies of transient stages in very thin Langmuir-Blodgett films", *Chem. Phys.*, **97**, 365 (1985).
15. C. A. Jones, G. J. Russell, M. C. Petty and G. G. Roberts, "A reflection high energy electron diffraction study of ultra-thin Langmuir-Blodgett films of  $\omega$ -tricosenoic acid", *Phil. Mag. B*, **54**, L89 (1986).
16. G. J. Russell in "Progress in crystal growth and characterisation", vol. 5, ed. B. R. Pamplin, Pergamon Press (1982).
17. P. R. Griffiths, "Chemical infrared Fourier transform spectroscopy", Wiley (1975).
18. W. Lesslauer, "X-ray diffraction from fatty acid multilayers. Significance of intensity data in low-angle diffraction", *Acta Cryst. B*, **30**, 1927 (1974).
19. M. Pomerantz and A. Segmüller, "High resolution X-ray diffraction from small numbers of Langmuir-Blodgett layers of manganese stearate", *Thin Solid Films*, **68**, 33 (1980).
20. R. H. Tredgold, A. J. Vickers, A. Hoorfar, P. Hodge and E. Khoshdel, "X-ray analysis of some porphyrin and polymer Langmuir-Blodgett films", *J. Phys. D*, **18**, 1139 (1985).
21. V. Skita, M. Filipkowski, A. F. Garito and J. K. Blasie, "Profile structures of very thin multilayers by X-ray diffraction using direct and refinement methods of analysis", *Phys. Rev. B*, **34**, 5826 (1986).
22. A. G. Chynoweth, "Dynamic method for measuring the pyroelectric effect with special reference to barium titanate", *J. Appl. Phys.*, **27**, 78 (1956).
23. A. Noblet, H. Ridelaire and G. Sylin, "Measurement of surface potentials", *J. Phys. E*, **17**, 234 (1984).
24. A. K. Jonscher, "Dielectric relaxation in solids", Chelsea Dielectrics Press, London (1983).
25. A. K. Jonscher, "Presentation and interpretation of dielectric data", *Thin Solid Films*, **50**, 187 (1978).
26. J. van Turnhout, "Thermally stimulated discharge of polymer electrets", Elsevier, Amsterdam (1975).

27. M. M. Perlman, "Thermally stimulated currents and voltages and dielectric properties", *J. Electrochem. Soc.*, **119**, 892 (1972).
28. J. Tanguy, "Effect of phase transition on the dielectric properties of thin organic layers", *J. Appl. Phys.*, **47**, 2792 (1976).
29. J. L. Gil-Zambrano and C. Juhasz, "Thermally stimulated discharge currents in polyvinyl butyral films", *J. Phys. D*, **14**, 1661 (1981).
30. J. L. Gil-Zambrano and C. Juhasz, "Space charge polarisation in nylon films", *J. Phys. D*, **15**, 119 (1982).
31. C. Juhasz and J. L. Gil-Zambrano, "Spontaneous electric currents from nylon films", *J. Phys. D*, **15**, 327 (1982).

## CHAPTER 5

1. G. L. Gaines, Jr., "Insoluble monolayers at liquid-gas interfaces", Interscience, New York (1966).
2. H. Sobotka, M. Demeny and M. Arnaki, "Multimolecular films of triiodostearic acid", *J. Coll. Sci.*, **14**, 281 (1959).
3. I. R. Peterson, G. J. Russell and G. G. Roberts, "A new model for the deposition of  $\omega$ -tricosenoic acid", *Thin Solid Films*, **109**, 371 (1983).
4. R. W. Sykes, Ph. D. thesis, University of Durham (1980).
5. G. W. Smith, M. F. Daniel, J. W. Barton and N. Ratcliffe, "Pyroelectric activity in non-centrosymmetric Langmuir-Blodgett multilayer films", *Thin Solid Films*, **132**, 125 (1985).
6. CRC Handbook of Chemistry and Physics, ed. R. C. Weast, CRC Press (1984).
7. A. Barraud, J. Leloup, A. Gouzerh and S. Palacin, "An automatic trough to make alternate layers", *Thin Solid Films*, **133**, 117 (1985).
8. C. Holley, "X-ray and optical properties of barium copper stearate films", *Phys. Rev.*, **53**, 534 (1938).
9. N. J. Harrick, "Internal reflection spectroscopy", Interscience, New York (1967).

10. C. A. Jones, M. C. Petty, G. G. Roberts, G. Davies, J. Yarwood, N. M. Ratcliffe and J. W. Barton, "Infrared studies of pyroelectric Langmuir-Blodgett films", *Thin Solid Films*, in the press.
11. I. R. Peterson and G. J. Russell, "Deposition mechanisms in Langmuir-Blodgett films", *Brit. Polym. J.*, **17**, 364 (1985).
12. L. H. Germer and K. H. Storks, "Arrangement of molecules in a single layer and in multiple layers", *J. Chem. Phys.*, **6**, 280 (1938).
13. F. Kimura, J. Umenura and T. Takenaka, "FTIR-ATR studies of Langmuir-Blodgett films of stearic acid with 1-9 monolayers", *Langmuir*, **2**, 96 (1986).
14. I. R. Peterson and G. J. Russell, "An electron diffraction study of  $\omega$ -tricosenoic acid Langmuir-Blodgett films", *Phil. Mag. A*, **49**, 463 (1984).
15. A. Bonnerot, P. A. Chollet, H. Frisby and M. Hoclet, "Infrared and electron diffraction studies of transient stages in very thin Langmuir-Blodgett films", *Chem. Phys.*, **97**, 365 (1985).
16. C. A. Jones, G. J. Russell, M. C. Petty and G. G. Roberts, "A reflection high-energy electron diffraction study of ultra-thin Langmuir-Blodgett films of  $\omega$ -tricosenoic acid", *Phil. Mag. B*, **54**, L89 (1986).
17. W. Knoll, M. R. Philpott and W. G. Golden, "Surface infrared and surface enhanced Raman vibrational spectra of monolayer assemblies in contact with rough metal surfaces", *J. Chem. Phys.*, **77**, 219 (1982).
18. G. R. Bird, G. Debuch and D. Möbius, "Preparation of a totally ordered monolayer by rapid epitaxial attachment", *J. Phys. Chem.*, **81**, 2657 (1977).
19. I. R. Peterson and G. J. Russell, "The deposition and structure of LB films of long chain fatty acids", *Thin Solid Films*, **134**, 143 (1985).
20. B. Belbeoch, M. Roullia and M. Tournarie, "Evidence of chain interdigitation in Langmuir-Blodgett films", *Thin Solid Films*, **134**, 89 (1985).

## CHAPTER 6

1. P. Christie, Ph. D. thesis, University of Durham (1985).
2. U. Khanna and V. K. Srivastava, "Studies of dielectric constant of some 'built-up' molecular films", *Thin Solid Films*, **12**, S25 (1972).

3. G. G. Roberts, P. S. Vincett and W. A. Barlow, "A.C. and D.C. conduction in fatty acid Langmuir films", *J. Phys. C*, **11**, 2077 (1978).
4. E. P. Honig and B. R. de Koning, "Transient and alternating electric currents in thin organic films", *J. Phys. C*, **11**, 3259 (1978).
5. G. Marc and J. Messier, "Dielectric losses in organic monomolecular layers", *J. Appl. Phys.*, **45**, 2832 (1974).
6. M. Careem and A. K. Jonscher, "Lattice and carrier contributions to the dielectric polarization of stearic acid multilayer films", *Phil. Mag.*, **35**, 1489 (1977).
7. C. A. Jones, M. C. Petty and G. G. Roberts, "Pyroelectricity in ultra-thin organic superlattices", *Proc. IEEE International Symposium on Applications of Ferroelectrics*, 195 (1986).
8. F. W. Sears and G. L. Salinger, "Thermodynamics, kinetic theory, and statistical thermodynamics", Addison-Wesley (1975).
9. W. Känzig, "Space charge layer near the surface of a ferroelectric", *Phys. Rev.*, **98**, 549 (1955).
10. P. E. Bloomfield, I. Lefkowitz and A. D. Aranoff, "Electric field distributions in dielectrics, with special emphasis on near-surface regions in ferroelectrics", *Phys. Rev. B*, **4**, 974 (1971).
11. L. M. Blinov, S. V. Ermakov and L. M. Korolev, "Surface pyroelectric effect in insulating films", *Sov. Phys. Solid State*, **14**, 3073 (1973).
12. O. G. Vendik and I. G. Mironenko, "The dimensional effect in thin ferroelectric layers", *Ferroelectrics*, **9**, 45 (1975).
13. G. W. Smith and T. J. Evans, "Optimization of thermal performance of Langmuir-Blodgett film pyroelectric devices", *Thin Solid Films*, **146**, 7 (1987).
14. L. M. Blinov, N. V. Dubinin, L. V. Mikhnev and S. G. Yudin, "Polar Langmuir-Blodgett films", *Thin Solid Films*, **120**, 161 (1984).
15. G. W. Smith, M. F. Daniel, J. W. Barton and N. Ratcliffe, "Pyroelectric activity in non-centrosymmetric Langmuir-Blodgett multilayer films", *Thin Solid Films*, **132**, 125 (1985).

## CHAPTER 7

1. S. Boguslawski, *Physik. Zeits.*, **15**, 283 (1914).
2. S. Boguslawski, "Pyroelektrizität auf Grund der Quantentheorie", *Physik. Zeits.*, **15**, 569 (1914).
3. S. Boguslawski, "Der Temperaturabhängigkeit der pyroelektrischen Erregung", *Physik. Zeits.*, **15**, 805 (1914).
4. W. Ackermann, "Beobachtungen über Pyroelektrizität von der Temperatur", *Annalen der Physik*, **46**, 197 (1915).
5. M. Born, "On the quantum theory of pyroelectricity", *Rev. Mod. Phys.*, **17**, 245 (1945).
6. S. B. Lang, "Pyroelectric coefficient of lithium sulphate monohydrate (4.2–320 K)", *Phys. Rev. B*, **4**, 3603 (1971).
7. C. Kittel, "Introduction to solid state physics", Wiley (1976).
8. N. D. Gavrilova, S. N. Drozhdin, V. K. Novik and E. G. Maksimov "Relationship between the pyroelectric coefficient and the lattice dynamics of the pyroelectrics", *Sol. State Comm.*, **48**, 129 (1983).
9. J. van Turnhout, "Thermally stimulated discharge of polymer electrets", Elsevier, Amsterdam (1975).
10. M. L. Miller and J. R. Murray, "Persistent polarization in polymers. II. Depolarization currents", *J. Polym. Sci. A2*, **4**, 697 (1966).
11. A. R. McGhie, G. McGibbon, A. Sharples and E. J. Stanley, "Thermally stimulated conductivity of poly(vinyl fluoride)", *Polymer*, **13**, 371 (1972).
12. M. M. Perlman, "Thermally stimulated currents and voltages and dielectric properties", *J. Electrochem. Soc.*, **119**, 892 (1972).
13. J. L. Gil-Zambrano and C. Juhasz, "Thermally stimulated discharge currents in polyvinyl butyral films", *J. Phys. D*, **14**, 1661 (1981).
14. J. L. Gil-Zambrano and C. Juhasz, "Space charge polarisation in nylon films", *J. Phys. D*, **15**, 119 (1982).
15. C. Juhasz and J. L. Gil-Zambrano, "Spontaneous electric currents from nylon films", *J. Phys. D*, **15**, 327 (1982).
16. J. Tanguy and P. Hesto, "Thermally stimulated currents in organic monomolecular layers", *Thin Solid Films*, **21**, 129 (1974).

17. J. Tanguy, "Effect of phase transition on the dielectric properties of thin organic layers", *J. Appl. Phys.*, **47**, 2792 (1976).
18. C. A. Jones, M. C. Petty, G. G. Roberts, G. H. Davies, J. Yarwood, N. M. Ratcliffe and J. W. Barton, "Infrared studies of pyroelectric Langmuir-Blodgett films", *Thin Solid Films*, in the press.
19. C. Naselli, J. F. Rabolt and J. D. Swalen, "Order-disorder transitions in Langmuir-Blodgett monolayers. I. Studies of two-dimensional melting by infrared spectroscopy", *J. Chem. Phys.*, **82**, 2136 (1985).
20. J. P. Rabe, J. F. Rabolt, C. A. Brown and J. D. Swalen, "Order-disorder transitions in Langmuir-Blodgett films. II. IR studies of the polymerization of Cd-octadecylfumarate and Cd-octadecylmaleate", *J. Chem. Phys.*, **84**, 4096 (1986).
21. L. Rothberg, G. S. Higashi, D. L. Allara and S. Garoff, "Thermal disordering of Langmuir-Blodgett films of cadmium stearate on sapphire", *Chem. Phys. Lett.*, **133**, 67 (1987).
22. A. C. Lilly, Jr., L. L. Stewart and R. M. Henderson, "Thermally stimulated currents in mylar, high temperature, low field case", *J. Appl. Phys.*, **41**, 2007 (1970).
23. G. Marc and J. Messier, "Non-linear dielectric properties of aluminium/ monomolecular layers of calcium behenate/ aluminium structures", *Thin Solid Films*, **68**, 275 (1980).
24. D. M. Taylor and M. G. B. Mahboubian-Jones, "The electrical properties of synthetic phospholipid Langmuir-Blodgett films", *Thin Solid Films*, **87**, 167 (1982).
25. R. W. Goranson and W. A. Zisman, "Electrical properties of multilayers", *J. Chem. Phys.*, **7**, 492 (1939).
26. G. G. Roberts, M. C. Petty and I. M. Dharmadasa, "Photovoltaic properties of cadmium telluride/ Langmuir film solar cells", *IEEE Proc.*, **128**, 197 (1981).
27. N. J. Evans, Ph. D. Thesis, University of Durham (1986).



## CHAPTER 8

1. O. A. Aktsipetrov, N. N. Akhmediev, E. D. Mishina and V. R. Novak, "Second harmonic generation on reflection from a monomolecular layer", *JETP Lett.*, **37**, 207 (1983).
2. I. R. Girling, N. A. Cade, P. V. Kolinsky, J. D. Earls, G. H. Cross and I. R. Peterson, "Observation of second harmonic generation from Langmuir-Blodgett multilayers of a hemicyanine dye", *Thin Solid Films*, **132**, 101 (1985).
3. I. R. Girling, N. A. Cade, P. V. Kolinsky and C. M. Montgomery, "Observation of second harmonic generation from a Langmuir-Blodgett monolayer of a merocyanine dye", *Electron. Lett.*, **21**, 169 (1985).
4. D. B. Neal, M. C. Petty, G. G. Roberts, M. M. Ahmad, W. J. Feast, I. R. Girling, N. A. Cade, P. V. Kolinsky and I. R. Peterson, "Second harmonic generation from LB superlattices containing two active components", *Electron. Lett.*, **22**, 460 (1986).
5. G. H. Cross, I. R. Girling, I. R. Peterson and N. A. Cade, "Linear Pockels response of a monolayer Langmuir-Blodgett film", *Electron. Lett.*, **22**, 1111 (1986).
6. D. B. Neal, M. C. Petty, G. G. Roberts, M. M. Ahmad, W. J. Feast, I. R. Girling, N. A. Cade, P. V. Kolinsky and I. R. Peterson, "Langmuir-Blodgett films for nonlinear optics", *IEEE International Symposium on the Applications of Ferroelectrics*, **89** (1986).
7. M. E. Lines and A. M. Glass, "Principles and applications of ferroelectrics and related materials", Oxford University Press (1977).
8. M. T. Fowler, Ph. D. Thesis, University of Durham (1985).
9. D. B. Neal, Ph. D. Thesis, University of Durham (1987).
10. G. Lieser, B. Tieke and G. Wegner, "Structure, phase transitions and polymerizability of multilayers of some diacetylene monocarboxylic acids", *Thin Solid Films*, **68**, 77 (1980).
11. C. A. Jones, M. C. Petty, G. G. Roberts, G. H. Davies, J. Yarwood, N. M. Ratcliffe and J. W. Barton, "Infrared studies of pyroelectric Langmuir-Blodgett films", *Thin Solid Films*, in the press.

12. G. W. Smith, M. F. Daniel, J. W. Barton and N. M. Ratcliffe, "Pyroelectric activity in non-centrosymmetric Langmuir-Blodgett multilayer films", *Thin Solid Films*, **132**, 125 (1985).
13. L. M. Blinov, L. A. Beresnev, N. M. Shtykov and Z. M. Elashvili, "Pyroelectric properties of chiral smectic phases", *J. Physique*, **40**, C3-269 (1979).
14. P. Christie, M. C. Petty, G. G. Roberts, D. H. Richards, D. Service and M. J. Stewart, "The preparation and dielectric properties of polybutadiene Langmuir-Blodgett films", *Thin Solid Films*, **134**, 75 (1985).
15. P. Christie, Ph. D. Thesis, University of Durham (1985).
16. M. J. Stewart, Private communication.
17. S. Baker, Ph. D. Thesis, University of Durham (1985).
18. G. L. Gaines, Jr., "Insoluble monolayers at liquid-gas interfaces", Interscience, New York (1966).
19. E. Stenhagen, "Built-up films of esters", *Trans. Faraday Soc.*, **34**, 1328 (1938).
20. A. Cemel, T. Fort and J. B. Lando, "Polymerization of vinyl stearate multilayers", *J. Polym. Sci. A1*, **10**, 2061 (1972).
21. K. Fukuda and T. Shiozawa, "Conditions for formation and structural characterization of X type and Y type multilayers of long-chain esters", *Thin Solid Films*, **68**, 55 (1980).
22. G. S. Galleti and A. Giuseppe-Elie, "Vinyl stearate for Langmuir-Blodgett film applications", *Thin Solid Films*, **132**, 163 (1985).
23. C. Holley, "X-ray and optical properties of barium copper stearate films", *Phys. Rev.*, **53**, 534 (1938).
24. I. Langmuir, "Surface electrification due to the recession of aqueous solutions from hydrophobic surfaces", *Phys. Rev.*, **60**, 1190 (1938).

## CHAPTER 9

1. A. Ruaudel-Teixier, M. Vandevyver and A. Barraud, "Novel conducting LB films", *Mol. Cryst. Liq. Cryst.*, **120**, 319 (1985).

2. M. Vandevyver, P. Lesieur, J. Richard, A. Ruaudel-Tiexier, and A. Barraud, "Langmuir-Blodgett conducting film and its precursor", *Mol. Cryst. Liq. Cryst.*, **134**, 337 (1986).
3. M. Fujiki and H. Tabei, "TTF-TCNQ Langmuir-Blodgett films", *Synth. Met.*, **18**, 815 (1987).

## APPENDIX 1

### PUBLICATIONS

1. P. Christie, C. A. Jones, M. C. Petty and G. G. Roberts, "Dynamic pyroelectric response of Langmuir-Blodgett film infrared detectors", *J. Phys. D*, **19**, L167 (1986).
2. C. A. Jones, G. J. Russell, M. C. Petty and G. G. Roberts, "A reflection high energy electron diffraction study of ultra-thin Langmuir-Blodgett films of  $\omega$ -tricosenoic acid", *Phil. Mag. B*, **54**, L89 (1986).
3. C. A. Jones, M. C. Petty and G. G. Roberts, "Pyroelectricity in ultra-thin organic superlattices", *Proc. IEEE International Symposium on Applications of Ferroelectrics*, 195 (1986).
4. C. A. Jones, M. C. Petty, G. G. Roberts, G. Davies, J. Yarwood, N. M. Ratcliffe and J. W. Barton, "Infrared studies of pyroelectric Langmuir-Blodgett films", *Thin Solid Films*, in the press.
5. C. A. Jones, M. C. Petty and G. G. Roberts, "Langmuir-Blodgett films: a new class of pyroelectric materials", *IEEE Transactions on Ultrasonics, Ferroelectrics and Frequency Control*, in the press.
6. C. A. Jones, M. C. Petty, G. Davies and J. Yarwood, "Thermally stimulated discharge of alternate layer Langmuir-Blodgett film structures", *J. Phys. D*, in the press.
7. C. A. Jones, M. C. Petty and G. G. Roberts, "Polarisation processes in pyroelectric LB films", *Proc. 3rd International Conference on Langmuir-Blodgett films* (1987), in the press.
8. G. Davies, J. Yarwood, M. C. Petty and C. A. Jones, "Fourier-transform infra-red studies of alternate layer Langmuir-Blodgett films", *Proc. 3rd International Conference on Langmuir-Blodgett films* (1987), in the press.

